VTOL Final Report

High Altitude Mountain Rescue Aircraft (HAMRAC)

DSE Group 1

TU Delft

This page is intentionally left blank.

VTOL Final Report

High Altitude Mountain Rescue Aircraft (HAMRAC)

by

DSE Group 1

Andreini, Matthew	4267958
Bentvelsen, Falco	4158040
Diercks, Ties	4362373
Goossenaerts, Sieglinde	4291093
Huang, Joey	4159772
Kooij, Robert	4444531
Noordam, Leon	4049470
Soengas, José	4235762
Steinbusch, Giel	4479289
Splunteren, Max van	4345614
White, Archie	4438248

In partial fulfilment of the requirements for the degree of

Bachelor of Science
in Aerospace Engineering

Design Synthesis Exercise (AE3200)

Distributed to:

Dr. ir. R. van Paassen,	TU Delft, tutor
Mr. R. Martinez,	TU Delft, coach
Mr. V. Villalba Corbacho,	TU Delft, coach

Version History:	
23-1-19	Draft v1 submitted
29-1-19	Final v1 submitted
29-1-19	Final v2 submitted

January 2019

TU Delft

Contents

List of Abbreviations

Abbreviation	Description
A&P	Airframe and Powerplant
AAIP	Approved Aircraft Inspection Program
ACARS	Aircraft Communication Addressing and Reporting System
ADI	Attitude Director Indicator
AFCS	Automatic Flight Control System
AGL	Above Ground Level
AMS	ACARS Message Security
AP	Autopilot
APPR	Approach
APU	Auxiliary Power Unit
AI	Autorotation Index
ATC	Air Traffic Control
ATT	Attitude Retention Mode
BVI	Blade Vortex Interaction
CFD	Computational Fluid Dynamics
CG	Center Of Gravity
CO	Carbon Oxide
CO2	Carbondioxide
CPL	Coupled Mode
CRFP	Carbon Fibre Reinforced Polymer
CS	Certification Specification
DSE	Design Synthesis Exercise
DMAP	Digital Map
DP	Design Parameter
DVE	Deteriorated Visual Environment
EASA	European Aviation Safety Agency
EE	Embodied Energy
EMS	Emergency Medical Services
EOS	Electro Optical Design
ESHP	Equivalent Shaft Horsepower
ESSRA	Equivalent Solidity Single Rotor Approximation
FAA	Federal Aviation Administration
FAR	Federal Aviation Regulations
FBD	Free-Body Diagram
FBW	Fly-By-Wire
FD	Flight Director
FMECA	Failure Mode, Effects and Criticality Analysis
GPS	Global Positioning System
GVE	Good Visual Environments
HAMRAC	High Altitude Mountain Rescue AirCraft
HC	Hydrocarbon
HD	High-Definition
HEEL	Helicopter Emergency Egress Lightning
HH	Hot & High
HQR	Handling Qualities Rating
IA	Inspection Authorization
IFF	Identification Friend or Foe
IFR	Instrument Flight Rules
IMU	Inertial Measurement Unit
ISA	International Standard Atmosphere
LCC	Life-Cycle Cost
LED	Light-Emitting Diode
LOC	Localizer (Instrument Landing System)

Abbreviation	Description
LTE	Loss of Tail Rotor Effectiveness
MDT	Mean Down Time
MDO	Multidisciplinary Design Optimisation
ME	Million Euro's
METAR	MEteorological Aerodrome Reports
MFD	Multifunctional Displays
MPMT	Mean Preventive Maintenance Time
MRO	Maintenance, Repair and Overhaul
MTBF	Mean Time Between Failures
MTBM	Mean Time Between Maintenance
MTOW	Maximum Take-Off Weight
MTTM	Mean Time to Maintain
MTTR	Mean Time to Repair
NACA	National Advisory Committee for Aeronautics
NASA	National Aeronautics and Space Administration
NAV/COM	Navigation Communication
NAVD	Navigation Display
NLR	Nederlands Lucht- en Ruimtevaartcentrum
NOx	Nitrogen Oxide
OEI	One Engine Inoperative
OEW	Operating Empty Weight
OHT	Offshore Helicopter Transfer
OPS	Operations
PP	Performance Parameter
QA	Quality Assurance
RADAR	Radio Detection and Ranging
RAMS	Reliability, Availability, Maintainability and Safety
ROI	Return On Investment
RSHP	Rotor Shaft Horsepower
SAR	Search and Rescue
SAS	Stability Augmentation System
SATCOM	Satellite Communication
SFC	Specific Fuel Consumption
SH	Stakeholder
SHP	Shaft Horse Power
SUV	Sport Utility Vehicle
TAF	Terminal Aerodrome Forecast
TAS	True Airspeed
TCAS	Traffic Alert and Collision Avoidance System
TRI	Tail Rotor Interaction
UCE	Usable Cue Environment
UHF	Ultra High Frequency
UD	Uni-Directional
US	United States
USD	United States Dollars
VFS	Vertical Flight Society
VHF	Very High Frequency
VMS	Vehicle Management System
VOR	Very High Frequency Omni-Directional Range Station
VTOL	Vertical Take-Off and Landing

List of Symbols

Symbols	Description	
κ_{ov}	Overlap constant of tandem helicopter	[-]
$\kappa_{ov,inter}$	Overlap constant of intermeshing helicopter	[-]
ρ	Density of air	[kg/m^3]
ω	Angular velocity of the rotor	[rad/s]
Ω	Rotational Speed	[rad/s]
μ	Advance Ratio	[-]
$\mu_{viscosity}$	Dynamic Viscosity of the air	
η_m	Mechanical efficiency of the rotor system	[-]
θ	Angle offset between the rotor and the vertical plane of the rotorcraft	[radians]
$V_{i,hov}$	Induced velocity at hover	[m/s]
$V_{i,cr}$	Induced velocity during cruise	[m/s]
V_i	Induced velocity	[m/s]
V_{sfr}	The Airspeed at highest specific flight range	[m/s]
V_∞	True Airspeed	[m/s]
V_t	Tip speed	[m/s]
V_{blade}	Blade speed	[m/s]
V_c	Cruise Speed	[m/s]
C_l	Lift Coefficient	[-]
C_T	Thrust Coefficient	[-]
A_a	Airfoil area	[m^2]
I_R	Rotational Inertia	[m^4]
I_{zz}	Moment of Inertia around the Z-axis	[mm^4]
I_{yy}	Moment of Inertia around the Y-axis	[mm^4]
I_{xz}	Moment of Inertia around the X & Z-axis	[mm^4]
A_i	Inherent Availability	[-]
A_o	Operational Availability	[-]
P_i	Induced Power	[kW]
$P_{i,cr}$	Power Induced during Cruise	[kW]
P_{pd}	Profile Drag Power	[kW]
P_{par}	Parasite Drag Power	[kW]
P_{cl}	Climbing Power	[kW]
P_{tr}	Power Tail Rotor	[kW]
P_{TO}	Total power Required	[kW]
P_{min}	Minimum Power Rating	[kW]
P_{hov}	Hover Power	[kW]
$P_{i,hov}$	Induced Power at Hover	[kW]
α	Angle of Attack	[radians]
α_{TPP}	Tip Path Plane Angle	[rad]
$C_{D,p}$	Profile Drag Coefficient	[-]
$C_{L,max}$	Maximum Lift Coefficient	[-]
$C_{m,0}$	Pitching moment coefficient at zero lift coefficient	[-]
C_m	Moment Coefficient	[-]
σ	Solidity	[-]
σ_y	Resultant Bending stress around y-axis	[MPa]
$\sigma_{vonmises}$	Von Mises Stress	[MPa]
σ_{axial}	Axial Stress of the Blades	[MPa]
σ_{bend}	Bending Stress of the Blades	[MPa]
d	Distance between two rotors	[m]
m	Mass of rotorcraft	[kg]
D	Diameter of a rotor	[m]
$dMach$	Delta Mach	[-]
D_{cd}	Delta Drag Coefficient	[-]
M	Mach Number	[-]
$M_{bending}$	Bending Moment	[Nm]
M_b	Moment of the Blade	[Nm]
M_{dd}	Drag Divergence Mach Number	[-]
R	Radius of Rotor	[m]
Re	Reynolds Number	[-]
SFC	Specific Fuel Consumption	[$g/N \cdot s$]
F_{used}	Fuel Used	[kg]

Symbols	Description	
W	Weight of rotorcraft	[N]
W_{fuel}	Fuel Weight	[kg]
W_{gross}	Gross Weight	[kg]
T	Thrust provided by one set of rotor blade	[N]
T_{RR}	Thrust produced by a second set of rotor blades	[N]
L	Total lift produced by the rotorcraft	[N]
S	Blade Disc Area	[m^2]
S_f	Wetted area	[m^2]
DL	Disc Loading	[kg/m^2]
$\bar{c}$	Chord Ratio	[-]
$\bar{z}$	Z-Direction Distance for the bending stresses	[m]
$\bar{x}$	X-Direction Distance for the bending stresses	[m]
c	Blade Chord	[m]
A	Aspect Ratio	[-]
$A_{skin,ij}$	Area of each Skin segment	[m^2]
A_{spar}	Spar Area	[m^2]
t_{skin}	Skin Thickness	[m]
N_b	Number of blades	[-]
x_i	Skin Segment X-distance	[m]
y_i	Skin Segment Y-distance	[m]
z_i	Skin Segment Z-distance	[m]
x_{spar}	X-distance of the spar	[m]
z_{spar}	Z-distance of the spar	[m]
h_{spar}	Height of the spar	[m]
h	Distance spar to the tip	[m]
b	Spar thickness	[m]
a	Distance in z-axis from the top of the spar minus skin thickness	[m]
EI	Flexural Rigidity	[$Pa \cdot m^4$]
$EI_{profile}$	Flexural Rigidity of the blade profile	[$Pa \cdot m^4$]
EI_{core}	Flexural Rigidity of blade core	[$Pa \cdot m^4$]
P_i	Centrifugal Force	[MPa]
$\rho_{material}$	Material Density	[kg/m^3]
ϕ	Deflection angle of the blade	[Degrees]
q_b	Base shear flow	[N/m]
$q_{b,i}$	Base shear flow for each segment	[N/m]
S_x	Shear force in x-axis	[N]
S_z	Shear force in z-axis	[N]
$p_{0,i}$	Moment arm for each shear segment	[m]
$A_{0,i}$	Enclosed Area	[m^2]
$q_{s0,i}$	Redundant Shear flow	[N/m]
G	Shear Modulus	[MPa]
r_i	Cross-Sectional Radius of a tubular section	[m]
L_i	Axial force on each rotorshaft	[N]
τ	Shear stress due to the torque of the rotorshaft	[MPa]
$B_{i,stringer}$	Boom area stringer	[m^2]
B_i	Total boom area	[m^2]
$q_{0,R}$	Redundant shear flow in cell	[N/m]
A_R	Enclosed Area of the Tubular cross-section	[m^2]
X_u	Drag Damping	[-]
M_u	Speed Static Stability	[-]
M_q	Pitching Damping	[-]
M_w	Angle of Attack Stability	[-]
Z_w	Heave Damping	[-]
L_p	Roll Mode	[-]
N_r	Spiral Mode	[-]
L_v	Dutch Roll Mode	[-]
t_{part}	Time of the mission part	[-]
$P_{installed}$	Power installed	[kW]

Executive Summary

Problem Statement The popularity of high altitude climbing has seen a significant increase over the last two decades, especially in the Himalayas. The commercialisation that has followed from the rapidly increasing number of climbers, has resulted in less experienced climbers, often with insufficient gear attempting to summit the highest mountains on earth. As a result of both of these trends, the number of incidents and injuries that has occurred within these mountains has increased dramatically, and so has the demand for emergency medical services, mainly in the form of mountainside helicopter evacuations. The current highest altitude rescue mission that has ever been performed reached an altitude of 7010 m while many accidents and life-threatening situations occur at higher altitudes. In addition, this helicopter evacuation was achieved under optimal circumstances, using an Ecureuil AS350 B3 helicopter. Therefore, there is a critical need for a rescue helicopter that can help stranded climbers at high altitudes and in sub-optimal weather conditions. This Design Synthesis Exercise shall fulfil this need through the design of the HAMRAC: High Altitude Mountain Rescue Aircraft. The project was initiated by two main stakeholders: Dr. ir. M.M. van Paassen, principal tutor at the faculty of Aerospace Engineering at Delft University of Technology, and secondly the Vertical Flight Society (VFS), which can be regarded as an external customer.

Mission Introduction The HAMRAC is designed for an extreme reference mission profile it has to be able to perform. The reference mission is from the international airport of Kathmandu to the top of Mount Everest with a refuel stop at the heliport of a medical clinic in Khunde. This mission reaches an altitude of 8950 m and has to be performed within three hours. If the aircraft is able to perform this mission, it can perform rescue missions at almost every spot within the Himalaya range. This mission profile also complies with the requirements set by the VFS. The profile is visualised in Figure 1. The mountain tops the HAMRAC will encounter during this mission have also been integrated, by planned fly-overs.

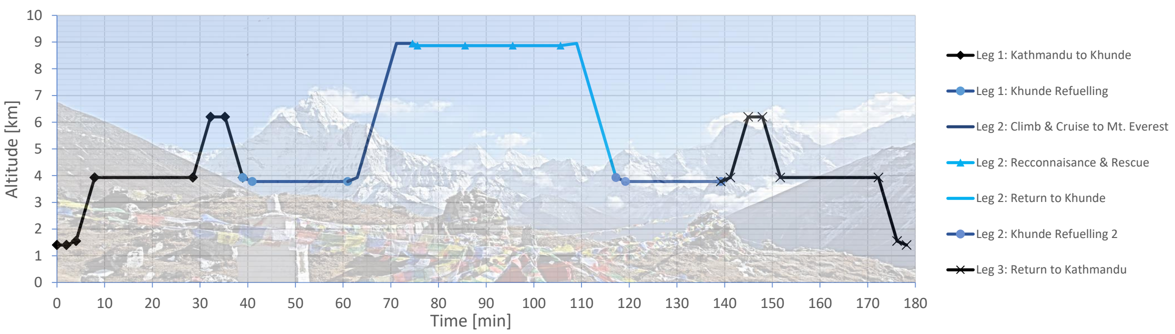

Figure 1: *Mission profile: altitude & fuel weight over design mission time*

Concept Development The HAMRAC was the winning configuration after an elaborated trade-off was performed. In previous design phases, 64 different configurations have been analysed, after which the non-feasible options were eliminated. This narrowed the trade-off down to 4 feasible options: the conventional, tandem, intermeshing and coaxial configurations. At this stage, an analysis at more detailed level had to be performed, in order to ensure the trade-off would result in the best option as the winner. Different criteria have been determined, and a weight has been assigned to each criterion based on their relative importance. The coaxial configuration outperformed all the other configurations on almost every important technical criterion, such as hover and cruise performance, structural efficiency and stability & control characteristics. In order to verify the trade-off results, several sensitivity tests have been performed, resulting in the coaxial still being the best configuration.

Figure 2: *The HAMRAC conducting a hoisting operation in the Himalayas*

Design Overview The HAMRAC is an extreme altitude mountain rescue helicopter that makes use of a coaxial rotor configuration to achieve altitudes that exceed the abilities of all current mountain rescue aircraft. This allows it to perform high-altitude missions significantly faster than current rescue options with improved safety for both rescuees and personnel, without the need for an on-foot expedition. The use of two engines means that this helicopter is still safe to operate with one engine inoperative, reducing the risk of accidents during operation. This also allows for the use of the aircraft in urban areas, and as such it is in accordance with Category A rotorcraft requirements. This makes the HAMRAC adaptable for a wide range of purposes outside of mountain rescue.

Performance Overview The HAMRAC is equipped to perform rescue missions both at high altitude and, with some adaptions, at sea level. This dual use is aided by a stationary transmission change that allows for a different rotor speed when flying at low altitudes. This means that missions can in principle be performed at any altitude up to 8950m, without compromising on the rotor performance. In addition to this the HAMRAC will be controllable in any foreseeable flight condition. This allows for rescues to take place in conditions in which other rotorcraft would be grounded, allowing for rescues to be performed within six hours of a distress call.

Table 1: *Main characteristics of the HAMRAC*

Characteristic	Value
Pilots	2
Rescue crew	2
Rescuee capacity	2
Empty weight [kg]	1347.5
Max. take-off weight [kg]	2095.5
Max. rate of climb [m/s]	10.16
Range [km]	318
Cruise speed [m/s]	77.2
Powerplant	2 x T800-LHT-800 (774 kW)
Service ceiling [m]	8950

Table 2: *Main geometric properties of the HAMRAC*

Dimension	Value [m]
Length	12
Width	2.1
Height	3.7
Rotor radius	5.5
Rotor spacing	0.45

Rotor Design The coaxial configuration removes the need for a tail-rotor, allowing the HAMRAC to transfer all its engine power directly into providing thrust, leading to an increase in efficiency in comparison to standard rotorcraft. The use of a coaxial rotor also leads to improved hovering and cruise capabilities, when compared to other helicopters in its class. The elimination of the dissymmetry of lift from the coaxial rotor means that it can reach rescue sites faster than any of the competition, at any altitude. The rotor itself is constructed from carbon fibre to reduce weight and employs multiple Boeing Vertol airfoils, for increased rotor performance across a wide range of altitudes. The further inclusion of a fairing between the coaxial rotors decreases the drag on the rotor improving the cruise efficiency of the vehicle.

Rotor Hub One of the main design disadvantages of most coaxial helicopters is their complicated rotor hub, which leads to a significant drag increase during cruise and heavy hydraulic systems. The HAMRAC solves this problem by using servo-flaps in combination with a gimbal instead of a second swashplate in order to control the rotorcraft. This design feature leads to reduced weight of the control system, reduced maintainability and a reduction in parasitic drag. Furthermore, a hingeless and bearingless rotor system was integrated in the design, which results in a decreased number of parts in the rotor hub and allows for the use of carbon fibre materials. This further reduces the weight of the rotor hub. Finally, a rotor hub fairing reduces the drag resulting from it even more.

Cabin Design The cabin of the HAMRAC is specialised for use within rescue operations. A rear loading door allows for the easy loading of rescuees during a mission. Specialised avionics ensure that the HAMRAC is able to locate rescuees during adverse conditions and during night operations. On board medical supplies and oxygen supply ensures that rescuees can receive immediate medical attention once on board. This makes it an ideal supplement to fleets, for a range of emergency services. Additionally, Aluminium construction ensures a lightweight cabin, that can resist CSA specified landing loads and ensures that 90% of the materials used within the construction of the HAMRAC are recyclable.

Cost Financially the HAMRAC performs similarly to rival aircraft, with an estimated hourly operational cost of 1100$in comparison to the Airbus H135 (1144$). An estimated development cost of 83.7 million EUR and a unit production cost of 1.9 million EUR, lead to a sale price per HAMRAC of 3.5 million EUR. The expected return on this project is explained below.

Return on Investment Several markets were identified in which the HAMRAC has a strong competitive position resulting from the design and performance features that were mentioned in the previous paragraphs. Next to the extreme altitude rescue market for which the HAMRAC is primarily designed, the search and rescue market at lower altitudes and sea level presents promising opportunities resulting from the high cruise speed of the HAMRAC and its ability to withstand harsh weather conditions. Other opportunities are present in the offshore and emergency medical service industry. A careful analysis on these markets, their size, growth prospects and the relevant performance of the HAMRAC compared to existing vehicles resulted in an estimation of the number of HAMRACs that could be expected to be sold during the first ten years of the operational phase of the program. According to this analysis, around 95 HAMRACs could be sold in the period 2022 to 2032. With a target price of 3.5 million EUR, this would lead to a return of investment of 26% after the first 14 years (including the development phases) of the program.

Design Conclusions Following the analysis, verification and validation of the work conducted in this report several conclusions can be made. The first is that the HAMRAC aircraft is for the most part a feasible concept vehicle and in addition to meeting the initial mission requirements, the HAMRAC is suitable for operation within a variety of roles and operational theatres. This ensures the opportunity of expansion within many aircraft markets. In addition to the many market opportunities, the HAMRAC is able to perform competitively against current rotorcraft of a comparable price within these markets. This makes the HAMRAC concept stand out when compared to competitive rotorcraft.

Following these conclusions several recommendations for further design analysis have been made, to improve the sophistication of the design concept. These are that a further investigation should be made into the composite blade design, making use of a more sophisticated analysis software. If the blades still fail to meet structural requirements a re-design of the blades should be completed allowing for an increase in blade thickness. In addition, the use of more sophisticated CFD software and a full stability model would provide a clearer insight on the aerodynamic performance and characteristics of the HAMRAC. Completion of these further analyses should confirm the feasibility and provide a more accurate approximation of the capabilities of the HAMRAC. According to the current schedule and assuming further investment, after additional design, testing and obtaining certification the HAMRAC program will enter its manufacturing phase at the start of 2022 and will be fully operational in the second half of 2022.

1 Introduction

With the popularity of mountain climbing increasing every year, the increase in mountain tourism also results in a growing number of people involved in accidents at high altitudes. Rescues at this altitude are extremely difficult, dangerous and take a long time to perform. Current helicopters are not designed to operate at such an extreme altitude. The majority of helicopters are designed to fly at sea level or slightly above. This leads to an opportunity for a new design that not only reaches the summit of Mount Everest at 8848m, but also performs a rescue mission at this altitude.

The goal of this design exercise was to develop a preliminary design of a high altitude mountain rescue aircraft that is able to perform its mission at the summit of Mount Everest, HAMRAC for short. This presented a set of engineering challenges which must be overcome. Firstly, the air becomes increasingly thin with altitude, which affects both the aerodynamic characteristics and engine performance. Secondly, performing the entire mission including two refuelling stops, within three hours. These are just some of the obstacles that had to be overcome by the design. Further design requirements are presented by the customer and derived during the design process.

To lead this project to a successful outcome, a project definition was produced which included a project organisation that introduced the role of each team member. To get a sense of the market and the profitability of this aircraft type, an extensive market research has been conducted. Furthermore, a SWOT analysis has been made to determine the potential opportunities for the HAMRAC, in the current market. Next the resource budgets were set in order to have a clear guideline throughout the process of designing the HAMRAC. This was followed by a trade-off which determined what top level configuration was best for this mission. This led to the detailed design phase of the HAMRAC, each department creating innovative solutions for the set requirements. In this section of the report the design choices are made and substantiated, and key performance values for the HAMRAC are identified. Next the choices that were made have been verified and validated in order to ensure the correctness. This was then followed by a departmental sensitivity analysis which established the degree of feasibility of the design. Then a cost breakdown and resource allocation has been made for the phase after the detailed design. Furthermore, the system characteristics of the HAMRAC were described which included the sustainability development strategy that has been implemented in the design. Following with the further development of the HAMRAC, this chapter investigates and plans all the phases including the ones after the detailed design. Finally, the conclusion is presented and recommendations following the design analysis have been elaborated on.

2
Project Definition

2.1 Mission Objective

The number of people attempting to climb the Himalayas has been increasing in the past few years[1]. More people are performing this highly difficult mission without the necessary training and experience, therefore there has been an increase in casualties and incidents in the Himalayas where the peak altitude is at 8,848 meters. Rescue missions at high altitude commonly use helicopters for their capability of vertical flight and for being able to land or hover at normally inaccessible locations. However, helicopter performance at high altitudes is typically marginal. The altitude record for helicopter landing to date stands at 8,848 meters altitude. However, this landing was part of a record attempt, not a routine flight. Rescue missions at these altitudes cannot wait for optimal conditions and need sufficient margin of performance and safety to be feasible also under adverse conditions. This left an opportunity for a rescue vehicle. The mission objective can be described with a mission need statement which leads to a project objective statement. These are given in this section.

Mission Need Statement

Considering the increase in casualties in the Himalayas and the lack of rescue vehicles that can reach the peak altitude of the Himalayas, the following mission need statement has been identified:

Mountaineers must have the possibility to be rescued at extreme altitudes.

Project Objective Statement

In order to address the mission need statement in greater detail and to take into account the project characteristics, the project objective statement has been established as well, which can be found below:

Design an air vehicle that is able to perform rescue missions at 8870 meter altitude at a purchase price that should not exceed 3.5 million EUR, with a group of 11 students during a period of 10 weeks.

2.2 Project Organisation

During the project, the individual team members tried to adhere to a clear organisational structure as much as possible, in order to work in a structured and efficient way. However, the group focused on flexibility towards deadlines and as it became clearer during the project which task would have a higher workload. As a result of this, the organogram went through some changes, as one would expect considering that the first versions were made in the first two days of the project. Figure 2.1 shows the final iteration of the organogram.

[1] URL `https://haexpeditions.com/wp-content/uploads/2018/09/Attempts-and-Summits-of-Mount-Everest-by-Year.pdf` [cited 14 November 2018]

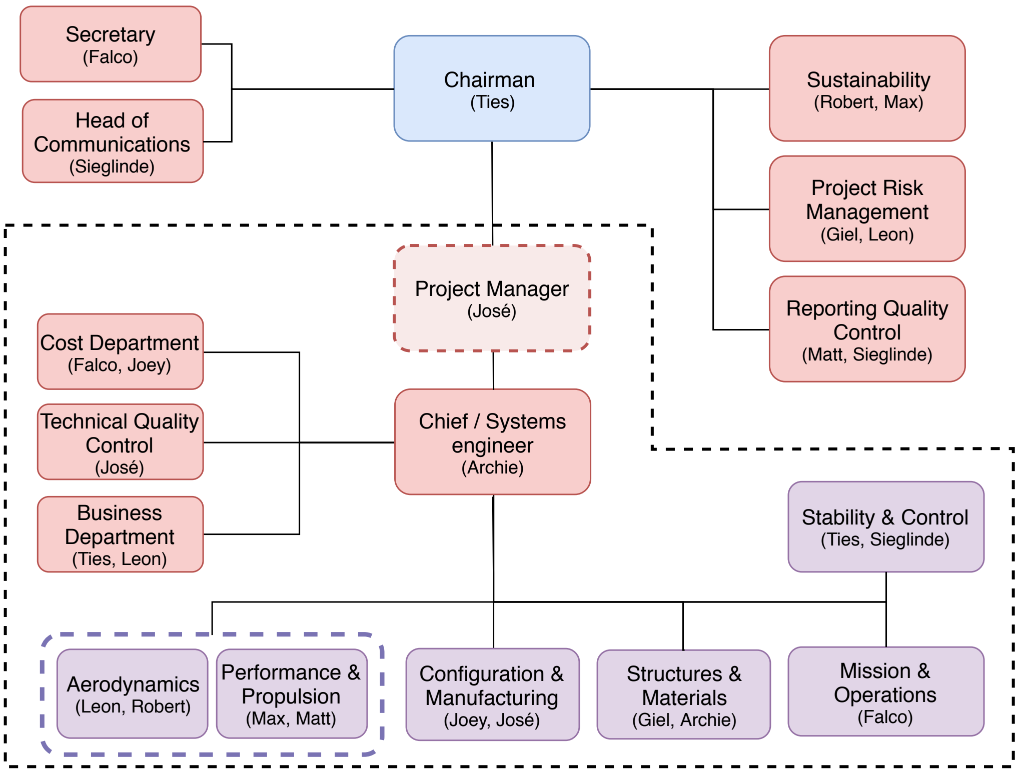

Figure 2.1: *Organisational structure. Red indicates management tasks, purple technical tasks, and blue the project leader. Elements within the dashed lines indicate a technical focus.*

Apart from reallocation of human resources to different organisational roles during the project, there were two main changes made to organisational structure. To begin with, it was found that the Aerodynamics and the Performance and Propulsion departments strongly interacted and had much overlap. It was therefore decided that those two departments would be merged into one large department with four team members working in it and renamed the 'Perfaero' department. This allowed for a more efficient design process with additional meeting within this department. Furthermore, the responsibilities could be more clearly assigned.

Another addition was to include a project manager. The chairman held this role up to the conceptual trade-off. This worked generally well, but taking into account the personal development goals of team members, this new role was created. The project manager focused on technical and non-technical tasks distribution and monitoring. There was some overlap between part of the project manager's functions and the Chief engineer as well. The implementation of SCRUM's where weekly sprints were done by the team, proved successful in achieving internal weekly goals.

2.3 Method & Approach

Before the project's inception, the approach for designing such an innovative vehicle was developed. With the design of the HAMRAC consisting on a large number of comprehensive subsystem analyses, the approach to the design was crucial for its success.

Based on the group's understanding and external advice, we refrained from developing a stability & control numerical model. Instead, the decision was made to focus on a rotor blade performance model, and on structural models. Since this mission is quite demanding, a lot of emphasis was put into mission profile and operations. Furthermore, sustainability was a big influence on the design of the HAMRAC. Every departmental subsystem design choice that has been made was approved by the sustainability managers. This meant that all the design choice that were introduced were sustainable to the furthest extent.

2.4 Functional Breakdown

The functional break down diagrams are shown in Figure 2.2 and Figure 2.3.

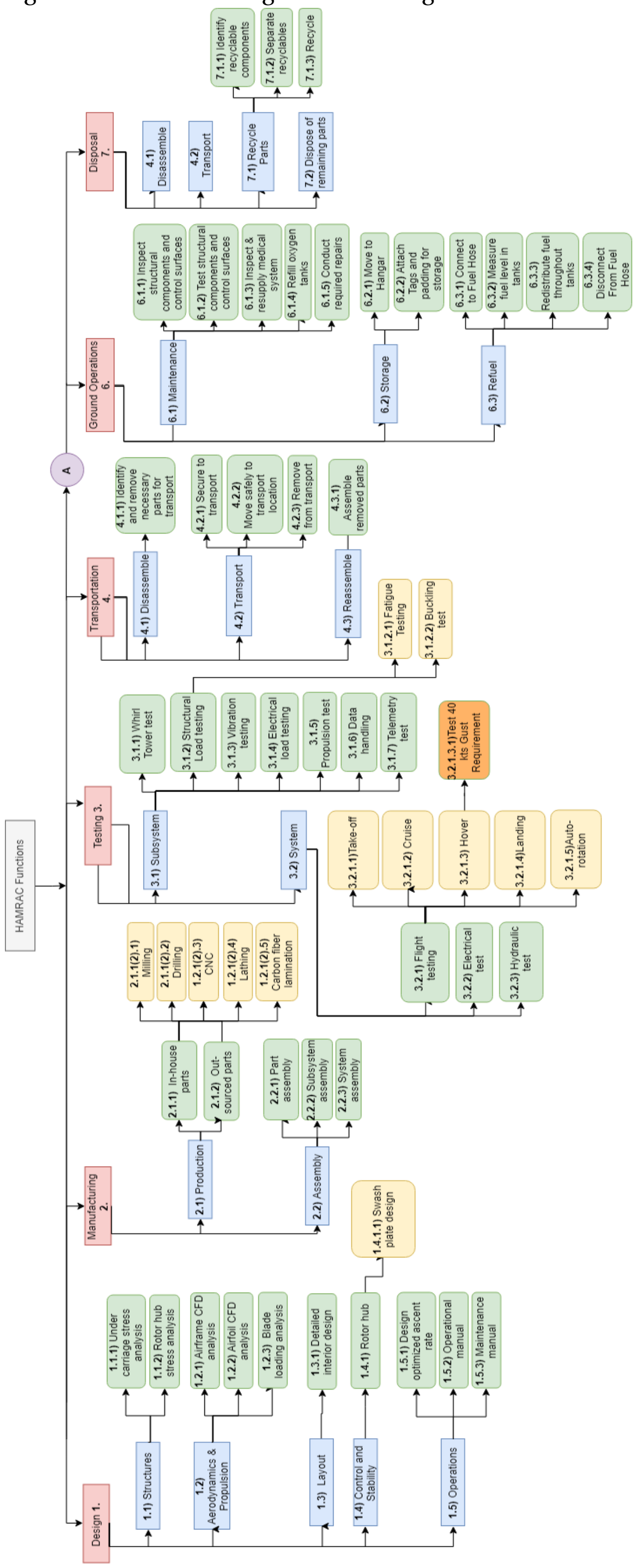

Figure 2.2: *The functional breakdown diagram for the HAMRAC project*

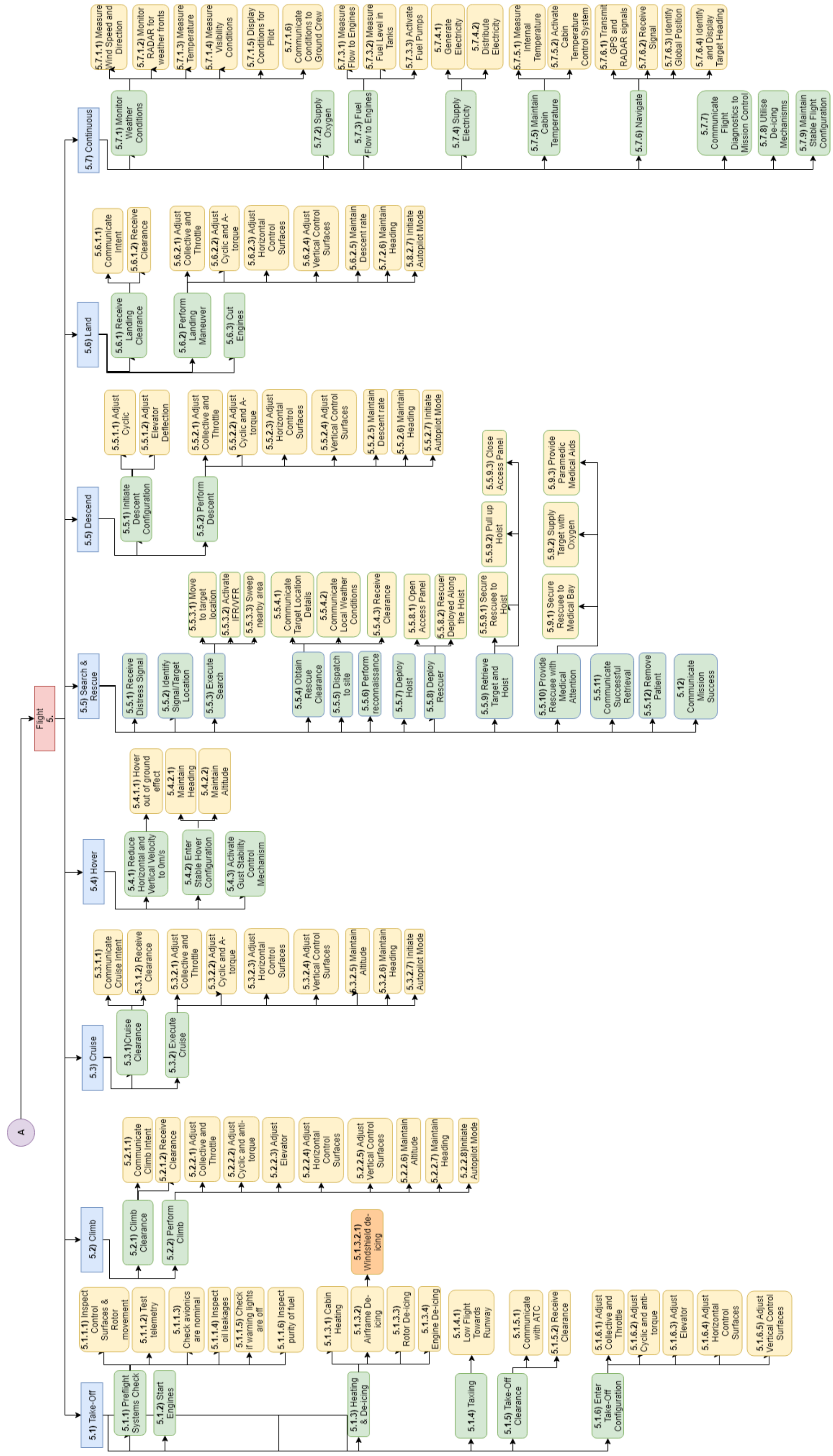

Figure 2.3: *The flight functional breakdown diagram for the HAMRAC project*

2.5 Functional Analysis

The functional flow diagram is shown in Figure 2.4

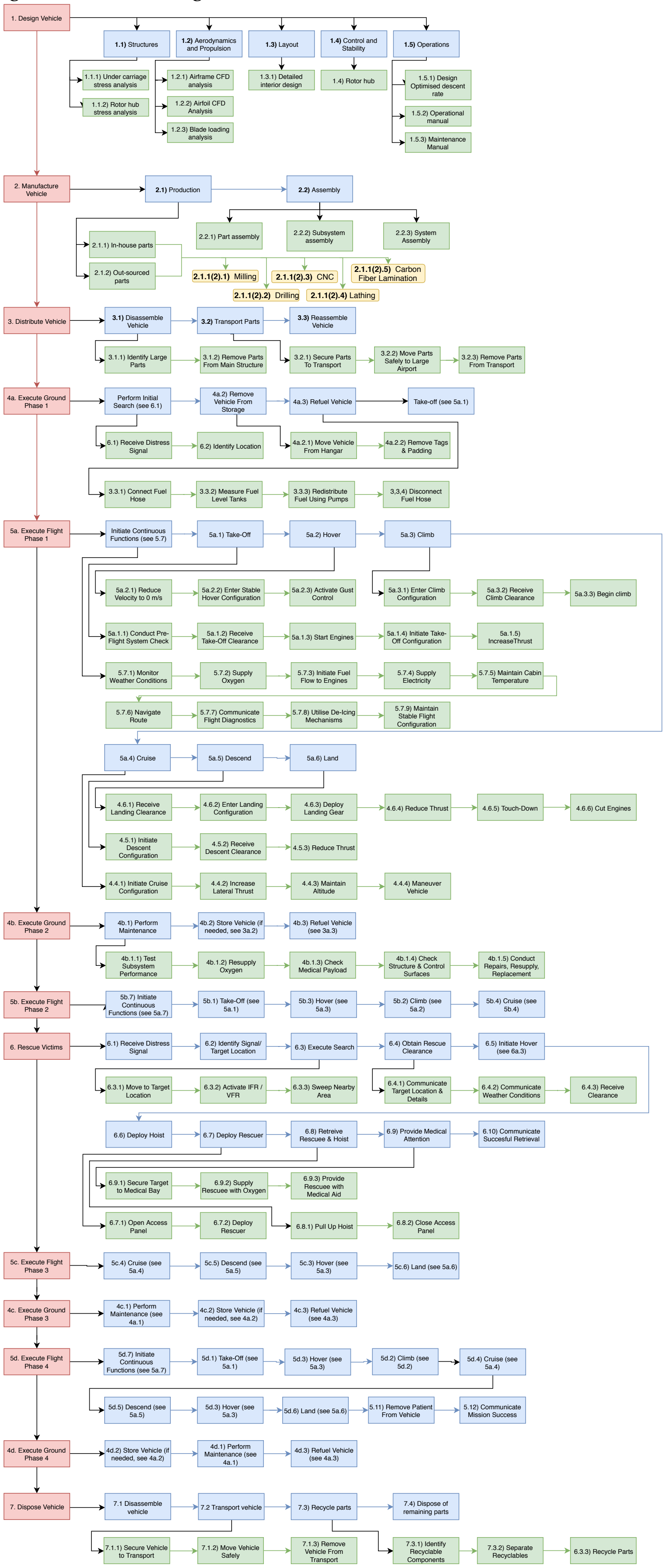

Figure 2.4: *The functional flow diagram for the HAMRAC project*

3

Market Analysis

In order to get a sense of the market opportunity and to understand how the design would perform in relation to the current available helicopters, a market analysis is conducted. At first, the HAMRAC was evaluated as a sinle-purpose vehicle for the primary market. After investigating multiple potential markets, they treated the HAMRAC as a multipurpose vehicle. As such, it has the potential to outperform its competitors in several markets. First, the entire helicopter market needs to be examined, which is done in section 3.1. Next, the primary high altitude mountain rescue market is defined in section 3.2. In section 3.3 the other potential markets are discussed which is followed by a forecast of the sales in section 3.4. This chapter is concluded by a SWOT analysis of the HAMRAC, which is given in section 3.5.

3.1 Helicopter Market

In order to gain a better understanding of the potential markets for the HAMRAC, one should have a general understanding of the global helicopter market. At the moment there are five 'large' private companies producing helicopters, which can be found in Table 3.1, which outlines the market shares within the civil and para-public helicopter sector[1].

Table 3.1: *Helicopter manufacturer market breakdown in the civil (and para-public) sector*

Manufacturer	**Market share [%]**	**Annual Deliveries**
Airbus	50	409
Bell	18	147
Leonardo	17	139
Russian Helicopters	11	90
Other	3	25
Sikorsky	1	8

Next to the deliveries in this table, many helicopters are delivered within the public and military sector. Sikorsky, for instance, only has a one percent market share of the civil and para-public helicopter market, according to Table 3.1, but it sold a total of 172 helicopters in the year 2017 [19]. The military market can therefore be considered to be significant and should not be neglected in this analysis.

3.2 Primary Market

In this section, the primary market for the HAMRAC is defined, its size is estimated, trends within it are identified and the market opportunity is quantified.

Definition The main market for the rescue vehicle, following from the user requirements, consists of all mountain ranges with peaks exceeding 6000m, as extreme altitude rescue operations can be performed at

[1] URL `https://www.airbus.com/helicopters/key-figures.html` [cited 21 November 2018]

these locations. Current rescue helicopters have the capability to perform rescues below this altitude. For this analysis, the focus is put on the Himalayan mountain range in Asia, which separates the plains of the Indian subcontinent from the Tibetan Plateau. The Himalayan mountain range consists of many of the Earth's highest peaks, including the highest, Mount Everest. The Himalayas include over fifty mountains exceeding 7200 m in elevation, including ten of the fourteen peaks that exceed 8000 m [2]. The peaks that exceed 8000 m above sea-level are the following: Mount Everest, K2, Kangchenjunga, Lhotse, Makalu, Cho Oyu, Dhaulagiri I, Manaslu, Nanga Parbat and Annapurna I. Next to these previously unreachable peaks, lower mountain ranges, like the Alps, might also benefit from the high performance of the HAMRAC, which is considered in section 3.3.

The reasons for not taking the other 6000+ m mountains around the world into account in this analysis are the high number of yearly ascends in the Himalayan area, the exceptional number of high-altitude mountains and the fact that travel insurers estimate the weekly number of rescue missions at about 80 during the climbing season[3]. To get an idea of the relative magnitude of this number, one could compare it with the number of helicopter evacuations that happen at the Kilimanjaro (the only mountain close to 6000 m on the African continent) every week: about one[4]. Furthermore, the highest mountain in the Alps and the Andes are respectively, only 4,810 and 6,961 m high. This means that the Himalayan Mountain Range dominantly represents the extreme altitude helicopter rescue market and justifies the decision to regard the Himalayan Mountain range itself as the primary market.

Currently, the only line of helicopters that is consistently used in this extreme altitude market, is the Eurocopter AS350 'Écureuil' helicopter line, also known as the Airbus Helicopters H125. Currently over 3,300 of these helicopters are used all around the world for different purposes, of which the AS350 B3 model is primarily used for high altitude missions and operations[5]. This helicopter holds exceptional records, such as performing the highest helicopter evacuation ever recorded at a staggering altitude of 7,010 m[6]. The price of a new H125 (or AS350B) ranges from 1.7 million EUR to 2.1 million EUR[7,8]. The operating cost of this helicopter are around 590 EUR per hour. This includes fuel cost, maintenance and scheduled parts replacement[9].

Size and Trends In order to establish the current (up to 6000m) market size of high-altitude mountain rescue missions in the Himalayan mountain range area, an estimate of the number of yearly rescue operations, based on the reported number of rescue missions per week, is combined with the average cost per rescue mission. Insurers report that these costs per rescue mission and medical check-up range from €9000 to €17,000. These numbers would result in a market size ranging from 10 million EUR to 19 million EUR per year in the Himalayan mountain range alone. This is assuming that 60% of the costs of the insurance claims follow from the helicopter evacuation[10], and that the climbing season lasts for around five months per year.

The number of people attempting to climb mountains in the Himalayan mountain range has been increasing strongly since around 1990, when this activity first started to become commercialised. This is illustrated by the number of successful attempts to summit the mount Everest, as visualised in Figure 3.1. In 2018, the record of the number of summits was broken again with a total of 715 successful summits[12]. Add to this the number of failed attempts, the number of sherpas on the mountain and the climbers attempting to summit other mountains in the Himalayas, that has been increasing at this pace as well. Following from this, it can be

[2] URL https://www.wikiwand.com/en/Himalayas [cited 21 November 2018]
[3] URL https://inews.co.uk/news/long-reads/everest-kathmandu-nepal%2Dhow-himalayan-treks-raise-millions-from-scam-helicopter-rescues/ [cited 21 November 2018]
[4] URL https://www.markhorrell.com/blog/2018/the-great-nepal-helicopter-rescue-fraud-an-introduction/ [cited 12 January 2019]
[5] URL http://www.aviationpros.com/press_release/10782913/american-eurocopter-celebrates-200th-american-made-as350-helicopter [cited 21 November 2018]
[6] URL http://aviationweek.com/business-aviation/world-s-highest-helicopter-rescue [cited 21 November 2018]
[7] URL https://www.avbuyer.com/articles/helicopter-comparison/bell-407-vs-airbus-h125-109789 [cited 21 November 2018]
[8] URL https://www.bjtonline.com/aircraft/airbus-helicopters-as350b3-2b1 [cited 21 November 2018]
[9] URL https://www.conklindd.com/CDALibrary/ACCostSummary.aspx [cited 21 November 2018]
[10] URL https://gearjunkie.com/nepal-government-helicopter-fake-rescue-insurance-scam-everest [cited 22 November 2018]
[11] URL https://www.statista.com/chart/1157/successful-mount-everest-ascents-per-year/ [cited 21 November 2018]
[12] URL https://gearjunkie.com/2018-everest-climbing-season-records [cited 21 November 2018]

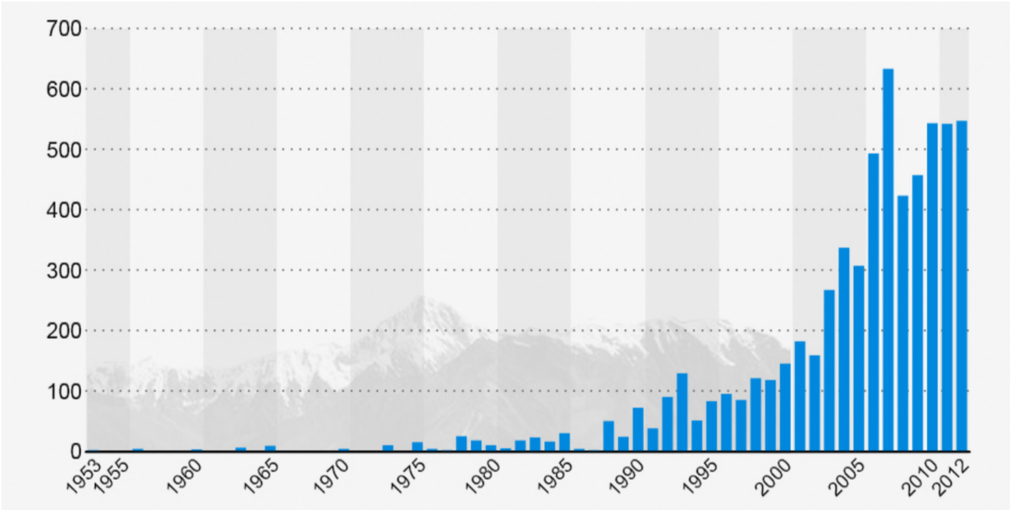

Figure 3.1: *Number of successful Mount Everest attempts from 1953 to 2012*[11]

expected that this increase in the number of people wanting to climb in this region strongly pushes the demand for helicopter rescue operations. It therefore results in a steady growth prospect in the upcoming years.

It is crucial to note that current helicopter evacuations can only be performed up to around 6000m. Especially considering that the occurrence of problems only increases the higher a climber gets, one could state there is a large potential market for high altitude rescue missions. This is illustrated by Figure 3.2, which shows that most of the deaths on the Mount Everest occurred at high altitudes (6000+m). It is not without reason that the region that surpasses the altitude of 8000m is known as "the death zone"[13]. This increase in the death rate is a direct consequence from the increase in the occurrence of high altitude sicknesses at that altitude.

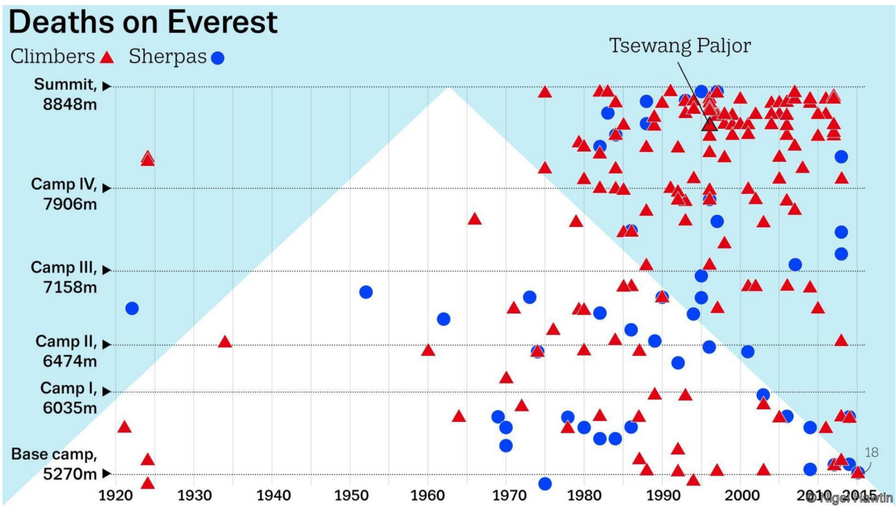

Figure 3.2: *Relation between deaths on the Mount Everest and the altitude at which they happened*[14]

Therefore, it can be concluded that the capability of the HAMRAC to perform rescue missions at the altitudes of the summits of the Himalaya's highest peaks could represent a significant increase in the size of the helicopter mountain rescue market in the Himalayas. In addition, rescue service providers (either private companies or public organisations) could ask significantly more money for these high altitude operations than

[13]URL `https://www.telegraph.co.uk/health%2Dfitness/body/life%2Din%2Dthe%2Ddeath%2Dzone%2Dwhats%2Dit%2Dlike%2Dto%2Dclimb%2Dabove%2D8000m/` [cited 21 November 2018]

[14]URL `https://www.statista.com/chart/1157/successful-mount-everest-ascents-per-year/` [cited 18 January 2019].

for lower altitude rescue operations, as there are currently no competing services. Therefore, it is estimated that this would lead to an additional market of around 5 to 10 million EUR on a yearly basis.

Market Opportunity Taking into account the existing market and new market at high altitudes that the HAMRAC would create, one could estimate a combined total market size of around 15 to 29 million EUR per year for helicopter mountain rescue missions in the Himalayas. The 5 to 10 million EUR new extreme altitude segment of this market could be obtained relatively easily by the HAMRAC, due to the fact that current helicopters can only reach altitudes of around 6000m under most weather conditions. This would, taking into account the 900,000 EUR average operation costs including depreciation established in section 12.3, justify the presence of around 12 to 30 rescue helicopters. Due to its excellent high altitude performance and extreme altitude capabilities, it could be expected that this would lead to the sale of about 10-20 HAMRACs in the first ten years of sales. These could be sold at the target price of 3.5 million EUR, considering the superb performance in comparison with its main competitor, the AS350, and the fact that the life cycle costs are predominantly determined by its operational costs. The fact that its operational costs are higher than for the AS350 is justified by both its increased flying performance in cruise and at altitude, and the fact that it is in size and rescue performance, for instance by having medical beds, rather comparable to the currently available H135 rescue helicopter that is used for rescues at lower altitudes. This helicopter has similar operational cost to the HAMRAC as will be discussed in section 12.3).

3.3 Potential Markets

Now that the current markets for the general helicopters and the market for typical high altitude mountain rescue vehicles are determined, additional markets are discussed in order to determine which could be applicable for the HAMRAC. These markets are not a part of the mission profile, which was leading in the design of the HAMRAC, but the eventual design led to the discovery that the HAMRAC could be used for other markets as well. These markets are the search & rescue market (SAR), the offshore helicopter transfer (OHT) market, emergency medical services (EMS) and finally the hot and high market (HH).

3.3.1 Search & Rescue

Definition Until recently, the search and rescue operations were mainly done by the air force, navy, interior ministry or other similar entities. The last few years, private operators are emerging in this market. This is closely related to the expanding of the oil & gas industry towards less reachable locations, and thus more expensive missions for the local governmental operator. Therefore, it is safe to conclude that this market is been driven by governmental operators and private companies.

Pricing At this moment the Eurocopter AS365 and Augusta Westland AW139 are the most used SAR-helicopters, having a sale price of 7.5 million EUR and 12 million EUR, respectively[15]. These aircrafts are heavier, bigger and more powerful helicopters, and can carry more payload.

Size & Trends There is a trend emerging where the government is outsourcing and/or working closely with the private operators. Various operators are competing for a five-year contract, to perform the rescue missions for a particular governmental organisation. A decade ago, two or three sales a year were made in this market, however aging fleets of the military and a growing demand from oil & gas companies results in a demand of at least ten specialist aircraft a year [16]

Market Opportunity Although this seems a highly applicable market for the HAMRAC, the stability for hovering at sea-level with more extreme weather conditions needs to be re-evaluated leading to a possible redesign for this purpose. The expectation is that the performance of the HAMRAC will be as required with minor changes in the design as is. Since the HAMRAC can perform well and is stable during forward motion at sea-level altitude, due to the coaxial configuration in combination with a variable rotational frequency, the HAMRAC will be applicable for this market, since a higher speed leads to a higher rescue success rate. Also, since the HAMRAC is designed for high altitude rescue missions, the lifting performance at sea-level conditions will exceed that of existing helicopters. This will make the HAMRAC a very good option for operators

[15] URL `https://en.wikipedia.org/wiki/Search_and_rescue` [cited 22 January 2019]
[16] `http://www.airbushelicopters.com/w1/jrotor/79/Strategy.html` [cited 22 January 2019]

performing search and rescue mission for all weather conditions. A rough estimate of sales would be average of one per year for the first five years, and two per year after the first five years to ten years. This results in a total of 15 HAMRACS sold after ten years. Since the prices of the current SAR-helicopters is above 7 million EUR, the HAMRAC will be a cheap solution for this market. The customer gets a lighter and smaller aircraft, able to perform SAR-missions for maximum of two rescues with the original configuration. It is possible to perform a small reconfiguration and re-determination of maximum payload at sea level, resulting in the possibility of rescuing more persons at once.

3.3.2 Offshore Helicopter Transfers

Definition With thousands of oil rigs all over the world at remote offshore locations helicopters are most favourable to be used in order to perform a successful transfer. The probability of access is 87% for a helicopter versus 51% for a vessel, which is mainly governed by weather conditions[17].

Pricing All sorts of helicopters are used for this purpose and prices are varying from 3 million EUR for a light-weight Augusta-Westland 119 Koala[18] to the heavier AW189, with a price of 15 million EUR[19]. The price ranges for this market was determined by the use of a brochure regarding the offshore market published by Leonardo, the manufacturer of Augusta-Westland, which is a solid estimate of the price range for this market[20]

Size & Trends The offshore market struggled with low utilisation from 2013 to 2016, due to over-ordering during the peak oil and gas years[21]. The market is slowly recovering, but a new submarket has arisen already: the offshore wind market. Light twin engine helicopters tends to be used for hoist operations, lowering crews onto the turbine from the air[17], which is the case for fast troubleshooting and scheduled servicing. In 2018 there were no more than 30 aircraft worldwide dedicated to providing wind power support[17]. This estimated market size of the offshore wind market will be at least 100 aircraft by 2021[17], of which a small portion will be the small, twin-engine helicopters.

Market Opportunity This seems a highly applicable market for the HAMRAC, but the stability for hovering at sea-level with more extreme weather conditions needs to be re-evaluated leading to a possible re-design for this purpose. However, the expectation is that the performance of the HAMRAC will be as required with minor changes in the design as is. Although it is very hard to make an estimation of the size of the complete offshore market, the offshore wind market seems to be a very good fit for the HAMRAC. The HAMRAC could perform the hoisting operations for scheduled service and fast troubleshooting at turbines fast and safe, since it was originally designed to withstand the extreme weather at high altitude and the increased cruise performance in comparison with conventional helicopters. This in combination with the back door hoist system, leads to a higher success rate and probability of access. With a market size of 100 within ten years of which a portion are medium-sized helicopters, 15 HAMRACs could be a safe estimation for the number of sales in that time-span. The sale price for the HAMRAC is 3.5 million EUR, which is more expensive than the cheapest helicopter of the Augusta brochure, but the HAMRAC has a higher cruise speed, is more powerful and has a lower maximum take-off weight.

3.3.3 Emergency Medical Services

Definition When an ambulance is not fast enough to a dedicated location, an ambulance could not transfer a person fast enough to the hospital or the location is simply not reachable for an ambulance, a helicopter is used instead. The helicopters that are mainly used for this purpose are the Airbus H125[22] and the Airbus H135[23], with a market share of more than 50%, according to Airbus[24]. Helicopters that are being used at ski resorts are part of this market and therefore present additional market opportunities for the HAMRAC.

[17] URL `https://www.rotorandwing.com/2018/02/27/winding-new-offshore-opportunities/` [cited 21 January 19]
[18] URL `https://en.wikipedia.org/wiki/AgustaWestland_AW119_Koala` [cited 22 January 2019]
[19] URL `https://www.bjtonline.com/aircraft/leonardo-helicopters-aw189` [cited 22 January 2019]
[20] URL `https://www.leonardocompany.com/documents/63265270/69072454/body_Catalogo_Prodotti_OilandGas_.pdf` [cited 22 January]
[21] URL `https://www.giiresearch.com/report/dw300118-world-offshore-oil-gas-helicopter-market-forecast.html` [cited 21 January 2019]
[22] URL `https://www.airbus.com/helicopters/civil-helicopters/light-single/h125.html` [cited 21 January 2019]
[23] URL `https://www.bjtonline.com/aircraft/airbus-helicopters-h135-t3` [cited 21 January 2019]
[24] `https://www.airbus.com/helicopters/civil-missions/ems.html` [cited 21 January 2019]

Pricing Since the two Airbus helicopters are more than 50% of the market, the sale price of these varies from 5.7 million EUR for a H135[25] to 2.5 million EUR for the H125[26]. It should be notified that the H125 has only one engine.

Size & Trends At this moment there are six EMS-helicopters being used in the Netherlands[27] and 89 in Germany[28], the rest of the helicopters used for EMS purposes in Europe can be seen in Figure 3.3.

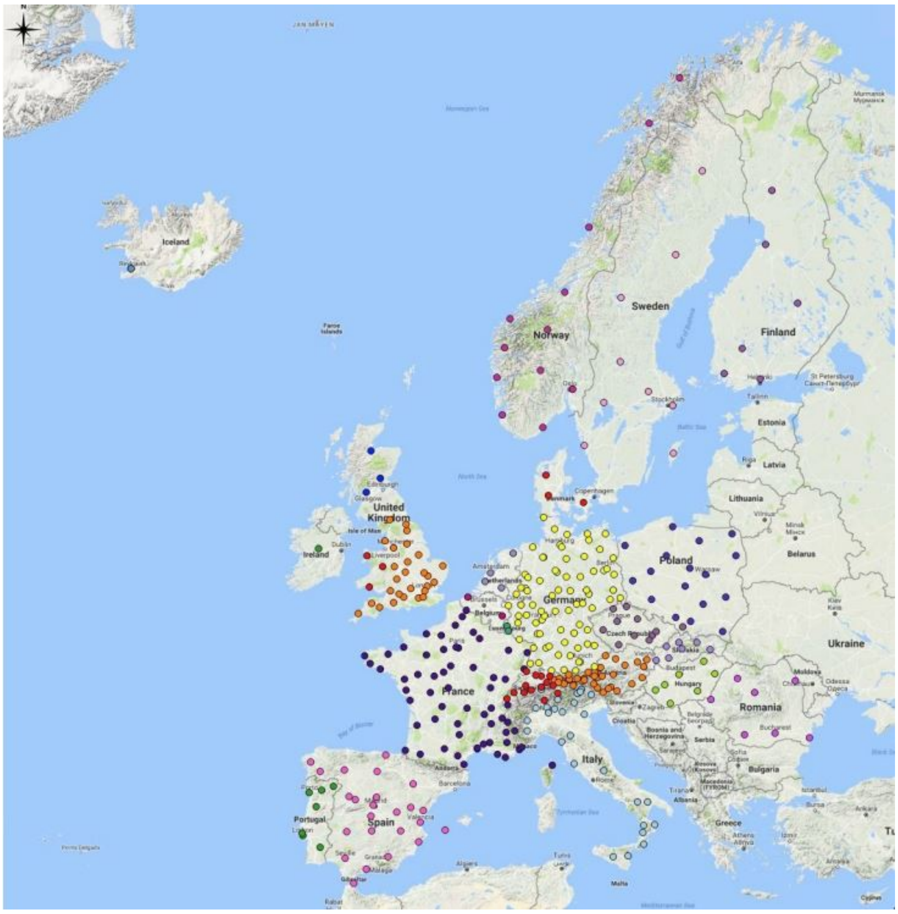

Figure 3.3: *Number of HEMS in Europe in 2017*[29]

The global EMS market is growing around 5% per year and at the moment it accounts for more than half of the helicopter market, which has a total value of 26.2 billion EUR in 2016[30]. Since there are no exact numbers on the number of helicopters in the market, but in Europe alone there are several hundred helicopters[30] and the US market has at least 370 helicopters right now in this market[30], one can conclude that this market is roughly 500 helicopters large in 2018. With a growth of 5% per year this can lead to 855 helicopters in 2032.

Market Opportunity since the global market is growing with 5% per year and the EMS market accounts for half of the helicopter market, there is a very good opportunity to penetrate this market. However, the US market is hard to penetrate, since laws in the more developed countries are very strict regarding foreign entities

[25] https://www.bjtonline.com/aircraft/airbus-helicopters-h135-p3 [cited 21 January 2019]
[26] https://www.bjtonline.com/aircraft/airbus-helicopters-h125 [cited 21 January 2019]
[27] URL https://www.umcg.nl/NL/UMCG/Afdelingen/mobiel_medisch_team_MMT/informatie_voor_kinderen/Helikopter_hoeveel_traumahelikopters_zijn_er_in_Nederland/Paginas/default.aspx [cited 21 January 2019]
[28] URL https://www.reuters.com/article/us%2Dhealth%2Demergencies%2Dhelicopters%2Deurope/helicopter%2Demergency%2Dmedical%2Dservices%2Duneven%2Dacross%2Deurope%2DidUSKCN1NH2GL [cited 21 January 2019]
[29] URL https://epostersonline.com/asgbi2017/node/1302?view=true [cited 21 January 2019]
[30] URL http://digitaledition.rotorandwing.com/october-november-2018/evolving-helicopter-ems/ [cited 18 January 2019]

entering this market[31]. A good opportunity is penetrating markets in countries that are relatively new to the EMS market and have a high need for air medical services, such as India[31]. The market in Europe is fairly stable and mature and Asia-Pacific can be considered an upcoming growth market[31]. With several hundred helicopters in this market and the upcoming markets in India and Asia-pacific, it would be a good strategy to focus the most on the upcoming market, and focus on the matured markets, which needs to replace their fleet as well. A rough estimate would be 50 helicopters within ten years, which would mean a market share of around 6% in about ten years. In order to do this, the noise of the HAMRAC should be re-evaluated, which might lead to a re-design of the tip of the rotor blades, since these produces the most noise for a coaxial helicopter. The stability for hovering at sea-level also needs to be re-evaluated leading to a possible re-design for this purpose. The expectation is that the performance of the HAMRAC will be as required with minor changes in the design as is. The sale price of the HAMRAC is 3.5 million EUR which is lower than the H135 and higher than the H125. The HAMRAC is more functional compared to the H125, with a higher cruise speed, a higher maximum take-off weight is more powerful and have a higher maximum hover altitude. The HAMRAC can carry less passengers than the H135, but is more powerful, have a higher cruise speed, have a higher hover altitude and a lower maximum take-off weight. The price of the HAMRAC is in between both of the Airbuses, with better performances compared to the H125 and being a good competitor for the H135's outstanding track-record for EMS purposes.

3.3.4 Hot & High

Definition A significant problem for current helicopters are so-called "hot and high operations". In these situations, both engine power and lift decrease due to the high temperature or the increase in altitude. If the rotorcraft, in addition is flying at a high altitude, the additional decrease in density can result in the inability to generate enough lift to control the aircraft[32]. This combination of environmental factors generally leads to bad operational performance of the rotorcraft. To get an idea to which extent this problem is actually relevant, one could consider the fact that the US (and Canadian) military actually leased Russian Mi-17 helicopters in order to be able to fly in high areas in Afghanistan, as the performance of their own Blackhawks was insufficient[33,34]. This fact is seen as politically controversial, and shows to what extent "hot and high" flight conditions can cause problems to aircraft.

Pricing The pricing for this market varies too much to state in one number, since this market is very broad, with many segments having different competitive rotorcraft prices.

Size & Trends The size of the hot and high market is relatively difficult to define, as it is a very broad market, as a large variety of helicopter operations encounter these flight circumstances. Examples could range from attack helicopters being employed in Afghanistan, to troop transport and firefighting in California. The strategy that could be used to penetrate this market is to perform a proper market segmentation and assess for which purposes the HAMRAC could perform at a level that could be competitive to currently used models. A segment that could be looked into is for instance the lightweight military rotorcraft segment. The US Army recently ordered 150 new of these rotorcraft in 2017[35], but there are many complaints about the fact that this helicopter has insufficient performance in the hot and high environment in Afghanistan, where they are going to be used. Another market that could be interesting to analyse in a further stage could be the firefighting market. This market has been growing rapidly over the last decades, probably due to climate change[36]. The fires result in extremely hot, low density air. This has a detrimental effect on the performance of most helicopters. California Firefighting (Cal Fire) has expressed the wish to buy around 12 helicopters in the upcoming years for a price of around 12 million USD each[37]. In addition, this market led to around 74

[31] URL `http://digitaledition.rotorandwing.com/october-november-2018/evolving-helicopter-ems/` [cited 18 January 2019]

[32] URL `https://www.skybrary.aero/index.php/Hot_and_High_Operations` [cited 18 January 2019]

[33] URL `https://sputniknews.com/military/201806161065458559%2DPentagon%2DAdmits%2DRussian%2DMi%2D17%2DOften%2DSuperior%2DBlack%2DHawks/` [cited 18 January 2019]

[34] URL `https://www.militaryaerospace.com/articles/2013/06/mi17-helicopter-buy.html` [cited 18 January 2018]

[35] URL `http://www.thedrive.com/the-war-zone/14159/afghanistan-is-getting-more-ill-suited-attack-choppers-it-may-not-even-be-able-to-fly` [cited 18 January 2019]

[36] URL `https://www.scpr.org/news/2016/08/19/63757/why-fighting-california-s-wildfires--more-than/` [cited 21 January 2019]

[37] URL `https://www.sacbee.com/news/politics-government/the-state-worker/article207343214.html` [cited 21 January 2019]

million USD in sales for the K-max, a helicopter with similar 'hot and high' and high altitude performance as the HAMRAC, to the U.S. Forest Service[38].

Market Opportunity At this point, it is difficult to assess the number of HAMRACs that can possibly be sold in the hot and high market. It is, however, an extremely relevant market as its conditions are similar to high altitude conditions for which the HAMRAC is specifically designed: low density combined with low engine performance. By designing some alternative versions, for instance for firefighting instead of high altitude rescue, the HAMRAC could possibly perform really well in these situations. The helicopters Cal Fire currently uses (the Vietnam era Bell UH-1 "Huey") for firefighting are in size and lifting capacity comparable to the HAMRAC. This market is for now not taken into account for calculating the break-even point and short term profitability, but should be taken into account when assessing the long-term profitability of the HAMRAC program.

3.4 Forecast Sales 2022-2032

For the forecast of the sales it is assumed that sales can start after two years of engineering, testing and producing, as was described in chapter 14. To give an estimate regarding the total potential sales over a time span of ten years is highly inaccurate, since it is very hard to predict future changes in for instance, regulations and other competitors. Furthermore, it is necessary to say that some of the markets can only be considered after doing some possible re-design of the original HAMRAC, which is designed for the high altitude performance. These re-design phases can be done after some first sales has been done and the HAMRAC is getting more and more exposure due to the possible unique performances at high altitude. This would require a more advanced business strategy and product development strategy. If these factors are planned correctly, a rough estimate of the possible sales can be found in Table 3.2, leading to a total sales of 140:

Table 3.2: *HAMRAC sales forecast 2022-2032*

Market	**Sales**	**Complications**
HAMR	15	-
SAR	15	Hovering Stability
OHT	15	Hovering Stability
EMS	50	Hovering Stability/Noise
HH	0	-
Total	**95**	

Since the primary market is really specific and therefore the smallest market, one can conclude that the whole program of the HAMRAC would not be profitable with a minimum sale price of 3.5 million EUR. This means the other, bigger markets can be entered with minor changes in design, leading to a profitable program, as will be described in section 12.5.

[38]URL `http://www.businessair.com/aircraft-press-releases/firefighting-market-strong-k-max-helicopters` [cited 21 January 2019]

3.5 SWOT Analysis

The SWOT-analysis is a widely used tool for determining the competitive position of the product in the existing and potential markets. It includes internal strengths, internal weaknesses, external threats and finally external opportunities. The SWOT-analysis can be found in Figure 3.4.

	Helpful to achieving the objective	**Harmful** to achieving the objective
Internal Origin	**Strengths:** • The HAMRAC is operational throughout a large altitude spectrum, ranging from sea-level to extremely high altitudes due to its variable rotor speed. • The HAMRAC can reach relatively high cruise speeds with high stability due to its coaxial configuration (no dissymmetry of lift). • Due to its back door hoisting operations, it is capable of rescuing patients with a large range of complicated injuries and problem (including complicated fractures, etc.) • Reduced rotor hub drag through fairing and servo-flap mechanism. • The HAMRAC has a high hover efficiency due to its coaxial configuration.	**Weaknesses**: • The HAMRAC development team currently does not have a strong reputation and existing sales channels in the helicopter industry. • The development team has limited financial and human resources at the moment and will have to attract serious investors. • The HAMRAC has relatively high maintenance costs due to the relatively complex design(coaxial configuration). • Operations are complicated due to the requirement to change rotational frequency manually. • Due to its coaxial configurations, noise performance might be worse than some competitors.
External Origin	**Opportunities**: • There is a clear need for high altitude helicopter rescue, while no current solutions exist. • Hot and high flight circumstances are very similar to high altitude circumstances. • The offshore market is expected to see an increase in demand of fast and light helicopters with excellent hover performance (under extreme weather), due to strong growth in the wind energy market • The Helicopter Emergency Medical Service (HEMS) market can be considered half of the global helicopter market and has an expected growth of 5% per year. Especially, India and Asia-Pacific have a high demand of new HEMS helicopters. • The Search and Rescue (SAR) market, previously dominated by governmental agencies,is privatising at the moment, pushing the demand for fast SAR capable helicopters.	**Threats**: • Changes in FAA or EASA regulations could cause problems for the HAMRAC wrt. obtaining certification. • Certain competitors in the helicopter market have a lot of knowledge, development experience and financial resources. • Other aircraft manufacturers could develop a cheaper or better performing product, or update an existing product (fi. the AS350) is to have higher performance • An Army could identify the need for similar vehicles and comes up with a development program itself in order to preserve technology.

Figure 3.4: *The SWOT analysis performed for the HAMRAC*

4

Resource Allocation

In this chapter, the preliminary mass and power budgets are presented with their respective method of calculation. These budgets have been determined to set a guideline for mass and power throughout the entire project. Section 4.2 elaborates on the mass budget of the HAMRAC with section 4.1 elaborating on the power budget.

4.1 Mass Budget

The approach taken for the mass budget calculation is threefold. The use of statistics is employed to determined subsystem and component masses. Statistics have not been used to determine subsystem or component masses that have been selected already at this point in the design. For their particular subsystems or components, the statistical outputs have nevertheless been used to verify the statistical method and their masses have been included in the mass budget for completion. A contingency margin of 15% has been introduced, for the systems that have not frozen their mass estimation yet.

For the statistical mass estimation, the society of aeronautical weight engineers [56] concatenation of statistical weight estimation equations has been used. A few assumptions were used, for the selection of the appropriate equations:

- The rotor group weight estimation equation is generic in the sense that it applies to all type of rotorcraft. The co-axial design factor has been taken into consideration by using six blades and the respective rotor radius, tip speed and chord length.
- For the body frame mass estimation, a single-rotor configuration is used instead of a tandem, since it is most similar structurally.
- For the landing gear, the skid type configuration is chosen.
- For flight control group mass, a turbine engine is assumed.
- For the engine mass a shaft turbine of over 1000 hp is assumed.

A few noteworthy mentions during the mass budget process are listed below:

- During the statistical weight estimation of air conditioning and anti-icing components, only the anti-icing of the windshield is accounted for. Therefore, the outcome for this statistical function is underestimating the true value since rotor, airframe and engine de-icing are also included in the HAMRAC. This underestimation is addressed for by adding a 30% margin to this weight prediction. 30% is chosen because it is believed to make the budget conservative.
- The weight of the furnishing equipment is likely to be very conservative. In reality the rotorcraft will only possess the essential furnishment for the mission objective. For this reason, its budget has been reduced by 30%.
- The hoist system mass is largely underestimated using statistics. However, it is assumed there is low correlation between the hoist weight estimation and the other weight estimations, so the statistical weight estimation in [56] is still relevant for the mass budget.

- The statistical mass estimation for the engine mass was found to be 99% of the already selected engine mass. This serves as a basic form of verification for the statistical weight estimation used.

The final mass budget values are presented below in Table 4.1.

Table 4.1: *Mass budgets for the HAMRAC*

Subsystem/Component	Mass [kg]
Rotor Group	255
Stabiliser Group	34
Airframe	201
Landing Gear	30
Control Subsystem	79
Engine	300
Powertrain	37
Instruments	25
Hydraulics	13
Electrical Subsystem	72
Furnishings	100
Air co. & Anti-icing	39
Hoist system	50
OEW	**1235**

4.2 Power Budget

The power budget for the HAMRAC is presented in this section. The most power consuming components are within the avionics subsystem, however they do not account for the majority of power consumed. The avionics subsystem includes components used for de-icing, life supports, lighting and communications as demonstrated in 7.1. Most power will be delivered to the engine and lost to transmissions. Presented below in Table 4.2 are the relevant subsystem power budgets and the total power budget.

Table 4.2: *Power budget for HAMRAC*

Subsystem	Power [kW]
Propulsion	800
Avionics	15
Hoist	2
Total	**817**

A few considerations are relevant for the power budget. In order to meet Class A category, it must be possible to operate with one engine inoperative. The battery must be one that allow for single engine failure and engine start-up. All subsystems must be operable during descent when less power is provided by the engine.

5
Trade-Off Summary

The HAMRAC project was initiated with a completely open view on how the design of the rescue vehicle for this mission should be approached. After a brainstorm and structured design option tree analysis, 64 unique conceptual designs that could potentially meet the design requirements were defined. This selection was narrowed to four feasible options; a conventional, coaxial, tandem or intermeshing rotorcraft.

An extensive trade-off was performed between these configurations, the method of which is presented in section 5.1. The results of the trade-off to arrive at the coaxial configuration for the HAMRAC are presented in section 5.2. A sensitivity analysis is performed in section 5.3 to evaluate the robustness of this result.

5.1 Method

The scoring per criterion of these configurations is executed as described by Table 5.1. Any design that was deemed to have 'unacceptable' performance for aspects of the mission was ruled out in the initial concept selection. The criteria on which to base the trade-off and corresponding weights to give them are based on helicopter-specific and statistical research. They are ranked based on the requirements of the helicopter and assigned weights using an Analytical Hierarchy Process, ensuring the relative importance of the criteria for the helicopter is taken into account [38]. These relative importances were established by listing which requirements would be most crucially influential in the mission's success or failure. The criteria and their relative weights are presented in Table 5.2. Designs that meet the 'technical' criteria of actually performing the high-altitude mission are given greater importance than non-technical criteria.

Table 5.1: *Scoring description for the HAMRAC configuration trade-off*

Score	Description	Colour
5	Excellent Performance	Cyan
4	Good Performance	Green
3	Satisfactory Performance	Yellow
2	Marginal performance	Orange
1	Poor Performance	Red

Table 5.2: *Trade-off criteria and corresponding weights*

Criterion	Weight [%]
Hover Performance	27.2
Cruise Performance	24.4
Structural Mass	14.0
Stability & Control	13.3
Cost	9.5
Reliability	6.9
Sustainability	4.7

5.2 Results

The driving factors for each of these criteria are summarised here. In high-altitude hover, the driving constraint on performance is the induced power that is required to hover and perform the rescue. This power required for hover at 8950m is checked for reference aircraft and adjusted with respect to MTOW. For cruise performance, aerodynamics are the limiting factor. All configurations can achieve sufficient forward speed to perform the mission within the required time span. The maximum speed obtainable is determined by how fast the advancing blade reaches Mach 1. The conventional helicopter experiences unfavourable retreating blade stall before this condition is met, therefore performing worst with respect to forward speed.

In analysing the structural mass per configuration, the configuration-dependent structural elements are reviewed. These are the airframe, the engine system, the rotor blades, control system and the driveline and transmission. Preliminary load calculations combined with statistical analysis offer information on the relative weights of these systems. A qualitative stability analysis is performed, highlighting the inherent (dis)-advantages of the different configurations. Despite increased complexity, it is found that the inherent torque cancellation and lack of lift dissymmetry in twin rotor configurations offers favourable stability and control characteristics.

Cost is evaluated by the unit cost and where possible takes into account development cost and maintenance, repair and operations (MRO) cost. Both are evaluated from statistics. As an abundance of data and expertise on the conventional rotorcraft is already built up, this design scores best cost-wise. Reliability of the different designs is investigated by comparing the complexity of their respective powertrains, the possibility of autorotation and the inherent risks stemming from mechanical interdependencies. It is concluded that more complex configurations always hold a greater reliability risk. The sustainability is evaluated with respect to pollution, noise and embodied energy. This last criterion comprises the energy that goes into development and operation of the rotorcraft: development testing, structural and component complexity, maintenance and facilities are considered.

The final trade-off table can be viewed in Table 5.3. The colour coding and scoring is executed as described above. It can be concluded that the coaxial configuration has the overall best performance. It outperforms the other configurations during both hover and cruise and is very structurally efficient. Due to its two counter-rotating rotor blades, the (cruise) flight envelope limiting effects of dissymmetry of lift cancel out, which allows for high cruise speeds. In addition, no tail rotor is required to obtain directional control and stability, which increases the structural efficiency. Furthermore, this has the advantage that the significant risk of Loss of Tail Rotor Effectiveness (LTE) at altitude is eliminated. Because the axis of rotation of both rotors coincides and this axis is close to the center of gravity, the moments induced by the rotor systems are minimal, adding to the structural efficiency. Finally, the induced power of a coaxial configuration is relatively low compared to other configurations due to its low disc-loading, resulting in improved hover efficiency.

Table 5.3: *Final trade-off table of the four concept rotorcraft configurations*

Criterion Weight	**Conventional**	**Coaxial**	**Tandem**	**Intermeshing**
Hover Performance 27.2%	[red] 1	[green] 4	[green] 4	[green] 4
Cruise Performance 24.4%	[orange] 2	[cyan] 5	[yellow] 3	[green] 4
Structures 14%	[orange] 2	[green] 4	[yellow] 3	[yellow] 3
Stability & Control 13.3%	[orange] 2	[green] 4	[green] 4	[yellow] 3
Cost 9.5%	[cyan] 5	[orange] 2	[yellow] 3	[green] 4
Reliability & Risk 6.9%	[green] 4	[yellow] 3	[yellow] 3	[yellow] 3
Sustainability 4.7%	[yellow] 3	[orange] 2	[orange] 2	[yellow] 3
Total	[orange] 2.20	[yellow] 3.89	[yellow] 3.60	[yellow] 3.61

5.3 Sensitivity Analysis

To verify whether the trade-off is performed correctly, a four-part sensitivity analysis is performed. Firstly, in Table 5.4 the full trade-off weight is divided only over the technical criteria, keeping its difference in relative importance constant. With this analysis it can be deduced whether the least weighted criteria have an impact on the outcome of the trade-off. Next, the weights of all criteria are set to be equal (each 14.3%) in Table 5.5 to determine the mutual influence of these criteria.

Finally, the subjectivity of the scoring is tested with two scenarios. The bias per departmental trade-off is investigated by introducing a change in score. In the first subjectivity scenario in Table 5.6, the 2's are changed to a 3 and vice versa. This subjective scoring might occur when project members are using different definitions of marginal and satisfactory. The second subjectivity analysis evaluates a scenario where the project members are biased in assigning extreme values, the 5 or 1. So, every 1 is changed to a 2, and every 5 is changed to a 4. This will result in a denser scoring. The result can be found in Table 5.7.

Table 5.4: *All the weight is divided over the technical part of the project*

	Conventional	**Coaxial**	**Tandem**	**Intermeshing**
Hover Performance 31.25	[red] 1	[green] 4	[green] 4	[green] 4
Cruise Performance 25	[orange] 2	[cyan] 5	[green] 4	[green] 4
Structures 25	[orange] 2	[green] 4	[yellow] 3	[yellow] 3
Stability & Control 18.75	[orange] 2	[green] 4	[green] 4	[yellow] 3
Total Score	[orange] 1.69	[green] 4.25	[green] 3.50	[green] 3.56

Table 5.5: *All the weight is equally divided over the criteria*

	Conventional	**Coaxial**	**Tandem**	**Intermeshing**
Total Score	[yellow] 2.71	[yellow] 3.43	[yellow] 3.14	[yellow] 3.43

Table 5.6: *Subjectiveness of marginal vs satisfactory scoring*

	Conventional	**Coaxial**	**Tandem**	**Intermeshing**
Total Score	[yellow] 2.67	[green] 3.96	[yellow] 2.86	[yellow] 3.22

Table 5.7: *Subjectiveness of extreme scoring*

	Conventional	**Coaxial**	**Tandem**	**Intermeshing**
Total Score	[orange] 2.47	[green] 3.65	[yellow] 3.36	[green] 3.61

On the technical criteria in Table 5.4, the coaxial design is the clear winner. When averaging all criteria in Table 5.5, the coaxial design still wins but by little margin; this suggests that it is not the best in the non-technical criteria. In the first subjectivity scenario, Table 5.6, the coaxial concept still wins the trade-off. This indicates that subjectivity of the group regarding the grade definition is not driving the outcome of the trade-off. In the second subjectivity scenario Table 5.7, the coaxial configuration wins the trade-off, although the intermeshing is a good runner-up. This indicates that recklessness in giving extreme scores is not driving for the outcome of the trade-off either. With the coaxial rotorcraft consistently scoring highest within the sensitivity analyses, it is concluded that the coaxial rotorcraft is robustly the best design option and that the trade-off was well-executed.

6

Operations & Logistics

In this chapter, the reference mission profile according to the Vertical Flight Society (VFS) competition is presented in section 6.1 [14]. An alternative mission and the range that the HAMRAC is capable of achieving is presented in section 6.2, after which the operational conditions and environmental challenges are shown in section 6.3. After this, operations and communications specific for the HAMRAC are displayed.

6.1 Reference Mission

The mission according the VFS requirements is used to determine the fuel weight and the time allocation. The reference mission is from the international airport of Kathmandu to the top of Mount Everest with a refuel stop at the heliport of a medical clinic in Khunde. The profile minimises flight time over the Gaurishankar Conservation Area by performing an early climb and cruising for some time at 6200m to pass the Tengi Ragi Tau mountain pass. The reference mission profile is the most demanding and therefore ensures the possibility of rescues at other mountains than the highest peak of the world, Mount Everest. The people on board include the pilot, two crew and the two rescuees picked up on the summit of Mt. Everest.

6.1.1 Mission Profile

Several mission profiles were analysed. After a study of the Himalayan topology, the profile was found. This mission profile complies with the requirements from the VFS competition [14]. Although the VFS requirements do not explicitly state an intermediate climb and descent are necessary, no real-life profile is possible without lengthening the distance significantly, more on this can be found in section 6.2. The reference mission profile was iterated numerous times with the Performance & Propulsion and Aerodynamics departments to motivate design choices. The mission profile is shown in Figure 6.1. Climbing phases and descending phases are planned to fly over all mountain ranges encountered with the clearances defined in section 6.3 with the shortest distance possible. The refuel stops at Khunde are deemed necessary to reduce fuel weight and to change the rotor RPM. The high and low reconnaissance (Recce) of the hover site are represented as one single Recce phase in this report. A more detailed description of each mission part can be found in subsection 6.1.3.

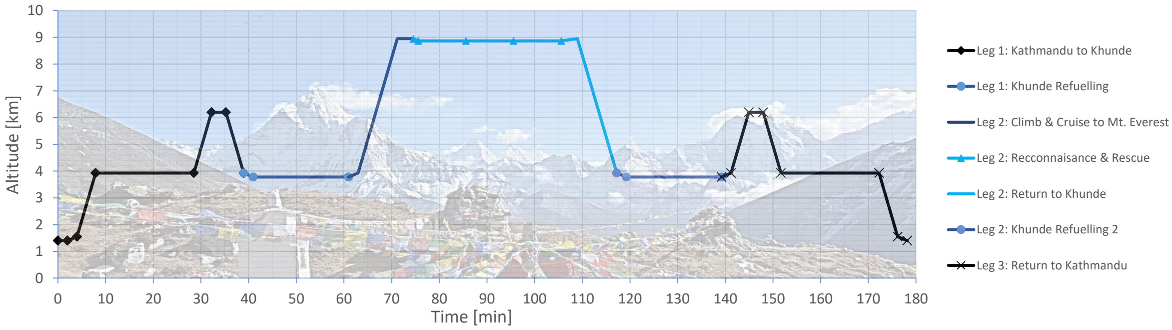

Figure 6.1: *Mission Profile: altitude & fuel weight over design mission time* [1]

6.1.2 Climb & Descent

Experts at NLR indicate climb and descent mission phases are usually not considered separately for helicopter operations because of the low altitude of flight. The HAMRAC has an exceptional, different mission profile with extreme altitude flying and clearance constraints due to mountain ranges present. Initial calculations showed that 22% of the initial fuel tank capacity is used for the climbing phase from 3780m to 8950m, therefore the fuel calculations consider them separately. Climb is performed at the best rate-of-climb speed [7]. The descent is performed at the same vertical and horizontal speed to avoid obstacles by taking a similar route back to landing zones. Higher than normal helicopter ascend and sink rates are required to achieve the mission within 180 minutes. These ascend and sink rates are maximized at 10.16 m/s, similar to the Kaman H-43B "Huskie" and Bell H-40 [49]. To prevent a vortex ring state from forming during the fast descent, the forward airspeed must be at least 4.5 m/s and the throttle setting must be reduced [88].

Hot refuelling Required ascend and sink rates can be reduced by hot refuelling, in which the engine is not shut off during refuelling. Faster refuelling can be made possible by installing a fast fuel pump at the Khunde medical clinic heliport, although this would require adaptation of the local infrastructure. With the maximum allowable refuel rate of 227L/min, the fuel tank could be filled within three minutes. Hot refuelling is not used in the HAMRAC mission design but left as a possible operational upgrade for the operator. The design will be technically capable of handling hot refuelling by putting the fuel port beneath, at some distance of hot engine areas and if fuel with a high flash point is used (jet A-1) [20].

6.1.3 Fuel Weight & Profile Details

To calculate the fuel weight, the method proposed by the Federal Office of Aviation from a country well known for mountainous helicopter operations, Switzerland, is used. To represent the actual fuel usage in real life as closely as possible, throttle settings during different mission parts are taken into account. For this method, the specific fuel consumption is assumed to be a linear function of the throttle setting. The fuel weight is calculated using a reference database for throttle settings in different flight phases and presented in Table 6.1. A throttle reduction factor per mission part is multiplied with the installed horsepower, SHP, with Equation 6.1 to find the fuel flow per second, which in turn is multiplied with the time of each mission part to find the part fuel consumption. The resulting fuel in column 'Part fuel calculated' has an uncertainty margin of 15% [80]. To prepare for a worst-case scenario, this margin is added to the fuel weight found. This can be seen in column 'Fuel used', being cumulated in column 'Fuel used total'. The column 'Part fuel verification' will be explained in subsection 11.1.1. The equation comes from the Swiss Guidance on determination of helicopter emissions [80].

$$\begin{aligned}\text{Fuel flow} = &\text{Throttle Factor} \cdot (4.0539 \cdot 10^{-18} \cdot SHP^5 - 3.16298 \cdot 10^{-14} \cdot SHP^4 \\ &+ 9.2087 \cdot 10^{-11} \cdot SHP^3 - 1.2156 \cdot 10^{-7} \cdot SHP^2 + 1.1476 \cdot 10^{-4} \cdot SHP + 0.01256)\end{aligned} \tag{6.1}$$

No fuel is estimated to be used during the refuelling phases, since it can be replaced instantly. Furthermore, no fuel is subtracted for the reduced power required during descending flight. This introduces a slight overdesign of the fuel tank capacity. The total time required for the mission is within the three hours by a slight margin of 110 seconds. Some resulting details for the mission parts are shown in Table 6.1. More details can be provided upon request to the Mission & Operations department.

Leg two determines the maximum fuel weight, which is a defining variable to determine the fuel tank size and the maximum take-off weight. With the 10% fuel margin at landing [14], and the 15% method uncertainty margin, the maximum fuel weight is 493 kg.

[1] URL `http://www.everest3d.de/` [cited 14 January 2019]

Table 6.1: *Details of the VFS mission including mission time, fuel weight and fuel fractions*

Mission part	Time [min]	Time-stamp [min]	Altitude change [m]	Cruise [km]	Horizontal speed [m/s]	Vertical speed [m/s]	Part fuel calculated [kg]	Part fuel verification [kg]	Fuel used [kg]	Fuel used total [kg]	Fuel Weight [kg]	Payload Weight [kg]	Weight fraction [-]
Idle & Flight check	2	0					5	14	5	5	350	405	1.0209
Take-off 1	2	2	150				14	14	16	21	345	405	0.9926
Climb to 3930m	4	4	2378	8.0	34.0	10.2	26	28	30	51	329	405	0.9860
Cruise at 3930m	21	8		98.8	80.0		137	145	158	209	299	405	0.9248
Climb to 6200m	4	28	2270	7.6	34.0	10.2	25	26	29	238	141	405	0.9853
Cruise at 6200m	3	32		13.0	72.0		20	21	23	261	112	405	0.9879
Descend to 3930m	4	35	-2270	7.6	34.0	10.2	25	26	29	289	89	405	0.9849
Recce & Landing 1	2	39	-150				10	14	11	301	60	405	0.9940
Refuel 1	20	41									49	405	1.2392
Take-off 2	2	61	150				14	14	16	16	493	405	0.9931
Climb to 8950m	8	63	5020	16.8	34.0	10.2	55	58	63	79	477	405	0.9723
Cruise at 8950m	3	71		11.2	55.0		23	24	26	105	414	405	0.9883
Recce	1	75	-80				7	7	8	113	388	405	0.9965
Hover Rescue Start	10	76					67	71	77	190	380	405	0.9649
Hover Rescue 1 pax	10	86					67	71	77	266	303	405	1.0039
Hover Rescue 2 pax	10	96					67	71	77	343	226	490	1.0039
Cruise at 8950m	3	106	80	11.2	55.0		23	24	26	369	150	575	0.9877
Descent to 3930m	8	109	-5020	16.8	34.0	10.2	55	58	63	432	124	575	0.9699
Recce & Landing 2	2	117	-150				10	14	11	444	60	575	0.9945
Refuel 2	20	119									49	575	1.1459
Take-off 3	2	139	150				14	14	16	16	345	575	0.9932
Climb to 6200m	4	141	2270	7.6	34.0	10.2	25	26	29	44	329	575	0.9876
Cruise at 6200m	3	145		13.0	72.0		20	21	23	68	300	575	0.9898
Descend to 3930m	4	148	-2270	7.6	34.0	10.2	25	26	29	96	277	575	0.9873
Cruise at 3930m	21	152		98.8	80.0		137	145	158	254	248	575	0.9289
Descent to 1552m	4	172	-2378	8.0	34.0	10.2	26	28	30	284	90	575	0.9855
Recce & Landing 3	2	176	-150				10	14	11	295	60	575	0.9945
End of mission		178									49	575	
Total / Maximum							**904**	**976**	**1039**	**444**	**493**		

6.2 Range & Alternative Mission

The HAMRAC is not only capable of rescuing mountaineers from Mount Everest but is a versatile extreme altitude rescue aircraft. To show operators its potential, alternative mission profiles are presented.

Payload range diagrams are presented in Figure 6.2 for the maximum cruise distance. The payload range mission profiles include idling, take-off, climb to the design cruise height of 3930m altitude, cruise, descent to the airport altitude, landing and a 10% fuel margin. The first profile starts and lands at sea level altitude, whilst the second starts at the reference airport of Kathmandu. The thrust T, power P, specific fuel consumption SFC and design cruise speed are set constant and evaluated at half fuel weight with Equation 6.2 [83]. It can be observed that the payload range diagram has no 'flat top'. This is because the fuel tank is optimised for maximum range with maximum payload and no extra fuel can be taken on board. An extra fuel tank can be added in the detailed design phase.

$$Range = \frac{T \cdot V_{cruise}}{P \cdot SFC} \cdot \left(-ln(1 - \frac{W_{Fuel}}{W_{Gross}}) \right) \tag{6.2}$$

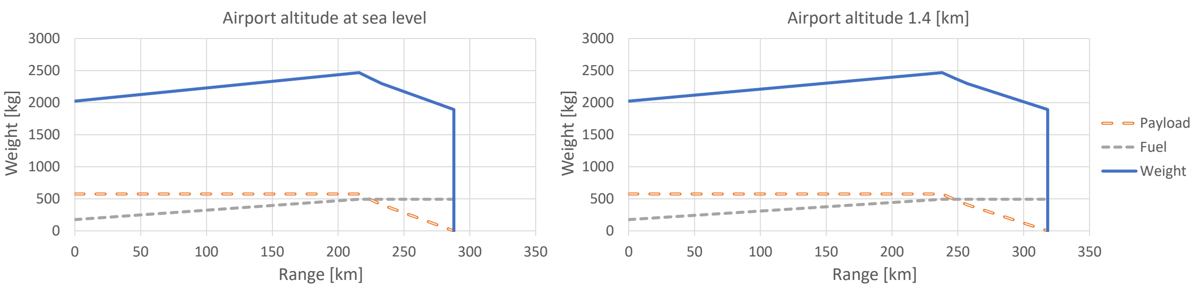

Figure 6.2: *Payload range diagrams*

An **alternative mission** can also be flown by operators from Kathmandu via Khunde to mt. Everest and back. For the HAMRAC design, the requirements of the VFS are strictly adhered to. Operators could however choose for a longer flight. This seems a big disadvantage, but has advantages. The Gaurishankar conservation area is completely circumnavigated, which is more environmentally friendly. Furthermore, cruise is performed all the way between Kathmandu, KTM, and Khunde at the more efficient design cruise altitude of 3930m. The routes are shown in Figure 6.3. No scale is shown in the image because the view is tilted, therefore distances in the bottom of the image might seem shorter than they are in reality.

Figure 6.3: *VFS mission (top route) and alternative mission (lower route) for the rescue at the top of Mt. Everest, using Google Earth*

For this alternative mission profile, similar fuel calculations are performed as for the VFS mission profile. The cruise distance between Kathmandu and Khunde is increased from 135km to 160km. Since the slow and fuel intensive clearing of the Tsengi Ragi Tau mountain pass is not necessary, the flight time and fuel consumed is reduced nonetheless. The total fuel consumed for the mission decreases from 1039kg to 1007kg and the mission time is reduced from 178 minutes to 174 minutes. Since the leg Khunde to rescue at the top of Mt. Everest and back to Khunde is defining for the fuel tank sizing, the fuel tank size does not need to be adapted for this mission profile.

Instead of refuelling at the Khunde clinic heliport, Syangboche airport could have been used as an intermediate stop. At the moment this is not deemed viable, since political conflict has left this airport derelict[2].

6.3 Operational Conditions

The HAMRAC operates in extreme environments. The design is possible of breaking the current record of 7010m for highest mountain rescue at an altitude with ease. To estimate conditions, the International Standard Atmosphere is used to determine temperature, density and pressure ranges at operating altitudes [42]. Although the reference mission in section 6.1 does not include sea level operations, sea level operations are considered to make production and testing outside the Himalayas possible.

6.3.1 Visibility

Clouds and fog in the mountains occur frequently and can cause a degraded visual environment [36]. Other causes of degraded visual environment are whiteout and brownout. Flights are planned under visual meteorological conditions, but mountain weather can change rapidly and instrument flight is considered a selling point for operators. The design is therefore made capable to operate under instrument flight rules (IFR). Night flight is technically possible, although to be prevented whenever possible, and cannot be done under visual flight rules (VFR) because mountains and cables strung across valleys are not illuminated [7].

[2] URLhttps://www.aviationnepal.com/syangboche-airport-deprived-of-flight-operation-from-past-decade-2/ Cited 28 January 2019

6.3.2 Clearances

Sudden engine failure or wind gusts can cause collisions with mountain faces. Therefore, the following clearances above ground level, AGL, from obstacles should be maintained during mountain operations [81]. In flight 200m AGL, hover initial reconnaissance (recce) 150m AGL, furthermore landing and take-off procedures start and end at 150m AGL. Furthermore, pilots must be aware and attentive of wires and cables strung across valleys.

6.3.3 Pressure Change

To perform the mission profile as described in section 6.1, high ascent and descent rates are required. Since the HAMRAC must be able to receive rescuees during hover at altitude, the vehicle has an unpressurised cabin. Crew and passengers could experience problems with lack of head pressure normalisation if they have a cold due to blockage of their Eustachian tube [42]. A possible measure to reduce the chance of headaches with passengers with blocked Eustachian tubes is to introduce pressure regulating diving-style helmets in the inventory, replacing the regular oxygen system. To prevent crew headaches, crew are not allowed to work when suffering from a serious cold. Possible passenger discomfort is negligible compared to suffering or perishing on the mountain faces of the Himalayas, and therefore considered acceptable.

6.3.4 Temperature

It is freezing cold with a temperature of $-43.2\,^{\circ}$C (230 K) at the top of Mount Everest. Since conditions vary between hot and cold days, even colder temperatures occur in extreme altitude operations. Average temperature ranges between 288 K at sea level conditions to 230 K in International Standard Atmosphere at 8950m [36]. Jet fuel specifications for available fuel in Nepal[3] require a freezing point of 226 K (Jet A-1). Furthermore, large temperature differences can cause water contamination in the fuel to separate out in the fuel tank and form ice crystals, as can be seen in Figure 6.4. Although total freezing does not instantly occur at the freezing point, hydrocarbon wax crystals will form, freezing free water will obstruct the fuel system and engine filter icing will occur [13]. Therefore, an engine oil heat exchanger is incorporated in the design to heat the fuel in subsection 7.4.3, preventing the need for environmentally harmful anti-icing additives.

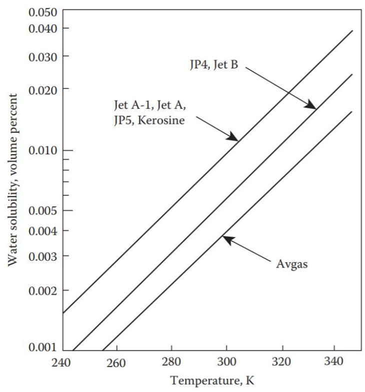

Figure 6.4: *Water solubility of jet fuels at temperature [13]*

Structural Icing Freezing temperatures cause structural icing. Structural icing is a problem between 0 °C and $-20\,^{\circ}$C as can be seen in Figure 6.5. These conditions occur in ISA between 2300m and 5400m [36]. The HAMRAC design has de-icing systems for the rotors, airframe, pitot tube [8], which are described in section 7.1.

Outside Air Temperature Range	Icing Type
0 °C to –10 °C	Clear
–10 °C to –15 °C	Mixed clear and rime
–15 °C to –20°C	Rime

Figure 6.5: *Temperature ranges for structural ice formation [6].*

[3] URL `https://dlca.logcluster.org/display/public/DLCA/2.2.1+Nepal+Tribhuvan+International+Airport+Kathmandu` [cited 09 January 2019]

6.3.5 Other Variables Influencing the Design

Other parameters of importance to the HAMRAC design are:

- Air density is lower at altitude, this is incorporated in all design calculations. Furthermore, when a mission is performed, density altitude corrections are made by the pilot [7].
- Mountain winds can be strong, turbulent and unpredictable [36]. Special operational procedures must be followed in mountainous operations [81]. The HAMRAC design is capable of controlled operation in wind gusts of 21m/s.
- Oxygen levels are 1/3 of sea level oxygen. Therefore, the HAMRAC is outfitted with oxygen masks for breathing. A pressurised cabin is considered not viable for a search & rescue helicopter, because rescuees need to be loaded at altitude.
- Thunderstorms form a serious risk for operations due to turbulence, downdrafts and potential lightning strikes. Therefore, a clearance of 20 miles is maintained from thunderstorms[4]
- Avalanches pose a potential risk for rescue missions in mountainous operations. A further analysis on triggering avalanches is presented in section 13.4.

6.4 Operational Flow

In this section, operations are described from a pilot's point of view. Both mountain related operations and procedures that must be performed differently or more thoroughly than usual due to the HAMRAC mission are shown in Figure 6.6.

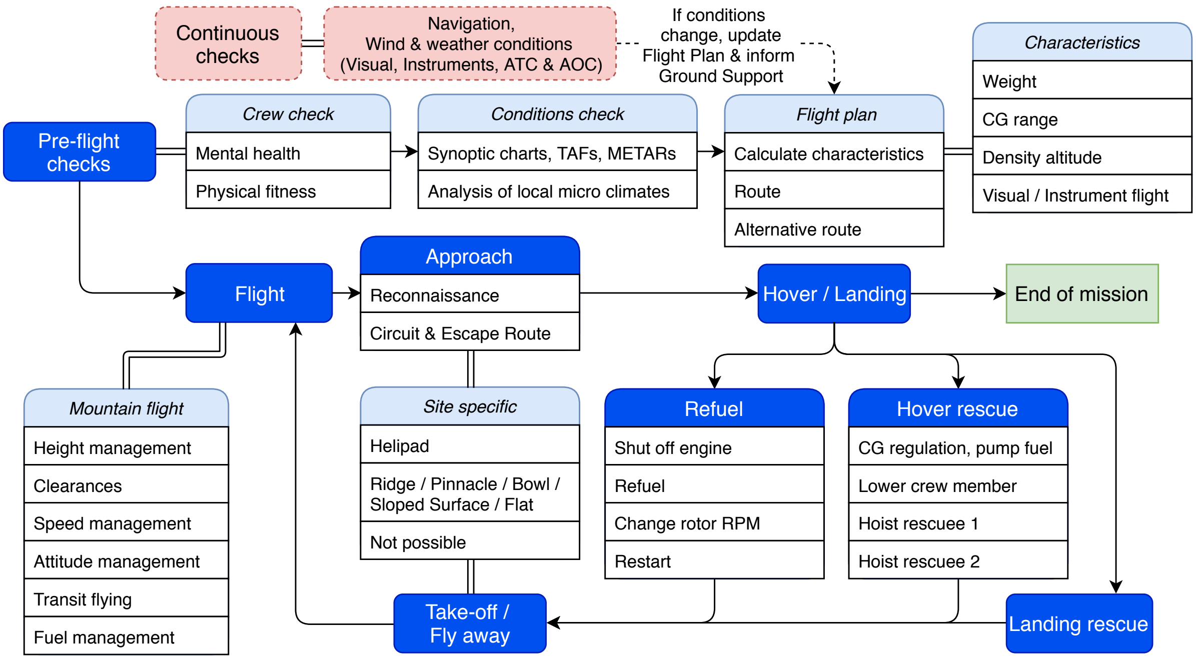

Figure 6.6: *Operational flow specific for HAMRAC [7] [76] [81]*

Safety is crucial in the challenging environment of mountain operations. A more elaborate mountain operations description can be found in the handbook [81]. In Figures 2.2 and 2.3 the operations performed are described from the system's point of view. Normal helicopter operations are taken as a baseline and not presented here for the purpose of conciseness. They can be found in the flying handbook [7]. One aspect pilot and crew need to be attentative of is their physical and mental health for performing under changing circumstances. More information on this can be found in the mountain operations handbook [81].

Rescuee Retrieval Protocol During the retrieval of rescuees, there is a sequence of steps that must be followed. The reason being that under strenuous situations, following predefined steps leads to effective action with no time required for figuring procedures on-the-go. The reason only one crew attends the rescuees is

[4] URL `https://www.faa.gov/documentlibrary/media/advisory_circular/ac%2000-24c.pdf` [cited 19 January 2019]

that space is significantly limited in between beds. The crew member ,that is not attending the rescuees should rather sit in the aft than forward seats, so the c.g range is not increased. Below, the sequence is enumerated:

1. The two crew members move from fronts seats to rear door hatch location.
2. The rear door hatch is opened by crew member two, and crew member one is hoisted down by crew member two.
3. One rescuee is attended to by crew member one, fixed to the hoist and brought up by crew member two.
4. Crew member two uses the hoist system to place the rescuee on one bed, fixes the rescuee to the bed and then releases the hoist from the rescuee.
5. Crew member two hoists the hoist down.
6. Step 3 and 4 are repeated if another rescuee needs to be rescued.
7. Crew member two hoists the hoist down and crew member one is retrieved.
8. The rear door hatch is closed.
9. One crew member attends to the rescuees while the other is seated in the rear seat.

6.5 Communication Flow

During all the mission phases of the HAMRAC, a line of communication needs to be maintained in order to ensure safe operation. The different entities and subsystems that are directly or indirectly interacting with the pilot are depicted in a flow diagram in Figure 6.7. Internal data flows for the stability & control are shown in separate diagrams in chapter 10, whilst subsection 7.3.3 shows the electrical block diagram. For every party that is communicating with the pilot, the method of communication is also depicted. Two-way communication is represented in Figure 6.7 by arrows on both ends of the line.

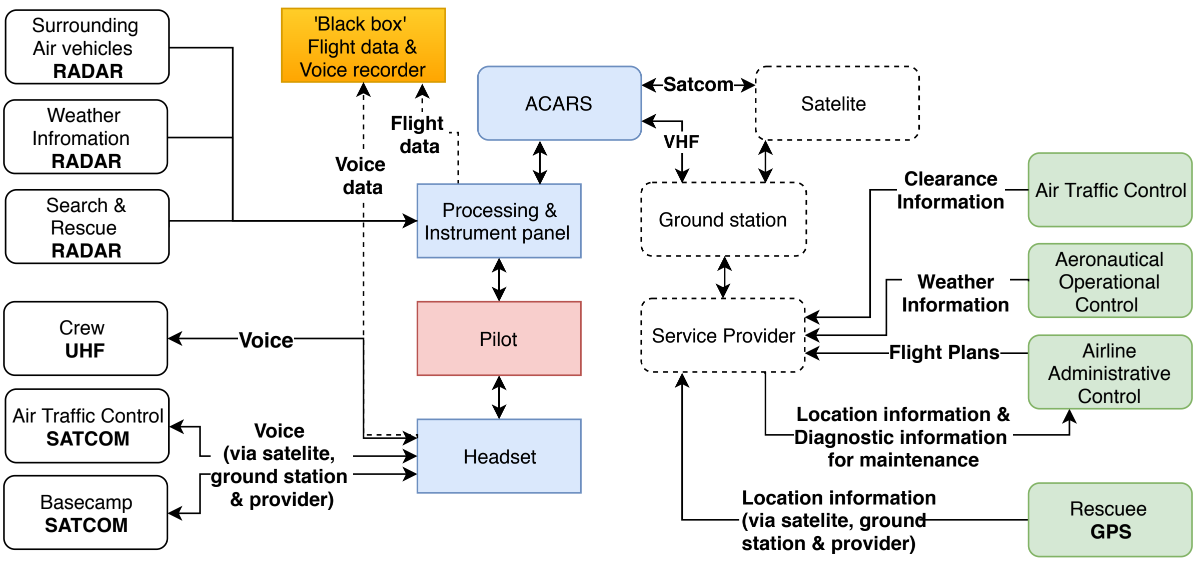

Figure 6.7: *Communication flow diagram for the HAMRAC*

The Aircraft Communication Addressing and Reporting System (ACARS) is a data-link system that receives and shows messages from different ground-based communication types. The HAMRAC will operate in remote areas where Very High Frequency (VHF) communication is not always possible due to mountains blocking the signal. Therefore, satellite communication (SATCOM) is used when flying in remote locations. Switching from VHF to SATCOM is done automatically by the ACARS when the VHF signal is not strong enough. The ACARS can also automatically communicate diagnostic information of component sensors to aid in predictive maintenance. The ACARS uses ARINC 823P1 standard ACARS Message Security (AMS) as bus protocol for external communications to protect sensitive business information communicated [41].

7

Configuration & Layout

This chapter shall give you an insight in the design of the HAMRAC both internally and externally. First, in section 7.1, the avionics configuration is given and explained thoroughly why certain systems are a necessity for the mission profile. Secondly, section 7.2, the general layout of the HAMRAC can be found that is supported with technical sketches from CATIA. Additional information has been given focused on the dimensions, weights and performance. Thirdly, in section 7.3, the internal subsystem layout is shown along with its geometric properties and alongside the electrical block diagram can be viewed. Lastly, in section 7.4, the external main subsystems can viewed, such as the engines, powertrain, rotor blades etc. Additionally, a thorough center of gravity shift analysis has been made for critical cases in order to comply with stability requirements. Furthermore, external 3D renders are given of specific parts to show the design decisions that have been made throughout the project.

7.1 Avionics

In this section, the avionics used in the HAMRAC are described.

Electro Optical System (EOS) FLIR's Star SAFIRE ®230-HD[1] can provide an EOS with the following characteristics:

- Infrared camera
- Daylight HD colour camera
- Laser range finder
- Embedded IMU/GPS and Geo-Functions

The infrared and daylight HD colour camera are useful for the identification of the target. There is a large temperature difference between living potential rescuees and the snow and ice around them. This difference can be captured by an infrared camera. Similarly, the difference in colour between snow and climbing equipment and clothes can be captured by the daylight HD colour camera. The laser range finder will provide the crew with data regarding their relative position to the rescuee as the laser range finder is embedded with, IMU/GPS and geo-function capabilities. The EOS is capable of geo-stabilization, geopointing and automatic moving map[2], which will reduce the pilot work load during the search phase of the mission.

Instrument Panel The instrumental panel design shall be an intuitive human machine interface that reduces crew work load and also has autopilot capabilities. Airbus's Helionix ®[3] cockpit avionics system will be used as reference for the design and is illustrated in Figure 7.1. It is a glass cockpit consisting of 3 multifunction displays (MFD) and one backup (3), glass cockpit flight navigation display.

[1] `https://www.flir.com/support/products/star-safire-230-hd#Resources`
[2] URL `https://www.flir.com/globalassets/imported-assets/document/star-safire-230-hd-datasheet-en.pdf` [cited 22 January 2019]
[3] URL `http://www.helicopters.airbus.com/website/en/ref/Airbus-operators-weigh-in-on-Helionix_404.html` [cited 22 January 2019]

Figure 7.1: *Heliolix cockpit avionics system* [4]

Noticeable features in Figure 7.1 that are relevant to the design of HAMRAC's cockpits avionics system are labelled. On the right-hand side is the flight navigation display (FND) (1), providing the pilot with three useful pieces of information. From top-to-bottom, it displays flight information, navigation information, alarms and caution lights respectively. The same functional display can be found on the left-hand-side of Figure 7.1, for the co-pilot in this configuration.
In the center of Figure 7.1 (2), an MFD provides the pilot with the ability to visualize six functions (4). The five mention-worthy features, starting from the left, are: FND, Navigation Display (NAVD), Vehicle Management System (VMS), Digital Map (DMAP) and Miscellaneous (Misc). The FND function can display the exact same things at the right MFD. The NAVD function will provide the pilot with information pertaining to the flight plan. The vehicle management system (VMS) function, provides the pilot with information such as oil temperature, fuel available, N1 & N2. The digital map (DMAP) function simply displays a digital map. Miscellaneous (Misc) function can be used to display what is seen by external cameras. Its applicability is quite relevant since we can integrate it with the EOS used during search and rescue.

Helicopter Emergency Egress Lighting (HEEL) HEEL is a lighting system that marks crew and passenger emergency exits[5]. Because this system is capable of unambiguously identifying emergency exits under extreme cabin conditions, such as smoke or water filled & submerged, it is chosen to be implemented into the HAMRAC.

Search, Rescue & Weather Avoidance Radar Telephonics's RDR-1600 radar provides a lightweight onboard airborne weather radar with "extremely low power consumption"[6].
The RDR-1600 radar can complement the EOS because in addition to its weather functions, it has three specialized search and rescues modes:

- **Search 1:** Includes enhanced sea clutter rejection for small boats/buoy detection
- **Search 2:** Precision ground mapping for higher resolution applications
- **Search 3:** Normal ground mapping for use in detecting prominent land objects or coastlines

The latter two being most relevant for the mission profile.
Other avionic systems to be included in the HAMRAC are also included in Table 7.1. Notable mentions in this table are the pitot static tube. Given a −43.2 °C, is the average temperature in ISA at 8950 m, a heated pitot static tube is required. An off the shelf solution for this is Aeroprobe's ®Heated Air Data Probe. It is designed for systems needing de-icing capabilities consuming a mere 160 W of power[7]. Another noticeable mention is the amount of power required to heat the cabin. It is desirable that the temperature inside the cabin be

[5] URL `https://www.astronics.com/subproducts?productgroup=emergency%20systems` [cited 22 January 2019]
[6] URL `https://www.telephonics.com/product/rdr-1600` [cited 22 January 2019]
[5] URL `https://www.youtube.com/watch?v=a9ExJCnLDJw&t=81s` [cited 17 January 2019]
[6] URL `https://www.airbushelicoptersinc.com/images/products/H135/135_T3H_P3H%20Technical_Data_low_resolution.pdf` [cited 17 January 2019]
[7] URL `http://www.aeroprobe.com/wp-content/uploads/2017/05/Heated-Air-Data-Probe.pdf` [cited 23 January 2019]

raised to above zero temperatures as soon as possible. We believe that enabling this, improves crew comfort and reduces working fatigue. Patients under serious stress will also benefit from an ambient temperature that brings comfort to their body. It takes 6000 W to bring the volume of the HAMRAC's cabin from −45 °C to 15 °C in 96 seconds. However, this amount of time does not consider heat losses across the aluminium airframe or leaks, so therefore the amount of time to heat the cabin would be larger than 96 seconds. JENOPTIK's 6000 W[8] is used in large aircraft and will be used to support the operations of the HAMRAC.

De-icing Considerations Since the HAMRAC will operate at temperatures as low as −45 °Celsius, a design that accounts for subsystem icing is required. This is a twofold design problem where both high accuracy ice sensing and heating is required. Ice detectors that use magnetostrictive technology drive a sensing probe to resonate at its natural frequency. The accretion of ice on the probe, shifts resonance frequency, which can be used to accurately detect ice accretion as little as 0.0254 mm [9].
Electrothermal technology permits continuous heater operation on structural elements (metal or composite) such as rotor blades, engine inlets and gear box fairings [10] [11]. The disadvantage of electrothermal heating is its high power consumption. It should be noted however, there are several regimes of structural icing. The coldest not exceeding −20 degrees Celsius. If the appropriate monitoring and control is performed successfully up to −20 degrees Celsius, lower temperatures are not expected to affect the performance of the vehicle in terms of structural icing. From Didier Delsalle's recount on landing on Mount Everest's summit, windows were kept open to prevent the windshield from icing up. Structural icing only occurred at an ambient temperature lower than −20 degrees, because the humidity of his breath was higher than that. Therefore, the option of having the windows open or using the windshield de-icing heater will be investigated, where power required is the main consideration [12].
Additional considerations are required to account for minimum operational temperatures of avionic components. The availability of component such as electrically heated pitot tubes are obvious choices for the design, and the same approach is required for communication and navigation antennas.

Table 7.1: *Main avionics components required for search & rescue rotorcraft configuration*

Component	Description	Quantity	Peak Power [W]
EOS	1	350	[-]
Instrument Panel	Helionix	1	160
Radar	Weather and Search & Rescue	1	40
Pitot static	Electrically heated & on pilot side	1	160
Magnetometer	Garmin GMU 11	1	[-]
Inertial Measuring Unit		1	$300 * 10^{-3}$
Flight Data Continuous Recorder	a.k.a Black box	1	10
Search light	Aid landing and search & rescue	1	1600
Anti-collision warning light	red flashing LED	1	[-]
Headsets		3	$250 \cdot 10^{-3}$
Engine fire extinguishing system		1	[-]
Emergency Locator Transponder		1	10
Cockpit utility light		1	2.24
Digital icing rate sensors		9	[-]
Rotor de-icing		6	300
Engine de-icing		2	40
Airframe de-icing		[tbd]	
Windshield wiper		[tbd]	
Transponder		1	250
Windshield wiper	Visibility	2	[-]
Radar Altimeter		1	15
VHF/UHF/L-Band Antenna	Communication	2	100
TCAS antenna	Communication	1	1000
ATC/IFF	Communication	1	3000
VOR/LOC/Glide Slope Antenna	Communication	1	[-]
SATCOM	Communication	1	60
Audio Panel	Communication	1	33
Satellite transceiver		1	16
UHF/Satcom/GPS Antenna	Communication	1	200
Cabin air duct heater	Humans in cabin	1	6000
Total		33	13157.09

[8] URL `https://www.jenoptik.com/products/aviation-subsystems/heating-systems/heaters` [cited 22 January 2019]
[9] `http://www.goodrichdeicing.com/images/uploads/documents/Rotor_Ice_Protection_Systems_RIPS.pdf`
[10] `http://www.goodrichdeicing.com/images/uploads/documents/Rotor_Ice_Protection_Systems_RIPS.pdf`
[11] `http://www.coxandco.com/products/low_power_ice_protection_systems.html`
[12] `https://www.verticalmag.com/features/landing-everest-didier-delsalle-recalls-record-flight/`

7.2 Design Configuration

In this section, the general layout of the HAMRAC is shown, which is a re-configured co-axial type of rotorcraft with a rear hatch for rescue operations. In the first paragraph, the technical sketches are presented, which gives a general view and dimensions of the side, top and front part of the air vehicle. Additionally, a table is presented which gives an overview of the general information. In the second paragraph, information regarding the performance of the HAMRAC is stated.

General Layout and Dimensions Three sketches are presented along with the dimensions of the HAMRAC, this gives a general overview of the external layout configuration. These sketches are the top, side and front view in Figure 7.2, Figure 7.3 and Figure 7.4 respectively.
Some important remarks regarding the design is the implementation of a backdoor to conduct the rescue operation, which can be seen in Figure 7.3, with an entrance height of approximately 1.4m. More information regarding the rear hatch will be given in section 7.4. Furthermore, a co-axial configuration is included in the design with a rotor spacing of 0.45m, with an additional hub fairing in between these rotors to reduce the drag and increase streamline efficiency. On top of these rotor blades, servo flaps are added at approximately 75% of the rotor blade length. Additionally, the use of the end plates at each end of the horizontal stabilisers in order to reduce the induced drag. Lastly, the external subsystems such as the engines and fuel tanks can be found in section 7.4, which has not been included in the CAD design due to time constraints.

In Table 7.2 the dimensions of the design and the general information regarding the stabilisers and rotor blades can be found for a better overview and in Table 7.3 the weight estimations can be found.

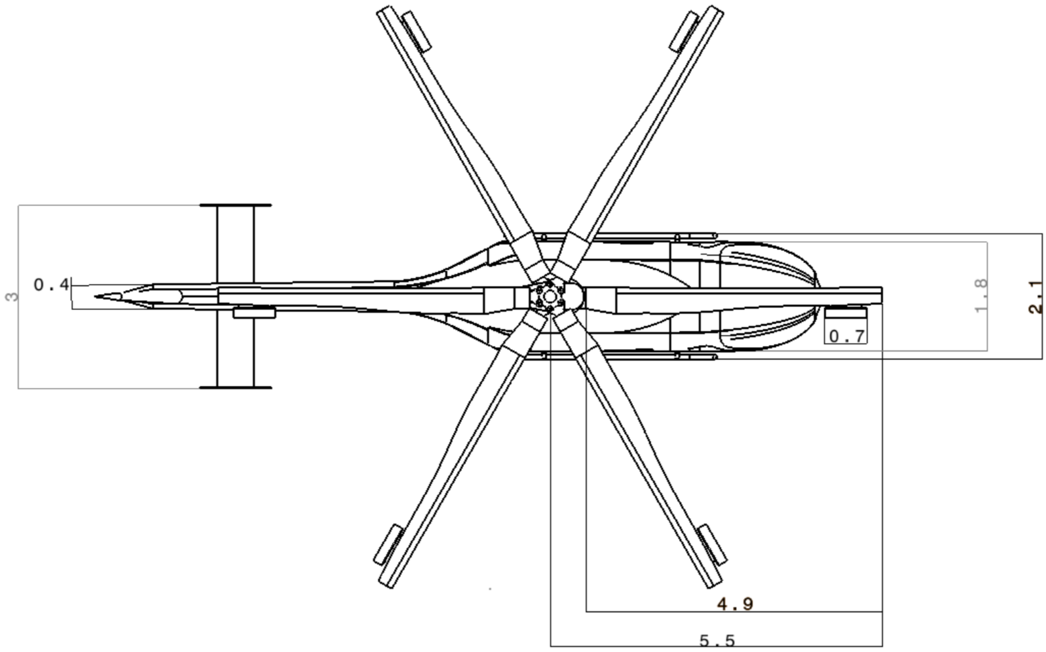

Figure 7.2: *Top view dimensions of the HAMRAC in meters*

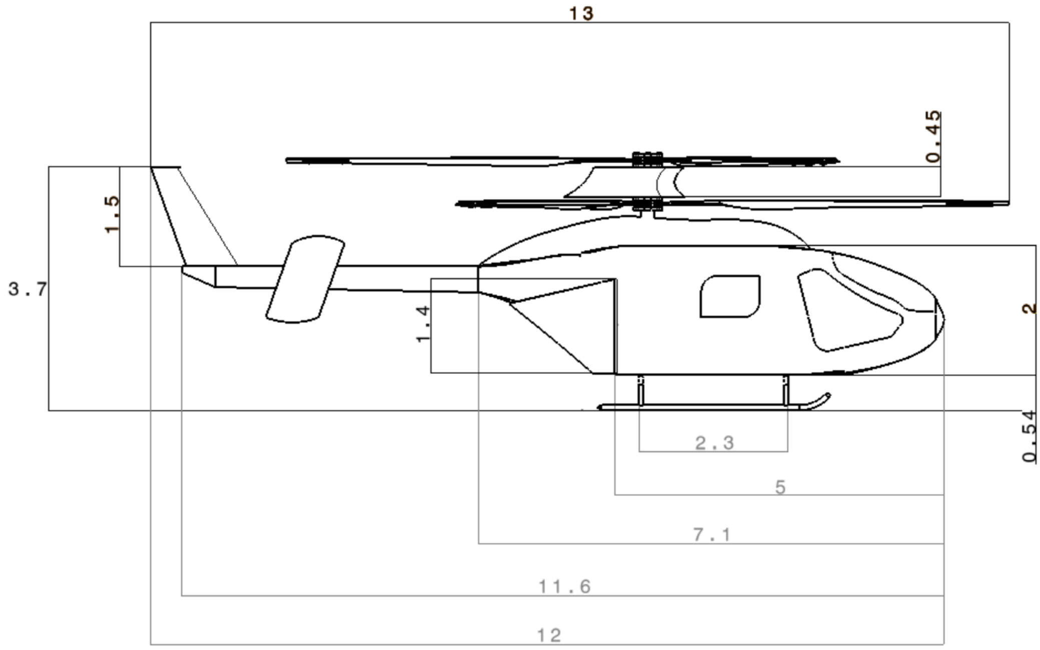

Figure 7.3: *Side view dimensions of the HAMRAC in meters*

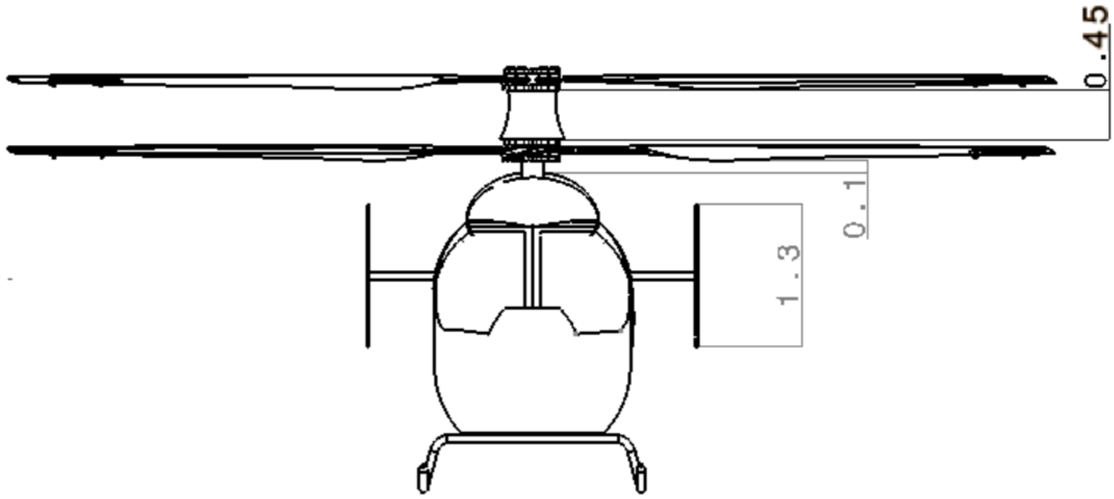

Figure 7.4: *Front view dimensions of the HAMRAC in meters*

Table 7.2: *General layout parameters and sizing information*

Parameter	Value	Unit
Airframe		
Max. Length	12	m
Max. Width	2.1	m
Cabin Length	5	m
Cabin Width	1.8	m
Tail Length	4.5	m
Height Rear Hatch	1.4	m
Width Rear Hatch	1.8	m
Area Backdoor	4.5	m^2
Rotorhub		
Rotorhub Height	0.95	m
Rotor spacing	0.45	m
Rotor blades		
Number of blades	6	-
Rotor Radius	5.5	m
Taper Ratio	0.61	-
Root Chord	0.46	m
M.A.C. Chord	0.36	m
Max. Thickness	0.0316	m
Skids		
Total Length	3.5	m
Total Width	2.1	m
Mid-spacing	2.3	m
Stabilizers		
Horizontal Tail Span	3	m
Horizontal Tail Area	1.8	m^2
Horizontal Tail Sweep Angle	0	degrees
Horizontal Tail Aspect Ratio	16.2	-
Vertical Tail Surface	3.2	m

Table 7.3: *Weight parameters*

Weights	Value	Unit
MTOW	2095.5	kg
OEW	1347.5	kg
Max. Fuel Weight	493	kg
Max. Landing Weight	2095.5	kg
Max. Payload Weight	748	kg

Performance information In Table 7.4, the general performance and propulsion parameters can be found for the HAMRAC. The choice of using two engines has been made by the propulsion department in order to meet the requirements from FAR category A to be more reliable and able to sustain greater safety. From a design choice perspective, choosing a single engine would not have much benefits except for making the engine compartment more aerodynamically shaped, but that would not out weight the results one get from a safety and reliability standpoint. Additionally, the reference rotorcraft (Airbus H135) that has been used to model the HAMRAC has the same twin engine configuration and still excels in cruise speed. Furthermore, the performance adheres to the required mission profile given by the stakeholders.

Table 7.4: *General performance parameters*

Propulsion	Value	Unit
Number of Engines	2	-
Engine types	T800-LHT-800	-
Manufacturer	LHTEC	
Max. Power	774	kW
	1038	SHP
Performance		
Max. Operating Altitude	9000	m
Service Ceiling	8950	m
Cruise Speed (@ 3930 m)	77.2	m/s
Max. Operating speed	88	m/s
Never Exceed Speed	92	m/s
Max. Range (No Payload)	318	km
Max. Range (With Payload)	216	km
Max. Rate of Climb	10.6	m/s

7.3 Internal Configuration

In this section, the internal configuration layout is explained and viewed. One of the big changes that has been mentioned in section 7.2 is putting the hoist system at the rear of the vehicle. Therefore in subsection 7.3.1 an explanation has been given about the hoist system and the overall rescue scheme. Furthermore, in subsection 7.3.3 the electric block diagram can be viewed to give an overall impression of the electrical wiring both externally and internally for the HAMRAC.

7.3.1 Internal Layout Configuration

The internal layout configuration can be viewed in Figure 7.5. It consists of a front compartment, middle compartment and a back compartment. The front contains the avionics and two pilot seats, the middle compartment includes four seats for the crew: two in the front and two at the rear. Additionally, the middle compartment also includes the two medical beds for the rescuees and EMS equipment that can be found at the side walls. EMS equipment locations is not specifically fixed, so it is possible to move the EMS to the upper side of the compartment. Lastly, the back compartment is used for the hoist system and the rear doors.

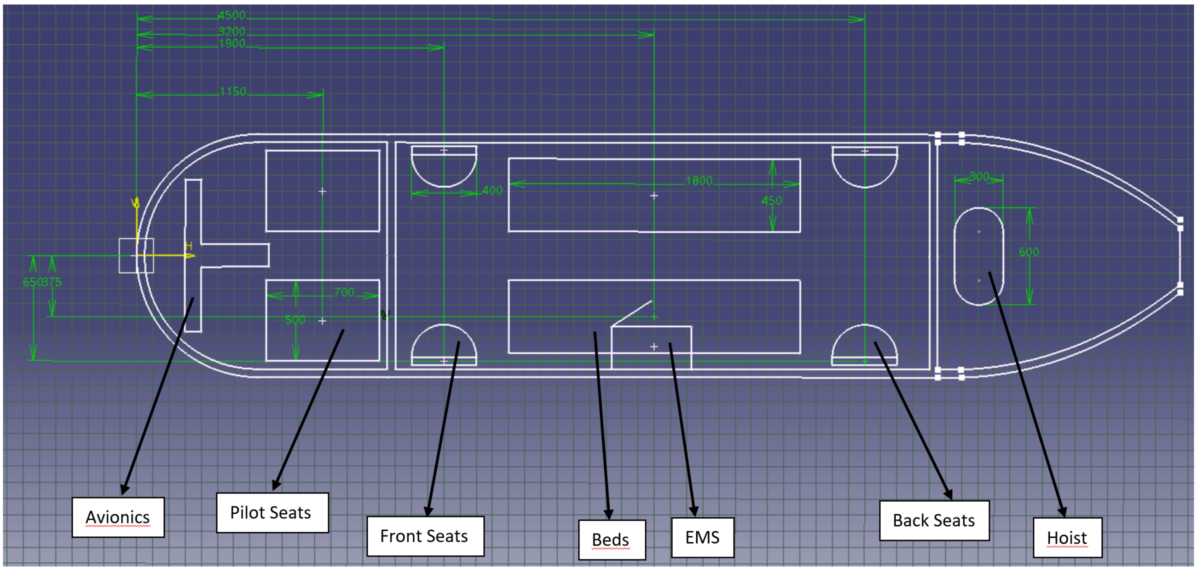

Figure 7.5: *Top view sketch showing internal layout system*

7.3.2 Rescue Operations and Hoist System

For the operation to be a success, off-the-shelf medical equipment will be available to support the rescuees during their transfer back to the international airport. Equipment such as an Oxygen Support System and a defibrillator will be available to aid the crew to perform their job effectively.

When approaching the design problem of integrating internal configuration with the search and rescue operation it was found that, the internal cabin dimensions were a hard requirement. This was so, because as a means of achieving an OEW of 1400 kg, the cabin size had to be of limited size. Based on this, and under the assumption of $180 \cdot 45$ cm bed for the rescuee, it was found that the space for moving between two beds would be too narrow, for the type of efforts the crew would have to perform on them. Therefore, it was decided that, to reduce crew workload, an internal hoist system would be used integrated with a rear hatch to the rotorcraft. The workload is reduced because the hoist can carry a person above the bed height, and the crew member can swing and operate the hoist such that it places the patient directly on the bed. By introducing a slot, with roller bearings, the hoist moves longitudinally along the inside of the cabin. The rear roof extends beyond the rear floor, therefore allowing for enough clearance with the airframe, such that the hoist can operate externally too. The hoist should then be able to bring crew or rescuee inside during hover.

It is a requirement from the VFS that the hoist system be rated for a 300kg load. The SkyHoist800 is an off the shelf solution, chosen as the hoist to be used for HAMRAC's operation, as it is rated for a 300 kg load, operating at 4.2 kW with a system target weight of 50 kg [13]. The component is rendered in Figure 7.7, however it is assumed that in-house adaptations to the casing are needed. A casing that can be operated within a slot must be designed such that the hoist system can be electrically moved forward and aft during operations.

The rear hatch design concept has been implemented before in the H145 from Airbus search and rescue configuration as can be seen in in Figure 7.6.

Figure 7.6: *Airbus H145 rear hatch for search & rescue configuration*[13]

Figure 7.7: *SkyHoist800*[14]

7.3.3 Electrical Block Diagram

Electrical power is needed to power the avionics and other electronic systems in the HAMRAC. The purpose of the electrical system is to bring power from the engine to the equipment that need the power to function [23]. This can be done by implementing alternators in between the engine and battery in order to convert mechanical energy into electrical energy. This should be done in a safe and reliable manner by adding switches to be able to select which alternator to use. Additionally, the battery needs sufficient power to start the engines and potentially light sources as well.

The equipment is divided over the avionics, internal and external bus. This division is made because in case of short circuit, it is favourable that most of the components will keep working. Between the busses and electrical components, fuses are placed to provide overload protection of the circuit. This is needed since this might initiate unwanted fires in the electrical wires. Before this would happen, the fuses melt and the power circuit to the component is interrupted. It is essential that spare fuses will be present in the HAMRAC such that, in case it melted, the fuse can be replaced during flight. In Figure 7.8 the preliminary electrical block diagram can be seen, where there are three different buses, and in every link of the equipment a fuse is placed. The battery is charged by the engine, and this can be verified by the ammeter.

[13] URL `https://www.jenoptik.com/products/aviation-subsystems/rescue-hoists-cargo-winches` [cited 22 January 2019]
[14] URL `https://i.pinimg.com/736x/bb/a8/53/bba853a588e24663c1e0f06b571a40ae.jpg` [cited 22 January 2019]

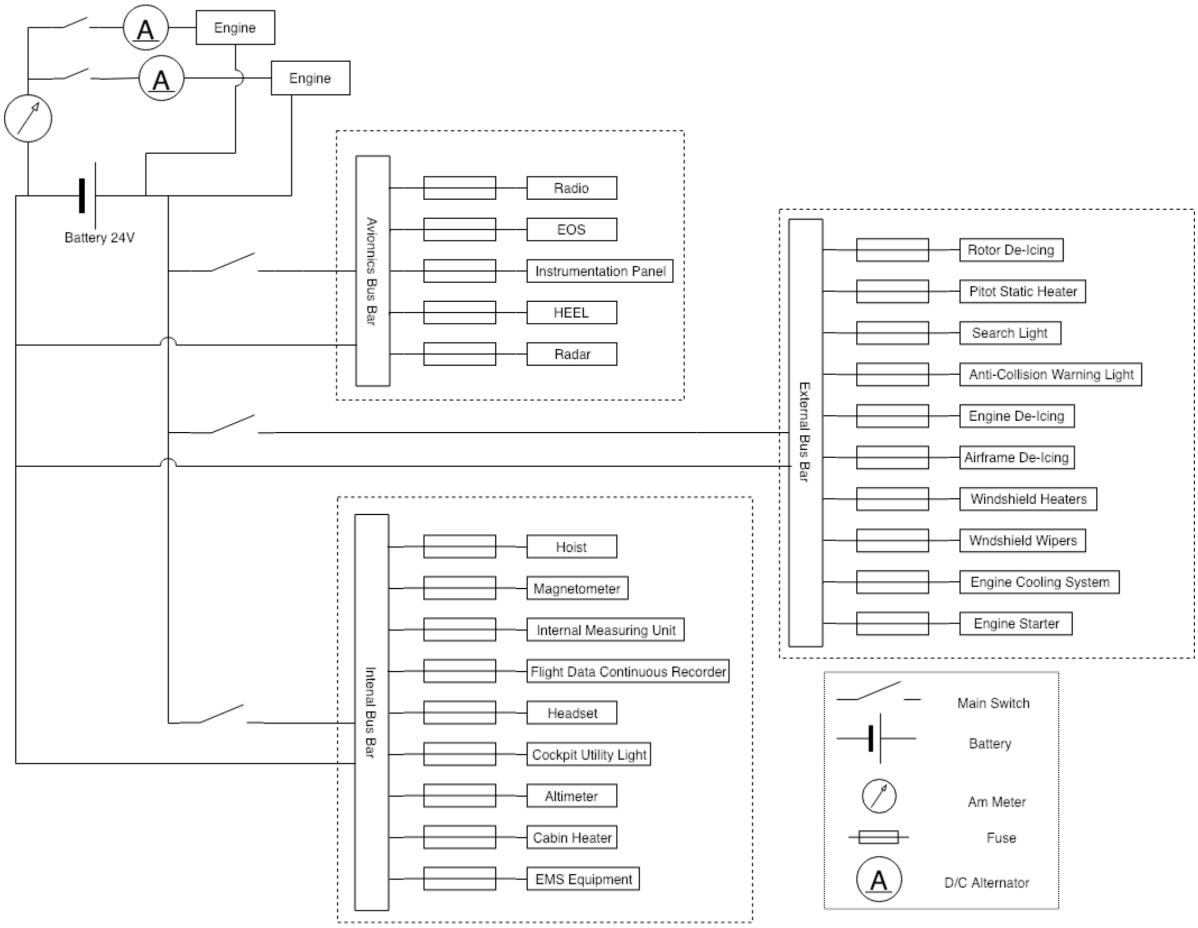

Figure 7.8: *Electric block diagram of the HAMRAC*

In this first design of the electrical block diagram some simplifications were made. For further development of the HAMRAC, the electrical block diagram should be extended with equipment such as starting motors and battery relays [7].

7.4 External Configuration

In this section, the external configuration of the HAMRAC is visualised and the layout configuration choices are stated and further explained. This will be split up in the following subsections: firstly, subsection 7.4.1 explaining the main subsystem locations, secondly subsection 7.4.2 explains the critical locations of the center of gravity of each subsystem, thirdly subsection 7.4.3 describes the fuel system, and lastly subsection 7.4.4 contains the three dimensional sketches and renders of the HAMRAC design.

7.4.1 Subsystem Layout and Center of Gravity

The subsystem layout has mostly been chosen based on conventional subsystem placement. This layout can be viewed in Figure 7.9 on the next page.

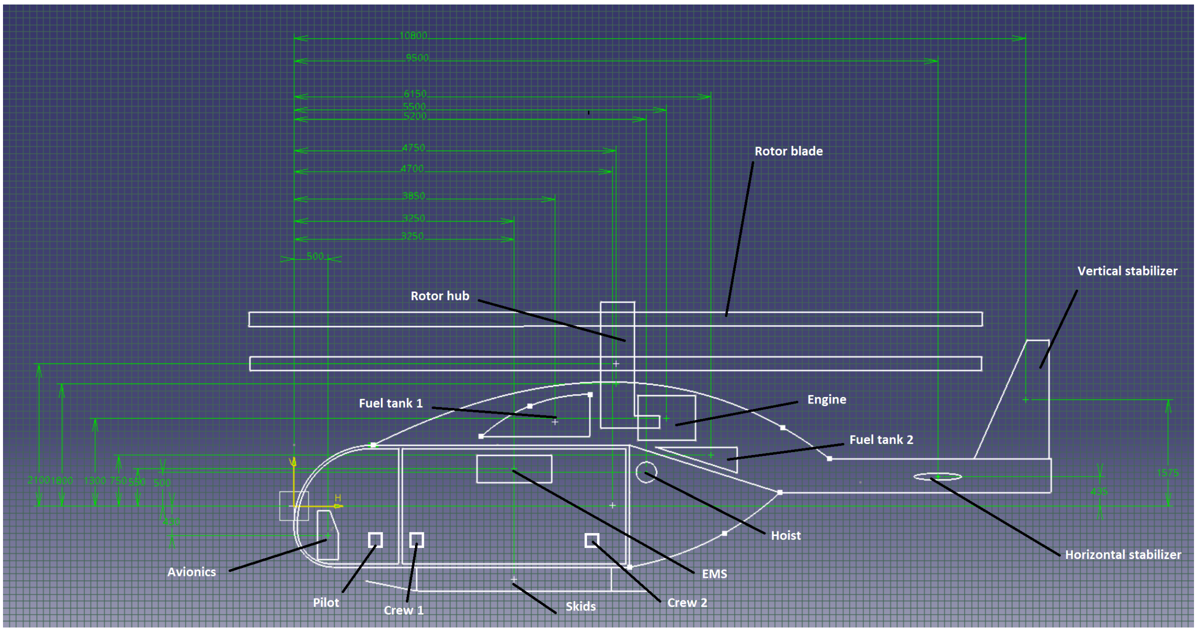

Figure 7.9: *Side view of the main subsystems location of the HAMRAC*

The center of gravity for the OEW condition is determined based on the distribution of subsystem locations. During an iterative process, the appropriate fuel distribution is determined. It is found that a 50-50 division of initial fuel mass distribution between front and aft tank, results in the smallest overall center of gravity range. The MTOW center of gravity position is then found based on three crew seated and full fuel tanks. The seating arrangement of 3 crew is one where, one crew is in pilot seat, and the other two crew are seated in the forward cabin seats. This results in the MTOW c.g being quite forward at the start of the mission. This initial fuel distribution and seating come as an understanding of a rear c.g shift, during operations. This MTOW c.g position allows for an overall reduction of maximum c.g range during the execution of the reference mission profile. As can be seen in Figure 7.10, had the cabin crew been in the rear cabin seats during take-off, the initial hover c.g (2), would have been further back. This would result in a c.g position which is further back from the rotor c.g, which is undesirable. After take-off, there are four critical loading conditions in the reference mission, as specified below. The XX-YY fuel distribution notations, refers to the percentage of fuel in front a rear tank respectively:

- **Case 1:** First refuelling stop, with three crew, 10% total fuel (0-100) and crew sat at front. The fuel is consumed in the front tank such that the c.g shift takes a rearwards direction.
- **Case 2:** Beginning of hover, with three crew, 70% fuel (80-20) and crew at rear hatch cabin position. Most of the fuel is consumed from the rear tank after refueling so that when the crew begin the rescue phase, the c.g is not shifted too rearwards, due to their aft position within the cabin.
- **Case 3:** End of hover, with three crew and two rescuees, 30% fuel (0-100) and crew sat at rear. During hover, fuel must be all pumped rearwards, so that as recuees are placed in their respective beds, the c.g will not shift to forwards.
- **Case 4:** Second refuelling stop with three crew and two rescuees, 10% fuel (100-0), and crew sat at front. The fuel is entirely distributed to the front tank between end of hover and begin of refuel landing. If the fuel had not been distributed to the front, the 3-4 step, would have had a strong shift towards the rearwards and finished rear of the OEW c.g position.

After this analysis, it is understood that a zero fuel tank is not desirable since sludge/residue more easily enters engine and fuel filters. This distribution should therefore be used as reference, while complying with the above mentioned factors.
Given the seating and fuel distributions throughout the operation, the stability and control standards shown in section 10.2 are met because a center of gravity range of 16.4 cm is achieved. The analysis for the three cases is reported in Table 7.5, where the origin of the coordinate system starts at the nose of the rotorcraft, and x is positive aft-wards. The center of gravity positions are also shown graphically in Figure 7.10 throughout the entire mission.

7.4.2 Critical Center of Gravity Locations

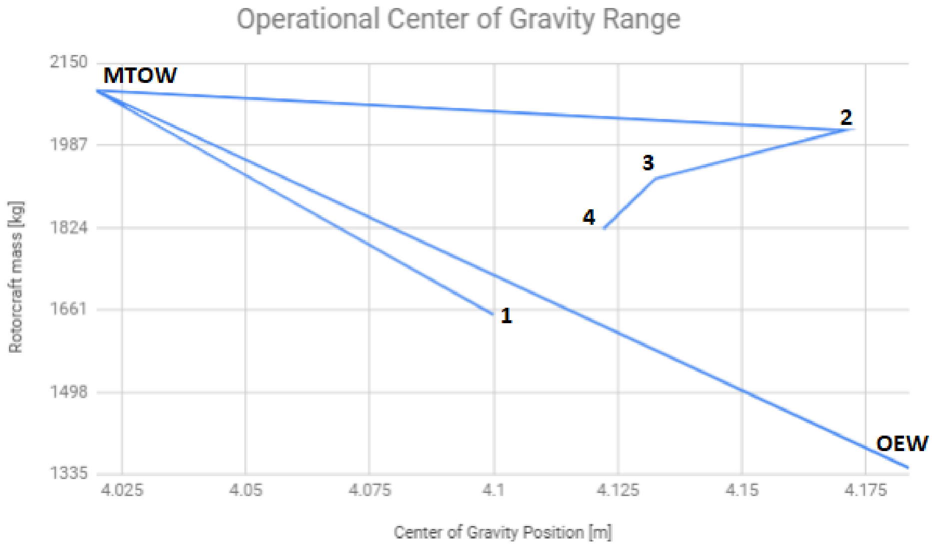

Figure 7.10: *The center of gravity shifts during HAMRAC's operational configurations*

Table 7.5: *HAMRAC's center of gravity location during operation*

Case	C.G Position [mm]	Element	Mass [kg]	C.G Shift [mm]
OEW	**4183.76**		**1347.5**	
MTOW	**4019.805539**		**2095.486667**	**-163.96**
3 crew @ 10% fuel	1700	Cabin Crew 1	85	
	1700	Cabin Crew 2	85	
	3750	Front Fuel Tank [1]	0	
	6000	Rear Fuel Tank [2]	49.3	
	4099.906746		**1651.786667**	**-83.86297025**
3 crew @ 70% fuel	4800	Cabin Crew 1	85	
	4800	Cabin Crew 2	85	
	3750	Front Fuel Tank [1]	276.08	
	6000	Rear Fuel Tank [2]	138.04	
	4170.676438		**2016.606667**	**-13.09327845**
3 crew + 2 pax @ 30% fuel	4500	Cabin Crew 1	85	
	4500	Cabin Crew 2	85	
	3250	Rescuees	170	
	3750	Front Fuel Tank [1]	0	
	6000	Rear Fuel Tank [2]	147.9	
	4132.487507		**1920.386667**	**-51.28220906**
3 crew + 2 pax @ 10% fuel	1700	Cabin Crew 1	85	
	1700	Cabin Crew 2	85	
	3250	Rescuees	170	
	3750	Front Fuel Tank [1]	49.3	
	6000	Rear Fuel Tank [2]	0	
	4122.077758		**1821.786667**	**-61.69195873**

The results are only possible however if the fuel flow between both fuel tanks is controlled. It can be observed in Table 7.5, that as soon as hover begins, the fuel needs to be pumped rearwards. The fuel weights in the Table are according to VFS requirement, always at least 10% reserve fuel [14].

7.4.3 Fuel System

Fuel Tank Sizing The fuel tank sizing is determined by taking the optimised fuel weight found with the mission profile in subsection 6.1.3 and multiplying it with the sea level density of jet A-1 fuel. This volume is used to size the fuel system according to small rotorcraft certification specifications to find a total fuel tank volume of 625L. This includes an expansion space of 2% [11]. To account for the required baffles, extra space for unusable fuel, and a margin for CG regulation due to pumping another 10% margin is added to this, giving an internal fuel tank volume of 344L for both the front and aft tank.

Fuel Heating Fuel heating is necessary due to cold weather operations. Ignition performance is negatively affected by a reduction in fuel temperature [13]. Fuel should be kept at least 3 °C above the freezing point for safe operation. Several concepts are compared, and for the HAMRAC design an engine oil heat exchanger is chosen due to its negligible fuel consumption penalty and, the low weight and the low complexity of the system compared to the runner up, electrical heating [16]. During the detailed design phase, a thermodynamic analysis can be made to calculate more precise requirements on the insulating properties of the fuel tank walls and fuel lines. Low fuel temperature is only becoming a risk above the landing rescue altitude of 6400m, so the HAMRAC does not require heated storage at landing sites.

7.4.4 External 3D CATIA Sketches

In the subsection, the complete design of the HAMRAC is visualised and various locations of the design will be shown in detail to visualise certain design choices the group has made.

First, a full render of the complete layout of the HAMRAC can be seen in Figure 7.11. The overall design of the hull and the dimensions are based on a reference helicopter, the Airbus H135. Slight modifications to the length were introduced to accommodate two rescuees comfortably. Furthermore, several sections of the hull have been modified in order to increase the aerodynamic efficiency, which is explained in section 8.4. One of the noticeable modifications is the implementation of a rear hatch. This is due to the location of the rescue operation, which occurs at the rear of the airframe. This will be further explained in this subsection.

Figure 7.11: *Render of the complete layout of the HAMRAC, using Keyshot 6 64 Pro.*

Following from the airframe, the rotor blades were designed based on the output dimensions given by the aerodynamic department stated in section 8.3. The renders can be found in Figure 7.12 and the top view in Figure 7.13. It can be noticed that the rotor blade has an angle of twist in several sections over the length, additionally there is a taper ratio which can be noticed in the top view picture.

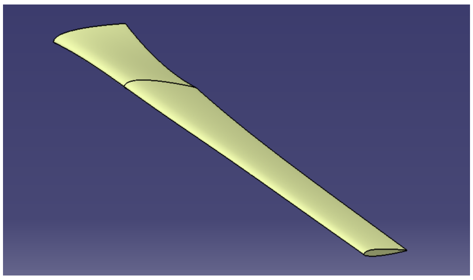

Figure 7.12: *CATIA render of the rotor blade*

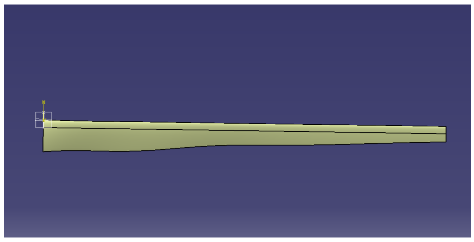

Figure 7.13: *CATIA render of the top view of the rotor blade*

Next, the connection between the rotor blades and the main rotorhub were designed based on a bearingless and hingeless rotorhub system, which is explained in section 10.3. This design connects the rotor blades onto a torque tube as can be seen in Figure 7.14 and the torque tube is connected to the main rotorhub in the end. Control parts of the blades are not visualised in this section due to the complexity, but this is explained in the department of stability and control in section 10.3. Furthermore, in order to reduce the drag due to the rotor spacing, a hub fairing has been included which can be seen in Figure 7.15.

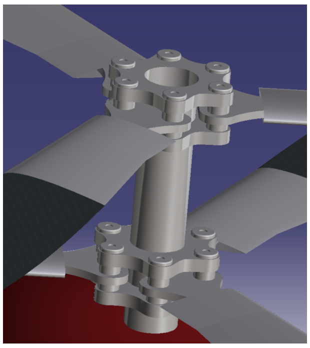

Figure 7.14: *CATIA assembly of the rotorhub and the torque tube*

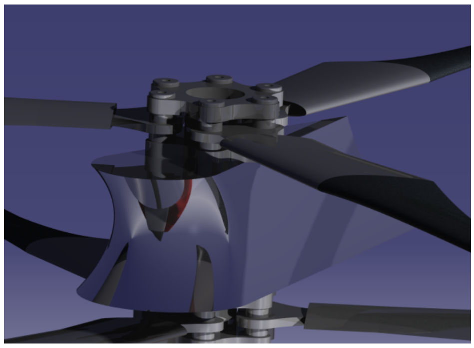

Figure 7.15: *CATIA render of the hub fairing*

The layout of the skids is presented in Figure 7.16, the design approach of the skids is based on the most conventional non-retractable skids that are currently used. Several options were thought of such as the retractable wheels, the conventional skids and the newly designed adaptive landing system which can be viewed in section 8.4. However, retractable wheels would end up using actuators and extra space in the cabin floor which was not beneficial from a structural view, furthermore using wheels in mountainous areas are not efficient due to the possibilities of slipping. The conventional skids are simple and efficient to use for mountainous area with minimal drag.

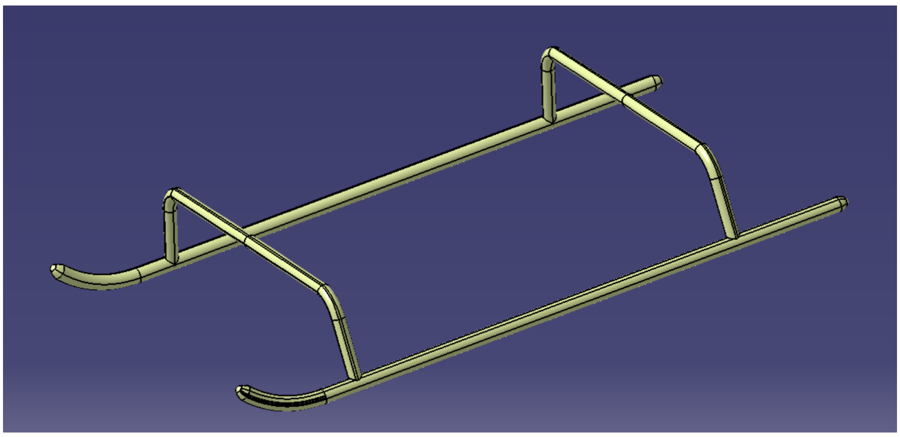

Figure 7.16: *CATIA render of the skids*

Furthermore, during the design process of the layout configuration, a group decision has been made to implement a rescue operation from the rear side of the HAMRAC inspired by the rear hatch of the Airbus H135 and the rear entrance of the Chinook. This has a few advantages over the normal conventional way of rescuing from the side, which are: less drag from the hoist system and a hoist rail system which can be retracted to hoist the rescuee more efficiently. The efficiency matter is based on the fact that a hoisting rail system can be positioned inside the fuselage in order to directly bring the rescuee on to the medical beds, which is a difficult task if one must overcome an angle when rescuing from the side. However, stability wise, this may impose larger center of gravity shifts, but this has been avoided by adjusting the subsystem locations. The rear side and the hoist rail system can be seen in Figure 7.17. An additional camera system is implemented at the rear to oversee the external environment during the operation of the hatch.

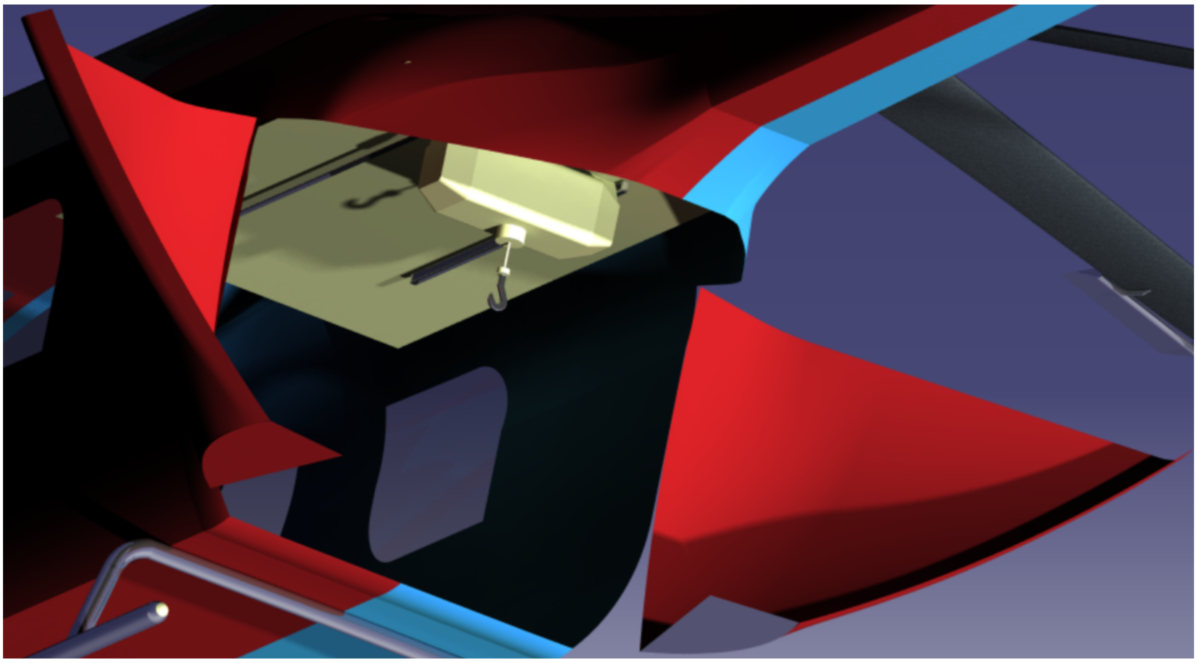

Figure 7.17: *CATIA render of the backdoor mechanism and the hoist system*

8 Aerodynamics & Performance

This chapter will cover the design choices considering the aerodynamic and performance characteristics. First the initial parameters were determined, leading to an initial weight and rotor size estimation, which is given in section 8.1. The outcome of this was used for optimisation via a Multidisciplinary Design Optimisation, which can be found in section 8.2. This resulted in the final outer dimensions of the rotor blades. The next phase was to determine the shape of the rotor blades, i.e. the airfoil design phase, which can be found in section 8.3. This resulted in multiple airfoils along the span of the rotor blade. Furthermore, the fuselage and additional aerodynamic considerations will be elaborated on in section 8.4. The fuselage shape will be analysed and a drag estimation will be made. Moreover, a fairing for the rotor mast and hub will be designed.

8.1 Initial Rotorsystem Sizing

Several approaches were found that could be used to determine the initial sizing of the rotor system. The method to determine the initial sizing was discussed with dr. M.D. Pavel. Findings after initial research on preliminary design of coaxial rotors was discussed. The steps that were discussed are used as one method for this sizing phase. For the purpose of convenience this method is called method 1. In order to verify the outcome, the output of the first method is used as input for a second method, written by Krenik [4]. This method uses a different approach than method 1 and could therefore be used as a validation of the first outcome. Lastly, dr M.D. Pavel referred to a paper of a former TU Delft student regarding the preliminary design of a coaxial rotorcraft [55], which was used as a guideline and a second validation for the first two methods. This interrelation can be found in Figure 8.1, which describes the flow of this process. All the results can be found in Table 8.2, where the similarities and outcomes will be discussed briefly. The output of this initial sizing will be used as input for the optimisation phase.

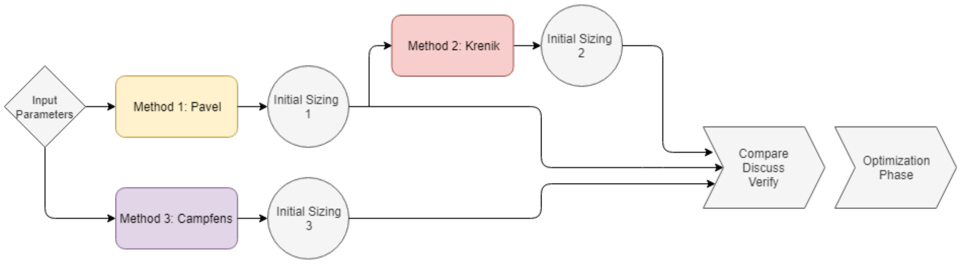

Figure 8.1: *Flow diagram of initial sizing of the rotor system*

During the literature research of this design phase, some additional parameters and constraints for the design were determined:

- The maximum flight speed is around 15% higher than the cruise speed, equal to 161 kts. This was determined after analysing 10 different helicopters.
- The never exceed speed is 10% higher than the maximum flight speed, which is equal to 177 knots [55].

- The maximum take-off weight (MTOW) for the HAMRAC was determined to be 2567 kg, as described in subsection 8.1.1.
- The maximum altitude during this mission is 8950m, as described in subsection 6.1.1.
- Blade tip Mach number cannot exceed 0.85 at cruise speed at maximum altitude [4].
- Blade tip Mach number cannot exceed 0.92 at never exceeding speed at maximum altitude [55].
- Advance ratio should not exceed 0.45, otherwise wings should be added [22].

8.1.1 Initial Weight Estimation

To begin the initial sizing, a Class-I weight estimation will be used to estimate the maximum take-off weight of the HAMRAC. This is done by comparing the OEW with the MTOW for several coaxial rotorcraft: the Cierva CR Twin / CR.LTH-1[1], the Kamov Ka 26[2], the EDM Aerotec CoAX 2D/2R[3], the Kamov Ka 226[4], and the Kamov Ka32A[5]. The plot of OEW against MTOW for coaxial rotorcraft is shown in Figure 8.2. Interpolating the data using linear regression for the required maximum OEW of the HAMRAC [14], gives a projected MTOW of 2567kg.

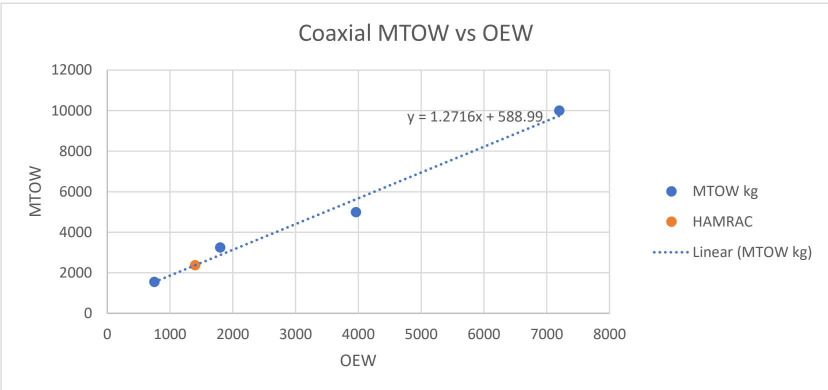

Figure 8.2: *A plot of OEW against MTOW for coaxial rotorcraft*

8.1.2 Method 1

After some consultation with dr. M.D. Pavel, the following procedure was advised:

1. Determine disc loading statistically (disc load versus MTOW graph)
2. Determine radius from first principles
3. Determine rotational frequency, using blade Mach number reaches maximum 0.85
4. Determine solidity from first principles
5. Determine chord and number of blades mathematically
6. Determine thrust coefficient statistically (thrust coefficient versus MTOW graph)
7. Determine advance ratio

Disc Loading The disc load is statistically determined to be 20 kg/m^2, which was determined from figure 16 from Filippone [3].

Radius The radius was determined by using Equation 8.1, resulting in a radius of 4.46m.

$$R = \sqrt{\frac{W}{2 \cdot DL \cdot \pi}} \tag{8.1}$$

[1] URL `http://all-aero.com/index.php/35-helicopters/copters/2359-cievra-cr-twin` [cited 20 December 2018] ; `http://avia-pro.net/blog/vertolyot-cierva-cr-twin-tehnicheskie-harakteristiki-foto` [cited 20 December 2018
[2] URL `http://www.flugzeuginfo.net/acdata_php/acdata_ka26_en.php` [cited 20 December 2018]
[3] URL `https://www.edm-aerotec.de/index.php?id=2` [cited 20 December 2018]
[4] URL `https://www.aircraftcompare.com/helicopter-airplane/Kamov-Ka-226-Sergei/274` [cited 20 December 2018]
[5] URL `https://www.aircraftcompare.com/compare-airplanes/Airplanes/2` [cited 20 December 2018]

Rotational Frequency Using Equation 8.2 and Equation 8.3, with a design blade tip Mach number of 0.85 at cruise speed, the rotational frequency becomes 41.8 rad/s.

$$M_{Bc} = \frac{V_c + U}{a} \tag{8.2}$$

$$U = \Omega R \tag{8.3}$$

The rotational frequency is used in order to determine the Mach numbers on the blade at never exceeding speed condition, which can be found in Table 8.2.

Solidity Using figure 20 of Filippone [3], a rotor solidity of 0.065 is found to relate to the chosen diameter of 10.2 m, which results in a combined solidity of 0.13.

Chord and Number of Blades Using Equation 8.4, the chord is 0.23m with four blades per rotor with an aspect ratio of 19.5 and the chord is 0.30m with three blades per rotor with an aspect ratio of 14.7.

$$\sigma = \frac{N_b \cdot c}{\pi \cdot R} \tag{8.4}$$

Due to overlapping of both rotors, the solidity is determined by using the number of blades of both rotors and the area of a single rotor [30].

Thrust Coefficient The thrust coefficient is determined using figure 19 of Krenik [4], resulting in a blade loading of 0.075, resulting in a thrust coefficient of 0.007 using Equation 8.5.

$$C_t/\sigma = \frac{sM_{to}g}{\rho c N_b R U^2} \tag{8.5}$$

Advance Ratio Using Equation 8.6 and Equation 8.3 the advance ratio was determined to be 0.43.

$$\mu_c = \frac{V_c}{U} \tag{8.6}$$

8.1.3 Method 2

This method, used by dr. Krenik [4], starts off with determining the rotor blade chord, rotor blade length, rotational frequency of the rotor and the rotor speed statistically with respect to the maximum take-off weight, which can be seen in Krenik [4]. This results in the following design parameters:

- Statistically, the blade chord should be between 0.19 and 0.45m, with the median around 0.32m. This design parameter is set at 0.23m, since number of blades is relatively high compared to conventional helicopters, which implies a smaller chord per rotor blade in order to have a 'normal' solidity.
- Statistically, the rotor radius should be between 3.5 and 7.0m, with the median around 5.5m. This design parameter is set at 4.46m. Lift at high altitude is harder to generate due to small density, which implies a higher radius. On the other hand, there are more blades apparent in comparison to a conventional helicopter, which already increases the overall solidity, this implies a smaller radius, in order to have a 'normal' solidity.
- Statistically, the rotational frequency should be between 25 and 42rad/s, with the median around 40rad/s. This design parameter is set to 41.8 rad/s. Lift at high altitude is harder to generate due to small density, which can be resolved to increase the velocity over the airfoil. This implies a relatively high rotational frequency.
- The number of blades should be between two and four. Since lift is harder to generate at high altitude due to small density , this design parameter is set to four blades per rotor.

With these parameters the chord ratio, rotor solidity, blade tip speed, Mach number at cruise speed and advance ratio at cruise speed was determined.

Chord Ratio The boundary conditions of this chord ratio are roughly set to 0.04 and 0.08. The chord ratio calculation is given in Equation 8.7, and is within boundary conditions.

$$\bar{c} = \frac{c}{R} = 0.048 \tag{8.7}$$

Rotor Solidity The boundary conditions of this characteristic are roughly set to 0.03 and 0.12. The rotor solidity is determined with Equation 8.4 and determined to be 0.12. This is at the limit of the upper boundary condition, which would suggest an over-designed rotor for sea-level conditions. However, the HAMRAC should be able to generate enough lift at extremely high altitude, which results in a higher radius and a higher chord, since the density is very low at extremely high altitude.

Blade Tip Speed The blade tip speed limit varies between 180 m/s and 220 m/s, since the blade tip speed is limited by the rotational frequency, the rotor length and the desired advance ratio and blade mach number. The blade tip speed is calculated using Equation 8.3 and determined to be 172.5 m/s. This is below the boundary conditions, which is due to the fact that the blade reaches Mach 0.85 faster at high altitude.

Mach Number (Blade Tip) at Cruise Speed In most cases a blade tip Mach number of 0.85 is used as a target value for the design. The boundaries are roughly set at 0.75 and 0.9. The Mach number at blade tip is calculated using Equation 8.2 and determined to be 0.86, which is at the upper boundary condition limit. This again proves the narrow design space for this extreme altitude, when comparing the upper boundary limit of the blade tip Mach number with the lower boundary limit of the rotational frequency of the rotor. The Mach number was also determined for the never exceeding speed conditions, which can be found in Table 8.2.

Advance Ratio at Cruise Speed The advance ratio is calculated using Equation 8.6 and determined to be 0.41. Normally a value of 0.3 can be defined as a good target, but since the rotor speed is relatively low for the given maximum take-off weight, the advance ratio is higher.

Method 2: 3 Rotor blades The same procedure was followed in order to determine the characteristics regarding three blades per rotor, as can be seen in Table 8.2.

8.1.4 Method 3

This method, which was used by J.A. Campfens [55], uses different sources related to conventional helicopters and verifies the applicability for coaxial rotorcrafts in order to develop a method for preliminary sizing of coaxial rotor crafts. This method is used to verify the first two methods and has been used as guide through the different steps in this design phase. This method approach is as follows:

- Evaluation of rotor diameter
- Evaluation of rotor tip speed in hover
- Evaluation of rotor solidity
- Evaluation of blade chord and number of blades

Rotor Diameter Using Equation 8.1 in combination with a disc loading of 20 kg/m^2, using figure 1 of Campfens [55], resulting in a radius of 4.46 m.

Rotor tip speed in hover Using Figure 5 of Campfens results in a rotor tip speed of 225 m/s, which provides a rotational frequency of 48.2 rad/s. The advance ratio then becomes 0.33, using Equation 8.6 and 8.3. The blade Mach number is 0.98, which is too high. This can be explained by the fact that figure 5 seems highly inaccurate.

Rotor solidity Using Equation 8.8 and the advance ratio and figure 7 of Campfens [55] results in a solidity of 0.12.

$$\sigma = \frac{DL}{\rho U^2} = 0.12 \tag{8.8}$$

Blade chord and number of blades As given in Campfens [55], the aspect ratio should be higher than 14 in order to achieve strong aerodynamic performance, and lower than 20 in order to limit structural mass. Using Equation 8.4, results in Table 8.1.

Table 8.1: *Number of blades and corresponding chord and aspect ratio*

N_B [-]	c [m]	A [-]
2	0.44	10.15
3	0.29	15.2
4	0.22	20.3

This means that according to Campfens [55], two blades per rotor almost exceeds the lower limit, and four exceeds the upper limit of the aspect ratio. The blade Mach numbers and advance ratio can be calculated using Equation 8.2, 8.3 and 8.6 which can be found in Table 8.2.

8.1.5 Results & Verification

The three different methods result in Table 8.2:

Table 8.2: *Results of Preliminary Sizing*

	Method 1	Method 2	Method 3
Disc Loading [kg/m^2]	20	20	20
Radius [m]	4.46	4.46	4.46
Chord (3 blades) [m]	0.304	0.304	0.293
Chord (4 blades) [m]	0.227	0.227	0.220
Solidity (3 blades) [-]	0.130	0.12	0.125
Solidity (4 Blades) [-]	0.130	0.12	0.125
Aspect Ratio (3 Blades) [-]	14.7	14.7	15.3
Aspect Ratio (4 Blades) [-]	19.6	19.6	20.3
Rotational Frequency [rad/s]	41.8	41.8	48.202
Thrust Coefficient [-]	0.007	0.009	0.009
Blade Mach (Cruise Speed) [-]	0.85	0.85	0.944
Blade Mach (Never Exceeding Speed) [-]	0.91	0.91	1.0
Advance ratio (Cruise Speed) [-]	0.39	0.39	0.34

As can be seen in Table 8.2 most of the parameters have an identical value for all the three methods. Since, the output of method 1 (chord and radius) was used as input for method 2, therefore it is very logical these values are identical. However, the third method uses different figures to determine the input (disc load), which results in a slightly different outcome. The difference will be elaborated on in the next paragraphs.

Rotational frequency The rotational frequency of the third method is greater than in method 1 and method 2, which is due to fact that Campfens [55] uses more inaccurate figures in comparison to Krenik [4] and Dr. M.D. Pavel [3]. This higher rotational frequency lead to a Mach number on the blade tips that exceeds the Mach limit constraint.

Aspect Ratio The aspect ratio for all the three methods is just above the lower limit of 14 with the 3-rotorblade configuration, the minimum aspect ratio needed for aerodynamic performance according to Campfens [55]. The aspect ratio is around the upper limit of 20 for all the three methods, the maximum aspect ratio allowed for structural performance [55]. Krenik [4], however, sets the statistical boundaries for the chord ratio, as determined in Equation 8.7, at 0.04 and 0.08. The inverse of the chord ratio is equal to the aspect ratio, which corresponds to statistical boundaries of 12.5 and 25.

Verification The use of three methods with almost the same outcome results in a direct verification of the initial sizing phase/method. The verification is even more convincing, since the differences are discussed and explained.

8.1.6 Determination of Number of Blades

With these boundaries for the aspect ratio in mind, both three and four blades are still optional. A further analysis regarding the number of blades per rotor will be performed. As can be seen in Figure 8.3, for the maximum take-off weight of 2500-2600 kg three blades tend to be the most common number of blades, however four is not directly excluded.

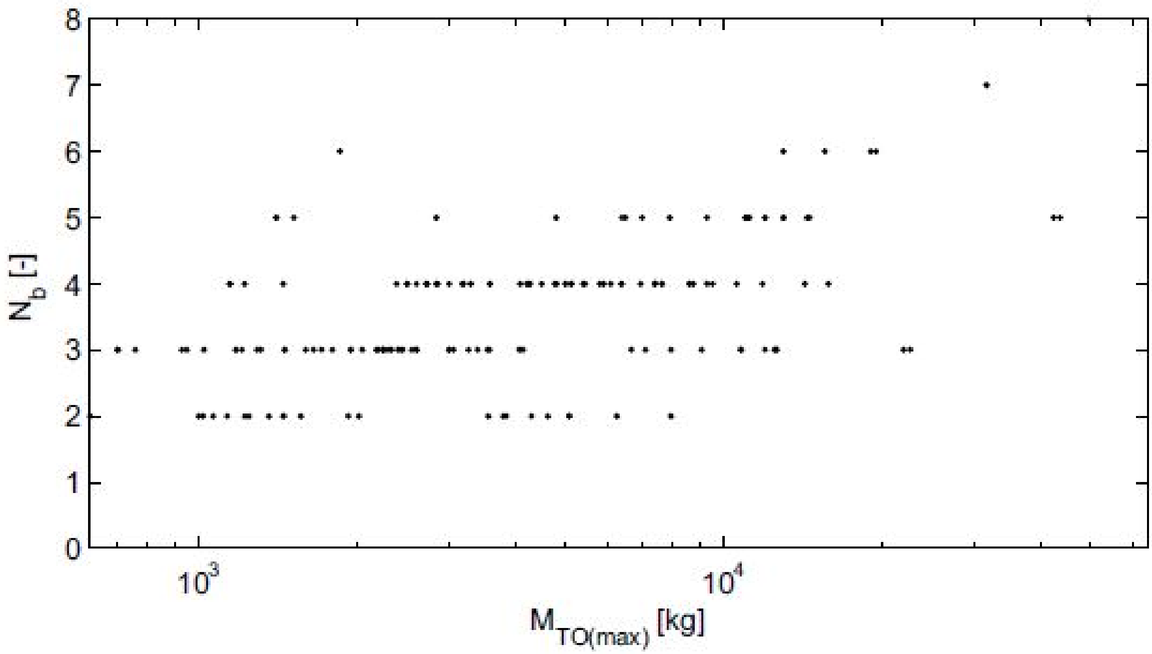

Figure 8.3: *Statistical representation of number of blades with respect to MTOW, from Krenik [4]*

Since statistics and general knowledge does not lead to a definitive conclusion, the weight per configuration is further investigated. The structures department has therefore conducted an investigation into which rotor system will lead to the largest mass, using a numerical model. The findings have been verified by an analytical model determined by the Performance and Aerodynamics department.

Analytical An initial analytical estimation for the maximum relative stress between a three and four blade rotor configuration is done. The three and four blade configurations will be referred to as case 1 and case 2 respectively. Several assumptions are made to perform this analysis:

- The height, y, of both blade profiles is equal.
- The rotor radii, R, are equal.
- A thin-walled blade profile is assumed
- The rotor can be modelled as an I-beam.
- Bending is the critical load condition
- The resultant lift force, L, acts at same location along the span of the blade in both cases.

The bending moment, M, for both cases is different, since the magnitude of the loading on each blade will differ. For case 1, it will be assumed the lift force is divided into three equal loads (since there are three blades), whereas in case 2 it is divided into four. Since the stresses for one blade is analysed, these should then be divided further by two, since one two rotors are present in a coaxial rotor system.

- 3 blades load on blade: $L/6$.
- 4 blades load on blade: $L/8$.

The moment equation is shown in Equation 8.9. Since, for both cases, the resultant force acts at the same position, for a relative stress comparison, the distance, d, is not further required in this analysis, and the bending moments, for each case are $\frac{L}{6}$ and $\frac{L}{8}$, respectively.

$$M = L \cdot d \tag{8.9}$$

To analyse bending stresses, the generic bending stress equation is used:

$$\sigma = \frac{M \cdot y}{I} \tag{8.10}$$

The maximum bending stress will occur at the region furthest from the neutral axis, so the stress will be analysed on the top flange. y is therefore defined as the distance from neutral axis to the furthest point (in y-direction) from the neutral axis. This is y_1 and y_2 for cases 1 and 2, respectively. The moment stress for case 1 then becomes:

$$\sigma_1 = \frac{\frac{L}{6} \cdot y_1}{I_1} \tag{8.11}$$

Where d is omitted. Given the thin-walled assumption, the moment of inertia for our modelled I-beam, for case 1 may be written as:

$$I = \frac{1}{12} * c_1 \cdot y_1^3 \tag{8.12}$$

Where c_1 is the cord length for case 1 blade profile. If we substitute the inertia, Equation 8.11 becomes:

$$\sigma_1 = \frac{\frac{L}{6} \cdot y_1}{\frac{1}{12} \cdot c_1 \cdot y_1^3} \tag{8.13}$$

Now, the chord lengths for case 1 and 2 respectively are assumed as $c_1 = 0.22$ m and $c_2 = 0.29$ m, as specified earlier in Table 8.1. And according to our structural department, the relation of profile height to cord length is specified as $0.12 \cdot c$ in subsection 9.2.1. A profile height of 2.64 and 3.48 cm is therefore used for case 1 and 2 respectively. Since, y corresponds to half the profile height, the ratio of stresses can be rewritten as shown in Equations 8.14 and 8.15.
The maximum bending stress for case 1, can now be re-written as:

$$\sigma_1 = \frac{\frac{L}{6} \cdot \frac{2.64 \cdot c_1}{2}}{\frac{1}{12} \cdot c_1 \cdot (\frac{2.62 \cdot c_1}{2})^3} = \frac{8 \cdot L}{2.64^2 \cdot c_1^3} [Pa] \tag{8.14}$$

$$\sigma_2 = \frac{48 \cdot L}{3.48^2 \cdot c_2^3} [Pa] \tag{8.15}$$

Through this analytic approach, it is found that a four blade rotor configuration leads to 1.51 times the maximum bending stress when compared to a three blade rotor configuration. For this reason, the three blade rotor configuration to be the best option when considering structural stress.

Numerical The structural department performed a numerical analysis regarding the number of rotor blades, which can be seen in subsection 9.2.1. This numerical analysis is a general numerical analysis of the weight of the rotor blades if the rotorsystem can cope with the bending stresses. This results in the conclusion that the weight with four blades is 34% higher than the weight with three blades.

Conclusion Based on the numerical analysis of the number of blades with regarding to the structural aspects of the HAMRAC, one can conclude that three rotor blades is the better option for this design, as concluded in subsection 9.2.1. This is verified by the conclusion of the analytical model, that the use of three blades per rotor results in a lighter subsystem mass. Therefore the final design will have three blades per rotor.

8.2 Rotor Blade Sizing

This section details the design of the rotor with respect to both the power requirements of the mission and the aerodynamics of the flight conditions. First, subsection 8.2.1 covers the statistical constraints that most rotorcraft are designed around, then subsection 8.2.2 will detail the multi-disciplinary method used and results obtained.

8.2.1 Statistical Constraints

Using literature and several sources regarding statistical data of typical rotorsystem characteristics, with respect to the maximum take-off weight of a rotorcraft, results in several statistical constraints. In order to reduce the design space, which results directly into less iterations being needed for the design optimization of this subsystem. The statistical constraints from section 8.1 can be expanded on from Krenik [4] and are given in Table 8.3:

Table 8.3: *Statistical boundaries for coaxial rotorcraft*

Constraint	Symbol	Unit	Minimum	Maximum
Blade chord	c	[m]	0.19	0.45
Rotor radius	R	[m]	3	7.5
Rotational frequency	Ω	[rad/s]	25	42
Number of blades	N_b	[-]	3	4
Aspect ratio	A	[-]	12.5	25
Solidity	σ	[-]	0.06	0.24
Blade loading	C_t/σ	[-]	0.07	0.1
Tip speed	V_{tip}	[m/s]	156	193
Advance Ratio	μ	[-]	0.25	4

8.2.2 Multidisciplinary Design Optimisation

Now that the initial sizing has been performed and verified, the optimisation phase can be initiated. This optimisation must be done in a multidisciplinary manner, as the design of the rotor is both dependent on the power requirements and the aerodynamic requirements of the mission. The architecture used to develop the multidisciplinary design is the collaborative optimisation as detailed by Martins and Lambe [58]. Collaborative optimisation has the advantage of being able to work in parallel by copying current design parameters to perform analysis by each discipline and then sharing the updates of the copies of the data.

Power Considerations To determine the power requirements of a rotorcraft, its preliminary power curve is generated, which is a graph of power required as a function of airspeed. The graph will first be calculated first for level, horizontal, forward flight, and then again for non-level, climbing, forward flight. It is comprised of four parts, given by dr. M.D. Pavel [22].

$$P_{t0} = P_i + P_{pd} + P_{par} + P_{cl} \tag{8.16}$$

The induced power, P_i, profile drag power, P_{pd} , and parasite drag power, P_{par} is given by Equation 8.17a, b, and c respectively. Power required to climb, P_{cl}, is zero in horizontal flight.

$$P_i = T \cdot v_i \tag{8.17a}$$

$$P_{pd} = \frac{\sigma C_{\overline{D,par}}}{8} \cdot \rho \cdot (\Omega R)^3 \cdot \pi R^2 \cdot (1+3\mu^2) \tag{8.17b}$$

$$P_{par} = 0.5 \sum (C_D \cdot S) \cdot \rho \cdot V_\infty^3 \tag{8.17c}$$

To perform the power calculations, the equivalent solidity single rotor approach (ESSRA) is used [30]. The ESSRA allows a coaxial rotorcraft to be analysed with the same approach as a conventional helicopter, which is the method given by dr. M.D. Pavel [22]. The ESSRA also tends to approximate the power requirements 5% higher than needed, indicating that the method will provide feasible, if only slightly over designed, results.

From the power curve, a few important values can be determined. These values are to be used when optimising the design of the HAMRAC and are as follows:

- $P_{t0,hov}$: Minimum power required to hover.
- P_{min}: The minimum power required for forward flight.
- $V_{p,min}$: The airspeed to flight at minimum power.
- V_{sfc}: The specific flight range airspeed closest to the design cruise speed of 140 kts.

- V_{max}: The maximum airspeed attainable according to installed power.

With the power curve for level, horizontal, forward flight determined, the power curve for non-level, horizontal, forward flight can be calculated by determining the rate of climb given by Filipe [31]. The tip path plane and airspeed of the rotorcraft can then be determined, which is used to determine power requirements from the same equations.

$$V_{cl} = 2 \cdot \frac{P_a - P_{TO}}{W} \tag{8.18}$$

$$\alpha_{TPP} = \frac{P_{excess} - P_{par}}{W \cdot V_\infty} \tag{8.19}$$

Parameter optimisation To perform the optimisation several different designs of the HAMRAC will be developed. These designs will be optimised for different conditions and with respect to different design parameters. The conditions that will be optimised for are as follows:

- P_hov: Minimum power required to hover.
- V_{cl}: Maximum rate of climb.
- V_{sfc}: The specific flight range airspeed closest to the design cruise speed of 140 kts.

The design parameters used for the optimisation are as follows:

- R: Radius of the rotor
- c: Chord of the rotor
- Ω: Angular velocity of the rotor

This process will generate a total of nine designs. Each of these designs will then be evaluated in a brief trade-off with respect to budget constraints. This is done to evaluate how sensitive the design will be with respect to the design parameters, as to allow the designer to predict how the results will change as the parameters are changed when optimising [58]. The design can then be iterated on, to try to find a 'middle ground' between optimising for two parameters, instead of optimising for just one. This is done by fixing the more sensitive design parameter and altering two of the less sensitive ones. This will generate more designs that have more desired results for P_hov, V_{cl}, and V_{sfr}.

With each design, the performance characteristics can be determined from the power curve associated with that design. The performance characteristics that can be determined are given in subsection 8.2.2. These performance characteristics indicate to the designers how well that particular design is expected to perform with respect to specific requirements. A V_{sfc} close to 140kts is desirable to meet the V_{cr} requirement of 140kts, as it indicates that the HAMRAC will be able to fly further, as V_{sfc} is an indicator of maximum range. Due to constraints for V_{max} and V_{NE}, the sizing of the engine can be done with respect to maximum airspeed, V_C, as V_C should be close to, but not below, V_{max} required, as the HAMRAC will not be allowed to fly above its V_{max} value, and so a V_C that is much above V_{max} indicates that the engine is over-designed or that it is likely to be too heavy, as engine mass scales proportionally with engine power available.

Design Space Once different designs for the HAMRAC are generated, the different parameters are compared to each other to check their compatibility with reference data. This is done with the use of a design space, as shown Figures 8.4 and 8.5. The design space for the HAMRAC was generated by comparing statistical data to determine general maximum and minimum values used in rotorcraft design to predict the design space for a rotorcraft operating under the conditions that the HAMRAC is to operate in, specifically its configuration, blade number, weight, and maximum operating altitude. This was done by calculating allowable values for the design parameters to the maximum and minimum boundaries given in Table 8.3. The boundaries used to determine the design space of the HAMRAC are solidity, advance ratio, aspect ratio, and tip speed. The resultant design space is two 2-D graphs with overlapping boxes indicating which values of R, c, and Ω are feasible for the HAMRAC. The use of this design space is to not only check that the values given in the optimisation procedures are within allowable constraints, but also to check the compatibility of the chosen parameters with each other.

To further refine the design, the blade loading was used to optimise the design for cruise and climb at 1402m from the international airport, the cruise and climb at 3930m to 6200m for refuelling and the cruise and climb from the refuelling at 3930m to 8950m, the hover at 8950m. However, an analysis of the blade loading demonstrated that it is impossible for any single rotor configuration to meet the required mission profile. Therefore, the angular velocity of the HAMRAC will be changed mid-mission. This change will be a discrete change, and will occur during refuelling, when the HAMRAC is on the ground. This will be done through the use of a gearbox system, disengaging the main rotor transmission for low altitude to engage the main rotor transmission for high altitude for outgoing flight, and vice versa for returning flight. The 'low altitude operation' will consist of the take-off from the international airport, the cruise at 3930m, the climb to 6200m to pass over the mountain range, and the descent to the refuelling station at 3780m. The 'high altitude operation' will consist of the take-off from the refuelling station at 3780m, to the maximum required altitude for rescue operation at 8950m, and then the return to the refuelling station, where low altitude will commence to finish the mission.

The low altitude angular velocity, Ω_{low} will be chosen to meet requirements for take-off, cruise, climb, and descent operations between 1402m and 6200m, and the high altitude angular velocity, Ω_{high}, will be chosen to meet requirements for take-off, cruise, climb, and descent operations between 3780m and 8950m.

Finally, to ensure that the design chosen is feasible, the design parameters are checked against aerodynamic constraints. This is done last as the aerodynamic constraints do not constrain the design of the HAMRAC, but do limit its operation, and therefore the different operating conditions of the HAMRAC are used to check that the design is feasible under all design conditions. The aerodynamic constraints used to check the feasibility of the design are the tip Mach number, the advance ratio, and the blade loading. If it is found that the chosen design is not feasible, then the parameters for that design will be altered to make it feasible while retaining the intent of the design, using the sensitivity analysis. Once the design has been checked for feasibility, the model can be updated with the new, updated numbers, and then the method can be reiterated on.

Alterations During the first iteration, it was found that some of the statistical boundaries did not accurately reflect the design space of the HAMRAC. The tip speed statistics taken from literature included both low altitude and medium altitude, whereas the altitude requirement of the HAMRAC is higher than the statistics. This problem was identified when the tip Mach number could not be met in more cases of the given statistics, indicating that the statistics used were not valid for this design. For future iterations, the tip speed statistic has been changed to meet the tip Mach number constraint.

Additionally, it was found that the solidity of the rotor was not accurate. The solidity constraints given in literature were for single rotor configurations, and the ESSRA was not applicable to this statistic, as the statistics were based on feasibility and practicality of rotor dynamics. Additionally, Coleman [30] used solidity of each rotor to compare different designs and based the solidity (per rotor) on the given statistical constraints. Therefore, the solidity constraint was changed to be solidity per rotor, instead of equivalent solidity. These changes (after the tip speed statistic and solidity were changed) are shown in Table 8.4. This decrease in power required to hover resulted in another engine to be feasible for consideration.

For the second iteration, the blade loading was considered more thoroughly, and it was found that this limit was impossible to meet with any single configuration. This is because the altitude difference results in a density range that is (relatively) larger than the allowable blade loading range; the maximum density is 2.2 times that of the minimum density, whereas the maximum blade loading is 1.7 times that of the minimum blade loading, and Equation 8.20 illustrates that the blade loading is (inversely) proportional to the ambient density.

$$\frac{C_T}{\sigma} = \frac{T}{\rho \cdot A_b \cdot (\Omega R)^2} \tag{8.20}$$

Typically, the design blade loading for helicopter operations is between 0.07 and 0.1 [78]. This is to prevent both advancing blade stall when the blade loading is too high, and retreating blade stall when the blade loading is too low. If the blade loading is too high, then the air will be too dense for the rotor to catch to generate lift, and the rotorcraft will stall. If the blade loading is too low, then the blades will not be able to generate enough lift with the air that does pass through the blades, and the rotorcraft will also stall. To avoid advancing blade stall due to blade loading, the maximum allowable blade loading is 0.12, given by Leishman [64].

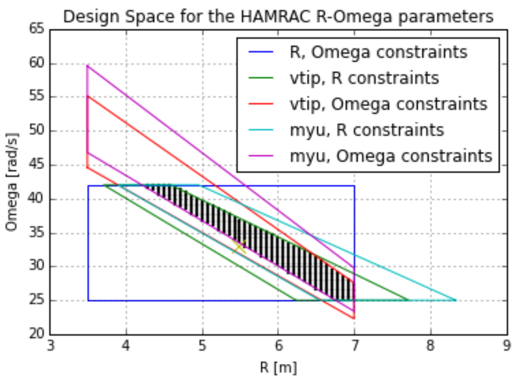

Figure 8.4: *Radius-Omega design space*

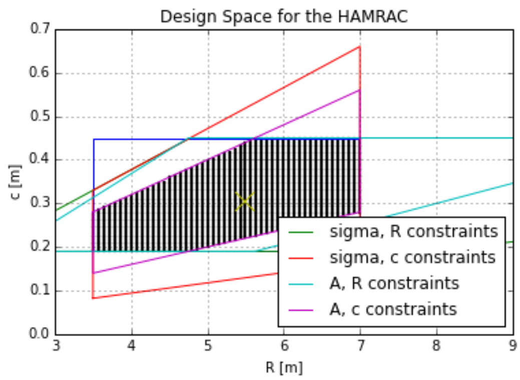

Figure 8.5: *Radius-chord design space*

Minimum values for blade stall are not given in literature, only design minimum values. Therefore, it will be assumed that there is a similar region between the typical, lower design value and the allowable minimum. This allowable minimum will be estimated at 0.6, as it is expected that the range between the allowable minimum and typical design minimum will be similar to the allowable maximum and typical design maximum, but will also be a conservative estimate due to the limited amount of literature on the phenomena.

If a constant angular velocity was taken, then the lower limit of the blade loading would occur during take-off from the international airport with a value of 0.0456. This value was deemed unacceptable, as it is 34% below the typical design minimum. As the maximum allowable value is only 20% above the maximum typical design value, retreating blade stall is expected to occur at such low values.

Additionally, the cruise speeds for the HAMRAC have been changed during this optimisation in order to more accurately represent the mission profile and to more accurately meet the blade loading constraint. It was decided to allow the HAMRAC to fly faster at its cruise by lowering the angular velocity for low altitude flight, and then to restrict the airspeed at high altitude. This requires the pilot to be aware of this high altitude maximum airspeed.

Results The design space for MDO of the HAMRAC is shown in Figures 8.4 and 8.5. The results of the first redesign optimisation are shown in Table 8.4, the results of the second redesign optimisation are shown in Table 8.5, and the final check with the results given in section 9.2.

Table 8.4: *First optimisation results*

Parameter	Unit	Initial Design Value	2nd Design Value	Percent Change %
$\mathbf{P_{hov}}$	**[kW]**	423	400	5.75
R	**[m]**	4.46	5.55	23
c	**[m]**	0.227	0.304	34
Ω	**[rad/s]**	41	33	-19

Table 8.5: *Second optimisation results*

Parameter	Unit	2nd Design Value	3rd Design Value	Percent Change %
$\mathbf{P_{hov}}$	**[kW]**	400	359	-10.25
R	**[m]**	5.55	5.5	1
c	**[m]**	0.304	0.36	18.4
Ω	**[rad/s]**	33	35	6

Table 8.6: *Third optimisation results*

Parameter	Unit	3rd Design Value	4th Design Value	Percent Change %
$\mathbf{P_{hov}}$	**[kW]**	359	362	0.8
R	**[m]**	5.5	5.5	0
c	**[m]**	0.36	0.4	11.1
Ω	**[rad/s]**	35	33	-5.7

8.3 Airfoil Design

After the preliminary sizing of the rotor system had been selected, the next step was to determine the airfoil design in more detail. In order to do this, a new literature research was performed to define a new set of subsystem requirements for the rotor blade itself. The requirements are explained briefly, before they are analysed numerically. After the numerical analysis, the possible performance of the airfoils was evaluated and finally the rotor blade design was determined.

8.3.1 Airfoil Requirements

The general requirements for a ‘good’ helicopter rotor airfoil for a conventional helicopter [64]. This was combined with two articles [62] [86] which are more in depth regarding values for certain Mach numbers and resulted in the following subsystem requirements, which will be discussed briefly in this subsection:

- **[SYS-RTR-117/1-C:PER]** The maximum lift coefficient shall be higher than 1.4 at a Mach number of 0.4 at cruise conditions.
- **[SYS-RTR-118/1-C:PER]** The maximum lift coefficient shall be higher than 1.2 at a Mach number of 0.5 at cruise conditions.
- **[SYS-RTR-119/1-C:PER]** The drag divergence number at zero-lift coefficient shall be higher than 0.70 at cruise conditions.
- **[SYS-RTR-120/1-C:PER]** The pitching moment shall be lower than -0.015 at the drag divergence Mach number at cruise conditions.
- **[SYS-RTR-121/1-C:PER]** The pitching moment shall be equal than +/-0.01 or closer to 0 at a Mach number between 0.2 and 0.5 when the lift coefficient is zero.
- **[SYS-RTR-122/1-C:PER]** Value of lift over drag ratio (L/D) shall be at least 100 at Mach 0.6 with the lift coefficient varying between 0.6 and 0.7 at cruise conditions.

[SYS-RTR-117/1-C:PER] This requirement is crucial for the performance of the inner part of the rotor blade, which is from 0 to 1.6m from the rotor hub. At 1.6m from the hub, Mach 0.4 is reached during forward flight at cruise altitude. In order to delay stall at the retreating blade and to decrease vibrations at high flight speeds, a high value of the lift coefficient is needed. Minimum required values of the maximum lift coefficient varies between 1.4 according to Noonan [62] and 1.6, as requirement for to-be developed airfoils according to Kania [86]. Although Noonan is the older source, a value of 1.4 should be a good starting point. For the final design choice, a particular airfoil was not considered for this section if this requirement was not met. The highest value of the lift coefficient was the best fitted airfoil for this part of the rotor blade.

[SYS-RTR-117/1-C:PER] This requirement is crucial for the performance of the outer part (1.7-4.4m) of the rotor blade. At 2.7m from the rotor hub, Mach 0.5 is reached during forward flight at cruise altitude. The reasons for this are the same as for [SYS-RTR-117/1-C:PER]. According to Noonan [62] a value of 1.2 should be the minimum. The higher the lift coefficient at this Mach number the better a certain airfoil performs with respect to this requirement.

[SYS-RTR-117/1-C:PER] The drag divergence Mach number is the Mach number where the drag coefficient increases drastically for a small increase in the Mach number. The higher the drag divergence Mach number the better this airfoil performs over the length of the rotor blade. This requirement is the most important requirement for the design of the outer part of the blade. According to Noonan [62] the drag divergence number should be at least 0.7, which coincides with the blade tip Mach number at the cruise conditions. For the highest altitude with a forward speed of 55 m/s, the blade tip Mach number will reach Mach 0.82. Therefore, airfoils with a drag divergence number less than 0.7 were not considered for the design choice. A drag divergence number equal or higher than 0.7 was an indicator to what extend this airfoil could be used along the span.

[SYS-RTR-117/1-C:PER] At the drag divergence Mach number the pitching moment should be negative in order to cope with the momentum that is generated due to the increase in drag. According to Noonan [62] this value should be at least -0.015 or lower. Therefore, an airfoil that does not meet this requirement was not considered for this part of the rotor blade.

[SYS-RTR-117/1-C:PER] An important requirement for the airfoil design is the near zero pitching moment at zero-lift, for Mach numbers between 0.3 and 0.5,- in order to have pitch-link loads and blade torsion loads that are as low as possible [62]. This same requirement is also beneficial for decreasing the loads for the control system and for reducing the blade twist [86]. Airfoils that did not meet this requirement were not considered for this part of the rotor blade.

[SYS-RTR-117/1-C:PER] In order to decrease the power that is necessary for hovering at altitude and to improve the hover efficiency, the lift over drag ratio should be as high as possible at Mach 0.6. In addition, the lift coefficient should be between 0.6 and 0.7 at cruise conditions [86]. Since all literature focuses only on the conditions at sea-level, for this project the lift over drag ratio at the highest operational hover altitude were taken into account as well.

8.3.2 Method

The first thing to do is to determine the possible airfoils that are possible for the rotor design. With the use of Leishman [64] a set of 11 modern airfoils were found, which will be discussed in subsection 8.3.3. The next step was to perform a numerical analysis on each of the airfoils in order to determine which airfoil meets the requirements for this mission. For this numerical analysis some initial parameters had to be determined, which are typical for the given cruise and hover altitudes. Finally, the numerical analysis leads to evaluation of each airfoil regarding the requirements. Based on that evaluation the final design of the rotor blades was determined.

8.3.3 Considered Airfoils

There are several airfoils that were optional for this rotor system, which will be discussed briefly.

NACA0012 This symmetrical airfoil was the most popular design choice for the early helicopters. These airfoils have a low pitching moment about the quarter chord and a good low speed as well as good high-speed performance, resulting in a relatively high maximum lift and a relatively high drag divergence Mach number [64].

NACA23012 This cambered airfoil has been used as baseline for many modern helicopter airfoil sections. This airfoil develops a high maximum lift and a low profile drag. In addition, the pitching-moment coefficient is very small compared to the NACA0012 [57].

VR Series These airfoils are developed by Boeing (Vertol) and are designed to represent the best compromise regarding maximum lift capability at the lower Mach numbers at the retreating blade while maximizing the drag divergence Mach number, meeting hover requirements and control load limitations. These characteristics are mostly represented by the **VR-12** and **VR-15** [64]. For the design of the rotor blade the **VR7**, **VR12**, **VR14** and **VR15** were evaluated.

OA-Family These airfoils are developed by ONERA following the same recipe to design an airfoil with a high maximum lift coefficient at low Mach numbers and a high drag divergence Mach number. The OA-206 is a thin supercritical-like airfoil, with a high drag divergence Mach number and, potentially, a large improvement in advancing blade performance. The OA-209 is a compromise between advancing and retreating blade requirements, with maximum lift coefficient characteristics similar to the NACA0012 while having an increase in drag divergence Mach number [64]. For the design of the rotor blade **OA206**, **OA209**, **OA212**, **OA213** were evaluated.

8.3.4 Numerical Analysis

For the numerical analysis of the airfoils the widely-used software of XFoil[6] was used. The following input was used for XFoil:

- The chord was set to 0.304m.
- The cruise altitude was set to be 3930m.
- The density at cruise altitude was set to be 0.825 kg/m^3.
- The dynamic viscosity[7] was set to be $1.68*10^{-5}$ $kg/m \cdot s$.
- The temperature at cruise altitude was set to be $-10.5\,°C$
- The speed of sound at cruise altitude was set to be 324.86 m/s.
- The rotational frequency at cruise altitude was set to be 28 rad/s.

XFoil also needed the Reynolds number in order to analyse the airfoils. The following equation was used to determine the Reynolds number:

$$Re = \frac{\rho \cdot v \cdot c}{\mu} \tag{8.21}$$

where ρ is the density, V is the velocity of the airflow, c is the chord and μ is the dynamic viscosity of the air (at altitude). The leads to the following Reynolds number for every Mach number at cruise conditions:

Table 8.7: *Reynolds Number at different Mach values*

Mach	Reynolds 10^6 [-]
0.40	2.8
0.50	3.7
0.60	4.7
0.65	5.2
0.70	5.7
0.76	6.2
0.80	6.7
0.85	7.2

Maximum lift coefficient at Mach = 0.4 and Mach = 0.5 The maximum lift coefficient could be easily found with the use of XFoil. The results can be seen in Table 8.8.

Table 8.8: *Maximum lift coefficient for variable Mach numbers*

Airfoil	$C_{L_{max}}$ (M=0.4)	$C_{L_{max}}$ (M=0.5)
NACA0012	1.29	1.14
NACA23012	1.54	1.49
NACA23015	1.57	1.57
VR7	1.38	1.37
VR12	1.62	1.63
VR14	1.43	1.35
VR15	1.32	1.27
OA206	0.95	0.91
OA209	1.54	1.44
OA212	1.40	1.35
OA213	1.55	1.54

Drag Divergence Number The drag divergence number could not be easily found with the use of XFoil. In order to determine the drag divergence number, the drag coefficient at zero-lift was determined separately for every Mach number. These drag coefficients with respect to the Mach number can be seen in Figure 8.6,

[6] URL `https://web.mit.edu/drela/Public/web/xfoil/` [cited 15 January 2019]
[7] UL `https://www.engineeringtoolbox.com/dry-air-properties-d_973.html` [cited 15 January 2019]

where the intersection of the curves of the airfoils with the value of 0.0115 is used as value for the drag divergence Mach number.

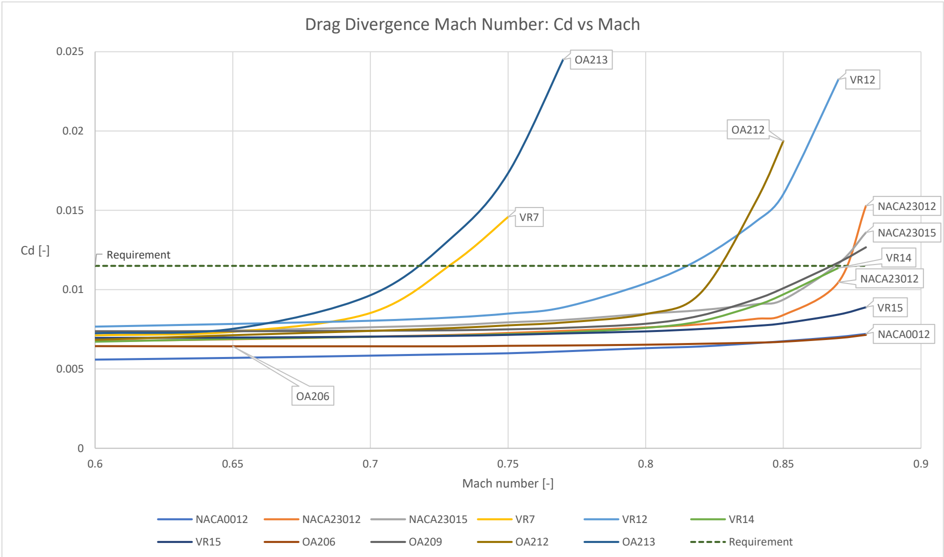

Figure 8.6: *Drag divergence Mach number*

Pitching Moment (at drag divergence Mach number) The pitching moment over the whole range of Mach numbers was determined in the same manner as the drag divergence number. The results can be seen in Figure 8.7, where the value of -0.015 is dashed, which is the required value at the drag divergence number:

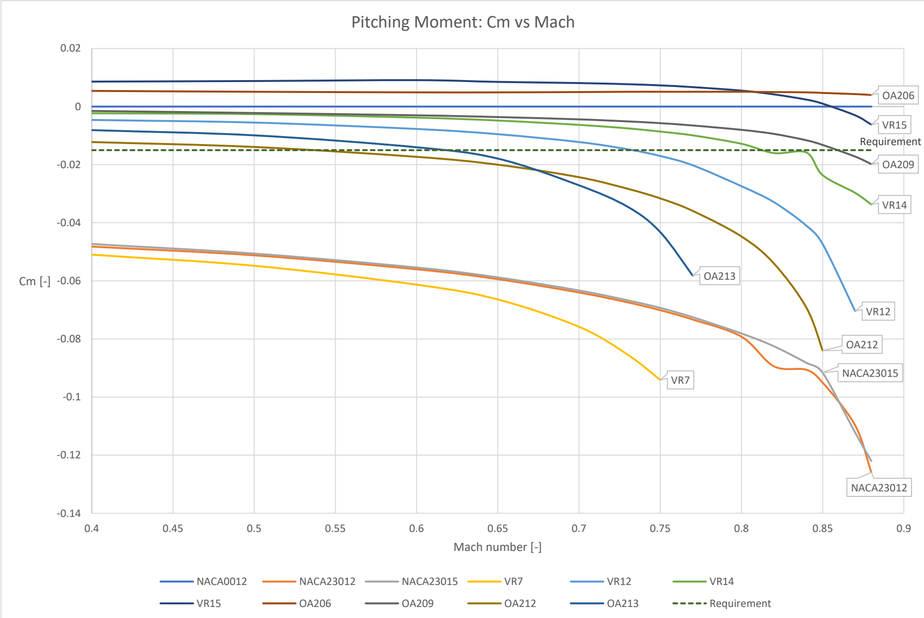

Figure 8.7: *Pitching moment at cruise altitude*

Lift over drag ratio for Mach 0.6 with lift coefficient varying between 0.6 and 0.7 Since this requirement is specific for the hover performance, it was important to determine the lift over drag ratio for the cruise altitude and for the highest altitude. These two values together determined the best airfoil for this requirement. Using XFoil, the conclusion was drawn that the maximum lift over drag ratio with the lift coefficient in the range of 0.6 to 0.7, was found to increase linearly. Therefore, only the values for the lift coefficient of 0.7 are presented for both the highest and cruise altitudes. Note that the forward speed at the highest altitude (8950m) is 55m/s, which changes the Reynolds number input for XFoil. The results can be found in Table 8.9, together with a performance difference between the two altitudes:

Table 8.9: *Lift over drag ratio (lift coefficient = 0.7, Mach = 0.6)*

Airfoil	3987m	8950m	Performance Difference
NACA0012	90.67	84.96	−6%
NACA23012	121.08	115.87	−4%
NACA23015	107.43	100.87	−6%
VR7	127.62	122.98	−4%
VR12	101.68	92.92	−9%
VR14	112.29	105.16	−6%
VR15	109.04	100.22	−8%
OA206	92.01	83.72	−9%
OA209	104.86	101.46	−3%
OA212	103.96	95.7	−8%
OA213	99.2	90.21	−9%

8.3.5 Evaluation

As can be seen in Table 8.10, the logical statement was made that there is simply not one airfoil that will perform the best overall. A trade-off could be performed, but it is more common to divide the rotor blade in several sections, divided by Mach numbers over the length of the rotor blade.

Table 8.10: *Evaluation of airfoils*

Airfoil	C_L @ 0.4	C_L @ 0.5	M_{dd}	CM @ M_{dd}	CM @ low M	L/D
NACA0012	1.29	NA	>0.87	0	0	90.67
NACA23012	1.5373	1.4896	0.86	-0.11	-0.0482	121.08
NACA23015	1.5693	1.5694	0.86	-0.11	-0.0473	107.43
VR7	1.3772	NA	0.73	-0.09	-0.05098	127.62
VR12	1.62	1.63	0.82	-0.03	-0.0046	101.68
VR14	1.43	1.35	0.86	-0.03	-0.0015	112.3
VR15	1.32	NA	>0.87	<0.01	0.0086	109.04
OA206	0.95	NA	>0.87	0.01	0.0054	92.01
OA209	1.54	1.44	0.86	-0.015	-0.0015	104.86
OA212	1.4	1.35	0.83	-0.05	-0.0122	103.96
OA213	1.53	1.53	0.72	-0.03	-0.0081	99.2

Mach 0.3 to 0.5 As can be seen the VR12 has the highest maximum lift coefficient for Mach 0.4 and 0.5. The second requirement is the nearly zero moment coefficient which also still applies for the VR12. At cruise altitude this section corresponds from 0 to 3.2m, which is 58% of the rotor blade length.

Mach 0.6 As can be seen in the graph for the pitching moment, the only profiles that are still having a nearly zero pitching moment are the VR12, OA209, OA206 and VR14 and VR15. Since the VR12 is already decreasing the pitching moment with increasing Mach number at Mach 0.6, a change in airfoil is necessary around this Mach number. A good estimate for a better profile at a Mach number of 0.6 is the maximum lift over drag ratio. VR14 has the highest lift over drag, so this would be the best option for this section. Mach 0.6 corresponds to $4.4m$, which corresponds to 80% of the rotor blade length.

Mach 0.6 and beyond As can be seen in the drag divergence and pitching moment graph, VR14 performs best together with OA206, regarding the pitching moment. At the drag divergence Mach number of 0.86, VR14 is less than -0.015, which proves that this is the best option for the tip. Mach 0.6 and beyond corresponds to the length of $4.4m$ and the tip of 5.5m or 80% to 100% of the rotor blade length.

8.3.6 Sections Design

After the evaluation of the airfoils for particular Mach numbers, the sections phase started. In this part, the airfoil per section was determined, and was optimised for twist and taper. The final design parameters were summarised and can be found in Table 8.14.

Airfoil Selection As can be seen in Table 8.10, and later described for the multiple Mach numbers, a combination of VR12 and VR14 was determined to be the best solution for the rotor blade. From 0-4.4 m (0R-0.8R) VR12 was determined to be the best solution. From 4.4-5.5 m (0.8R-1R) was VR14 was determined to be the best solution.

Taper The taper was determined by optimising the baseline airfoil for maximum lift with minimal power required, which is equal to the maximal lift over drag ratio. The angles for these sections can be found using XFoil. For the taper, according to Leishman [64], taper reduces the profile power, which lead to the fact that the rotor can be operated at the same thrust with in improved figure of merit. These factors ultimately lead to a higher stall margin and thus a higher possible collective pitch, higher attainable rotor thrust and better overall hover efficiency. In order to check whether the performance of the rectangular rotor will decrease in performance the VR12 was used to check the drag coefficient and moment coefficient between Mach 0.8 and Mach 0.85 for a chord of 0.304 and 0.25m. These results can be found in Table 8.11:

Table 8.11: *Performance of airfoil with variable chord length*

VR12	M	C_d	C_m	D_{cd}/D_{Mach}	D_Cm/D_{Mach}
c=0.304	0.8	0.01051	-0.0276		
c=0.304	0.85	0.0162	-0.0476	11%	-40%
c=0.25	0.8	0.01091	-0.0284		
c=0.25	0.85	0.01674	-0.0483	12%	-40%

As can be seen, the drag divergence gradient increases only 1% and the moment coefficient remains the same. Therefore, introducing taper will not change the performance of the rectangular rotor blade too much. In order to keep things simple a taper ratio of 2:1 was introduced, which resulted in a chord of 46 cm at the root and 23 cm at the tip. All the chord length over the length of the rotor blade can be found in Table 8.14.

Twist Introducing the proper twist results in a redistribution of the lift over the blade, which reduces the induced power. This directly relates to an improvement of the figure of merit [64]. Blades with very large twist are beneficial for the hovering performance but suffer a reduced cruise performance and vice versa [64]. In order to find the optimum twist, one should optimise the twist for the minimum hover power, while not degrading the forward flight. There are several different ways to introduce the twist of the blade. Linear, quadratic and two linear with multiple airfoils are just a grasp of those [65]. Since the optimizing for minimum hover power is a time consuming process, which is beyond the scope of this project. A linear basic twist already increases the overall performance of the rotor blade. Most helicopter blade use a twist between 8 and 15 degrees [64]. A study shows that two sections with linear twist with two different airfoils result in a 2.2% reduction of power, while linear twist reduces the power with 1.3% if the optimisation is done correctly [65]. Optimising for minimum power at this stage was too advanced, since it requires to combine the MDO for power with XFoil. Therefore, in order to simplify this process the configuration was evaluated for two optimisation scenarios, namely the hover and cruise at cruise altitude, before the twist was determined. For the hover scenario the maximum lift coefficient over the rotor blade was leading for the twist and for cruise the maximum lift over drag ratio was leading for the twist. These can be seen in Table 8.12 and Table 8.13, where the rotor length sections were determined by the Mach number over the blade:

Table 8.12: *Twist optimised for 150kts at 8950m: Optimisation for C_L/C_D*

Dimensionless Radius r/R [-]	Airfoil	Mach	Re	$\frac{C_L}{C_D}_{max}$	$\alpha°$	C_L	C_D	C_M
0.182	VR12	0.3	1.9	113.5	7.6	1.13	0.00998	-0.0219
0.382	VR12	0.4	2.8	121.7	8.2	1.27	0.01047	-0.0169
0.582	VR12	0.5	3.7	125.3	8	1.35	0.01076	-0.009
0.8	VR14	0.6	4.7	128.8	5.1	0.95	0.00736	-0.0068
1	VR14	0.7	5.6	136.82	4.9	1.06	0.00779	0.0031

Table 8.13: *Twist optimised for hover at 3930 altitude*

Radius [m]	Airfoil	Mach	Re	$\frac{C_L}{C_D}$	$\alpha°$	$C_{L_{max}}$	C_D	C_M
0.182	VR12	0.3	1.9	47	15	1.6	0.03397	0.0353
0.382	VR12	0.4	2.8	49	14.1	1.62	0.0331	0.0455
0.582	VR12	0.5	3.7	61	12.2	1.6307	0.02672	0.054
0.8	VR14	0.6	4.7	81	7.6	1.3019	0.0164	0.0221
1	VR14	0.7	5.6	90	5.9	1.2523	0.01387	0.0172

One can conclude that for cruise the angles are roughly around 8 degrees for the inner part and varies between 15 and 12 degrees for the hover performance. Since the inner part of the blade is very important for the hover performance, the angle was set at 15 degrees for 1 m of the radius and linearly twisted to 13 degree at 3.2 m. This will not affect the cruise performance too much, since the optimised angle for this part is roughly constant at 8 degrees. For the second section (4.4-5.5 m) the cruise performance becomes more important. Therefore, the angles were set to 9 and 7.5 degrees for the last two sections. This will not influence the hover performance too much since the difference in angle between the VR12 and VR14 airfoil should be -3 degree for hover performance, which is -4 degree at the moment. This results in the following final twist distribution over the rotor blade length, which can be seen in Table 8.14.

Tip Shape The tips of the blades play a very important role in the aerodynamic performance of the rotor, since they encounter the highest dynamic pressure and highest Mach numbers, which can produce strong trailed tip vortices [64]. These vortices produce the most noise for a coaxial configuration. Since the blade Mach number at the tip is 0.7 at cruise altitude and 0.8 at high altitude in forward motion, the tip is less crucial than conventional helicopter. Since taper was already introduced the tip would have a tapered tip already, therefore there was no need to further introduce an additional tip shape. The tip is classified as a long tapered tip [64], as can be seen in Figure 8.8.

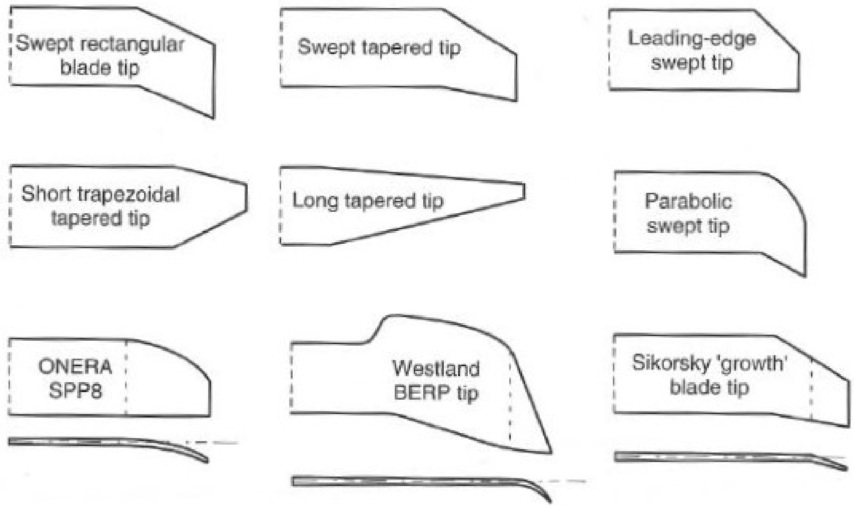

Figure 8.8: *Different tip shapes for helicopter blades*

Final Rotor Blade Dimensions All the airfoils, dimensions and angles of the rotor blade can be found in Table 8.14:

Table 8.14: *Rotor blade dimensions*

Radius [m]	Airfoil	Chord [m]	Angle [°]
0.6	VR12	0.435	15.5
1	VR12	0.418	15
2.1	VR12	0.372	14
3.2	VR12	0.326	13
4.4	VR14	0.276	9
5.5	VR14	0.230	7.5

8.4 Fuselage & Additional Aerodynamic Considerations

The fuselage is the largest part of the helicopter, and thus it has a significant impact on its aerodynamic performance. The fuselage and attachments should be designed in a streamlined manner to make the HAMRAC as aerodynamically efficient as possible. To do this, in this section different kinds of drag are analysed. Then the fuselage shape will be analysed for minimum drag and a rough drag estimate will be calculated. After the design of the fuselage is analysed, the rotor hub will be further analysed, where the rotor spacing is considered and fairings will be added to minimize the parasite drag. Finally, a decision will be made on the landing gear for the HAMRAC.

8.4.1 Drag Factors Identification

Since a rotorcraft can perform a large variety of operations with respect to an airplane, the drag can come from different angles. Whilst the drag types can occur at the same time, for simplification purposes they are

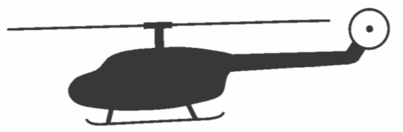

Figure 8.9: *Unstreamlined fuselage with large upsweep angle [64]*

Figure 8.10: *Streamlined fuselage with small upsweep angle [64]*

analysed independently. In reality, they may behave differently resulting in a reduced overall performance of the rotorcraft. In this section, only the parasitic drag caused by the non-lifting parts such as the fuselage and attachments are covered. Profile drag, due to the blades moving through the air, and induced drag, due to the orientation of the blades creating lift in the opposite direction of the movement will not be considered.

Horizontal Pressure Drag When the rotorcraft is moving forward the fuselage will experience drag in the opposite direction of the movement. This type of drag is relatively high compared to airplanes with the similar weight. The main reason for this is the contribution of the rotor shaft and hub. This can account for 30% or more of the total parasitic drag [64]. The other main contributor is the fuselage rear, which accounts for 20% or more of the total parasitic drag. This is due to flow separation, which occurs at the point where the fuselage and the tail are connected. High upsweep angles of the fuselage rear can result in large drag [64], because it results in early flow separation. This will lead to a high pressure at the front and a low pressure at the rear of the fuselage. The rear should have a more circular than square shape to delay the flow separation, and thereby reduce the drag. The aft shape of the helicopter is highly dependent on the mission. In Figure 8.9 an unstreamlined helicopter can be seen. The fuselage rear has a large upsweep angle increasing the horizontal pressure drag with respect to the streamlined helicopter with a small upsweep angle in Figure 8.10 [26]. On the top of the rotorcraft, a fairing should be placed to reduce the drag of the rotor shaft. This is not only beneficial for reducing the drag, but the air reaching the tail with control surfaces will be less turbulent. As a result, effectiveness of these surfaces is increased.

As mentioned in section 8.3 the Reynolds number at altitude is lower because the air is thin. This can be seen in Equation 8.22, where ρ is the density, L is the characteristic length, and V and μ are the velocity and the dynamic viscosity of the air, respectively. The flow tends to separate earlier at low Reynolds numbers. At high altitude the Reynolds number will be lower. To increase the Reynolds number, and thus delay flow separation at the rear of the helicopter, the length of the fuselage should be increased.

$$\mathrm{Re} = \frac{\rho \cdot L \cdot V}{\mu} \tag{8.22}$$

Viscous Drag To reduce the parasitic drag the fuselage length should increase. However, the rear of the fuselage should not increase by too much because more surface will result in more viscous drag. The friction between the air and the surface will increase with lower Reynolds number. The pressure drag varies with the square of the flow speed, where the viscous drag varies linear with the flow speed, which indicates the relative importance of the two when increasing airspeed.

Vertical Pressure Drag During hover it was assumed that the thrust is equal to the weight. However, because of the downwash creating vertical drag on the fuselage, more thrust needs to be provided. Typically, this can lead up to 5% of the aircraft weight for rotorcraft in case there are no extra wings attached [64]. To reduce the vertical drag as much as possible, the rotor should have a large spacing with the fuselage. However, the impact on the performance of the horizontal pressure drag of the rotor shaft is larger than the extra thrust that needs to be provided due to the downwash on the fuselage. Therefore, the lower rotor will be placed as close as possible to the fuselage such that the shaft under the lowest rotor won't be in the freestream during cruise.

Fuselage Side-Force When a rotorcraft is flying to the left or right a side-force will occur. Since conventional helicopters have a horizontal force produced by the tail rotor to counteract the torque of the main rotor, this side-force could result in stability problems. However, since the HAMRAC will have a coaxial configuration this problem won't occur. The side-forces can easily be counteracted by the main rotors.

8.4.2 Fuselage

Isolated components can be analysed fairly well, however, when integrated together, they may behave differently and the aerodynamic interactions produced between them may cause an unfavourable behaviour that may negatively impact the overall performance and handling qualities of the helicopter.

According to Stalewski [87] the three main aspects of currently used helicopters at high speeds that could be improved are the horizontal drag force, the vertical down force, and the large negative pitching moment. In Figure 8.11 the common shape of a light-weight helicopter can be seen. The front of the fuselage is sharp relative to the fuselage of the optimized fuselage in Figure 8.12. In the rear it can be seen that the sharp corner at the top of the old fuselage is flattened in the optimized fuselage. With this new design, the flow separation was delayed and therefore the drag was reduced by 7%. Furthermore, the down force was reduced by 20% and change the large negative pitching moment into positive. Since the helicopter will be designed for high speeds, the rear of the fuselage will be as smooth as possible, such that it is still possible to have a back door as discussed in chapter 7.

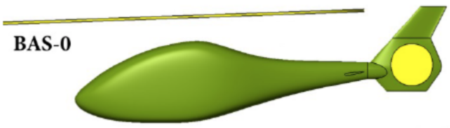

Figure 8.11: *Commonly used helicopter fuselage [87]*

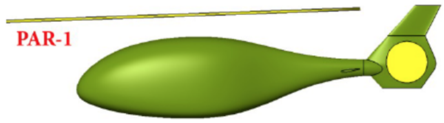

Figure 8.12: *Optimized helicopter fuselage with simulation of main and tail rotor influence [87]*

Now the fuselage is shaped, a rough drag estimate can be calculated. This estimate is based on the cruise speed of 72 m/s at 3930 m and can be seen in Equation 8.23.

$$D = c_D \cdot \frac{1}{2} \cdot \rho \cdot V^2 \cdot S = 0.1662 \cdot \frac{1}{2} \cdot 0.825 \cdot 72^2 \cdot 4.2 = 1493N \tag{8.23}$$

In this calculation, the drag coefficient is obtained from a reference helicopter which was tested without main rotor, with exhaust, skids and stabilizer [26]. From literature [26] [77], it can be found that the main rotor is a very large contributor to the parasite drag of the helicopter. This is due the fact that extra air is pushed against the fuselage by the main rotor. The cross sectional area of the helicopter fuselage was found on Catia to be 4.2 m^2. Including the main rotor in the drag estimate would increase the complexity. In this rough drag estimate, the drag of the skids is not taken into account. For further research it would be recommended to use CFD models to obtain a more accurate estimate of the parasite drag and the aerodynamic interference between the fuselage and components.

8.4.3 Rotor Hub Design

First the rotor spacing will be calculated for optimal performance, whereafter a fairing for the rotor mast and hub will be designed.

Rotor Spacing To minimize the induced power of the HAMRAC an analysis should be performed on the spacing between the two rotors. The aerodynamic interaction between the two rotors is the main aspect that should be taken into account, since the lower rotor is in the wake of the upper rotor. The main trade-off that has to be made is the difference between the hover and cruise phase of the mission. In hover the upper rotor thrust increases when the inter-rotor spacing increases, and the lower rotor thrust decreases. Since the rate of increase in the lower rotor thrust is higher than the rate of decrease in the upper rotor thrust, the overall thrust increases as the inter-rotor spacing decreases [75]. For hover this would indicate that the spacing between the rotors should be large. However, the disadvantages of a large inter-rotor spacing that occur during cruise, such as increased mass of the rotor hub and increased parasite drag due to the enlarged surface area in the free-stream, would limit this spacing. An optimization of the inter-rotor spacing was found by Andrew [67], which resulted in z/D=0.05, where z is the distance between the rotors and D is the diameter of the main rotor disc. This ratio indicates that the spacing is dependent on the size of the main rotor blades. With the radius of the disc set to 4.46 m the disc space can be calculated to be 0.45 m.

Rotor Mast Fairing As mentioned earlier, the shaft and hub of the helicopter are largely responsible for the parasitic drag of the rotor. Instead of leaving the shaft as a cylinder in the free stream, a fairing will be placed around the shaft. This fairing will be a NACA 0030 airfoil. This airfoil is chosen due to is very high thickness to chord ratio, which will result in a short chord relative to other airfoils. This is beneficial mainly because of structural reasons. Since there will be no angle of attack with respect to the free stream, no lift will be produced by the fairing. In chapter 9 the diameter of the mast was calculated to be 0.31 m.

When no fairing would be placed around the mast the drag would be 119 N as calculated in Equation 8.24, where the drag coefficient[8] for a cylinder was found to be 0.4.

$$D = c_D \cdot \frac{1}{2} \cdot \rho \cdot V^2 \cdot S = 0.4 \cdot \frac{1}{2} \cdot 0.825 \cdot 72.0^2 \cdot 0.45 \cdot 0.31 = 119N \tag{8.24}$$

The airfoil will be placed such that the mast is at 30% of the chord, which is the location of the maximum thickness of the airfoil. The thickness is 30% of the chord, and with a simple calculation the cord length can found to be 1.03 m. In Equation 8.25 the minimized drag of the shaped mast is calculated. A reference design can be seen in Figure 8.13.

$$D = 0.0083 \cdot \frac{1}{2} \cdot 0.825 \cdot 72.0^2 \cdot (0.45 \cdot 0.32) = 2.56N \tag{8.25}$$

With XFoil the profile drag of the NACA0030 was found to be 2.56 N. The fairing is optimized for 3930 m at a cruise speed of 72 m/s where the HAMRAC will cruise. The new fairing around the pole will lead to a significant drag reduction. In this calculation it was assumed that the fairing will increase the thickness of the mast by 1 cm.
The fairing will be placed in two counter-rotating components, the lower and upper rotor shafts. As can be seen in Figure 10.5 the outer shaft will be attached to the lower rotor and the inner shaft to the upper rotor. To have a non-rotating part in between the two rotors to which the fairing can be attached, another non-rotating shaft will be added. The outer shaft, connected to the lower rotor, the middle shaft is fixed and will hold the fairing, and the inner shaft is connected to the upper rotor. The fairing shaft shall have an assumed skin thickness of 3 mm, as little force acts upon this component. For the maintainability of the rotor mast, it should be possible to open one side the fairing to be able to check the rotor mast or perform maintenance actions[9].

Rotor Hub Fairing To reduce the drag of the rotor hub, it will be covered in a fairing as well. The main difference with the fairing of the mast is the fact that it will rotate with the blades and thus the freestream can come from every side. The best possible solution for this fairing will be a circular disc. The reference design can be seen in Figure 8.14.

Figure 8.13: *The Sikorsky S-97 Raider with a fairing over the mast*[10]

Figure 8.14: *The Sikorsky X2 with a circular fairing over the rotor hub*[11]

8.4.4 Landing Gear

To safely land the HAMRAC there are three different landing gear options. Wheels are placed under a lot of military or excessively powerful helicopters. The main advantage is that it gives the possibility to taxi over the

[8] URL `https://forum.solidworks.com/thread/113156` [cited 18 January 2019]
[9] URL `http://www.copters.com/R44_SkinsOff/Mast/Mast.html` [cited 18 January 2019]
[10] `http://www.hispaviacion.es/sikorsky-s-97-raider-el-helicoptero-de-asalto-mas-rapido-del-mundo/` [cited 16 January 2019]
[11] `https://www.wired.com/2010/08/sikorsky-x2-breaks-helicopter-speed-record/` [cited 16 January 2019]

airport. On the other side the wheels should be able to be stored inside the fuselage to remain aerodynamically efficient. The structure and the increase in fuselage size will increase the weight. Skids, however, can be placed under the fuselage and don't weigh as much as wheels. Also, during rescue missions they are useful to stand on for rescuers that want to look under the helicopter. The third solution would be to have an adaptive landing system containing four legs with each one degree of freedom[12]. With these four legs the HAMRAC would be able to land on rough terrain and slopes.
Since weight is a very important factor in the mission of the HAMRAC the skids will be used as landing gear. The adaptive landing gear is not necessary, because the HAMRAC does not have to land on slopes or rough terrain because it will hover at the rescue location. To minimize the drag of the skids a fairing will be placed around the vertical tubes attaching the skids to the fuselage.

8.5 Propulsion Subsystem Design

This section will detail the performance characteristics of the design of the HAMRAC. The performance characteristics are largely related to the power of the HAMRAC, both the power required for different flight conditions and by the power available. The power curve for the HAMRAC is shown in Figure 8.15 for level, horizontal, forward flight according to Marilena [22] and Equation 8.17a.

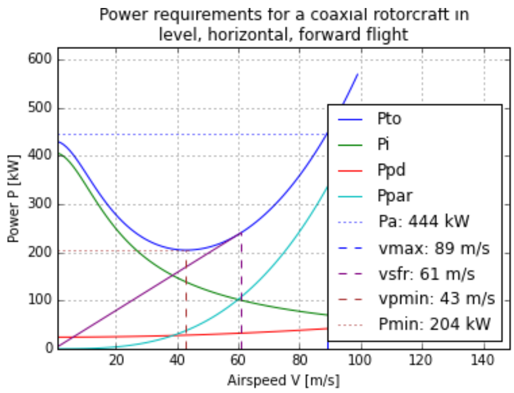

Figure 8.15: *Power required for level, horizontal, forward flight*

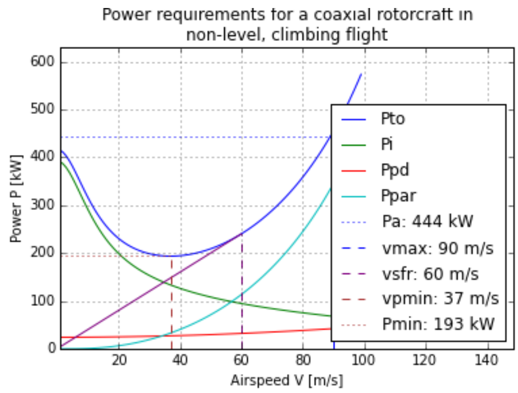

Figure 8.16: *Power required for non-level, climbing, forward flight*

With the power curve, the engine for the HAMRAC can be selected. This can be used to calculate the power curve for non-level, horizontal, forward flight, as shown in Figure 8.16 [31]. From the power curve, the characteristic airspeeds and power values can be determined. These airspeeds are shown in the list below:

- P_{hov}: 361 kW. Power required to hover.
- $P_{i,hov}$: 302 kW. Induced power at hover, used to determine figure of merit.
- P_{min}: 279 kW. Minimum power in flight.
- $V_{p,min}$: 43 m/s. Airspeed to fly at minimum power.
- V_{sfr}: 67 m/s. Airspeed to fly at maximum specific flight range.

With these performance characteristics, the design of the HAMRAC can be compared to the mission requirements.

8.5.1 Engine Selection

For the engine of the HAMRAC a number of possibilities can be implemented in the performance subsystem. These possibilities are presented in this subsection. First of all, a determination between piston and turbine engines is made. Next rationale behind single or twin-engine configuration is explained. Lastly the engine choice itself is made based upon an engine trade-off.

Type of Engine Two kinds of engines can be used for the propulsion system of the HAMRAC, a turbine engine or a piston engine. A reciprocating piston engine (Otto cycle) and a turbine engine (Brayton cycle) are inherently different in their operation. Piston engines are considered a constant volume process during

[12]URL `http://www.athlas.ethz.ch/en/` [cited 17 December 2018]

combustion and turbine engines constant pressure. For sea level conditions this would not be a problem. However, at altitude where the density decreases, a constant volume process sees an increased performance deterioration than a constant pressure process [40].

In combination with current engine technology this results in a higher total efficiency for turbine engines when compared to piston engines. There is only one downside to the efficiency of the turbine engine. It is only very efficient during high power loading. At low power loading the turbine engine efficiency decreases significantly. But most important of all, the power to weight ratio of a turbine engine is greater than a piston engine. This is due to the lesser number of rotating parts in the turbine engine. This results in another favourable characteristic of turbine engines, improved reliability. Since the HAMRAC is a rescue vehicle, reliability is very important. In conclusion the type of engine that will be installed on the HAMRAC will be a turbine engine.

Single or Twin Engine As helicopters rarely have failures due to the strict maintenance intervals and risk mitigation. However, it is possible that an engine failure occurs. When this happens either the helicopter should auto-rotate back to a safe place or it should have an additional engine that can handle the required power load of the helicopter. The latter is the case for a category A helicopter [11]. This rating is used for twin engine helicopters who can perform special take-off procedures and clear obstacles in close proximity of the take-off site. The HAMRAC is a search and rescue helicopter which means safety is of utmost importance. Furthermore, if the rotorcraft encounters an engine failure on the way to the hospital it should be able to still deliver the rescuees. Therefore, it has been decided to make the HAMRAC a category A helicopter.

According to CS27, the category A helicopter shall be able to reach a steady rate of climb of 0.76 m/s at 305m above the highest scheduled take-off location with one engine inoperative (OEI). For the case of the HAMRAC this is 6400m. Above this altitude the HAMRAC is not scheduled to perform a landing in the mission profile. Since, at higher altitudes the rescues will be performed by means of hoist.

This is the reason why the assumption is made that this is the highest landing altitude that has to be taken into account for the category A rating. For an engine failure above 6400m the autorotation performance should be good enough to return to a safe place. At altitudes above 6705m the power produced by one engine is not enough to attain a climb rate or 0.76 m/s or even hover when the altitude increases. When the latter is the case the engine that is still operative should support the aircraft in a safe decent to 6400m where it is able to operate safely. The aircraft then uses the excess power in an autorotation manoeuvre to keep the decent rate to the desired minimum for safe pressurised decent.

Requirements These two design choices in combination with the category A helicopter aim led to the creation of a number of new requirements:

- The HAMRAC shall have two engines.
- Each engine shall have enough power to let the HAMRAC take off from a 6400m altitude.
- Each engine shall have enough power to let the HAMRAC achieve a climb rate of 0.76 m/s at 6705m altitude.
- The engines shall be isolated in a way to be used independently.
- The propulsion system shall comply with all the tests given in CS27.

Engine Trade-off With the engine configuration finalised the only part left is the engine choice itself. This is done using a trade-off to determine which engine has the best characteristics for the mission. Most importantly the engine chosen shall have a mass that falls within the mass budget. Since the aircraft will have a twin engine configuration it will be hard to comply with the given mass budget. Furthermore, the cost budget will also be hard to comply with because of the twin engine configuration.

To determine the power required per engine at sea level to comply with the category A regulations. Take-off from 6400 m and being able to achieve a climb rate of 0.76 m/s with one engine in operative. The power to achieve this climb rate has been added to the power to hover at 6705 m. This came to a power level of 342 kW. This number is then converted to sea level power using density and temperature relations. The power of a turbine engine is proportionate to the density of the air that it is breathing [64]. Additionally, the power increases by 0.1% with every K it goes below 15 °C [2]. These relations result in a power required of 658 kW at sea level per engine. Next the steps that are taken to check for suitable engines are described:

- Find the maximum OEI and maximum continuous power at sea level.
- Determine whether the engine can deliver the required power setting.
- Calculate the maximum continuous power at 8900 m.
- Determine whether the twin engine configuration has enough power to function at 8900 m.
- Find the mass of the engine.
- Find the specific fuel consumption of the engine.

The outcome of the assessment with its respective suitable engines is presented in Table 8.15. Since the OEI requirement is the hardest to meet only these power values will be shown.

Table 8.15: *Trade-off table for engine choice*

Engine	P_a OEI at Sea Level [kW]	P_a OEI at 6700m [kW]	Mass [kg]	SFC [kg/h]
Safran Arriel 2E	710	369	120	267
Honeywell HTS900	723	375	142	230
LHTEC T800-LHT-800	774	402	149	212
Rolls Royce Gnome H1200	783	406	142	294
General Electric CT58-110	783	406	143	305
Safran TM 333 2B2	798	414	140	306

Before the engine choice can be finalised, the transmission losses need to be taken into account. Since the HAMRAC is a coaxial configuration it needs an extra transmission to produce the counter rotation. This means that both of the transmissions lose some power. The efficiency of helicopter transmissions for upwards of 2000 kW is 0.987 [17]. This is the transmission which provides the rotor with two different rotational speeds with optimal engine performance. For the coaxial transmission the same value is assumed, this results in a total efficiency of 0.974. This is the transmission which lets the masts counter rotate. Furthermore, the twin engine configuration requires another transmission. The engines need to be able to operate separately in case of an engine failure. Therefore the final efficiency of all the transmissions combined is 0.961.

The efficiency is then added on the power requirement which results in 685 kW of power. The electrical systems in the helicopter need power from the generator and in turn the generator need power from the engine as well. This power needed for the generator is budgeted at 10 kW which brings the total up to 695 kW. With this power rating the Safran Arriel 2E could be used as the engine. However, the specific fuel consumption is such that the benefit of this engine completely disappears. The Arriel 2E used 50 kg of fuel per hour more than the T800 with a difference in mass of only 29 kg.
This means that the next best option is the Honeywell HTS900 or the LHTEC T800-LHT-800. Even though the HTS900 produces less power the fuel consumption is 18 kg/h higher compared to the T800. However, the HTS900 is 7 kg lighter which results in a difference of 14 kg for the pair. Taking this all into account the T800 pair will be 22 kg lighter over a flight of 1 hour. Concluding, the engine that will be used for the HAMRAC will be a pair of LHTEC T800-LHT-800's. With these engines the HAMRAC has been overpowered. However, the fuel consumption and the weight of the engine are better compared to the other engines.

8.5.2 Propulsion subsystem components

In addition to the engine, the propulsion subsystem of a rotorcraft also includes additional components to enable and regulate engine function.

Main Rotor Transmission The purpose of the main rotor transmission is to transfer the axial rotation of the engine to the vertical rotation of the main rotors, and to reduce the engine RPM to the rotor RPM. The ratios that will be used to decrease the 23000 RPM [13] turbine speed to the correct rotor speed are, 68.5 : 1 for high altitude and 85 : 1 for low altitude.

Freewheeling Unit The freewheeling unit of a helicopter is used to disengage the rotor from the engine in case of engine failure to allow the pilot to enter autorotation. Additionally, it can be used to disengage one engine from the other and the rotor in case of one engine inoperative conditions.

Fuel Systems The fuel system of a rotorcraft has two parts: the fuel supply system and the engine fuel control system. The components of the fuel supply system are the fuel tank(s), fuel quantity gauges, a shut-off valve, fuel filter, a fuel line to the engine(s), and possibly a primer and fuel pumps. Details and specific purposes of these components are given in [7] and the components chosen for the HAMRAC will be considered for 14.

Electric Systems Rotorcraft are equipped with a battery to start the engine, provide limited power to the avionics display and radio, and provide central heating. For small rotorcraft, this battery produces 12 or 24V, and typically weighs 11 to 12 kg [28]. It is also required that a rotorcraft is able to fly and function during the event of failure of the electric system, and that failure of the engine does not cause the critical avionics and radio systems to fail as well.

[13] https://janes.ihs.com/Janes/Display/jae_0739-jae_[cited 28-01-2019]

9

Structural Characteristics

In this chapter the structural characteristics of the HAMRAC have been discussed. This has been done on subsystem level. Firstly, the initial considerations are discussed in section 9.1. Secondly, the main rotor has been analysed in section 9.2, followed up by the blade hub connection part in section 9.3 and the rotor shaft in section 9.4. Lastly, the airframe is discussed in section 9.5.

9.1 Initial Considerations

For the structural analysis of the HAMRAC, it was decided to independently design and evaluate the separate subsystems of the aircraft; the rotor blade, blade-hub connector, rotorshaft and airframe. The analysis procedures and the resulting equations used within the analysis are given within Aircraft Structures for Engineering Students, by T.H.G. Megson [82]. Before starting the analysis, a coordinate has to be set up, and the load factors have to be determined, which has been done in subsection 9.1.1 and subsection 9.1.2 respectively.

9.1.1 Coordinate System

Before starting the analysis, it is necessary to define a coordinate system for the aircraft. The aircrafts x axis runs along the center of the aircraft's fuselage with the positive direction towards the nose of the aircraft. The y axis runs from port to starboard and is positive on the starboard side of the aircraft. The z axis runs from the bottom to the top of the aircraft and is positive in the top direction.

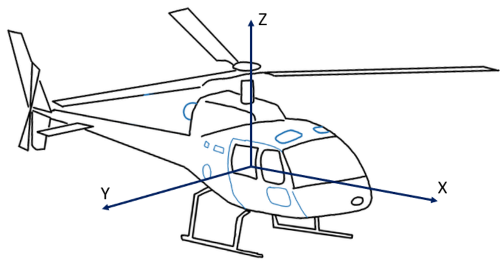

Figure 9.1: *Figure displaying the HAMRACs coordinate system*

9.1.2 Load Factors

As the HAMRAC is to be designed for operation in extreme weather conditions it is necessary that load factors are considered during the structural design. Load factors are provided from the EASA Certification Specifications (CS-27) [11]. Aerodynamic load factors due to manoeuvres and gusts range from +3.5 to -1.0. However, as the HAMRAC is operating in highly extreme weather conditions, an analysis should be made as to whether these load factors are exceeded during the operating conditions of the HAMRAC. If so then these load factors should be replaced by ones that are more relevant to the operating conditions.

Also specified in CS-27 guidelines is the use of a design load safety factor of 1.5. This is to account for any uncertainty in structural calculations, and to ensure that the HAMRAC is designed to resist any possible loading conditions that could arise during its lifetime. In combination with the aerodynamic load factors this results in a design load factor that ranges from -1.5 to +5.25.

Further load factors that must be considered in the structural design of the HAMRAC are the load factors that are induced by a hard landing. These will affect the point loads transferred to the airframe by the undercarriage. These load factors under emergency landing conditions are determined by EASA [11] and apply only to the aircraft structural element: upward (1.5g), downward (4.0g), sideward (2.0g), forward (4.0g).

9.2 Rotor Blade Design

In this section, the structural design of the rotor blades has been conducted. Firstly, the number of blades has been determined. Secondly, the blade discretisation has been elaborated, upon, followed up by an analysis of the blade loading and the blade stresses. The final structural design of the blades is discussed afterwards.

9.2.1 Evaluating the Number of Blades

It is very important for the Performance and Aerodynamics department to select an appropriate number of blades to use within each rotor, so that they can progress with the design of the rotor itself. In order to assist this design decision, the structures department were tasked with making a preliminary assessment of the structural mass of the two rotor configurations. In order to make this estimate, an analysis of the stresses due to bending (the governing stress mode, for the blades) was conducted. To model each blade simplistically, several major assumptions were made. Firstly, the two rotors shall use the same radius and shall have the same solidity, with a difference in blade chord length accounting for the difference in the blade design. Secondly each blade cross section shall be modelled as an I-beam, with the flanges being the same length as the chord and the spar height being 12% of the chord length (similar to NACA2312 airfoil). The chord of the three blade rotor is 0.304m and for the four blade rotor it is 0.227m. To this discretised beam, the moment distribution due to pure lift force was applied, see Equations 9.11 and 9.13. The resultant bending stresses within the cross section was then calculated using:

$$\sigma_y = \frac{I_{zz}M_x - I_{xz}M_z}{I_{xx}I_{zz} - I_{xz}^2} \cdot \bar{z} + \frac{I_{xx}M_z - I_{xz}M_x}{I_{xx}I_{zz} - I_{xz}^2} \cdot \bar{x} \tag{9.1}$$

The maximum magnitude bending stress was then identified in each beam. The calculation was then repeated for increasing skin thickness, until the maximum magnitude bending stress fell below the ultimate yield stress of an arbitrary material, in this case *Al 2024-T3*. The volume of each beam was then determined, and the mass for each rotor system calculated. Based on this analysis, the following results come forward:

$$\frac{\text{weight 6-blade rotorsystem}}{\text{weight 8-blade rotorsystem}} = 0.746 \tag{9.2}$$

As this ratio is smaller than one, it can be concluded that the 6-blade rotorsystem will result in a lighter rotor subsystem configuration.

9.2.2 Blade Discretisation

Before the blade can be analysed it must be discretised into a number of sections to allow for a blade design that varies throughout the structure. In this way a blade will be designed with each section optimised to withstand the loads that it shall experience throughout its operational lifetime, resulting in a lightweight blade structural design. It should be taken into account that whilst the solution accuracy increases each time and the optimisation of the blade also increases, the manufacturability decreases. To develop a blade with a near constant change in material thickness would prove to be very expensive and time consuming. For this reason, the structural analysis shall assume ten discrete cross-sections within the blade.

From the Performance and Aerodynamics department an initial rotor radius, airfoil type, twist, and taper have been determined. This provides enough geometric information to generate a structural model of the blade. Important to note is that for the first 60cm of the blades radius the blade shall be modelled as a tubular shaft, as this part will have a different design to the rest of the blade, as it has no airfoil. This is commonly seen within helicopter blade design as the interior of the rotor disc produces comparatively little lift. This interior section has therefore zero lift load assumed to be acting upon it, as will be discussed in section 9.3.

Firstly, airfoil coordinates were generated from AirfoilTools[1], this provided 86 discrete coordinate points around the skin of the airfoil. The airfoil used is the Boeing Vertol VR12 airfoil. In reality the HAMRAC uses a different airfoil (VR14) at the outer regions of the blade, however as the difference in the profile is marginal, it was decided to neglect this and use one airfoil, the VR12, over the span of the blade. To this the structures department added a single spar to the interior of the airfoil. This was placed at the thickest point within the airfoil, at 35% chord, to provide the maximum additional moment of inertia, with a spar thickness double that of the airfoils skin. The spar is composed of an additional 50 discrete coordinates. The decision to use a single spar came from research into the structural design of helicopter blades [63]. It was found that the bending moments due to lift are largely relieved due to the centrifugal forces on the blades, hence there are not as many structural elements resisting bending loads to be found in helicopter blades as in an aircraft wing. There is more emphasis placed upon increasing the stiffness of blades, due to the large deflections that are possible under the loading conditions. For this reason, a large proportion of helicopter blades are filled with honeycomb material. Hence the decision to use a single spar is further justified when you consider that in the rear part of the cross section a honeycomb material can then be applied. This follows the same structural mode that has been used for the structural analysis of blades by Li [63] for the structural analysis of helicopter blades, validating that the approach is suitable for blade analysis which is elaborated further on in section 11.1.

In order to convert the identified cross section into the coordinates for the helicopter blade, the radius was divided into sections, through using several discrete points along the blade. Each point has its own taper, chord and blade twist angle. These were then applied to the coordinates of the cross-section through multiplying the coordinates first by the chord, then the taper ratio value at each location, obtaining a gradually decreasing cross section as you move towards the blade tip. Blade twist was applied through identifying the twist angle at each point then multiplying each coordinate through a transformation matrix. Through this method discrete cross sections were identified across the span of the blade, each with its own taper, chord and twist, with the coordinates of each being given in the blade coordinate system. However, across each section, for the purposes of our analysis, it is assumed that only one sectional geometry shall be present. Therefore, the geometric properties for each section are assumed as being equal to those of the midpoint of the section. The coordinates of the midpoint of each section were then separately identified, using the taper, chord and twist of the midpoint of each section. This is assumed as being the cross-section geometry of that section. For example, if only two discretisation points were used then the cross-section geometry of the blades middle point would be assumed as being the geometry of the blade along its length.

Now that the cross-sectional coordinates for each section have been determined it is possible to calculate the centroid, areas, and moments of inertia for each of the cross-sections. In order to do this the skin of the airfoil was considered as being made up of small rectangular skin sections, of small thickness, each having a segment length of the distance between the two skin boundary points of each segment. The spar was considered just as a single rectangle, undergoing a small twist angle, with an area of its height multiplied by twice the skin thickness. The area of each skin segment is therefore equal to:

$$A_{skin_{ij}} = t_{skin} \cdot \sqrt{(x_j - x_i)^2 + (z_j - z_i)^2} \tag{9.3}$$

The sum of all of the skin areas plus the spar area being equal to the area of the cross section, within each blade section. Equation 9.3 also allowed for the determination of the centroid coordinates for each section in the blade.

$$\bar{x} = \frac{\sum(A_{skin_{ij}} \cdot (x_i + (x_j - x_i)/2)) + A_{spar} \cdot x_{spar}}{\sum(A_{skin_{ij}}) + A_{spar}}, \; \bar{z} = \frac{\sum(A_{skin_{ij}} \cdot (z_i + (z_j - z_i)/2)) + A_{spar} \cdot z_{spar}}{\sum(A_{skin_{ij}}) + A_{spar}} \tag{9.4}$$

Once the centroid location was identified and verified using XFoil, the moments of inertia for each blade section could then be determined. As the skin of the airfoil is not small in comparison to the profile area, the thin walled approximation cannot be used in this case. This means that both the inertial and the Steiner terms of the skin were taken into account. Each inertial term for the skin was first calculated for a flat rectangle then converted to the angle that the segment is at in relation to the principal axis, using equations 9.8.

$$I_{xx_{skin}} = \sum I'_{xx_{skin}} + \sum(A_{skin_{ij}} \cdot (x_i + (\frac{x_j - x_i}{2}) - \bar{x})^2), \; I_{zz_{skin}} = \sum I'_{zz_{skin}} + \sum(A_{skin_{ij}} \cdot (z_i + (\frac{z_j - z_i}{2}) - \bar{z})^2) \tag{9.5}$$

[1] http://airfoiltools.com/

$$I_{xz_{skin}} = \sum I'_{xz_{skin}} + \sum (A_{skin_{ij}} \cdot (x_i + (\frac{x_j - x_i}{2}) - \bar{x}) \cdot (z_i + (\frac{z_j - z_i}{2}) - \bar{z})) \tag{9.6}$$

Whereas for the spar:

$$I_{xx_{spar}} = \frac{1}{12} \cdot t_{spar} \cdot h_{spar}^3 + A_{spar} \cdot (\bar{x}_{spar} - \bar{x})^2),\ I_{zz_{spar}} = \frac{1}{12} \cdot t_{spar}^3 \cdot h_{spar} + A_{spar} \cdot (\bar{z}_{spar} - \bar{z})^2) \tag{9.7}$$

The $I_{xz_{spar}}$ is zero in this case due to symmetry. However, as the spar is twisted along with the cross-section the moments of inertia must be recalculated to account for the twist angle within each section. This does not apply for the skin at the moments of inertia have already been determined using the coordinates with twist already applied.

$$I'_{xx} = \frac{I_{xx} - I_{zz}}{2} + (\frac{I_{xx} - I_{zz}}{2} \cdot \cos(2\theta)),\ I'_{zz} = \frac{I_{xx} - I_{zz}}{2} - (\frac{I_{xx} - I_{zz}}{2} \cdot \cos(2\theta)),\ I'_{xz} = \frac{I_{xx} - I_{zz}}{2} \cdot \sin(2\theta) \tag{9.8}$$

Therefore for each section you need only sum the moments of inertia for the skin and spars, to determine the moments of inertia in each section of the blade.

Also included in each section is a region of $Al2024 - T3$ honeycomb material. This is assumed to have zero mass and also is assumed to have no effect upon the moment of inertia of the blade. However, this material shall increase the stiffness of the blade. The effect of this is taken into account through the following relationship, where the moment of inertia of the honeycomb is approximated as a triangle with the dimensions of the airfoil behind the spar.

$$EI = EI_{profile} + EI_{core} \tag{9.9}$$

$$EI_{core} = E_{Al} \cdot \frac{hb^3 - hab^2 + hba^2}{36} \tag{9.10}$$

Where h denotes the distance from the spar to the tip, b is the spar thickness minus twice the skin thickness and a is the distance in the z axis from the top of the spar minus the skin thickness, to the trailing edge.

9.2.3 Blade Loading

In order to determine the stresses within the blade the internal forces within the structure must be identified. The beam shall therefore be modelled as a cantilever beam. For each blade there are three main forces acting upon the blade. These are the lift, drag and centrifugal forces that act upon the blade. For each section the individual magnitudes of these forces shall first be identified. These will then later be combined to identify the blades internal normal force, shear force and bending moments across each section of the blade, as these will be assumed constant for each section. A free body diagram of the blade loading is shown in Figure 9.2. It is assumed that the shear forces that act on the blade act through the shear center at each location, meaning that there is zero aerodynamic torque assumed to be acting upon the blade. Furthermore, as the weight of the blade is itself negligible in comparison to the lift force produce by the blade, its effect shall be ignored for the purpose of this analysis.

Firstly, the lift force acting upon each section was determined. In reality the lift is a distributed load over each section following a quadratic distribution, as it is dependent of the velocity of each section, which increases as you approach the blade tip. However, the lift shall be approximated as a point load acting on each section. This will be assumed to act at a point two thirds along the length of each section, following from a linearly increasing distributed load, which approximately represents the increase in lift. The difference between the force location for a quadratic lift distribution and a linearly increasing one is assumed negligible for the length of the blade sections. The lift force for each section is then calculated using Equation 9.11.

$$L_i = \frac{1}{2} \cdot \rho_{air} \cdot C_{L_i} \cdot S_i \cdot (\omega y_i + V_{flight})^2 \tag{9.11}$$

Where y is the distance from the point of rotation at two thirds of the length of the section, and ω is the rotational frequency. The air speed that the aircraft is travelling at also must be taken into account within the lift equation. It should be noted however that each part of the disc shall see a different airspeed, but that the critical case is given by when the blade is perpendicular to the wind direction, but moving into the wind, as there is the greatest airspeed as seen by the blade. This equation also allows for the lift load to be determined

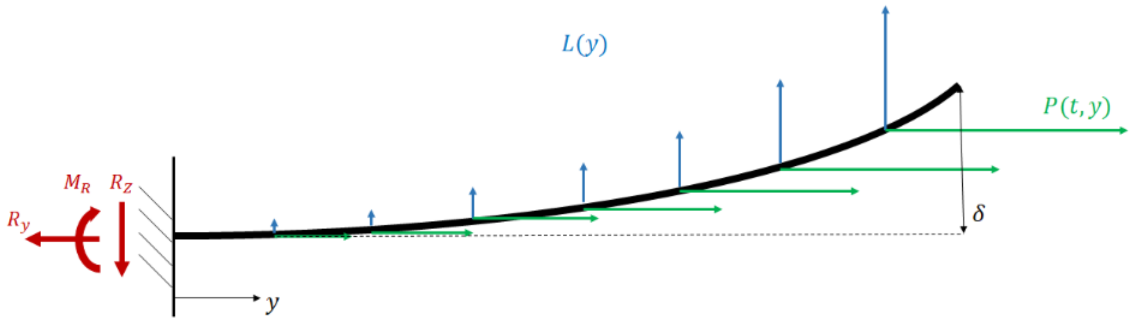

Figure 9.2: *Free body diagram of the blade loading. Note that centrifugal force P is dependent on skin thickness and radial position, whereas the Lift is dependent on radial position only.*

for lift coefficients that differ across the span. The drag force is then simply obtained by multiplying the lift force by the lift to drag ratio for each section.

The centrifugal force is also a distributed load, however this time in the axial direction and acts as a tensile force along the length of the blade. As the centrifugal force is also dependent on the rotational velocity, it follows the same quadratic distribution as the lift. Hence within each blade section the approximate point centrifugal force is assumed to act at the same location as the point lift force. Using this the centrifugal force within each section is determined as follows:

$$P_i = A_i \cdot l_i \cdot \rho_{material} \cdot \frac{y_i \cdot \omega^2}{2} \tag{9.12}$$

With the first three terms in the equation yielding the mass of each blade segment.

The normal force acting on the blade is then described by the loading due to the centrifugal force. The shear force is also described purely by the loading due to the lift and drag forces. The blades internal normal and shear forces can hence be determined across the span of the blade. However, in order to determine the internal bending moments further analysis is required.

As the centrifugal force is greater than the lift force acting upon the blade the bending moment acting upon the blade cannot be assumed due to purely lift but also due to the moment induced by the centrifugal force as the blade deflects due to the lift loading, with zero initial deflection. In order to calculate the internal bending moments acting within the blade an iterative approach was used. Firstly, the deflections due to purely the aerodynamic loading were calculated, using Macaulay step functions. Then the moment distribution due to the combined aerodynamic forces and the centrifugal forces was calculated, yielding an internal bending moment distribution across the blade.

$$M(y) = M_a + \sum(L_i[y - a_i]) - R_a y - \sum(P(\delta_i - \delta_j)[y - a_i]) + \sum(P\delta_i) \tag{9.13}$$

Note that this equation includes centrifugal terms, however these are zero for zero initial deflection. The deflections are then calculated through the following process. First the deflection angle ϕ is determined for the internal bending moment within each section. The deflection at the end of each section is then equal to the length of the segment multiplied by the deflection angle.

$$\frac{d\phi}{ds} = \frac{M_b}{EI_{xx}} \tag{9.14}$$

This equation shall then yield a new set of deflections for the blade. The process is then repeated using the new deflections. This continues for a number of iterations. If the blade is stiff enough then the blade deflections shall converge. A stiff material such as CFRP is therefore required. As a result of these findings the structures department chose to use Uni-Directional Carbon Fibre Reinforced Plastic, which has a high flexural strength and a Young's Modulus in the fibre direction of 135GPa and a density of 1600kg/m^3. 2000 iterations yield a final moment distribution for the combined aerodynamic and centrifugal loading and furthermore, the blade deflection. It should be noted by the reader that the loading distribution depends upon the blades thickness, due to the fact that the centrifugal force is dependent on the mass of each segment. Hence the distribution of loading shall be described at the end of the chapter, once a varying thickness has been selected across the blade.

9.2.4 Internal Stress

Due to the nature of the combined loading present on each rotor blade, there are three principal stresses within the structure, these are; axial, bending and shear stresses. All three must be taken into account for the purpose of this analysis, as each principal stress is relatively large due to the nature of the blade loading. These will be calculated and the Von Mises stress within the blade will then be determined using:

$$\sigma_{Von\ Mises} = \sqrt{(\sigma_{axial} + \sigma_{bend})^2 + 3 \cdot \tau_{xz}^2} \tag{9.15}$$

This will give the maximum stress within the blade for which to design the thickness of the blade elements.

The axial stress is fairly straightforward to evaluate as it induced purely by the axial force due to the centrifugal motion of the blades. This is known at each section of the blade and need only be divided by the cross-sectional area at each section to determine the stress.

$$\sigma_{axial} = \frac{P_i}{A_i} \tag{9.16}$$

The stress due to bending is also evaluated within each section through Equation 9.1. Where the moment about the x axis is the internal bending moment due to both the lift and centrifugal forces. The moment about the z axis is dependent purely due to the drag force.

This leaves only the shear stress that must be evaluated within the closed multi-sectional airfoil beam. Firstly, the two sections were split, with one section being ahead of the spar (a) and the other to the rear of the spar (b), at these locations the 'cuts' were made to allow for an analysis of the base shear flow. The starting location for section (a) is at the skin at the top of the spar, and for (b) it is at the trailing edge. The base shear flow is then evaluated around each section through the following.

$$q_b = -\frac{S_x I_{xx} - S_z I_{xz}}{I_{xx} I_{zz} - I_{xz}^2} \int_0^s (t \cdot x) ds - \frac{S_z I_{zz} - S_x I_{xz}}{I_{xx} I_{zz} - I_{xz}^2} \int_0^s (t \cdot z) ds \tag{9.17}$$

In order to know the full shear flow within the blades cross section the redundant shear flow must be calculated and added to the identified base shear flow within each section. This is done through first calculating the sum of moments, due to the base shear flow, about each section. The point about which the moments were taken was the same for both cross sections and was chosen as the bottom of the spar. So the moment for each section is determined through Equation 9.18.

$$M_i = \oint q_{b_i} p_{0_i} ds \tag{9.18}$$

This is related to the redundant shear flow through Equation 9.19.

$$0 = M_i + 2A_{0_i} q_{s0_i} \tag{9.19}$$

As this can only be evaluated per section and does not account for the other, another equation is required to derive the redundant shear flow within each section accounting for the influence of the other. This is the Bredt-Batho formula. Note that for the above equation and subsequent ones A_0 denotes the area enclosed by the section.

$$\frac{d\theta}{dy} = \frac{1}{2A_{0_i} G} \oint (q_{b_i} + q_{s_i}) \frac{ds}{t} \tag{9.20}$$

As the twist per unit length must be equal for both sections of the cross section, the following system of equations can be derived and solved to determine the redundant shear flows.

$$\begin{bmatrix} 2A_{0_a} & 2A_{0_b} \\ -\frac{1}{2A_{0_a}G} \oint \frac{1}{t} ds & \frac{1}{2A_{0_b}G} \oint \frac{1}{t} ds \end{bmatrix} \cdot \begin{bmatrix} q_{s_a} \\ q_{s_b} \end{bmatrix} = \begin{bmatrix} -(M_a + M_b) \\ (\frac{1}{2A_{0_a}G} \oint \frac{q_{b_a}}{t} ds - \frac{1}{2A_{0_b}G} \oint \frac{q_{b_b}}{t} ds) \end{bmatrix} \tag{9.21}$$

Now that the redundant shear within each section is determined, this can be added to the base shear flows within each section to determine the total shear flow distribution. Note that as the shear flow is assumed in opposite directions within the spar for each section, to determine shear in the spar the spar flow in (a) must be subtracted from the spar flow in (b). Now that the total shear distribution is known, the shear stress there is calculated by dividing it by the thickness at that point.

With all of the functions necessary to obtain the Von Mises stress distribution across the blade, it is now possible to determine the thickness at each point of the blade, such that the Von Mises stress does not exceed the materials yield stress.

9.2.5 Blade Design

As the loading is dependent upon the thickness of the blade, changing the thickness of the blade at any point changes both the stress at that location but also the distributed load across the blade. This makes solving for thickness particularly challenging unlike for aircraft where one can simply solve to find the thickness for a given load case at each point within the section. In order to optimise the blade for structural mass it was decided to first determine a thickness ratio that lead to the least mass across the blade. This is done by first selecting a thickness at the root. It was decided then to take at first the maximum possible thickness at the root, which for a chord of 0.4m and an airfoil of maximum thickness of 10.6% results in a thickness of 0.02m. So at the root section the thickness factor used shall be 1. At first different distributions of thickness were used including a linear distribution an exponential and a geometric distribution. From this it was identified that a geometric distribution ranging in thickness factor from 1 at the root to 0.15 at the tip produced the optimum mass whilst still ensuring no yield in the material. The values at each section were then manually changed until a minimum mass solution was determined. This solution for the blade contains the optimum thickness ratio that could still meet the strength requirements for the blade. The thickness ratio that came out of this analysis is shown in Table 9.1, along with the corresponding Von Mises stresses within each section. Also displayed is the loading diagrams for this thickness distribution in Figure 9.3a and the Von Mises stress distribution in the blade in Figure 9.3b.

Table 9.1: *Table displaying the blade's thickness and stress distribution*

Blade Segment	Thickness Factor	Thickness [m]	Max. Von Mises Stress [MPa]
1	1	0.0200	351.3
2	0.85	0.0170	355.3
3	0.71	0.0142	355.3
4	0.57	0.0114	354.3
5	0.43	0.0086	349.9
6	0.31	0.0062	319.7
7	0.23	0.0046	230.5
8	0.18	0.0036	131.1
9	0.15	0.0030	95.3

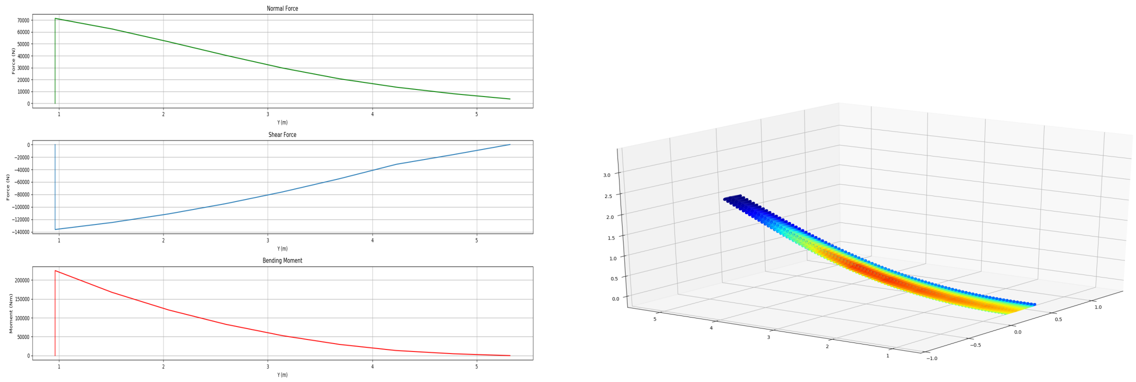

(a) *This figure displays the blade loading diagrams for the selected thickness distribution*

(b) *This figure displays the Von Mises stress distribution within each blade cross section and the maximum deflection at that point. Red denotes high stress and blue lower stress. Note that for the purpose of visualisation an increased number of segments have been used to display the stress distribution.*

Figure 9.3: *Figures displaying the internal loads and stresses within the blades*

This was determined for a load safety factor of 1.5, under the maximum (non-gust) lift conditions. Under these conditions the mass of the blade was identified as being equal to 52.2kg. This is at a flight speed of 80m/s at the altitude of the intermediate airport using a blade rotational frequency of 35rad/s. Unfortunately for when the maximum gust load factor of 3.5 was applied, the stress within all except the last section exceeds the yield stress. As the thickness at the root cannot be further increased due to the geometric constraints of the blade, the structures department recommends a further analysis of blade structural design following this report. The easiest way to increase the strength of the blade is through increasing its thickness. An increase in chord can be used to achieve this, while using the same airfoil as before. This is the chief recommendation of the structures department, though it shall of course require a post-DSE analysis into how this may affect the aerodynamics of the HAMRAC.

As can be seen in Figure 9.3b the deflections under the current load case also exceed the rotor spacing. The structures department have attempted to limit the deflections undergone by the blade through the addition of Aluminium Honeycomb to increase the stiffness of the blade, however this was unsuccessful. Increasing the skin thickness in the blades exterior sections will limit the deflections, through increasing the moment of inertia and centrifugal force, however this will increase the mass of the blade. Furthermore, increasing the thickness of the blade will also limit the deflections so the effect of this should first be investigated. The mass optimised skin thickness factors that have been determined can then be adapted (increased within the outer sections) until a skin thickness ratio is found that is optimised both for blade strength, structural mass and to limit the blade deflections.

Hence in summary the blade structural analysis has shown that further analysis is required for the HAMRAC blades. However, the work conducted in this report has laid an extensive foundation upon which this future analysis can be based, including several recommendations as how to achieve the increase in strength and stiffness that is required within the blades.

9.3 Blade Hub Connection Design

It is important that the connection between the lifting region of the blade and the hinge-less and bearing-less hub is strong enough to resist the loads transferred to it from the blade. This connection has been modelled as a tube with a gradually decreasing radius as it approaches the blade, with the radius at the blade being equal to 0.02m, to allow for a smooth material transition to the blade. This ensures the tube is as thick as the blade, at the connection. The blade and the hub connector shall both be made from the same material (UD CFRP). The forces acting upon the connector are the sum of centrifugal forces in the blade and the sum of the lift forces. The moment upon the connector is the resultant moment at the root of the lifting region of the blade, where y is 0.6m. The internal bending moment and shear forces in the connector could hence be determined. There is assumed to be no deflection of the connector, nor is it assumed to generate any lift itself or produce any centrifugal force itself, as there is relatively low velocity at this radial distance.

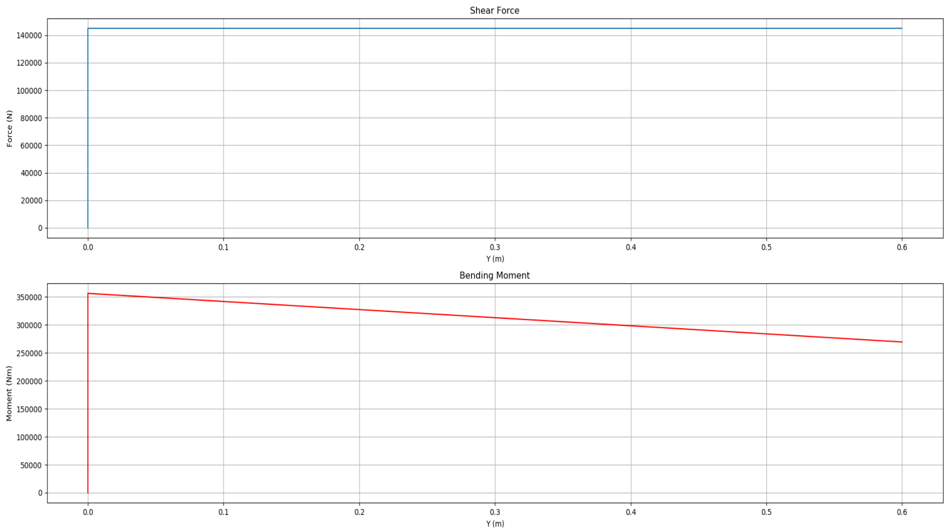

Figure 9.4: *Figure showing the bending moment and shear force loading of the hub connection (normal force is constant throughout the connection)*

The inertia of such a tubular section can be determined through the following equation. It should be noted that discretised points will be taken along the hub connection, so the inertia, radius and skin thickness will vary throughout.

$$I_{xx} = \frac{\pi}{4}(r_i^4 - (r_i - t_i)^4) \tag{9.22}$$

Equation 9.1 can be used to evaluate bending stress and Equation 9.16 can be used to evaluate the axial stress within the cross section. For the shear stress there is no need to use the multi-cell relationships, hence the base shear flow can be evaluated using Equation 9.17 and the moment due to this from Equation 9.18. Redundant shear flow is then simply evaluated from Equation 9.19. Shear stress is then determined by taking the combined redundant and base shear flows and dividing by the skin thickness at each location. The Von Mises in the hub connection is then simply determined through Equation 9.15. Unlike in the blade, the loading condition does not depend on the thickness of the tube. Hence it is simple to evaluate the thickness across the span of the tube, in order to resist the Von Mises stresses at each location. This has been evaluated under the maximum loading condition, for the same atmospheric and flight conditions as the blade, with a load safety factor of 1.5 and the maximum gust load of 3.5. In order to ensure an optimum weight to strength relationship for this component the thickness should vary across the component to ensure that at each location the stress is a near as possible to the yield stress of the material under the maximum loading conditions. This design process has yielded the following stress and thickness distribution for this component, for a component mass of 1.72kg.

Table 9.2: *Table displaying geometry and stress distribution for the hub connection*

y Location [m]	Cross-Sectional Radius [m]	Thickness [m]	Max. Von Mises Stress [MPa]
0.0	0.0222	0.0081	353.9
0.067	0.0218	0.0082	353.7
0.133	0.0216	0.0083	353.6
0.2	0.0213	0.0084	353.5
0.267	0.0211	0.0085	353.5
0.333	0.0209	0.0086	353.6
0.4	0.0207	0.0087	353.7
0.467	0.0204	0.0088	354.0
0.533	0.0202	0.0089	354.2
0.6	0.02	0.009	354.7

9.4 Rotorshaft Design

The rotorshaft is the shaft that provides the blades of the helicopter with a rotational velocity. For a conventional helicopter only one rotorshaft is used, however as the HAMRAC uses coaxial rotors, two separate rotorshafts must be considered. The one driving the top rotor is 0.63m tall, to allow for the rotor separation distance of 0.45m. The top driving shaft is rotating inside of the shaft for the lower rotor, with a separation distance between the two of 0.01m to allow for a smaller shaft to which the middle fairing is attached. The lower shaft has a height of only 0.14m to allow for a separation of 0.1m for the lower rotor from the fuselage, as can be seen in Figure 9.5. Each rotorshaft shall be constructed from $Al2024-T3$, a commonly used alloy within aerospace that has a material density of 2380kg/m^3. This shall keep production costs down and allow for these parts to be recycled at the end of the products life. Each shaft will be modelled as a circular tube, with a constant thickness and radius. The shaft will be analysed under maximum loading conditions, the same loading conditions that have been applied to the rotor hub connection. One must consider however that there are three separate blades attached to the shaft hence the loading is a combination of the loading that is transferred from each blade. Hence for blade 1, the loads from the blade shall be determined for a flight speed of +80m/s. Therefore, for blades 2 & 3 the loads must be calculated for the retreating blade, at its angular position and are hence given by the loading for a flight speed of -80· cos(60°) = 40 m/s. The axial force on each rotorshaft is therefore equal to:

$$L_i = L_1 + 2 \cdot L_{23} \tag{9.23}$$

Furthermore the bending moment applied to each shaft is equal to:

$$M_i = M_1 - 2 \cdot M_{23} \cdot \cos(60°) \tag{9.24}$$

The shear force acting upon the shaft is zero as the centrifugal forces from blades 2 and 3 cancel out the force from blade 1.

$$0 = P_1 - 2 \cdot P_{23} \cdot \cos(60°) \tag{9.25}$$

Also acting on the rotorshaft is the torque produced by each rotor:

$$T = \frac{Power}{\omega} \tag{9.26}$$

Where $Power$ denotes the maximum shaft power and ω the rotational frequency. Hence there is a constant bending moment, axial force and torque over each rotorshaft and due to the simplicity of the loading, loading diagrams will not be given. Furthermore, as each rotorshaft is a simple tube, the moment of inertia can be determined simply using Equation 9.22. Now that the loading has been determined, along with the moment of inertia, the stresses within each shaft can be calculated. Equation 9.1 can be used to evaluate bending stress and Equation 9.16 can be used to evaluate the axial stress within the cross section. The shear stress due to the torque can then be calculated using:

$$\tau = \frac{T}{2 \cdot A_{0_i} \cdot t_i} \tag{9.27}$$

The Von Mises stress distribution in the shaft can then be calculated using Equation 9.15. The results are displayed in Figure 9.5.

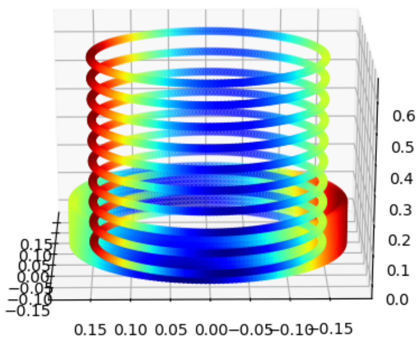

Figure 9.5: *Von Mises stress distribution within rotorshaft subsystem, where red denotes high stress and blue low stress*

As the shafts are counter rotating, there will be a maximum stress on the opposite side of the shaft to the other. The radius and thickness of the interior shaft shall first be determined in order to ensure the maximum stress is lower than that of the material $Al2024-T3$ (345MPa). Once again, the material properties will be optimised for a minimum overall mass by ensuring that the maximum Von Mises stress within the rotorshaft is as near to the yield stress as possible. The top rotor shaft radius will then dictate the radius of the lower shaft. It was found that increasing the radius of the shaft leads to a decrease in shaft mass as for a larger radius there is greater moment of inertia of the shaft and a greater resistance to the applied stress. This allows for a decrease in the thickness of the shaft hence a reduction in mass. However, as the radius increases, so will the drag produced by the rotorshaft. A compromise must therefore be reached between shaft mass and shaft drag. Due to this the radius of the top rotorshaft was constrained at 0.15m. Subsequently a thickness of 0.0265m was calculated, in order to resist the applied loads, leading to a shaft mass of 68.3kg, for a maximum Von Mises stress of 342.8MPa. For the lower shaft the radius is already determined as being equal to that of the top shaft plus 1cm gap plus its thickness. Therefore, its thickness need only be determined. This was found to be 0.01675m, leading for a total mass for the lower shaft of 11.8kg, for a maximum Von Mises stress of 340.6MPa. The mass of the total shaft system is therefore 80.1kg.

Now the mass of the HAMRACs total rotor system can be evaluated. It is constructed from the rotor shaft system, six rotor blades and six hub connections. The total mass of the rotor system is therefore 403.6kg. This exceeds the mass budgeted for the rotor system by 148.6kg. However, if the budget contingency factor is removed it only exceeds by 114.5kg. As the structures department has recommended an increase in the thickness of the blades to improve the strength and stiffness, this will also allow for a decrease in the mass of the blades, similar to how increasing the thickness of an aircraft wing will also lead to a decrease in mass. It is recommended to continue this analysis with thicker rotor blades to investigate how this may reduce the mass of the rotor-subsystem, as a mass reduction of only 19kg is required per blade to bring the subsystem within budget.

Additional recommendations for future structural analysis of the rotorcraft system are to consider the dynamic loading of the blade. Through this a vibrational analysis of the HAMRAC can be conducted. This will identify the natural frequency of components and ensure that components are designed in such a way that the rpm of the helicopter does not cause the components to oscillate in an unstable fashion. Further analysis into the fatigue behaviour is also recommended to ensure that parts are able to survive a pre-determined baseline number of cycles, as cyclic loading for rotorcraft occurs at a much faster frequency than for airplanes. This will also help the reader to identify the regularity of maintenance checks and the safe lifetime for HAMRAC components.

9.5 Airframe Design

In this section, the structural design of the airframe will be elaborated upon. Subsection 9.5.1 consists of a short introduction on rotorcraft airframes. The used assumptions during the analysis are elaborated in subsection 9.5.2, after which the load cases are determined in subsection 9.5.3. The analysis is performed in subsection 9.5.4. The results and recommendations of the structural design can be found in subsection 9.5.5. Lastly, the landing gear is briefly discussed in subsection 9.5.6

9.5.1 Introduction

The design of an airframe of a rotorcraft is significantly different to the design of an airplane airframe. There are some differences in terms of the load paths that constitute the structure. It consists of several parts, of which the bottom and body structure will be the only heavily loaded parts, and thus have to be strongest parts of the airframe. A typical example of an airframe structure is depicted in Figure 9.6a, where the body and bottom structures are numbers 2 and 7, respectively. There exist different types of rotorcraft airframe, but for the HAMRAC, a stressed skin construction will be used. This semi-monocoque construction has the advantages that it has a high strength to weight ratio and is easy to manufacture. Its body part consists of a framework of vertical and horizontal members covered with a metal skin, and its bottom consists of a monocoque structure[2].

[2]https://www.slideshare.net/partyrocka99/1-week-1-helicopter-structure[cited 20-1-19]

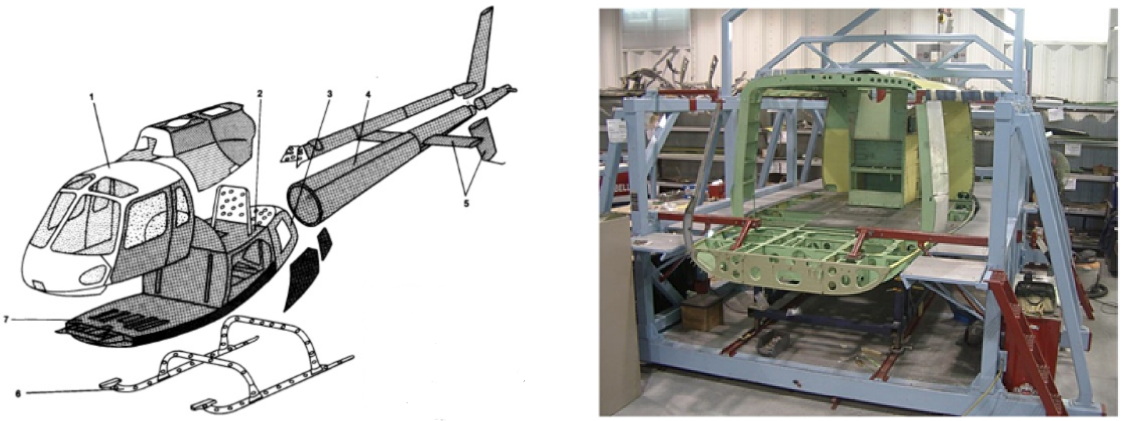

(a) *Example airframe structure* **(b)** *Frame of a Bell 412*

Figure 9.6: *Airframe figures*

9.5.2 Assumptions

For simplification purposes, a few assumptions have been made during the design. These assumptions are listed below:

- **Forces along axis other than the z axis can be neglected.** Only forces along the z axis have been considered. There will also be forces acting in other directions, such as drag, but it is assumed that these forces are relatively small and can be neglected.
- **The cross-section analysed is critical.** Due to time constraints, only one cross-section of the airframe has been analysed. The cross-section of the aircraft will differ a lot along its length, but the one analysed it assumed to be critical.
- **The cross-section can be idealised.** The cross-section is idealized, so booms have been placed along the cross-section. During idealisation it can be assumed that booms only carry direct stresses, and the skin takes all shear stresses. This follows the method outlined by Megson [82].
- **The resultant shear force acts through the shear center.** Due to this assumption, no twist will be induced in the cross-section.

9.5.3 Load Cases

The design of the airframe must be based on its critical load case. All load cases have been evaluated, and the conclusion has been drawn that either during the hover performance or the landing performance the airframe has to endure the highest loads. During hover, the lift produced by the main rotor will be highest, and during landing, the normal forces acting on the airframe through the skids will be highest. These two load cases have been further evaluated, and a shear diagram and a moment diagram of the forces have been made. Based on these diagrams, the maximum load case can be determined and this case is used in further analysis.

The magnitude and the locations of the weight forces are based on the mass and cg budget shown in section 7.4. The loading diagrams are depicted in Figure 9.7. Because equilibrium state has not been considered during these budgets, the moment diagrams do not perfectly end at zero as they should. For the hover case a load factor of 5.25g has been used, and for landing the load factor equals 6g, both including a safety factor of 1.5, as previously described in subsection 9.1.2. The absolute maximum value of the internal shear force is higher during the landing case, but the absolute maximum value of the internal moment is higher for the hover case, so from these diagrams it is not clear which case will be critical. Therefore, both cases have been considered in further analysis.

9.5.4 Analysis

The analysis has been conducted on a cross-section, based on the frame of a Bell 412. This frame is shown in Figure 9.6b. The bottom of the airframe has to be very strong in order to withstand the high shear forces acting on the airframe during landing. Between the attachment points of the skids the airframe has to be the

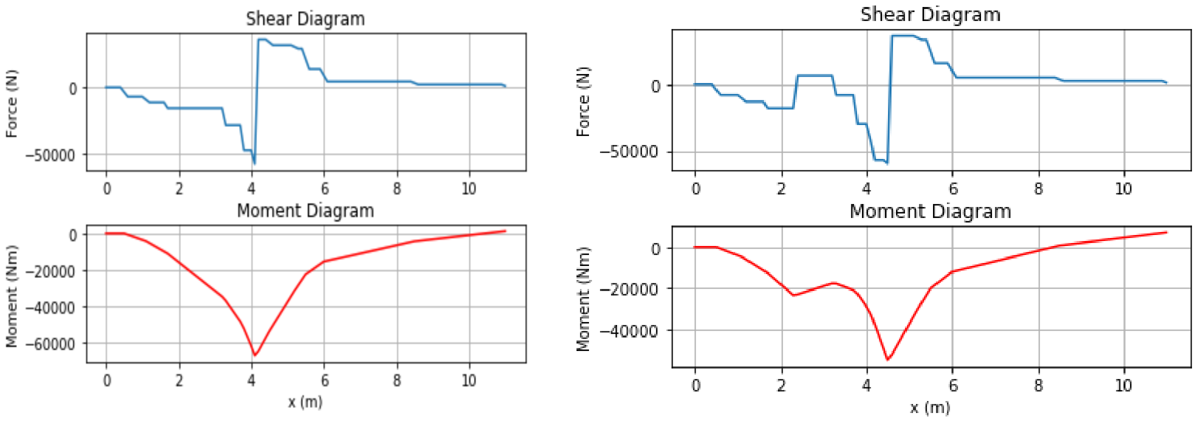

(a) *Hover case* **(b)** *Landing case*

Figure 9.7: *Loading diagrams of the airframe*

strongest, because here loads will be heaviest. A cross-section of this location has been analysed. A schematic sketch is shown in Figure 9.8a. The cross-section consists of an upper part which contains a relatively thin skin with equally spaced stringers along its length. The bottom part is a relatively thicker monocoque structure.

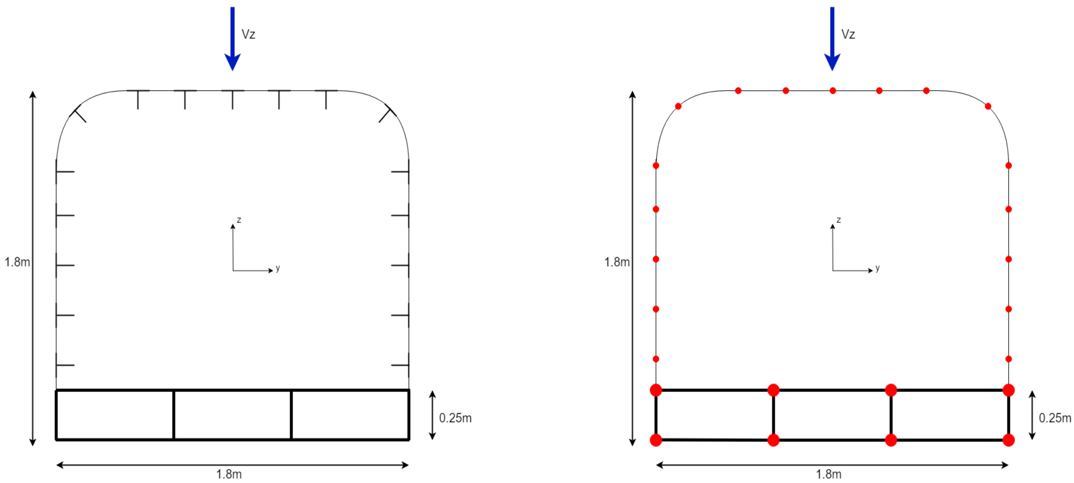

(a) *Cross-section non-idealized* **(b)** *Cross-section idealized*

Figure 9.8: *Critical cross-section of the airframe*

The first part of the analysis consists of the idealization of the cross-section, completed in accordance with the idealization process outlined in Megson [82]. Booms have been placed at stringers on the upper part and at intersections on the bottom part. This new idealized cross-section is sketched in Figure 9.8b. The next step is calculating the areas of the booms. This has been done using Equation 9.28. If the boom is not located at a stringer $B_{i,stringer}$ equals zero.

$$B_i = B_{i,stringer} + \sum_{j=1}^{N} \frac{t \cdot b}{6}(2 + \frac{\sigma_j}{\sigma_i}) \tag{9.28}$$

In this equation j is an adjacent boom, t is the thickness of the adjacent skin, b is the distance to the adjacent boom and N is the number of adjacent booms. The stresses within the booms are not known yet, but the stresses fractions are equal to the fractions of the distances from each boom to the neutral axis. The neutral axis goes through the centre of gravity, which has to calculated based on the non-idealized cross-section. After this is found, the boom areas can be calculated.

The next step is calculating the moment of inertia. Due to the idealization, the moment of inertia equals only the sum of the Steiner terms of the booms. The formula is shown in Equation 9.29.

$$I_{yy} = \sum_{n=1}^{N} B_i \cdot d^2 \tag{9.29}$$

In this equation, d is the distance from the boom to the neutral axis. After this, the bending stresses in the booms can be calculated, using a reduced form of Equation 9.1 for symmetry.

$$\sigma_x = \frac{M_y}{I_{yy}} \cdot z \tag{9.30}$$

Because the cross-section consists of multiple cells, both base shear flow and a redundant shear flow have to be calculated. In each cell a cut has been made, after which the base shear flow has been calculated. This has been done using Equation 9.31

$$q_{b,ij} = -\left(\frac{V_z}{I_{yy}}\right) \sum_{r=1}^{N} B_i z_r + q_i \tag{9.31}$$

After the base shear flow in each wall has been calculated, the redundant shear flow for each cell has to be found. The first step in doing this is calculating the moment induced by each base shear flow around an arbitrary point and sum to that the torques generated by the redundant shear flows, which should equal zero, shown Equation 9.32.

$$0 = \sum M_i + \sum_{R=1}^{N} 2A_R q_{0,R} \tag{9.32}$$

In this equation A_R equals the enclosed area of a cell and $q_{0,R}$ the redundant shear flow in that cell. This equation is the first of N+1 equations necessary to be able to compute all redundant shear flows. The other equations consist of the equation of twist of each cell, shown in Equation 9.33

$$\frac{d\theta}{dx} = \frac{1}{2A_R} \oint \frac{q ds}{Gt} \tag{9.33}$$

This leaves you with a set of five equations and five unknowns, being the four redundant shear flows for each cell, and as a fifth unknown $\frac{d\theta}{dx}G$. For each wall now the total shear flow can be found, by summing its base shear base with accompanying redundant shear flow(s). Now the shear stress wall can easily be found by dividing the total shear flow with its wall thickness.

$$\tau_{yz} = \frac{q}{t} \tag{9.34}$$

The last step of this analysis consists of calculating the Von Mises stresses at every part along the cross section using Equation 9.35

$$\sigma_{VonMises} = \sqrt{\sigma_x^2 + 3 \cdot \tau_{yz}^2} \tag{9.35}$$

9.5.5 Results and Recommendations

The analysis elaborated upon in subsection 9.5.4 has been modelled in python, and the outcome of this model is the ultimate Von Mises stress. In order to guarantee safety during all flight phases this Von Mises stress has to be lower than the yield stress of the used material, which will be an $Al2024-T3$ alloy. Simultaneously, the mass of the HAMRACs airframe should be kept as low as possible. Different variables could be adjusted in the model, such as the distances between the stringers, the stringer area and the skin thicknesses of both the upper and lower part of the cross-section. The mass of the body and bottom parts were calculated by multiplying the area of the cross-section with its estimated length along the x axis, taking into consideration that vertical frames will be located throughout these components as well. The entire airframe consists of more parts than just the body and bottom parts, so as a really rough estimate, a mass fraction of 50% has been taken for these two parts. By trial and error, the four variables have been tweaked such that the mass was as low as possible while still complying with the yield stress value criterion. The results are depicted in Table 9.3.

From the table it can be concluded that the thickness of the cross-section can be very thin and still the material would not yield. When compared to reality, these numbers do not seem reasonable, so it can be concluded that there are some mistakes within the analysis. The assumptions made might not have been valid for this model, or the forces acting on the airframe have been underestimated.

Table 9.3: *Results of the airframe analysis*

Characteristic	Value
Stringer pitch [m]	0.30
Stringer Area [m^2]	0.000150
Skin thickness upper part [m]	0.0002
Skin thickness bottom part [m]	0.00053
Yield stress alloy [MPa]	323
Maximum Von Mises stress [MPa]	324
Airframe mass [kg]	107.8

A few recommendations have been considered for in a further design phase:

- Do not only consider forces acting in z-direction, but also in x- and y-direction, as they might induce stresses that significantly influence the strength of the airframe.
- Do not only consider the yield of the material, but also consider buckling as a possible failure mode.

9.5.6 Landing Gear

For the landing gear of the HAMRAC it has been decided to use the landing gear that is manufactured by Airbus Helicopters for use in the H145/EC145, emergency response aircraft. The decision to use a pre-fabricated landing gear, is one that will save time and cost during the development phase of the HAMRAC. The testing and certification of landing gear can be a very lengthy process in the development phase of a helicopter, due to the fact that properly functioning landing gear is critical for the safety of the occupants. Whereas the purchasing of landing gear from this manufacturer ensures that it shall function properly without the need for additional certification. The landing gear need only be purchased from Airbus Helicopters and supplied to the manufacturing location of the HAMRAC.

The H145 land gear was selected as it is for a helicopter of similar specification to the HAMRAC. Its operational empty weight of 1919kg [46] exceeds that of the HAMRAC, ensuring that the gear will be able to resist the landing loads on the HAMRAC. Furthermore, the landing gear uses skids and is designed for use in rescue operations within mountainous regions. This ensures that it is suitable for use as landing gear for the HAMRAC. Additionally, the EMS configuration of the H145 makes use of rear loading doors [46], similar to the configuration of the HAMRAC. This also ensures that the landing gear will be able to support the aircraft when loaded from the rear. This landing gear will therefore be able to support the HAMRAC during any of its operating conditions.

The landing gear is of a lightweight tubular Aluminium construction and has a skid length of 2.4m [12]. The design of the gear is such that the bearing rings on the cross tubes swivel in their brackets, so that all forces are absorbed by bending the cross tubes only [12]. The long skid length ensures that the helicopter is stable on uneven ground and helps disable ground resonance [12]. The landing gear provides a fuselage ground clearance of 0.45m.

10

Stability & Control

In this chapter, the stability and control characteristics of the HAMRAC will be analysed. The focus is put on the design and mission-specific constraints. The chapter starts with section 10.1, in which the stability and control subsystem elements are highlighted. An initial strategy regarding achieving balance is defined in section 10.2 and a maximum range in center of gravity in which normal operations can be performed is determined. The chapter continues with a description of the flight controls in section 10.3, the rotor hub design in section 10.4 and the control surfaces in section 10.5. The stability of the rotorcraft is further analysed in section 10.6 and the expected behaviour modes are highlighted. section 10.7 subsequently discusses whether the HAMRAC is able to control these modes. After that, the flying qualities section 10.8 are discussed, describing whether the rotorcraft is also able to successfully manoeuvre its mission. Finally, the chapter concludes with a discussion in section 10.9 on the automatic flight control system needed to meet the requirements resulting from these required flying qualities.

10.1 Subsystem Description

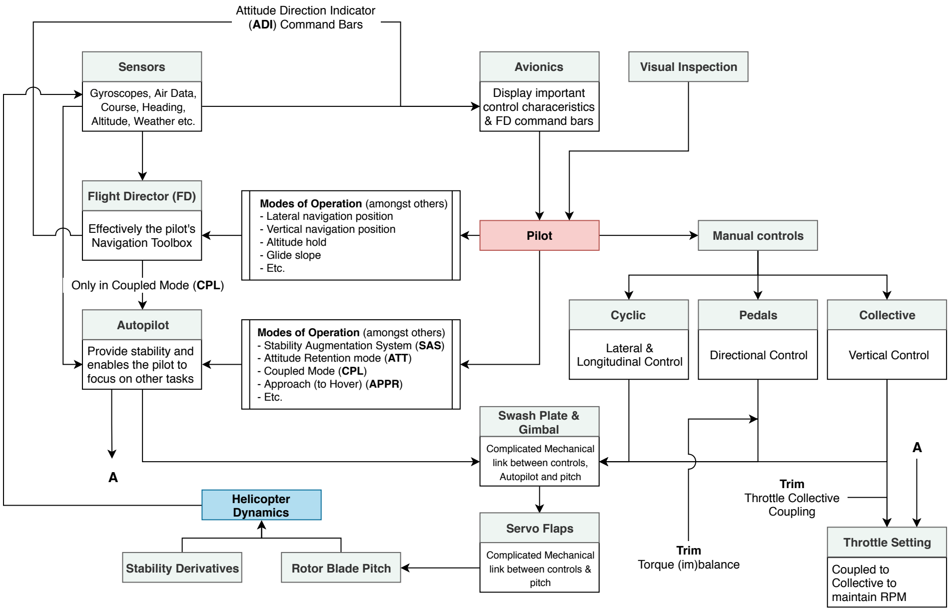

Figure 10.1: *Overview of the main elements of the stability and control system of the HAMRAC. Relations between pilot, actuators, computers, etc. are indicated by arrows.*

In Figure 10.1, an overview is provided of the main elements of the stability and control subsystem of the HAMRAC. As one can see and would expect, the subsystem consists of a large number of elements. Subsequent sections will discusses the main interactions that can be seen in this figure.

10.2 Achieving Balance

Before one can start to design or to analyse the stability characteristics of a helicopter, one must make sure that the rotorcraft is able to achieve balance in the first place, both during cruise and hover. Of these two situations, hover proves to be more limiting due to the ineffectiveness of control surfaces during this flight phase and will therefore be discussed in this section.

Importance and General Information Ideally, the center of gravity (CG) of a helicopter is located directly under the center of the rotor mast during hover, which would lead to the fuselage being in a horizontal position, as can be seen in Figure 10.2. For this scenario, cyclic input from the pilot is in principle only necessary to balance gusts.

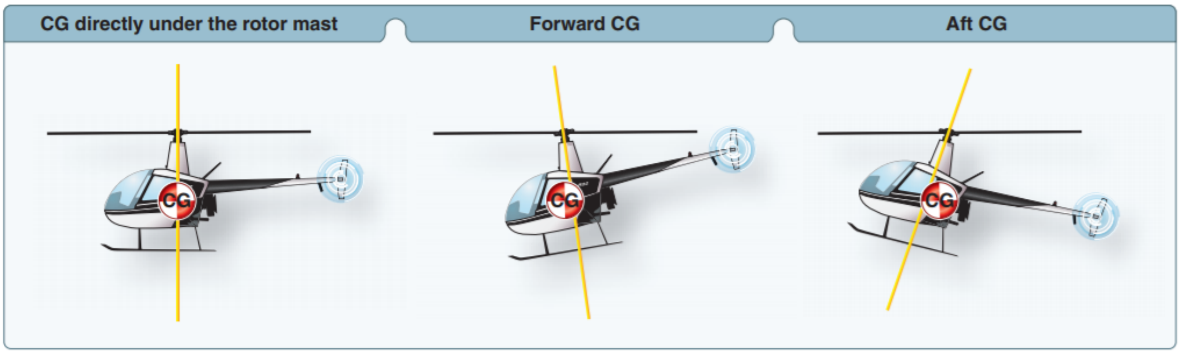

Figure 10.2: *Influence of the location of the CG on the balance of the HAMRAC [7]*

To consider what happens to the balance of a helicopter when the location of the CG is more forward or aft, it might be helpful to consider the helicopter to be a pendulum suspended from the rotor hub [7]. The fuselage pitch angle changes as the location of the CG changes in order to achieve balance, which can be seen in the middle and right sections of Figure 10.2. In these situations, the pilot has to apply cyclic control in order to tilt the rotor disc and make sure that the rotor does no exert lateral forces on the helicopter. However, there generally are strict limits regarding the range of these CG locations of the rotorcraft.

As keeping balance for extreme CG locations requires large displacements of the cyclic control, less cyclic control is available to cope with disturbances or perform general flight manoeuvres. For instance, if the CG would be located too much forward, the HAMRAC would have trouble to decelerate, cope with gusts from certain directions and it could be unable to perform the flare manoeuvre that is essential for a safe landing during autorotation. On the other hand, if the CG would be located too much aft of the rotor mast, the rotorcraft could be unable to hover under strong headwind conditions. In addition, it would not be able to reach high velocities during cruise. This could cause the fuel to deplete before the destiny of the flight is reached [5] [7]. These risks are especially relevant due to the high wind speeds that are part of the operational environment of the HAMRAC and helicopter requirements.

Center of Gravity Range Also the consideration whether it is possible to perform the hoist operation aft of the helicopter fuselage, as is explained in subsection 7.3.2, largely depends on the change in center of gravity location it causes. If this change would be too much aft due to the relatively large distance between the hoist system and the rotor mast, the risk of the HAMRAC being uncontrollable during hover would be too large. In order to assess whether this design feature is possible, it is important to know what the CG range is in which the helicopter can safely operate. To accurately calculate this range for the HAMRAC, a very complicated and extensive control model is necessary using data from flight- and wind tunnel tests. As this goes beyond the scope of this preliminary design, an analysis on center of gravity ranges of similar helicopters is performed.

Only the **longitudinal** center of gravity range is analysed in this section, as achieving lateral balance is in general not a large problem for a helicopter [5]. For this analysis, relevant data on the CG limits of rotorcraft that are in function and size similar to the HAMRAC was found and used. The reference CG ranges were found in official certification documents of the EASA[1,2,3] and are listed in Table 10.1. The numbers in this table are defined as the difference in the maximum forward and aft location of the center of gravity that are allowed during its operation. This means the center of gravity can be located at any point in between of these two CG locations, which is why it is called a “range” during this analysis. The CG ranges given vary linearly between the two values that are given in relation to their weight. For two of the three models, this range changes as the weight of the rotorcraft changes. Generally, the rotor mast is located towards the aft limit of this range, in order to have enough cyclic available to reach high cruise speeds.

Table 10.1: *CG ranges of reference rotorcraft for the HAMRAC*[4]

Helicopter Model	CG Range at Maximum Weight [cm]	CG Range at Minimum Weight [cm]	Empty Weight [kg]
Airbus AS350	26	38	1174
Airbus H135	19	39	1455
Airbus EC155	27	27	2618

In subsection 7.4.2 it was found that the difference in center of gravity location between the most forward and most aft limit during the operation of the HAMRAC is about 16.4cm. If one compares that with the numbers in Table 10.1, one could conclude that this is less than the ranges that where found for the reference aircraft. The CG ranges of the AS350 and H135 show that for comparable rotorcraft to the HAMRAC, the range actually can even be higher than 27cm, as the weight of the helicopter decreases during flight. Therefore, one can conclude that the current configuration of the HAMRAC should satisfy the CG limits that are required to keep it controllable and safe to operate under the conditions specified by the mission profile. Furthermore, as the hoisting operation that is performed at the back of the fuselage does not shift the CG position outside of this range, as explained in subsection 7.4.2, it can be concluded that this change with respect to the conventional location of the hoist system does not pose significant problems regarding controllability.

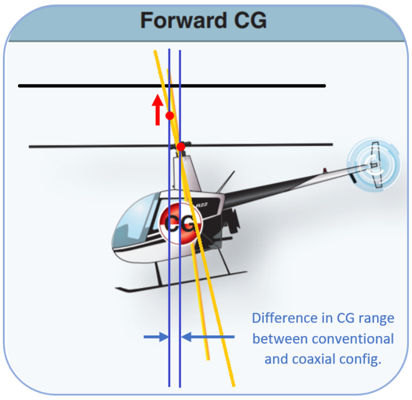

Figure 10.3: *Longer CG range for a coaxial rotorcraft. Exaggerated effect for clarity. The red dot indicates the point where the resulting lift from the rotors acts.*

Another element that supports this conclusion is the fact that the HAMRAC has a coaxial rotor configuration. This most likely results in an increased allowable CG range. Due to the fact that the resulting lift vector of the two rotor discs is generally located higher than for a conventional configuration, the helicopter could be considered to be a prolonged pendulum. As a result, a similar increase in collective control displacement (angle of the pendulum) results in a larger allowable CG position (forward or aft) for a coaxial configuration, compared to a conventional configuration. This phenomenon is visualised in Figure 10.3.

[1] URL `https://www.easa.europa.eu/sites/default/files/dfu/TCDS_EASA_R105_AH_SA365_AS365_EC155_Issue_04.pdf` [cited 16 January 2019]

[2] URL `https://www.easa.europa.eu/sites/default/files/dfu/TCDS_EASA_R009_AHD_EC135_Issue_14.pdf` [cited 16 January 2019]

[3] URL `https://www.easa.europa.eu/sites/default/files/dfu/TCDS_EASA_R008_AH_AS350_EC130_Issue_11.pdf` [cited 16 January 2019]

10.3 Helicopter Flight Controls

An important part of the Flight Control System of a helicopter consists of the actuators that enable the pilot to actually control the rotorcraft by displacing the cyclic, collective and pedal controls. Using these controls should finally result in constant (collective), differential (pedals) or cyclical pitch changes in all of the rotor blades. Although there are multiple ways to achieve this, most of the current helicopters use a complicated mechanical swashplate mechanism instead of a fly-by-wire (FBW) electrical system. The coaxial configuration of the HAMRAC complicates the transmission from pilot controls to pitch changes in the rotor blades, and commonly leads to a very complex swashplate system, as can be seen in Figure 10.4. This is one of the main disadvantages of this configuration, due to its increased complexity, weight and parasitic drag. Therefore, an extensive design analysis was performed in order to achieve high maintainability and control capabilities while keeping other aspects into strong consideration, most importantly drag, reliability, development cost and weight.

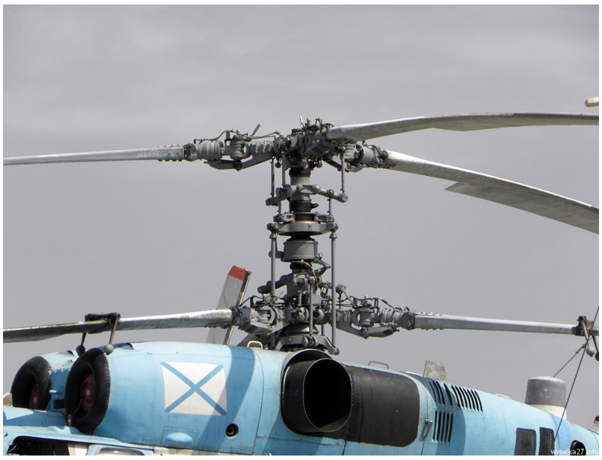

Figure 10.4: *Kamov Ka-27 rotor hub*[5].

Fly By Wire (FBW) While FBW controls are being used in many (generally larger) winged aircraft nowadays, almost all helicopters that are currently available on the market use mechanical control systems[6]. An FBW system was considered because of the potential of such a system to reduce the effects of complicated rotor hub. Replacing mechanical (and hydraulic) linkages by electric wiring and actuators on the blades could theoretically lead to a vast reduction in weight and complexity.

However, it was eventually decided to not include an FBW control system in the HAMRAC. The main reason for this is the fact that this technology is, at the moment, only in an early stage of development in the helicopter industry. Choosing this design feature would lead to a very extensive development program, the cost of which would, in this case, outweigh the potential benefits. This is illustrated by the enormous development costs and high purchase prices of both the Sikorsky RAH-66, which was later cancelled and the Airbus NH90: respectively 6.9 billion USD[7] (two rotorcraft built) and 12.6 billion USD[8] (about 300 rotorcraft built). A price tag moving to this direction would make the HAMRAC not competitive with respect to current competitors. In addition, the market is not fully convinced of this technology at the moment, which was shown by reactions to a recent crash of the Bell 525, the first commercial helicopter that uses an FBW control system [9].

[5] URL https://www.flickr.com/photos/hydrotechinc/8379753245 [cited 22 January 2019]
[6] URL https://www.flyingmag.com/aircraft/jets/fly-by-wire-fact-versus-science-fiction [cited 08 January 2019]
[7] URL https://en.wikipedia.org/wiki/NHIndustries_NH90 [cited 08 January 2019]
[8] URL https://www.airbus.com/helicopters/military-helicopters/specialised/nh90-tth-and-nfh.html [cited 08 January 2019]
[9] URL https://www.rotorandwing.com/2018/01/17/ntsb-approves-probable-cause-fatal-bell-helicopter-525-crash/ [cited 08 January 2019]

Servo Flaps Another possibility to counter the disadvantages posed by the coaxial swashplate mechanism that was considered, is the use of so called servo-flaps. This system changes the pitch angle of the individual rotor blades not by applying a moment (through a hydraulic force) directly to the blade itself, but instead generates a moment by deflecting small flaps that are located towards the tip of the blade, just behind the airfoil. This can be seen in Figure 7.2. As the arm of the flap at this point of the blade is relatively large compared to conventional systems acting at the root, the force required is significantly lower. In fact, it eliminates the need for hydraulic systems for control purposes [10]. The effectiveness and simplicity of this technology has been proven by its use in for instance the Kaman K-Max [10]. The question that remains, however, is whether this principle can also be applied to the current coaxial configuration. Research by NASA has shown that the use of servo-flaps and the elimination of the swash plate mechanism for a conventional helicopter can lead to a reduction of 40% in the weight of the flight control system, a reduction of 8% in gross weight, a reduction of 26% of parasitic drag during cruise and a significant reduction in maintenance costs [54]. These effects can only be expected to be even stronger for a coaxial configuration, as the double swashplate mechanism, that is generally used, is much more complicated than the one used for a conventional helicopter. Choosing the servo-flaps to be positioned behind the rotor blade like the K-max, instead of integrating them in the blade itself, leads to additional drag. However, due to the fact that the moment with respect to the rotation axis is larger there the servo-flaps can be smaller in size. In addition, the hub drag reduction and other advantages mentioned above are expected to outweigh the drag increase. Finally, by choosing this configuration, a technology is integrated that has been flight proven and can be integrated easily without resulting in a redesign of the blade itself, which was definitely something that was also taken into consideration.

In order to control the servo-flaps, Kaman generally uses the combination of a gimbal and control rods inside the rotor shaft, as can be seen in Figure 10.6. This is possible because of the low structural loads in the control system (compared to a hydraulic system). As a result, the swashplate mechanism can be replaced by a smaller gimbal. However, one encounters a problem when trying to apply this principle to a coaxial configuration, as it would be impossible to control the lower rotor blades from the inside of the shaft. The solution that is proposed for this problem can be explained using Figure 10.5. This figure shows a rotor hub configuration for a coaxial rotorcraft that does not use servo-flaps. For the HAMRAC, the linkages at the red dots would be changed into rods that are (indirectly) connected to the servo flaps, instead of to the rotor blade itself. In order to control the lower rotor blades, a conventional swashplate will be used (blue area in Figure 10.5). The lower swashplate in the figure, however, shall be replaced by a gimbal (purple area in Figure 10.6) similar to the one shown in Figure 10.6. Both the gimbal and the swashplate are mechanically connected to the controls of the pilot (yellow link in Figure 10.5).

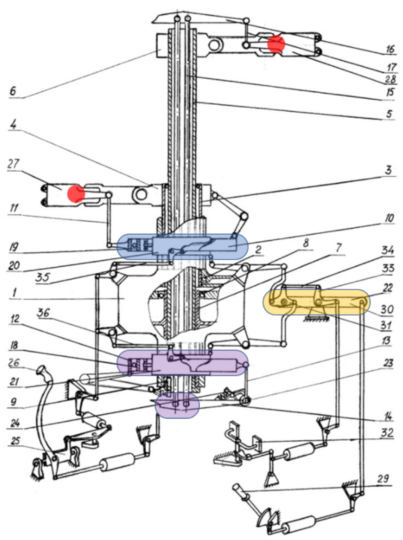

Figure 10.5: *Reference rotor hub configuration for a coaxial helicopter [66]. Areas of interest indicated by different colours.*

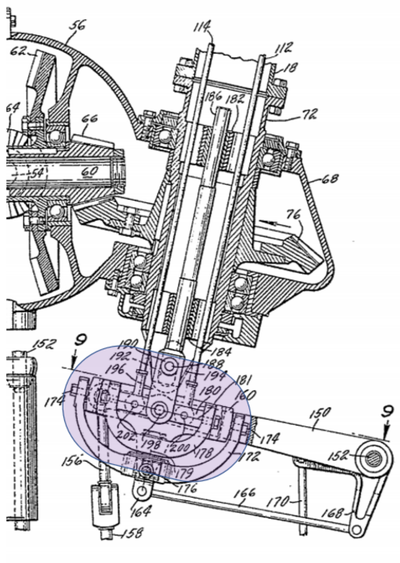

Figure 10.6: *Gimbal system used to control the servo flaps on the rotor blades Kaman K-140 (purple area) [29]*

This configuration results in a similar amount of parts to a configuration with two swashplates. However, it is using proven technology of the Kaman Aerospace Company, and eliminates the need for a heavy hydraulic system. This simplicity adds to the general reliability and reduces the cost of the control subsystem. In addition, it reduces the need for structurally strong, heavy rods. Finally, it reduces aerodynamic drag around the rotor hub during cruise. Because of these reasons, this control configuration is chosen over a possible configuration without servo-flaps and with two external swashplates. The 'standard' spanwise location of a servo flap is at 75% of the span of the rotor blade, as it is relatively free of high speed effects such as stall and drag divergence that occur more towards the tip while the airflow around it has sufficient speed to generate a moment that is large enough to pitch the blade [52], therefore the servo-flaps of the HAMRAC will initially be located at this location, and are to have a similar servo-flap size to rotor blade size ratio as the K-max. Actual performance tests in a further design phase will then lead to more iterations on the specific size and location. At the current location the Mach number is at most about 0.67, which is within the limits as an analysis from the Aerodynamic Department required it to be lower than 0.7.

10.4 Main Rotor Hub Design

In this section, the main rotor hub design is elaborated upon

10.4.1 Considerations of Bearingless and Hingeless Main Rotor Design

An aerodynamic requirement was derived which has direct implications on the main rotor hub design. This requirement is specified as:

- The HAMRAC's rotor hub should attribute to less than 20% of total rotorcraft drag.

As early as 1994 [48], it was predicted most future rotors would be built as bearingless rotors. The most recently developed helicopters that serve as a relevant reference for our design, Airbus' H135 and H145 have hingeless and bearingless, and hingeless rotor hubs, respectively. The reason hingeless and bearingless rotor designs are possible today, is attributed to the improvement in composite technology [48]. This type of rotor hub system design reduces operational costs [72] [84] and maintenance (due to the use of fewer parts), and allows for a better performing hub design (due to simple and clean aerodynamics) [48]. Additionally, due to reduced drag, a higher payload can be achieved [72] [84]. Since hub drag accounts for a significant part of the rotorcraft's drag, and there is a specific requirement to its limit, it is paramount that it is reduced, should it be feasible. In Figure 10.7, it can be observed that a bearingless hub system has both simpler and fewer parts than the other two systems (articulated and hingeless).

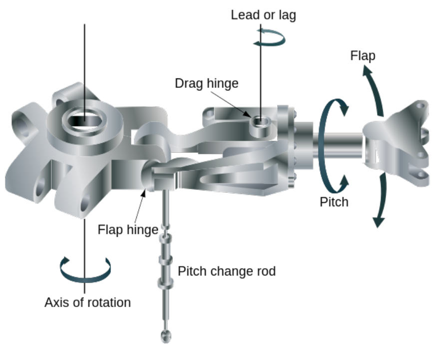

(a) *Fully Articulated Rotor Hub Design [37]*

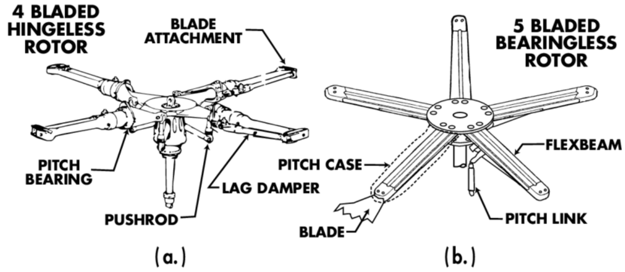

(b) *Hingeless and bearingless rotor hub design [7]*

Figure 10.7: *Several types of main rotor hub system*

As the years have progressed, bearingless technology developments have led to increased weight savings and a reduced number of parts. For example, Airbus' H135 main rotor hub system has a reduced weight of 50 kg and 40% less parts [44] compared to its predecessor the B0105. In Figure 10.8 a bearingless hub of the Airbus H145 can be observed.

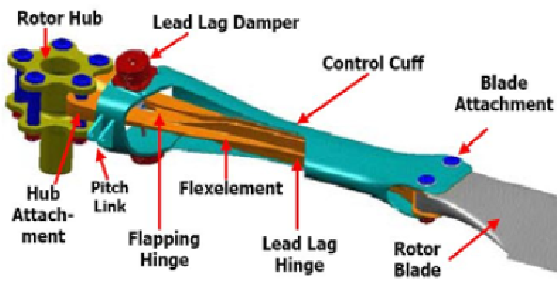

Figure 10.8: *Illustration of main components of bearingless main rotor hub system [34]*

The main distinguishing feature of a bearingless rotor is the torsionally soft flexbeam located between the main blade and hub [48]. The primary function of the flexbeam is to provide elastic hinges to enable flapping, lagging and feathering [34]. Its cross-sectional shape is designed to allow for a displacement in three directions in a single part [34]. Additionally, a control cuff or torque tube, encloses the flex beam. Its design must be sophisticated to meet the required lag and torsional stiffness with low aerodynamic drag [34]. Pitch control can be achieved by rotating the torsionally stiff torque tube through the servo-flap system. The damper system is another essential part to this bearingless rotor hub system.

Boeing built the first full-scale bearingless rotor, for the Bo 105 and flight tested it successfully [48]. The rotor system of the Bo 105 consisted of twin flexbeams (C-beams) and a single torque tube rod and did not have lag dampers as can be seen in Figure 10.9. The bearingless hub of the RAH-66 Comache can also be seen in that figure.

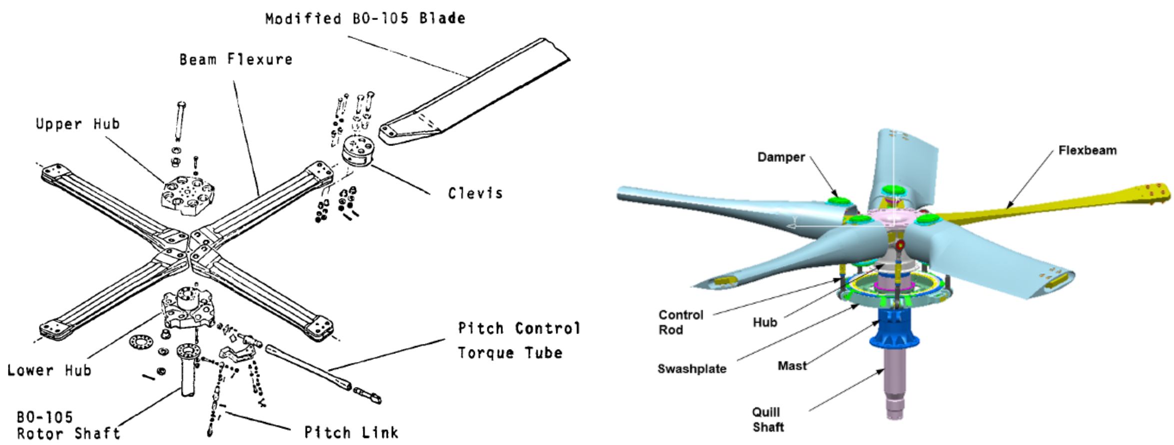

(a) *The first successfully flight tested bearingless rotor hub design (Bo 105) [48]*

(b) *The Comache's bearingless rotor hub design*[10]

Figure 10.9: *Successfully flight tested bearingless main rotor hub systems*

Due to design considerations, bearingless and hingeless are designed as soft-in-plane rotors. Soft-in-plane means that the lead-lag frequency is normally less than the shaft rotational frequency [11]. The problem is that a soft-in-plane rotors are more susceptible to air resonance instability than fully articulated systems. However, it has been found that reducing pitchlink stiffness increases the effectiveness of the torque tube and causes a stabilising influence on air resonance stability [48].

As well as this, due to inherently small lag displacements (at the root) of a soft-in-plane design, mechanical lag dampers which are usually used to deal with ground resonance instability, become ineffective. This rotor-

[10] URL `https://www.sikorskyarchives.com/RAH-66%20COMANCHE.php` [cited 22 January 2019]

[11] URL `http://helicopterforum.verticalreference.com/topic/14174-soft-in-plane-rotor-system-what/` [cited 22 January 2019]

body system instability can be reduced with elastomeric dampers and/or negative pitch-lag coupling [48]. In basic terms, negative pitch-lag coupling results in a feathering motion when a lag-wise shear reaction occurs. Elastomeric dampers are usually installed between the torque tube and the flex beam. And to introduce the desired negative pitch-lag coupling, the pitch link is slightly inclined. This has to be designed with caution since a negative pitch-lag coupling destabilizes ground resonance stability [48].

10.4.2 Design choices for the HAMRAC & further considerations

Type of Hub Mechanism Ideally, a crucial cross-strap type of hub mechanism is used, since it allows for a design with smaller number of parts and less weight than separation type hub mechanism. However, at this moment, no rotorcraft that uses a three blade rotor has been found to use a crucial cross-strap. Therefore, the possibility of using a crucial cross-strap for the HAMRAC must be further investigated through testing. The separation type hub mechanism can be seen above in, Figure 10.9a as Boeing first implemented it. The crucial cross-strap type has one flexbar per two blades. The flexbar used for this configuration can be seen in Figure 10.10.

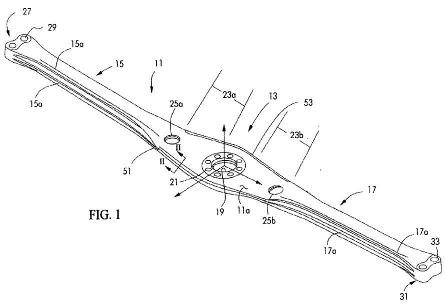

Figure 10.10: *A crucial cross-strap type flexbeam*[12]

Flexbeam Cross-section Several cross-section designs for the flexbeam must be investigated further through testing. The ones considered are: Double C-channels, X-type, H-type and Double H-types and are shown in Figure 10.11. Tests should be done to perform a comparative analysis of their bending (in lag direction) and torsional stiffness, but also an assessment should take place regarding the ease of manufacturing associated with the design, using composite materials. The cross-sections considered for this process are illustrated in Figure 10.11.

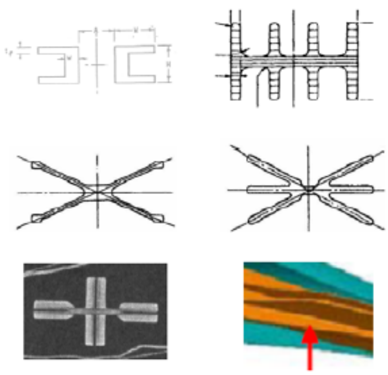

Figure 10.11: *Considered flexbeam cross-sections for design [34]*

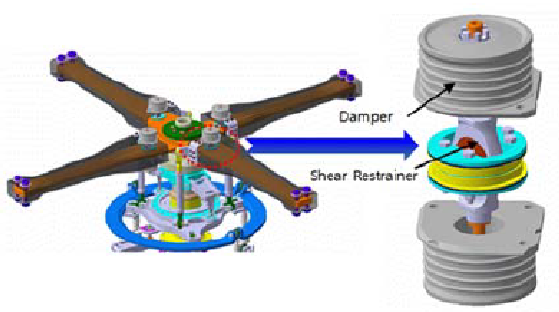

Figure 10.12: *Restrainer & damper System [34]*

Torque tube Two torque tube cross-sectional shapes shall be investigated, namely the circular and elliptical shapes. Structural and aerodynamic performance will be investigated as well. The requirements of the design should make sure that the torque tube provide an amount torsional stiffness that allows for changes

[12]URL `https://patents.google.com/patent/EP1088754A3` [cited 22 January 2019]

in blade pitch and that hub drag is reduced [34]. As stated before, the rotor hub system of a rotorcraft is one of the main sources of drag, and aerodynamics should therefore not be overlooked. To avoid interference between torque tube and flexbeam during blade pitch change, a kinematic analysis should be done to determine which torque tube shape best meets the lag and torsional requirements with least amount of interference [34].

Shear Restrainer & Damper System To reduce development costs, the shear restrainer and damper system will be outsourced. An example and its application location are shown in Figure 10.12. Again, for completion, it should be noted that the pitchlink, will work together with the elastomeric damper to improve air resonance stability.

Material Choice Manufacturing of the flexbar and torque tube will be performed in-house with a composite material. Glass fibre and carbon fibre have been considered for this purpose. Even though carbon fibre is more expensive than glass fibre, its tensile strength is higher and its coefficient of thermal expansion is lower. Since both these parts are not large, their main costs will derive from complexity of manufacturing and not material costs itself. The coefficient of thermal expansion is of quite important, since the HAMRAC will have a large operational temperature range as explained in section 6.3. For the above-mentioned reasons, carbon fibre is the material of choice for the design of these parts.

10.5 Control Surfaces Design

The HAMRAC will have horizontal and vertical stabilisers. First their purpose will be explained, where after the location will be determined.

10.5.1 Horizontal Stabiliser

Purpose There are two main reasons to include a horizontal stabiliser in the design of the HAMRAC. The first one is a result from the fact that helicopters in general are longitudinally unstable. The second reason is that a horizontal tail surface can counter for the negative pitch moment and the angle of attack instability that both increase with forward speed [24]. As a result of this, the fuselage can be kept more level with respect to the flight path and thereby the parasitic drag resulting from the body can be significantly reduced.

Location In order to minimise the weight that is added to the structure by the stabiliser, this horizontal surface is typically located at the radius of the rotor disc, or just after the rotor disc. As the distance to the center of gravity increases, the moment arm is larger and the required surface size is reduced. Choosing the location of the stabiliser to be inside the rotor wake results in a performance penalty, especially during hover, due to the download caused by the air moving down in the wake. However, when its location is just outside of the rotor wake, sudden download increases can occur when changing flight mode (for instance, cruise to hover) or when sudden gusts change the behaviour of the rotor wake. This can be seen in Figure 10.13 and can be a significant stability risk regarding the mission profile of the HAMRAC.

The horizontal stabiliser position is chosen to be within the rotor wake, in order to keep the download steady and thereby predictable and controllable during the critical hover phase of the mission. In addition, its location shall be as aft as possible within this wake in order to reduce its weight, size and thereby also the performance penalty it causes during hover. From [1], a horizontal stabilizer position of $0.33Z/R$ and $0.8X/R$, or 1.815 m below the top main rotor and a distance of 4.6m behind the rotor shaft can be calculated. This position complies with the statistical sizing analysis presented in [70]. This position maintains its constant downforce from the rotor wake at low speeds, which is preferable, and allows for increased handling qualities at large forward speeds to counteract the angle of attack instability. Its increased area, which is with 3 m^2 a lot higher than the 1.1 m^2 proposed by statistical analysis, serves to keep this control capability at low-density high altitudes and strong gust interference conditions. This area is validated by the Airbus H135, which is employed at relatively similar heights.

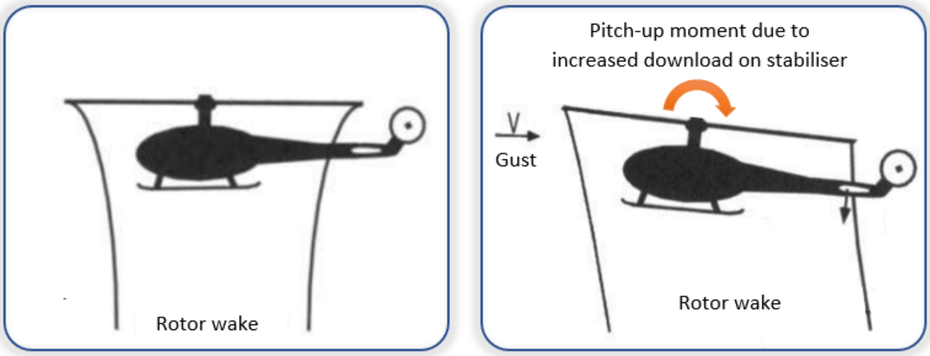

Figure 10.13: *Aft mounted stabiliser resulting in a sudden pitch moment as a result of gusts*

Stabilator Another design choice is to include a so-called stabilator. This is a variable-incidence horizontal stabiliser. The main reason for this decision is that a large reduction in the hover performance penalty due to the download on the tail surface can be achieved using large incidence angles [53]. In addition, being able to change the incidence angle of the stabiliser during hover and cruise can lead to increased longitudinal control power and optimal drag reduction. Especially when integrated with the helicopter autopilot to automatically adapt to different flight speeds and modes it can also reduce the workload on the pilot, which is an important consideration for the HAMRAC mission. These advantages strongly outweigh the weight penalty that results from the control system and thereby justify this design choice.

10.5.2 Vertical Stabiliser

Purpose A characteristic difference between a conventional and a coaxial helicopter configuration is the mechanism it uses to achieve directional balance and control. While a conventional helicopter needs a tail rotor, the chosen coaxial configuration uses torque imbalance: creating a pitch difference between the two rotor discs that keeps the combined lift about equal but creates a torque equilibrium or imbalance when directional control is required.

In autorotation, however, this situation changes. For the conventional helicopter, the main rotor does not generate torque and its rotation mechanically powers the tail rotor. Thereby it allows for good directional control performance. This is not the case for a coaxial configuration. As can be seen in Figure 10.14, the effectiveness of yaw control and the stability of the helicopter is both limited and unpredictable in autorotation. When operating at $(L/D)_{max}$, the lowest point of the graph in Figure 10.14, both an increase and a decrease in pitch result in a drag and thus a torque increase. As a result, the rotorcraft becomes uncontrollable with respect to direction [53]. This is the main reason for a coaxial configuration to require a large vertical fin with a moveable rudder. In addition, a large fin alleviates the requirements on the flight control system with respect to keeping precise torque balance.

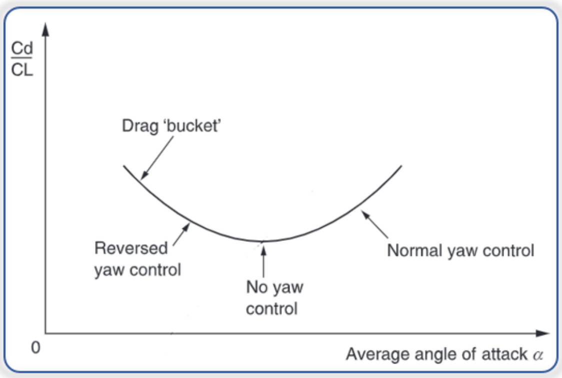

Figure 10.14: *Drag bucket for autorotation of a coaxial configuration [53]*

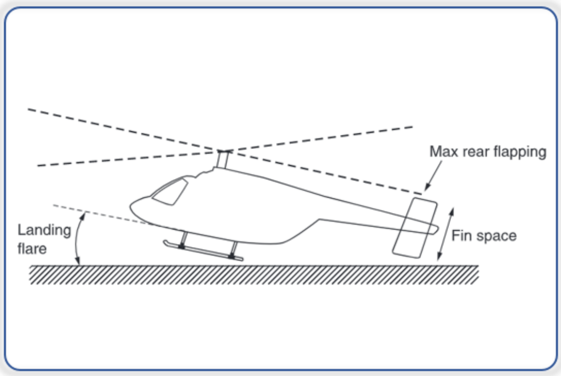

Figure 10.15: *Considerations with respect to tail sizing: flapping and landing flare [53]*

Location As the extra yaw control quality that a vertical fin offers is very much welcomed in coaxial designs, the fin area is significant. Contrary to conventional helicopters, the fin does not support a tail rotor. This means the structurally demanding task of supporting tail rotor vibrations is of no importance here, neither is interference of the fin with the tail rotor, and only the weight of the control linkages and 'empty' structure should be taken into account. It is therefore possible to place a large tail fin. The longitudinal distance from the rotor shaft is 6.43 m [70], a statistically average position. The tail area is 1.5 m^2, after the tail used on Airbus' H135.

10.6 Stability Analysis

Stability and control is concerned with the flying capacity of the helicopter. A distinctly unstable vehicle could never achieve the requirements of this demanding mission profile, an overly stable mission might not be controllable enough. It is the aim of this section to analyse the expected stability performance of the HAMRAC in the aforementioned configuration.

Stability is evaluated from a trim (steady state) condition, for instance the balanced hover situation obtained in section 10.2, and aims to analyse the aircraft response when small disturbances are applied on this trim condition. The aim of trim analysis is to gain insight into partial trims necessary for steady flight, the handling process of obtaining these trim conditions and identifying regions of the flight envelope where trim becomes difficult to obtain. This process is highly iterative and a somewhat accurate estimation requires highly specific and detailed modelling of the helicopter [43][89]. It is therefore decided to leave trim analysis of the HAMRAC to a subsequent paper. This chapter focuses on the altogether more top-level stability and control analysis following a trim assumption. This is more valuable to the design process because it provides an estimate of the (in)stability and subsequent handling that needs to be accounted for [74].

10.6.1 Stability Modes Analysis

Helicopter stability is a difficult subject that is far from comprehensively explored. One of the areas for which example data on which to base initial design is mostly lacking, is in coaxial rotorcraft analysis. The two main rotors discs and lack of tail rotor represent a change in the equations of motion, the linearisation assumption and the stability derivatives of a rotorcraft that is not easily quantified. However, reliable sources offer an elegant solution to this problem: reasonably accurate stability estimates on counter-rotating rotorcraft can be made by assuming an uncoupled response [83]. This assumption can be made because in a coaxial design, opposite blade flapping largely cancels the induced coupled pitching and rolling moments. Coupled yawing moments almost entirely eliminated as well, because there is no change in tail rotor thrust and blade angles of attack in trim counteract each other [74]. NASA further proves [15] the successful application of this simplification, which is used in the following analysis. Furthermore, hingeless rotors are used, as discussed in section 10.4.

These two top-level design choices respectively make the task of evaluating the rotorcraft stability easier and more representative of real-world rotorcraft stability. Note that in some cases, increasing instability actually has favourable effects on the helicopter handling capabilities; in the following discussion, 'unstable' is therefore not straightforwardly 'bad'. Often, pilots will choose slight instability over very stable modes, as they allow for better manoeuvering and the possibility to get out of tight spots [43][83].

The derivation of stability derivatives is a complex matter involving many inputs, and a full-scale stability model of the HAMRAC would be necessary to be able to quantify and optimise the stability derivatives [43][74][18][24]. As this is outside the scope of this project, a mode analysis is performed in which the expected migration of the stability modes from multiple reference rotorcraft (three conventional [43], one tandem [61][85][15]) are indicated. These rotorcraft are chosen because they use the same stability analysis methods and both indicate the progression of their derivatives over forward velocity. It needs to be noted that these aircraft have been extensively optimised and have different configurations than the coaxial aircraft at hand. We can, however, indicate general trends within the most important derivatives and therefore modes and extract some expectations for the coaxial configuration [59][61][15][43]. The stability derivatives are highly interconnected. Therefore, it is decided to bring forward to the discussion to the most influential factor for each. In considering the mass- and inertia-normalised derivative graphs over horizontal velocity, some interesting agreements are found.

Longitudinal Modes In hover and forward flight, the phugoid motion depends mainly on the X_u, M_u and M_q stability derivatives. The pitch subsidence is mainly influenced by M_w and M_q, the heave subsidence by Z_w [43][24].

The drag damping X_u (generally negative and increasingly so with speed) in hover for the tandem configuration has a rather high negative value compared to a conventional aircraft at low speeds [15]. This makes sense when considering that the blade profile drag is generally higher for a twin rotor configuration. In forward flight, this value becomes even more negative, because the fuselage drag is added, although it needs to be noted that the fuselage drag of the coaxial helicopter is expected to be significantly less than that of the Chinook. The coaxial drag damping X_u then behaves like the tandem at low speeds, and like the conventional configurations at high speeds [43][60].

Headwind disturbances in hover cause the rotor to flap, creating a statically destabilizing moment opposite to the disturbance [59]. The speed static stability M_u is therefore preferably somewhat positive at hover for good handling qualities, but high positive values also increase dynamic phugoid and gust responsiveness [61]. The M_u for the HAMRAC is expected to be high, due to the very large rotor moments created by the hingeless blades [43]. As the stabilisers are placed under the downwash of the rotors and therefore create download, they are influential in stabilizing M_u.

At high speeds, the heave mode frequency is influenced by the angle of attack stability M_w, which is close to zero at hover but increasingly positive at larger speeds and aft center of gravity location [59][60]. A positive angle of attack increase is further increased by a positive M_w value. The hingeless main rotors and the fuselage's aft center of gravity have a large destabilizing influence [83]. The horizontal stabiliser is essential in counteracting some of this effect and decreasing M_w again [24]. Horizontal stabilisers are therefore very much required to ensure stability for the high-speed flight phases of the HAMRAC. However, they are at high speed unable to fully counteract the rotor and fuselage contributions. The heave mode therefore becomes unstable at high speeds [61].

Conventional helicopters experience a stabilizing effect from pitch damping M_q, effectively counteracting a change in pitch rate [59]. This stabilizing effect is also present in coaxial rotors due to the main rotors differential thurst and is strengthened by the choice of hingeless blades and the presence of a horizontal stabiliser [60]. This increases the phugoid stability of coaxial helicopters, although it is not as influential as M_u [43]. It is however especially influential in stabilizing the pitch subsidence, easing the pilot's control task in hover, which is a desirable effect [9][33].

The response of the rotorcraft to vertical speed increments in hover for both a tandem and a conventional rotorcraft is stable and convergent, represented in a real negative heave subsidence [15][43]. As the helicopter is required to withstand heavy gusts from all directions, stable heave damping during the hover rescue mission is essential. The heave damping Z_w is inversely proportional with blade loading M_a/A_b. Rotorcraft in general, but particularly coaxial rotorcraft, experience very high blade loading. Combined with the lower density at high altitude, this results in more negative values for Z_w and therefore lower gust sensitivity, which is preferable for the high-altitude rescue mission in heavy gust conditions [43]. The gust sensitivity increases and becomes unstable with forward speed and fast upward velocity of the rotorcraft [43][15].

All this results in the prediction that the coaxial longitudinal modes will be comparable in shape and even a bit more stable compared to the conventional ones. The expected modes of the HAMRAC are depicted in Figure 10.16 and Figure 10.17. Similar drag damping, better speed stability and increased pitch damping result in a more damped pitch subsidence throughout the flight envelope and the absence of a short period. The heave subsidence is stable and controllable in hover, which is beneficial for the hoisting operation. However, the angle of attack instability at high speeds means the heave mode becomes unstable at high speeds. Furthermore, the rotorcraft displays an unstable oscillatory phugoid mode. With speed, the phugoid mode is expected to become less stable and oscillate less, which is why an autopilot system that recognizes this mode in an early phase is recommended. For all speeds, an investigation into the optimisation of a pitch attitude and pitch rate feedback system combined with an automatic stability augmentation system is required [43].

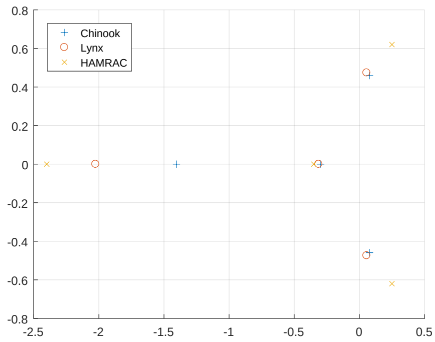

Figure 10.16: *The estimated eigenmodes at hover for the Chinook [15], Lynx [43] and HAMRAC*

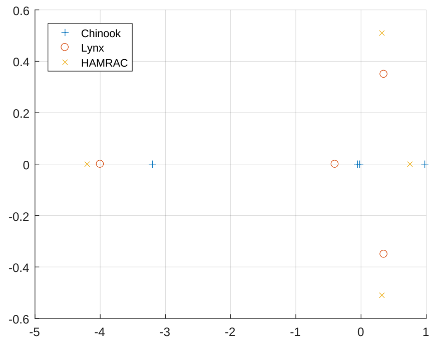

Figure 10.17: *The estimated eigenmodes at forward flight for the Chinook [15], Lynx [43] and HAMRAC*

Lateral Modes For the roll mode, spiral mode and Dutch roll mode, these are mainly influenced by respectively L_p, N_r and L_v. As it is relevant for the vertical stabiliser sizing, N_v is discussed as well [43][24].

The uncoupled roll motion is dominated by roll damping L_p. This damping is generally higher for coaxial rotorcraft than conventional ones, making the rotorcraft more stable and thereby slowing the roll response [9]. This is the effect of an increased rotor stiffness, to which the following all contribute: the number of rotor blades, increased blade stiffness, hingeless rotor selection and finally the increased distance between the upper rotor hub and the center of gravity in a coaxial rotorcraft design [59]. The roll subsidence is therefore heavily damped and converging, as well as somewhat increased with forward speed.

The spiral motion is in reference aircraft damped and converging, even if only barely so. The main contribution to N_r is generally the tail rotor [43][60]. In coaxial aircraft, this effect needs to be captured by fin area and main rotor differential. The order of magnitude in which the various rotorcraft are damped is quite similar. The coaxial rotorcraft is expected to be slightly stable as well for all horizontal speeds [59].

In the dihedral effect L_v, the main rotor and horizontal tail contributions are the most significant [43]. The hingeless rotors create a large, stabilizing moment here. The weathercock stability N_v is derived from the fuselage (destabilizing), tail rotor and vertical fin (both stabilizing) contributions [43]. As no tail rotor is present in the coaxial design, an increase in vertical fin area and the addition of significant end plates to the horizontal stabilisers and a rudder is well justified [59]. The effect of the fin on weathercock stability is especially significant during velocity perturbations at high speeds, vastly increasing the yawing stability in windy situations as a consequence [33]. The real stability increments gained from a fin are however only significant in forward flight, and the Dutch roll mode is expected to be unstable [61]. The slightly destabilizing N_v is instrumental in reducing the oscillation of the Dutch roll, which is preferable [59]. It needs to be noted that the Dutch roll mode handling qualities are likely poor in hover and become manageable with forward speed [60].

The lateral modes exhibit a very stable roll mode, a slightly stable spiral mode and unstable Dutch roll. An estimation of these lateral modes can be found in Figures 10.18 and 10.19. Special attention for the handling qualities of the Dutch roll in hover is required.

The stability modes are therefore expected to generally be stable, with an unstable heave, phugoid and Dutch roll mode. Wind tunnel tests to confirm these hypotheses are recommended.

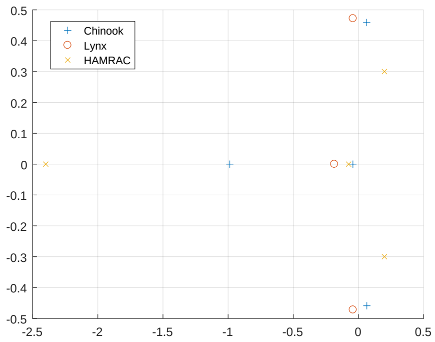

Figure 10.18: *The estimated eigenmodes at hover for the Chinook [15], Lynx [43] and HAMRAC*

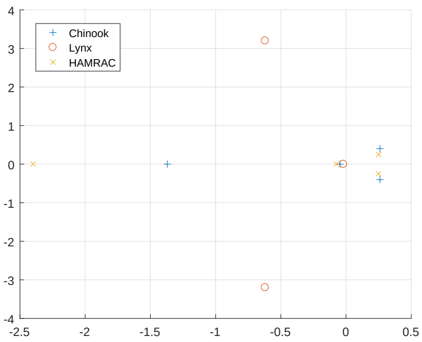

Figure 10.19: *The estimated eigenmodes at forward flight for the Chinook [15], Lynx [43] and HAMRAC*

10.7 Control Power

Control power is defined as the total moment that can be created by the control system about a given axis. Control sensitivity is the control moment generated per unit of control displacement. Damping is the moment that resists the initial rotor acceleration caused by a control moment [33]. Starting from the stability analysis, the goal of this section is to briefly describe the necessary controls and evaluate their effectiveness.

The coaxial hingeless rotor offers high control power. This high control power automatically implies high gust sensitivity, meaning an autopilot that recognizes these gusts and corrects for them is needed [33]. As discussed in subsection 10.6.1, the hingeless rotor also increases angle of attack instability, meaning a relatively larger horizontal tail surface is needed during cruise subsection 10.6.1, as well as an automatic control system that deals with the heave instability. This higher control power also results in increased pitch and roll damping, meaning these motions are easier to predict after control inputs.

The flight controls for the main rotor are subdivided in the collective pitch, longitudinal cyclic pitch, lateral cyclic pitch and differential collective pitch. For all these control inputs, the control power increases with advance ratio. Variation of the collective pitch is mechanically coupled with the thrust setting and strongly coupled to the pitching moment coefficients. The longitudinal cyclic control exhibits similar levels of coupled pitching moment at high speeds and has an influence on the thrust coefficient as well, especially in idle flight. The lateral cyclic control is as good as uncoupled. At hover, some yaw control is available from the differential collective pitch, but it is strongly coupled with the rotor thrust coefficient. This means a sequence of control inputs is required for effective yaw control. As forward speed increases, the yaw control provided by the differential collective remains quite constant but strong rolling moment coupling develops, making the differential collective more effective in roll than in yaw [9].

The horizontal tail control power in hover is negligible because of its rotor wake interference, supporting the choice for a horizontal tail that can be inclined when necessary. With increased forward speed, the horizontal tail's control power increases significantly. The rudder control power becomes predictably more effective in higher forward velocities as well [9]. This further proves the addition of a moveable rudder is a good design choice that increases the control power available in HAMRAC.

In scale models tested by NASA, it is concluded that although statically unstable in longitudinal direction, the hingeless coaxial rotorcraft is capable of sufficient control power to both overcome the instabilities present and manoeuvre the rotorcraft effectively [9]. The lateral motions are stable except for the Dutch roll, that is to be counteracted with rotor differential rotor collective in hover and rudder deflections in forward flight. It is concluded that the stability and control power on the hingeless rotorcraft allows for good manoeuvring capabilities. Caution is necessary regarding lags and overcontrolling by the pilot [43], which is why various automatic control systems are integrated in the rotorcraft. The HAMRAC will satisfy requirement [SH/VFS-02/2-P:CON] as it uses a hingeless coaxial rotor, providing large control power and various control surfaces to effectively manoeuvre in all circumstances.

10.8 Flying Qualities

As Padfield states [43], "*Good flying qualities make for safe and effective operations; all else being equal, less accidents will occur with an aircraft with good handling qualities compared with an aircraft with merely acceptable handling, and operations will be more productive*". Since the mission is demanding in all regards and both pilot error and uncontrollability due to insufficient handling qualities are a significant risk, it is proposed to keep a 'design for safety' approach in mind in all phases of the control system design [35]. Significant improvements in safety and degraded visual environment operations can be obtained by implementation of advanced flight control systems (for instance ADCFS on the Apache AV05 or VELSTAB on the Comanche) [43] but development cost must be weighed with incremental performance. This section aims to address various highly important considerations for the controllability of the HAMRAC and highlight the flying quality elements crucial for mission success, no matter how stable and controllable the aircraft might be.

In general, the coaxial rotorcraft has comparatively better flying qualities than most helicopters, less complicated coupling and better high-altitude performance [33] [21]. For the purpose of stability and control, this configuration is therefore the natural choice for the mission at hand. This is all the better, as the requirement that missions need to be able to be performed within 6 hours in 95% of the cases pushes the operating conditions and therefore flying qualities to its limits. It cannot be understated how important these are: flying qualities determine whether the rotorcraft can be flown safely and easily under all circumstances [35], and might conclusively decide whether the mission can be executed.

The standard for quantitatively evaluating the minimum required flying qualities post-design is ADS-33, which provides guidelines for the flyability of military rotorcraft [35]. Considering the highly challenging mission at hand, it does not seem a stretch to evaluate the HAMRAC like a military utility mission. This document will serve as a guideline in later stages of the stability and control design, such as flight tests and certification. Notably, the wind speeds specified for various manoeuvres and control power requirements during hover only go up to 35 kts. Additional testing on the heading maintenance of the HAMRAC for 35-40 kts wind speeds is therefore required. Hoisting operations need to be possible at around 25 kts, qualifying as 'moderate winds' in the ADS-33 standard [27].

The assessment of flying qualities commonly happens along the Cooper-Harper handling qualities rating scale (HQR), which is established from pilot's subjective opinions on the required workload to fly a task with a defined level of performance. Level 1 means the desired performance is achieved at minimum workload, level 2 means adequate performance is achieved at maximum pilot workload and level 3 means major deficiencies in control occur [35].

As the hover phase is the most taxing, safety is crucial here and it needs to be maintained for 30 minutes in the mission profile, a maximum level 2 HQR is required here. The rotorcraft needs to be able to comply with the requirements on both good and degraded visual environments (GVE and DVE) for utility military rotorcraft for all relevant mission task elements. For instance, the vertical axis control power necessary to maintain reasonable attitude control shall for level 2 HQR be able to achieve a vertical rate of at least 55 ft/min, 1.5 seconds after initiation of a rapid displacement of the collective control from trim [27]. It is assumed the pilot is able to execute fully attended operations during both the hover phases and high-speed cruise.

Another parameter worthy of testing and reiterating is the aircraft agility factor, which enables fast and safe operation maximisation. The agility, in contrast with the ADS-33, defines the upper limits of performance to expect from the aircraft. Agility is impeded by for instance low control power (which is not a problem for the HAMRAC), pilot error or reluctance to use the helicopter's maximum performance [43]. In defining the upper limits of performance, these last two factors prove that awareness of the human-machine interaction is crucial to mission success. In designing the aircraft and control sequences, agile performance is preferable. The hingeless rotor is not expected to introduce a lot of lag, and pilots should be trained to recognize the fine difference in when maximum performance is required and when overcontrolling introduces dangerous situations.

Finally, attention for the influence of the environment on control is required. The continuous tasks of a pilot are stabilization, guidance (short term manoeuvring) and navigation (long-term flight path definition). The stabilization task is rarely fully taken over by stability augmentation systems and therefore requires constant attention. The tasks of guidance and navigation require considerably more attention in DVE. Guidance in DVE can be improved somewhat by projecting augmented visual cues (e.g. infrared imaging) onto the pilot's visor [35].

The usable cue environment (UCE) standard help define the quality of the (augmented) visual cues available, and largely define the extent in which missions can be performed [43]. It seems reasonable to state that the HAMRAC will at current performance not be able to conduct a full close to terrain rescue mission in the Himalayas without any visual cues, flying fully on instruments and with only one pilot present. This limit on pilot workload seems to be the main limit on HAMRAC performance concerning stability and control. It furthermore needs to be noted that to obtain Level 2 FQR in for instance gusty DVE conditions, Level 1 FQR for good visual environment for the same manoeuvre and pilot needs to be attainable [35]. Stability is essential for divided attention or DVE operations, and helicopter stability is thus far not quite at the 'self-driving' level at which many fixed-wing aircraft are, and attempts to close the loop on this control sequence have so far been unsuccesful [43]. This analysis therefore poses the urgent recommendation to design a control system that both augments the pilot's spatial awareness and increases the autopilot capabilities, with the aim of achieving even further extended operational capabilities that would otherwise be unattainable due to lack of control.

10.9 Automatic Flight Control System

Apart from making the life of the pilot easier, having an advanced Automatic Flight Control Systems (AFCS) with Stability Augmentation Systems (SAS) is actually required by the FAA in order to obtain a certification to fly under Instrument Flight Rules (IFR)[13]. In addition, the strong winds and unpredictable weather conditions in mountainous areas require especially effective stability systems for the HAMRAC to be able to guarantee safety during hoisting operations at high altitude. The main parts of the AFCS are the Flight Director (FD) and the Autopilot (AP). These are discussed in more detail in the following paragraphs.

Flight Director The function that the FD fulfils consists of providing steering commands to the pilot in order to follow a desired flight path. Figure 10.20 shows its relation to sensors, the pilot and the Autopilot. This desired flight path is communicated to the FD by the pilot through a Mode Selector. The pilot can select different modes relating to the different flight modes, such as cruise, climb, approach and landing[14]. As output, the FD provides visual commands and information on the flight instruments of the helicopter, for instance on the Attitude Director Indicator (ADI). In other words, the FD itself has no servos or whatsoever that can exert active control, it is mainly there to assist the pilot in controlling the rotorcraft. However, as is explained in the next section, it can be coupled to the autopilot in order to provide this functionality[15].

[13] URL https://www.faa.gov/air_traffic/publications/atpubs/aip_html/part2_enr_section_6.1.html [cited 11 January 2019]

[14] URL http://www.helicoptermaintenancemagazine.com/article/understanding%2Dhelicopter%2Dautomatic%2Dflight%2Dcontrol%2Dsystems%2Dafcs [cited 14 January 2019

[15] URL http://www.flight-mechanic.com/automatic-flight-control-system-afcs-and-flight-director-systems/ [cited 14 January 2019]

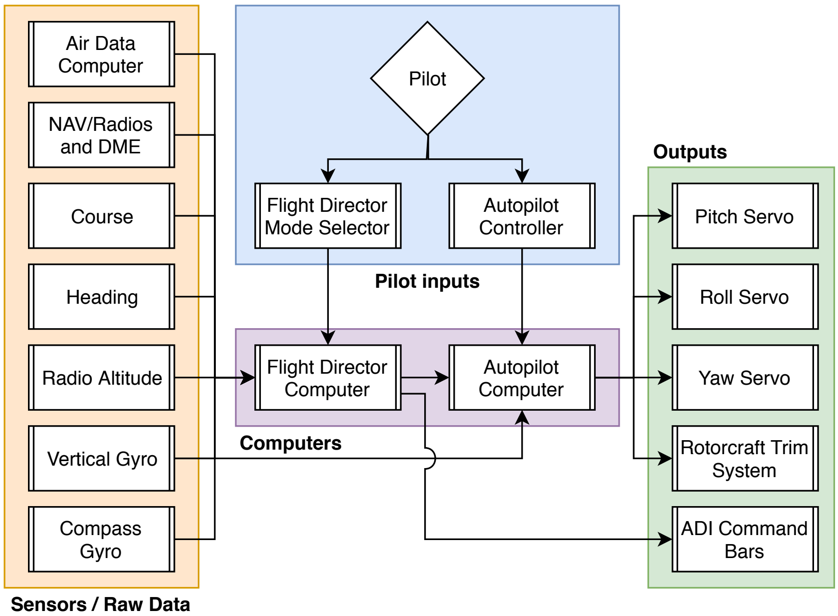

Figure 10.20: *Preliminary AFCS of the HAMRAC outlining the relationships between its main elements: sensors, pilot, Autopilot, Flight Director and some actuators*[16]

Autopilot Helicopters have autopilots with different levels of functionality and complexity. These range from helicopters that do not have an autopilot at all (only a flight director) to helicopters that detect hover situations and automatically engage a hover-specific Stability Augmentation System (SAS)[17]. Most helicopters do nowadays use some kind of Stability Augmentation System (SAS). This AFCS mode improves the controllability of the rotorcraft by damping oscillations and responding to short period disturbances. It is used in combination with other control modes. In addition, an autopilot generally has several different autopilot modes, such as an attitude hold mode (ATT), a mode that keeps the rotorcraft level (LVL) or a mode that keeps a constant vertical velocity (VS). Furthermore, advanced APs have a mode (CPL) in which the AP is coupled with the flight director, in order to automatically perform certain attitude changes and other manoeuvres.

Although many helicopters use a 3-axis autopilot, which provides pitch, yaw, and roll control by interfering with the mechanical control system linked to the cyclic, the decision was made to include a 4-axis autopilot for the HAMRAC. A 4-axis AP includes an actuator (or more for redundancy) to control the collective of the helicopter as well[18]. Although these systems are generally more expensive and complicated, it was concluded that the difficult and specific mission profile required such a system. The main reason for this is that it is crucial in mountainous areas, especially when flying under IFR conditions, to be able to achieve very precise climb angles. In a 3-axis system, this has to be done partly by the pilot through changing the collective control displacement while simultaneously used a horizontal airspeed hold mode (IAS)[19]. The HAMRAC can perform this manoeuvre by simply selecting a specific climb angle in the FD. Additionally, collective control can aid performance during the approach at the site where the hoist operation will take place. There exist several companies selling such systems to a variety of customers and show a good track record of getting for instance FAA certification. An example of such a company could be Safran Electronics & Defense, which provides AFCS to amongst others Augusta Westland, Bell and Eurocopter [20].

[16] URL `http://aelmahmoudy.users.sourceforge.net/electronix/egair/avionic.htm` [cited 14 January 2019.
[17] `https://www.garmin.com/en-US/blog/aviation/gfc-600h-revolutionary-helicopter-flight-control-system/`
[18] URL `http://www.helicoptermaintenancemagazine.com/article/understanding%2Dhelicopter%2Dautomatic%2Dflight%2Dcontrol%2Dsystems%2Dafcs` [cited 14 January 2019]
[19] URL `https://www.verticalmag.com/news/understanding-your-autopilot-pt-3-html/` [cited 14 January 2019
[20] URL `https://www.safran-electronics-defense.com/aerospace/helicopters/flight%2Dcontrol%2Dsystems` [cited 14 Janauary 2019]

11

Verification & Validation

In this chapter the verification and validation of the HAMRAC is treated. Firstly, the verification and validation processes of different departments on several subsystems has been described in section 11.1. After that, sensitivity analyses have been performed in section 11.2. Lastly, the compliance with the requirements and the feasibility of the design is described in section 11.3.

11.1 Subsystem Verification & Validation

In this section, subsystem verification and validation is discussed per department. Firstly, Operations and Logistics discusses their verification and validation, followed up by Structural Analysis. Power, Performance and Aerodynamics is discussed afterwards and lastly Stability and Control verification and validation is elaborated upon.

11.1.1 Operations and Logistics

Fuel weight verification is based on [80], another method is used to calculate the fuel weights. F_{used}, is calculated with Equation 11.1. The Specific Fuel Consumption (SFC) for the engine is assumed constant and multiplied with the time of the mission part, t_{part} [64]. In Table 6.1, the column 'Part fuel calculated' gives the fuel calculated with Equation 6.1. The verification fuel weight in column 'Part fuel verification' is in total somewhat higher, but well within the uncertainty margin of 15% from the Swiss Federal Office of Civil Aviation database calculation [80], which is set to +15% for the worst case scenario.

$$F_{used} = SFC \cdot P_{installed} \cdot t_{part} \tag{11.1}$$

Mission profile sensitivity analyses The operations are checked for sensitivity on varying inputs. The cruise speeds, climb speeds, descent speeds, refuel time and hover rescue time are varied one at a time. For each of these inputs the % change after which the mission profile is not achieved within the required three hours is given in Table 11.1.

11.1.2 Structural Analysis

This section will cover the verification and validation procedures used for the structural analysis models, including the blade, hub connection, rotorshaft and airframe.

Verification For all analysis models used within the structural design of the HAMRAC, software verification has been performed. In order to perform such verification several checks were made. Firstly, all inputs were verified to be in the correct format and verified to be using 'SI' units. Secondly all formulas used were verified as being correctly input into the code. Unit tests were subsequently run on these formulas to then verify that these were functioning properly and returning realistic results. When constructing the discretised models, lists were printed to verify the correct order of calculations. Furthermore, all discretised cross sections were plotted, before and after the twist and taper were integrated within the model to verify the correct coordinates and order of coordinates were being used within the model. All models were further verified to be using the

Table 11.1: *Sensitivity analysis of mission input parameters*

	Used value	Extreme value	Unit	Sensitivity threshold	Likely reason for parameter increase
Cruise speed @ 8950 m	55.0	43.5	[m/s]	-21%	Aerodynamic design, detours from nominal mission
Cruise speed @ 6200 m	72.0	55.2	[m/s]	-23%	Aerodynamic design, detours from nominal mission
Cruise speed @ 3930 m	80.0	76.6	[m/s]	-4%	Aerodynamic design, detours from nominal mission
Climb & Descent Vertical	10.2	9.3	[m/s]	-9%	Rescuee headaches, aerodynamic design, detours from nominal mission
Climb & Descent Horizontal	34.0	30.9	[m/s]	-9%	Aerodynamic design, detours from nominal mission
Take-off & landing times	120	138	[s]	15%	Pilot not sufficiently skilled, difficult weather conditions
Refuelling times	1200	1255	[s]	5%	Refuel stop infrastructure inadequate
Idling & flight checks time	120	230	[s]	92%	Hangar temperature too low
Reconnaissance before hover	60	170	[s]	183%	Difficult hover site
Hover rescue start	600	710	[s]	18%	Hoist failure, rescuee trapped, crew not sufficiently skilled
Hoisting time	1200	1310	[s]	9%	Hoist failure

same coordinate system. All results obtained by the analysis were printed to further verify that conditional statements were working. For example printing the stress at every location, to verify that it is indeed less than the material yield stress. A sensitivity analysis has in addition been performed on the model as described in subsection 11.2.4. The assumptions made in the construction of the analysis model must also be verified. The assumptions made in the inclusion of the honeycomb are verified as the honeycomb will only take a very small part of the loading. It also has an extremely small cross sectional area and therefore contributes only partially to the moment of inertia. Furthermore, its low density means it contributes negligible mass and the assumption of no mass is therefore valid. The assumption of zero torque acting upon the blade is verified as being valid as the load due to torque is significantly less than that of the centrifugal force or bending moment. However, for a complete analysis this should be considered within a more detailed model, especially since the material is made from composites. It should be checked that the material does not fail in torsion under the applied loads. For the hub connection the assumption that this part generates no lift or centrifugal force is verified due to the fact that the velocity at this part of the blade is negligible compared to the tip velocity. Furthermore, this component has a small mass in comparison to the blade, further decreasing the centrifugal force. For the airframe the assumptions follow those of the structural idealisation procedure outlined by Megson [82]. Indeed, the approach taken for the analysis of each component is further verified by the analysis procedures outlines in this book.

Results verification was also performed at several stages throughout the construction of each model. The first of these tests was performed upon the blade analysis model, where the determined area, centroid and moment of inertia of the airfoil skin were verified by using the results obtained from constructing the airfoil in XFoil. A less than 5% discrepancy, likely due to errors from discretisation verified that these were being calculated correctly. Verification of the loading conditions is performed through analysis of the loading diagrams. The shape of the slope of the loading diagram can for example verify that the correct bending moment is being determined from the shear force, as the slope of the bending moment graph is equal to the shear force. Furthermore, within all components the normal, shear force and bending moments should return to zero at either end of the component. This has verified that the correct internal forces and moments have been applied. Verification can also be performed through the comparison of obtained results and expected results. For example, a positive bending moment should induce a negative internal moment and should cause compression within the top of a beam and tension in the bottom. In this way the bending stress has been verified as acting in the correct direction within all models. The calculation of base shear flow can be verified through the constraint that the base shear flow must return to zero at the location where the 'cut' has been made within the cross section. As this happens within all of the components analysed this verifies the correct computation of base shear flows. Von Mises stress distribution can be verified through the plotting of the stress distribution. As the main loading is due to bending in the majority of the structural components, the Von Mises stress should mainly follow the same distribution as the bending stress which is verified as correct for the blade, hub connection and rotorshaft.

Validation Structural models used in the analysis have been validated versus helicopter structural components used in aerospace construction. The airframe model follows a similar construction to helicopter airframes used in industry. Loads on helicopter airframes are in general much less than seen within the airframes of aircraft. The calculated stringer pitch of 0.30m has been validated versus modern airframe construction. The blade construction used within the model has been validated in comparison to modern rotor blade construction. It is commonly seen that rotorcraft use a thick airfoil skin with a single spar and the rear half of the airfoil filled with honeycomb material, as seen in Figure 11.1. This is further validated by the structural model used by Li [63].

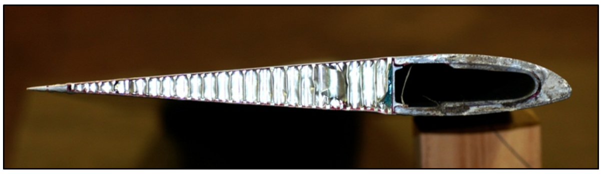

Figure 11.1: *Helicopter blade cross-section* [1]

However, the results of the blade model are not validated by modern rotor blade construction. The required skin thickness within the structural model exceeds the skin thicknesses used within modern construction. Furthermore, the blade deflections are much larger than those experienced by true helicopter blades, especially considering that only the safety factor is included and not a gust load factor. A revision of the model is therefore recommended with the inclusion of a FEM analysis procedure and for an increased blade thickness as concluded in subsection 9.2.5. The results of the rotorshaft analysis and hub connection are in accord with modern construction. The Sikorsky X2 for example has a rotorshaft mast of an approximately similar diameter to the HAMRAC. Furthermore, the use of such a hub connection has been verified by comparison with blades on other helicopters.

11.1.3 Power, Performance, and Aerodynamics

This section will cover the verification and validation procedures used for the power and performance models, including the MDO.

Verification To ensure the correctness of the data presented, the models used to generate the data must first be verified, then validated. This will detail the verification procedures done. First, the program was separated into a modular fashion. This was done to facilitate unit testing which was used both to check that the script was functioning properly during development as well as help identify where the script wasn't functioning as intended. Each module was structured such that it would take an input of data and either do something with the data or process the data and return the result of that process. This allows the data stream to be followed more easily when performing system testing, as well as improving readability of the code, such that each module is designed to do one thing instead of several. System testing was done by following the flow of the code through the procedure and checking that the inputs of each module were the correct ones, that the process was being performed in the correct order, and that the correct units were used when performing calculations.

To verify the MDO approach used, it is important to check that the values given in the MDO are consistent with the aerodynamic restrictions on the helicopter. This is important as the statistical boundaries also include mission and design elements, whereas the aerodynamic constraints cause a significant detriment to performance and have a high risk of causing accidents in operation. Therefore, all the values found during the MDO must be checked with the aerodynamic constraints. This also indicates an error in the model and demonstrates where the model must be changed to account for the operating conditions of the HAMRAC. When optimising for hover power, it was found that the angular velocity that results in the smallest hover power required fits with sea level tip speed constraints, but, due to the operating altitude, the tip Mach number exceeds allowable values. Therefore, the angular velocity is reduced to allow for the appropriate maximum tip mach. The angular velocity was chosen to be reduced as the design space indicated that changing the radius would require the chord to change, and the hover power optimisation analysis indicated that the

[1] URL `http://bst-tsb.gc.ca/ENG/rapports-reports/aviation/2011/a11o0205/a11o0205.asp` [cited 21 January 2019]

power required to hover is most sensitive to changes in chord length. Therefore, reducing the angular velocity allows for the aerodynamic constraints to be met while minimising the power required to hover.

To verify the engine selection, the engine selected was determined both 'forward' and 'backward,' by first determining the power required, and then selecting the possible engines that would fit such a profile (forward). Afterwards, the performance of the engine that was selected based on the considerations given in section 8.5 was calculated manually using the specifications given by the manufacturer to determine the maximum power required that that engine would still fit the requirements. If that power is larger than the projected HAMRAC power, then the selected engine was deemed verified.

Validation The first type of validation used was parameter variability. This allowed the model to check the results of given data and compare it to the results obtained by the model developed. If the model can reproduce given results from given data, it can therefore be assumed that it will produce reliable data from the design data. For this check, the both key values, such as the power required to hover, and the shape of the graphs are checked. A shape that differs from the expected one is an indicator that the model used an inappropriate assumption. For validating the ESSRA, the data given by dr. Pavel [22] was used and the power curve generated by the ESSRA model was compared to the provided. Next, the conversion from coaxial rotor parameters to their equivalent single rotor parameters were compared to the one given by Coleman [30]. It can then be assumed that the data generated by the model at the desired design parameters is within a similar accuracy to that which was generated by the model at the given parameters. Additionally, it is assumed that, since the data produced is accurate enough, that any further processing on that data by a verified module will also produce accurate data, as there is a lack of other models and historical data to compare to. The engine selection and design space procedures used followed the same verification and validation procedures, as these could be compared to similarly sized helicopters. For example, if it was found that the model predicted a weaker engine for high altitude than for a similar weight low altitude mission, then the model would be deemed invalid due to the power lost in engines at high altitude logically requires a stronger engine for a higher altitude.

The second method of validation used was parameter variability and sensitivity analysis. This was used largely when constructing the climb rate power curve due to both the lack of comparison data and difficulty of estimating excess power, making climb rates unpredictable. Therefore, a sensitivity analysis, as detailed in section 11.2, was used to validate that the numbers given by the model were reliable ones that accurately reflected real world values. When the numbers were found to indicate unrealistic data, such as minimum power required at hover, too large/small values of climb rate, or unexpected peaks or breaks in the curve, then it was deemed that the model was not accurately simulating the real world conditions. Verification would need to be repeated, especially after changes were made to the model, before it could be validated again. Due to the lack of information regarding the concept of blade loading in high altitude operations, the model predictions for blade loading cannot be fully validated. This will be covered in subsection 11.1.5.

11.1.4 Stability and Control

Verification In chapter 10, one can find a thorough discussion on the expected stability of the HAMRAC and methods to aid the pilot in control of the helicopter. As stability and control is a highly complicated subject on which no 'one size fits all' approach can be employed, care is taken that each statement is sufficiently backed up. Several highly referenced sources [74] [18] [43] lie at the basis of the claims made on the stability mode analysis. Sources are also verified against each other for anomalous claims, and the best and most extensively backed up literature on the subject of stability is used. Where extrapolations concerning the expected stability modes are made, the proposed evaluations are verified with the stability analyses these sources provide. Per mode, references to back up the claims on coaxial rotorcraft specifically are also sought out [59]. While the values are likely off, the shape and most orders of magnitude of the projected stability modes are expected to be accurate. This is sufficient for the current depth of the analysis, as the point in this the sections relating to the stability modes is to make perform an analysis on the general behaviour of the HAMRAC, not to precisely quantify every individual stability derivative. The sources show good agreement in their analyses and a lot of effort is put into estimating where the HAMRAC will fall in comparison to these analyses.

Validation Design-wise, all the analyses and control options used are already or have been in use in successfully flying helicopters, although the particular combination described here might be unique. An example is the gimbal control [10] of the upper rotor disc that is combined with more traditional swash-plate control of the lower disc. Each proposed system is therefore 'validated' technology. As the mission is demanding and will possibly drive both the skills of the pilot and the performance of the machine outside of general boundaries, preference is given to systems that ease the pilot's control task. Little information on the exact sizing of these control systems is to be found, indicating these design choices are highly specific per design. Where sizes are estimated, they are backed up by statistical methods and validated on reference aircraft.

In further design phases, it is recommended to put great effort into the establishment of a full trim and stability model and verify the outcomes of this model against the expectations backed up by literature. This requires an extensively worked out physical design and an accompanying full aerodynamic model to represent inflow, load and pressure distribution. As the outcomes of stability derivatives are highly individual per configuration and design choice, verification of this model is performed initially by a stability mode analysis, as performed in 10.6. A highly in-depth model is required is to get estimates that can safely represent reality. To validate this stability model, a scale model is required and extensive wind tunnel testing for the specific design has to be performed. After this, actual prototype flight tests are necessary to validate the results of both the wind tunnel and computer model tests.

11.1.5 Recommendations

Following verification and validation of the design procedures conducted within the HAMRAC project, several recommendations for future modifications to the analysis procedure have been identified and are presented here. The first recommendation to improve the accuracy of the performance of the HAMRAC in high altitude is to develop a model with an increased understanding of the phenomena and implications of blade loading at different altitudes. This is important as the HAMRAC is the first rotorcraft designed to operate at such a wide range of altitudes such that existing models and prediction methods are not sufficient to understanding this.

The second recommendation to improve the accuracy of the loading of the rotor blades is to include the torsional loading of the blades, that is induced by aerodynamic forces acting at a distance to the blades shear centre. The second recommendation stems from the validation of the structural design of the rotor blades. As the current blades are not feasible under the loading condition, yet make use of a skin thickness far greater than is used in current rotor blade design, it is recommended to repeat the structural analysis procedure, making use of a composite blade design software such as VABS, or through using a FEM analysis model.

11.2 Sensitivity Analysis

Because the design is very complex and depending on various assumptions it is necessary to further examine the feasibility of the design. In order to confirm that the right method has been used and that a small change in one of the parameters does not result in a catastrophic change in the design, a sensitivity analysis is performed. This is done for every department separate and elaborated on further in the next subsections.

11.2.1 Performance Sensitivity

Even though the performance department has a lot of inter linkage with the aerodynamics department, a clear division can be made in terms of subsystems. The engine and transmission of the HAMRAC are clearly in the performance department. Therefore, they will be examined separately in terms of feasibility and sensitivity. For the engine the choice was made to go for the engine which overpowered the HAMRAC by a small margin but would deliver a very good specific fuel consumption. If the engine would need to be switched because of unavailability this would not be a problem. There are a number of engines which are possible for the design of the HAMRAC that fit the requirements, slight adaptation would be necessary with different engines having different specific fuel consumptions. This would however not be catastrophic for the design.

In the case of unavailability of production of the transmission, which provides the possibility of two different rotational speeds for the rotor, the engine can solve this. The engine is able to spin 20 % slower than optimal, this however is not optimal for its fuel economy. This means that the engine will use more fuel when flying the first leg of the mission. This is not a problem since the fuel tank of the HAMRAC is designed for the second leg of the mission which is the most demanding. It therefore has theoretically enough designed fuel for this case. With these two cases the performance sensitivity can be assumed very low since it has no catastrophic results from small changes in the design.

11.2.2 Aerodynamic Sensitivity

The aerodynamic department has a lot more parameters which not only influence the design, but they also influence each other. All of these parameters will be elaborated on and their degree of sensitivity will be evaluated with respect to each other and, ultimately, the entire design. These different parameters are; number of rotor blades, rotor radius, chord, rotational frequency, airfoil, taper, twist and rotor spacing.

The first parameter that is going to be examined is the number of rotor blades. This was the first to be finalised in the design. This is a special parameter since it is not able to change in small increments, it has to be a discrete change, since there is no such thing as 2.5 rotor blades. However, the implications of this change are larger than expected. If the number would be changed from three to four rotor blades this would mean that a change has to be made in a number of departments. For instance, a new rotorhub needs to be designed, the power has to be re-evaluated, the loads on the blades need to be re-examined, are of large impact to the design. However, the influence on the other parameters is limited to a change in chord to make the rotor have a correct solidity and thus blade loading.

The remaining parameters have less of an influence on other departments since these are all, apart from rotor spacing, rotor blade characteristics. These characteristics all have the same tendency to not influence the entire design by much. However, the structural and power loads need to be re-examined after every change. The most important characteristics will be elaborated on, so the ones that have the most influence on the design. To begin with, the rotational frequency (ω) and radius (R) have a large influence on the power required for cruise since the equation involves a fifth degree term of tip speed, $\omega \cdot R$. The rotational frequency is also very sensitive to blade loading which why the design choice was made to have two different rotational frequencies for the different flight phases. Airfoil selection depends on various parameters mentioned above, different airfoils perform better under different circumstances. However, airfoils can have a larger effect on the design. Airfoils have very specific characteristics, a family of airfoils can be used but these airfoils need to be used at the right position on the rotor. If an airfoil is used that is designed for high speed operation is used at the root of the rotor where the speed is relatively low this could lead to catastrophic results. Similarly, if a low speed airfoil is used for high speed conditions the same can happen.

Taper, twist and rotor spacing have a lot less influence on the design since these are optimisation factors for the design. Twist has a decrease 2% in power required if linear twist is used and 6% if quadratic twist is used [65]. For taper it is even less, it has negligible impact on cruise performance. For hover performance, having taper increases the figure of merit and the high stall margin, which is beneficial to the hover efficiency [64]. But this increase in hover efficiency is only some percentages, therefore changing the taper results in a moderate impact to hover performance. That leaves rotor spacing which is mildly sensitive to the efficiency of cruise and hover [67]. This is due to the fact that in cruise small spacing is desirable because the mast of the helicopter causes an increase in parasitic drag. For hover a large spacing is desirable since the bottom rotor can then capture more clean air from alongside the top rotor, which increases hover efficiency.

Hover performance is not sensitive to taper [64], and it has no implications on cruise performance. Rotor spacing has only a mild effect on the efficiency of cruise and hover performance [67].

11.2.3 Stability and Control Sensitivity Analysis

Most stability and control design parameters that are determined in this report do not have a large influence on the overall design when changed. If another AFCS were chosen, for instance, no other subsystems would change. Changes in the position and size of the horizontal and vertical stabilisers would result in changes in the position of the center of gravity of the HAMRAC. These changes, however, would be relatively small compared to the total weight and structural integrity of the helicopter. In addition, these changes in control surfaces would result in changes in the stability derivatives of the design and its behaviour with respect to controllability and stability. These changes in derivatives can however be designed for and would probably lead to adjustments to the control system itself, not in other subsystems. With respect to flying qualities, one might need to add some sensors on the helicopter body, but no significant aerodynamic or structural changes are caused. Therefore, these design parameters and choices mentioned do not influence the overall design by a large extent.

If the determined maximum center of gravity range during operations would be smaller, this could result in large changes in the rotorcraft configuration. It could make it unsafe to perform the hoist from the back instead of the more conventional side of the rotorcraft. Furthermore, it could require the fuel and / or passengers to be located more closely towards the center of gravity of the helicopter, and thereby significantly change the layout and aerodynamic shape of the fuselage. In order to minimise the chances that this situation infers, the center of gravity range is limited to the smallest value that was found during the analysis of similar rotorcraft.

Finally, if during more detailed design or actual flight tests, it is found that servo-flaps do not provide sufficient performance regarding the control of the rotorcraft, it could lead to some significant changes in the design. The more traditional hydraulic double swash plate mechanism that would replace them would require a hydraulic system and increase drag during cruise significantly. This could lead to the HAMRAC not meeting cruise requirements and to problems with respect to layout and weight. To mitigate this risk, it was decided that the servo-flap mechanism should strongly resemble the system that is used on the K-max, as that system is proven in flight and could serve as an initial validation for its use on the HAMRAC.

11.2.4 Structural Sensitivity Analysis

For each subsystem within the structural analysis part a python model has been made, which are dependent on several variables. For the main rotor blades and the airframe, a sensitivity analysis has been performed. Several input variables have separately been given a 10% increase, and the influence that had on the outcome has been analysed and elaborated upon. Because the rotor hub part and the rotorshaft have no direct input values but only depend on output values from the main rotor, no sensitivity analysis has been performed on these parts.

Main rotor blades

The main rotor blade is a subsystem that depends on a lot of different parameters. In the main rotor model these input parameters can easily be changed, which will result in different outcomes. The outcome of this model is the maximum Von Mises stress at each section, the mass of each rotor blade, and the deflection along the span. In the sensitivity analysis of the main rotor blades, the load factor, taper ratio, root chord and forward flight speed have been given a 10% increase. The results of this analysis are shown in Table 11.2. It can be seen that the load factor does not influence the mass, but the Von Mises stress and the deflection have an almost identical relative increase. Also notable is that the increase in Von Mises stress and tip deflection are always equal in sign.

Table 11.2: *Sensitivity analysis of the main rotor blades*

Variable increased with 10%	Root Von Mises stress increase (%)	Mass increase (%)	Tip deflection increase (%)
Load factor	9.88	0.00	10.0
Taper ratio	4.51	2.00	0.04
Root chord	-1.37	9.99	-10.35
Forward flight speed	7.69	0.00	6.99

Airframe

Also on the airframe, a sensitivity analysis has been performed. As already explained in subsection 9.5.5, the airframe model has four input variables that can be adapted such that the Von Mises stresses and the airframe mass are kept as low as possible. In this sensitivity analysis, these four variables plus the maximum load factor have all been separately increased by 10%, and the effects these changes will have on the model outcome are analysed. The results of this sensitivity analysis are shown in Table 11.3. The outcome of this analysis seems reasonable: when the load is increased by a certain amount, the stresses should increase by the same amount which is the case. Also, an increase in area and skin thickness will result in a lower stress, but a higher mass, which is also the case. Lastly, it can be seen that the skin thickness of the bottom part is not as effective in carrying stress as the upper part, but causes a much bigger increase in weight.

Table 11.3: *Sensitivity analysis of the airframe*

Variable increased with 10%	Von Mises stress increase (%)	Mass increase (%)
Load factor	10.00	0.00
Stringer area	-0.70	2.50
Stringer distance	1.27	0.02
Skin thickness upper part	-0.68	1.06
Skin thickness bottom part	-0.06	6.45

11.3 Compliance Matrix & Feasibility

The logic for the requirement tags found in the compliance matrix below keeps a relation with the original numbering as used in the beginning of the project. The unique Requirement identifier is built up as following: It start with the origin of the requirement, which can be a stakeholder requirement (SH), a system requirement (SYS) or subsystem requirement (SYS-XXX). An indicator for requirements derived from the VFS document is possible (SYS/VFS) or (SH/VFS) Requirements at the subsystem level are distinguished at the third level. These are split into three main subsystems for now, namely: Propulsion (PP), Structures (STU), Avionics (AVI), Hoisting (HOI) and Rotors (RTR). This is followed by the number of the requirement, which is taken from the project plan and keeps numbering up. Numbers 30-40 have been renumbered from older duplicate numbers. Finally, for traceability, a three or four letter code is added to indicate where the requirement was discovered in the project requirement discovery tree. The HAMRAC team secretary can make this tree available upon request.

TAG	Description: The HAMRAC shall...	What has been done to comply?	Actual Value
SH-01:RES	Be able to perform a long-line rescue, at 8870m above sea-level, in the Himalayas.	Concluding from all the technical departments, it is theoretically able to perform a rescue at 8870m.	8870m
SH-02:VER	Be able to perform a vertical landing and take-off at an altitude of 6400m.	Class A certification for one engine inoperative landing & take-off at 6400m	6400m
SH-03:ENV	Be capable of performing a high altitude mountain rescue, during all climbing seasons, in the Himalayas.	Landing rescue can be performed up to 6400m and hover rescue up to 8848m during all climbing seasons.	Complies
SH-04:PLA	Be able to operate with limited or no adaptation of infrastructure in the target areas.	No hot refuelling is used in the reference mission profile.	Complies
SH-05:RES	Be able to rescue two people with a total weight of 170kg.	The layout, stability and hoist system design is conducted using two rescuees.	Complies
SH-06:SCH	In 95% of the cases, perform a rescue mission within 6 hours after the call for rescue in the target area (Himalayas).	A 4-axis autopilot and SAS system are included. Operational availability is maximised in a later design phase and also depends on operator policies.	To be verified in later design
SH-07:SUST	90% of the materials used in the HAMRAC shall be recyclable.	An analysis indicates this requirement is achievable. Deeper analysis must be done.	To be verified in later design
SH-08:OPS	Not exceed 2500€hourly operation costs.	A significantly lower operational cost is achieved	1010€/hour
SH-09:PUR	Not exceed 3.5 million EUR purchase price.	The purchase price is lower than the requirement.	3.44 Million EUR
SYS-10:VEL	Be able to cruise at 140kts at 4000m altitude.	Design cruise speed at 4000m is higher than the requirement.	150 kts
SH-12:RES	Be equipped with oxygen support system for 3 crew members and 2 rescuees.	Oxygen masks with oxygen supply for 5 persons are in the inventory.	Complies
SYS-30:RAN	Have a range of 150NM at 3000m altitude, with fuel reserves according to FAR.	Payload range for a mission from Kathmandu with cruise at 3930m gives a maximum range of 328km. At 3000m, 10 m/s higher cruise speeds are achieved, causing even higher range.	177NM
SYS-HOI-31:RES	Have a hoist system rated for 300kg load.	Hoist system is rated for 350kg load.	350kg
SYS/VFS-32:RES	Include a hoist system.	SkyHoist800 electrical hoist system.	Complies

SH/VFS-33:CON	Be well-controllable in any foreseeable flight condition.	A 4-axis autopilot and SAS system are included, no LTE in coaxial helicopters.	Complies
SYS-34:CON	Be dynamically and statically stable while hovering with assisted control system.	A 4-axis autopilot and SAS system are included.	Complies
SYS-35:PL	Be able to have a minimum payload of 575kg at 8870m altitude.	Design is optimised for this weight.	575kg
SYS/VFS-36:HOV	The control system shall be capable of maintaining heading in hover with wind from any azimuth up to 74km/h (40 kts) at 8950m.	Up to 35kts from most critical direction possible, investigation into 35-40kts necessary	To be verified in later design phase
SYS-37:CER	Meet small rotorcraft requirements (CS 27 FAR/EASA).	Design is made to be class A certifiable. Certification to be done in a later phase.	To be verified in later design phase
SYS/VFS-38:CER	Be configured with an avionics suite that meets minimum FAA requirements for single pilot day/night IFR operations.	Is included in the inventory.	Complies
SYS-39:STR	Not exceed 1400kg OEW.	OEW is within the budget for the preliminary design phase.	1348kg
SYS/VFS-40:CER	Be configured with all navigation/communication that meets minimum FAA requirements deemed relevant for a single pilot to safely perform the mission during day/night IFR operations.	Is included in the avionics design.	Complies
SYS-50:SEN	Be able to identify the distress signal during rescue using an on-board system.	Electrical Optical Signal & Radar is included.	Complies
SYS-AVI-53:TEM	Have an active temperature control system to control the temperature inside the cabin.	A cabin heat duct ensures warmth.	6000W
SYS-54:AVI	Be able to communicate with air traffic control.	ACARS, VHF and SATCOM, communications systems are included.	Complies
SYS-STU-57:MAN	The HAMRAC's integral structure shall not be assembled with permanent joints.	Airframe assembly shall be completed using rivets.	Partly Complies
SYS-59:MAN	The components of the HAMRAC shall be within the size to fit for transport to assembly facilities.	The components are identical to the reference H135 helicopter in dimensions.	Complies
SYS-60:STR	Have a Maximum take-off weight (MTOW) of 2500 kg.	The MTOW initially was estimated to be 2500kg. Current estimate is:	2468kg
SYS-PP-61:POW	Have Take-Off Power (TOP) of <2076SHP>in standard atmosphere at sea-level.	Use LHTEC T800 engines	Complies
SYS-PP-62:POW	Have a Maximum Continuous Power (MCP) of 1550kW in standard atmosphere at sea-level.	Two 774kW engines are installed.	1548kW
SYS-STU-63:STR	Have a fuel tank capacity of <344 Liters>.	Fuel tank sizing done according to small rotorcraft certification specifications.	2·344L
SYS-STU-64:STR	Have a cabin floor area of 8.65m^2.	Is included using margins during sizing in case for dimension increments.	Complies
SYS-STU-65:STR	Have a cabin volume of 14.71m^3.	Is included using margins during sizing in case for dimension increments.	Complies
SYS-AVI-67:TEM	Have a demisting system for front windscreens.	De-icing system is present.	Complies
SYS-AVI-68:SEN	Have a magnetic compass.	Magnetometer is included in the design	Complies
SYS-AVI-69:STR	Have an instrument panel vibration that shall not impede their function.	Will be determined by testing.	To be verified in test phase

SYS-PP-70:STR	Have a propulsion system's frequency that shall not interfere with the structural natural frequency.	Will be determined by testing.	To be verified in test phase
SYS-71:MIS	The HAMRAC's electrical system architecture shall be fail-safe and operable if one electrical component fails.	Fuses are added for every electrical component.	Complies
SYS-AVI-72:AVI	Have a primary flight display.	Is included in the HAMRAC avionics.	Complies
SYS-AVI-74:AVI	The primary flight display shall have an airspeed indicator.	Is included in the HAMRAC avionics.	Complies
SYS-AVI-75:AVI	The primary flight display shall have a vertical speed indicator.	Is included in the HAMRAC avionics.	Complies
SYS-AVI-76:AVI	The primary flight display shall have an altimeter.	Is included in the HAMRAC avionics.	Complies
SYS-AVI-77:AVI	The primary flight display shall have an attitude indicator.	Is included in the HAMRAC avionics.	Complies
SYS-AVI-78:AVI	The HAMRAC shall have a navigation display.	Is included in the HAMRAC avionics.	Complies
SYS-AVI-79:AVI	The navigation display shall show the flight plan.	Is included in the HAMRAC avionics.	Complies
SYS-80:STR	The structural integrity shall not be compromised when performing a landing at MTOW with vertical speed.	Landing gear absorbs loads and the airframe is built to a crash load factor of 4g.	Complies
SYS-81:STR	All load-bearing parts shall be designed with 1.5 design-load safety factor.	The design safety factor of 1.5 is included in the design	Complies
SYS-82:CON	Be controllable under 9.1 m/s vertical gusts.	A 4-axis control system is present, which also takes into account collective changes. Heave motion is stable in hover.	Complies
SYS-STU-83:STR	The structural integrity shall withstand a positive manoeuvring load of 3.5g.	The blades require redesign to withstand this load.	Redesign is necessary
SYS-86:POW	Be able to climb at a climb rate of 10.16 m/s.	Climb rate is limited for passenger comfort at this speed.	Complies
SYS-87:STR	Protect occupants from electrocution in the event of a lightning strike.	The metal airframe acts like a faraday cage to protect occupants from electrocution.	Complies
SYS-AVI-88:TEM	Have a pilot windshield wiper.	Is included in the HAMRAC design.	Complies
SYS-STU-90:STR	The rear hatch shall have 1600mm · 1400mm dimensions for accessibility to the interior of the vehicle.	Is included using margins during preliminary sizing in case for dimension increments.	Complies
SYS-HOI-91:SUST	The hoist system shall have an electrical hoist.	An electrical Skyhoist800 is used.	Complies
SYS-AVI-92:AVI	Be equipped with 3 headsets.	Is included in the HAMRAC inventory.	Complies
SYS-AVI-93:AVI	Be equipped with GPS system.	Is included in the avionics design.	Complies
SYS-AVI-94:RES	Have an emergency locator transmitter.	Is included in the avionics design.	Complies
SYS-AVI-95:TEM	Have de-icing equipment installed on all lift devices and control surfaces.	Rotor de-icing, airframe de-icing, pitot tube heating and fuel heating are included.	Complies
SYS-96:RES	Be equipped with a searchlight with a 1600W power rating.	Is included in the HAMRAC design.	Complies
SYS-97:SEN	Have a pitot-static system to determine aircraft speed.	A pitot tube with electrical heating is included in the design.	Complies
SH-97:SCH	A rescue mission shall be completed within 3 hours after departure from starting location.	The mission profile is achieved with 110 seconds to spare.	2.96hours
SYS-98:MIS	Climb from 3780m (12,400ft), to 8870m (29,100ft) with 3 crew and 2 rescuees and 10% fuel margin.	Is included in the mission profile and RTR subsystem requirements.	Complies

SYS-99:MIS	Cruise at an altitude of 3780m (12,400ft) for 135km (73NM) with 3 crew and 2 rescuees.	Is included in the mission profile, with cruise at 3930m for clearances, and RTR subsystem requirements.	Complies (@3930m)
SYS-100:MIS	Cruise at an altitude of 8870m (29,100ft) for 28km (73NM) with 3 crew and 2 rescuees.	Is included in the mission profile, with cruise at 8950m for clearances, and RTR subsystem requirements.	Complies (@8950m)
SYS-101:MIS	Be able to hover out of ground effect at 8870m (29,100ft) for 30 minutes with 3 crew and 1 rescuee.	Is included in the mission profile as 10 min with 0 rescuee, 1 rescuee and 2 rescuees respectively.	Complies
SYS-102:VFS	Be capable of performing the mission profile proposed by the Vertical Flight Society	Yes, including an extra mountain overpass at 6200 m altitude	Complies
SYS-105:SUST	The HAMRAC's average fuel consumption shall be less than all currently used air rescue vehicles in the Himalayas.	Engines with lowest specific fuel consumptions have been selected	Doesn't comply
SYS-106:SUST	The HAMRAC's power to payload ratio shall be higher than all currently used rescue air vehicles in the Himalayas.	The power to payload ratio at sea level is higher than current vehicles.	2.0455kw/kg
SYS-107:SUST	The HAMRAC's CO_2 emissions shall be less than all currently used rescue air vehicles in the Himalayas.	Engines with lowest specific fuel consumptions have been selected	Doesn't comply
SYS-108:SUST	The HAMRAC's noise level shall be less than all currently used rescue air vehicles in the Himalayas.	The noise level is +18dB compared to current mountain rescue air vehicles.	18dB higher
SYS-HOI-110:OPS	Be able to perform hoisting operations with wind speeds up to 13m/s	Hoisting operations are possible, limit is to be included in the operational manual.	Complies
SYS-PP-111:OPS	Be able to achieve a vertical clearance of 150m from the landing site.	The clearance for reconnaissance purposes is included in the mission profile.	Complies
SYS-PP-112:OPS	Be able to achieve a vertical clearance of 100m from the hovering site.	At the top of Mt. Everest this is possible, maximum hover altitude is 10km.	Complies
SYS-115:SUST	The HAMRAC's embodied energy level shall be lower than the current rescue air vehicles in the Himalayas.	No Hydraulic system, Existing skids, no tail rotor, low specific fuel consumption engines, no infrastructure change necessary.	To be verified in later design phase
SYS-AERO-116:PER	The HAMRAC's rotor hub should attribute to less than 20 % of the total rotorcraft drag.	Drag reduction by adding a fairing to the rotor hub. Fairing contributes less than 1%	Complies
SYS-RTR-117:PER	The maximum lift coefficient shall be higher than 1.4 at a Mach number of 0.4 at cruise conditions	The airfoil design is best-fitted with the rotor requirements.	1.62
SYS-RTR-118:PER	The drag divergence number at zero-lift coefficient shall be higher than 0.70 at cruise conditions.	Drag divergence at cruise for the airfoils is: VR12=0.82 & VR14=0.86.	Complies
SYS-RTR-119:PER	The pitching moment shall be lower than -0.015 at the drag divergence Mach number at cruise conditions.	The airfoil design is best-fitted with the rotor requirements.	-0.03
SYS-RTR-120:PER	The pitching moment shall be equal than +/-0.01 or closer to 0 at a Mach number between 0.2 and 0.5 when the lift coefficient is zero.	Pitching moment at zero lift for the airfoils is: VR12=0.0086,VR15=0.0054	Complies
SYS-RTR-121:PER	Value of lift over drag ratio (L/D) shall be at least 100 at Mach 0.6 with the lift coefficient varying between 0.6 and 0.7 at cruise conditions.	Lift over drag for the airfoils is: VR12=101, VR14=112.	Complies
SYS-RTR-1178:PER	The maximum lift coefficient shall be higher than 1.2 at a Mach number of 0.5 at cruise conditions.	The airfoil design is best-fitted with the rotor requirements.	1.63

From this compliance matrix, it is possible to discuss the feasibility of the HAMRAC design as presented throughout the report. In general, good compliance is found over the wide range of requirements. This section will highlight some of these requirements and explain whether the project is expected to be feasible, which changes or further investigations will have to be made and whether continuation of the design is perceived as a valid effort.

Firstly, the feasibility of the mission and operations is good, all requirements were complied with. After study of the refuelling stops between the international airport and Mount Everest, local infrastructure is deemed not capable of hot refuelling, so the mission profile is optimised without this option. The mission profile further requires high ascend and descend rates. As the use of pressure helmets is not common practice in helicopters, the descend rates are limited to 10.16 m/s, allowing the omission of possibly unfeasible pressure helmets. Furthermore, the rotorcraft design is made class A certifiable, certification shall be done in a later stage.

Aerodynamics-wise, the design is expected to be feasible. The airfoil design underwent several iterations to find a feasible fit. The development of a CFD model of the fuselage and landing gear aerodynamics is recommended. The rotor blade and fairing will need to be tested in a wind tunnel to determine their actual performance, but so far meet all requirements. The interference of the servo flap with the rotor blade should be tested. As the blade material is composite, manufacturing the complex shape does not present much of a problem compared to a metal design. Rotor hub manufacturing is feasible due to the existing technology used. The power performance is complicated through the different rotational speeds, vibrational testing will need to conclusively prove the safety and feasibility of this system. The twin engine gearbox is reliable, safe and proven technology.

Structurally, the blades and rotor hub carry the largest aerodynamic loads and are therefore crucial for feasibility. So far, the blades cannot comply with their requirement; they break under gust load but are otherwise capable of carrying the nominal loads and safety factor. To meet this gust load requirement, it is advised to increase the blade's stiffness and moment of inertia. The CFRP-Al honeycomb structure is feasible but expensive, and not recyclable. Both the rotor hub and rotor shaft are fully feasible and comply with their load requirements. The rotor hub is a small carbon fibre tube with varying thickness and inexpensive. The rotor shaft is made of aluminium. The results of the airframe analysis do not seem reasonable. They comply with the requirements, but not with reality. The thickness of the skin has a very low value, which would easily buckle. As a recommendation for further design phases, do not only consider forces acting in z-direction, but also in x- and y-direction, as they might induce stresses that significantly influence the strength of the airframe. Additionally, do not only consider the yield of the material, but also consider buckling as a possible failure mode. No analysis of the blade joints on the rivet level was made, which is why this requirement is not complied with.

In stability and control, the hingeless rotor blades ensure enough control power for the aircraft in all foreseeable conditions. The 4-axis autopilot helps the helicopter to become stable in both hover and forward flight. Further development of an autopilot and consideration of how to help crew fly through the degraded visibility environments will conclusively determine whether the aircraft can be flown in 95% of the cases. Current autopilots are capable of dealing with wind up to 35kts from the most critical direction, further investigation into 40kts from any azimuth is necessary and needs to be accounted for in further autopilot design.

Where sustainability is concerned, the rotorcraft is made of at least 90% recyclable materials. It therefore complies with the requirements, the precise percentage still needs to be determined. The noise requirement cannot be complied with. It is inherent to coaxial configurations' rotor wake interference to produce more noise. Efforts to reduce this noise can be made with silent tips, but the noise levels will not come down below the conventional aircrafts. Fuel consumption and CO_2 emission levels are not lower either despite the choice of engines with low specific fuel consumption: this is because the mission goes higher than comparable aircraft, therefore needs more power and fuel as well. The real problem here is that no truly comparable aircraft can be found. The embodied energy required compared to other rotorcraft will need to be verified in a later stage of the project.

12 Cost Breakdown

This chapter aims to establish the cost breakdown for the HAMRAC project. To do this, the lifecycle cost (LCC) for aerospace engineering is analysed and reconsidered for design, development, production, operation, and transport of a rotorcraft.

First, the purchase price of the HAMRAC will be estimated using a logarithmic regression of aircraft given by Roskam [51] as a function of MTOW. The projected purchase price, given by Equation 12.1, accounts for inflation, as aerospace projects typically require a market projection for the future when estimating costs. Therefore, the market cost will be used using the 1989 market, accounting for this inflation. It is assumed that all unknown market parameters are negligible in this preliminary estimation. The projected purchase price is 1.9 million USD in 1989. This is equivalent to 3.92 million USD in 2018[1], or 3.44 million EUR. This is within the required purchase price of 3.5 million EUR. This projected purchase price will be used to determine the return on investment for the HAMRAC in section 12.5

$$AMP_{1989} = \log_{-1} 2.3341 + 1.0586 \log(W_{TO}[lbs]) \tag{12.1}$$

The LCC for an aerospace engineering project is shown in Figure 12.1. The LCC is broken down into four sections: development, production, operation, and disposal, which will each be addressed in the following sections. The total cost breakdown for the HAMRAC project is given in Figure 12.2.

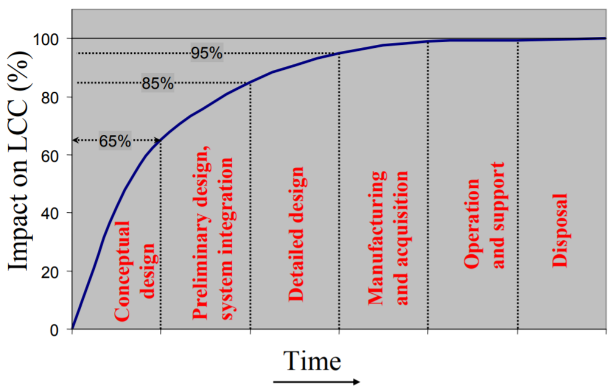

Figure 12.1: *Lifecycle cost diagram [50]*

12.1 Development Cost

The future costs related to the development of the HAMRAC are the costs to finalise the systems integration and to complete the final design for the HAMRAC. These tasks are given by Roskam [51] as the non-recurring

[1] URL `https://www.usinflationcalculator.com/` [cited 23 January 2019]

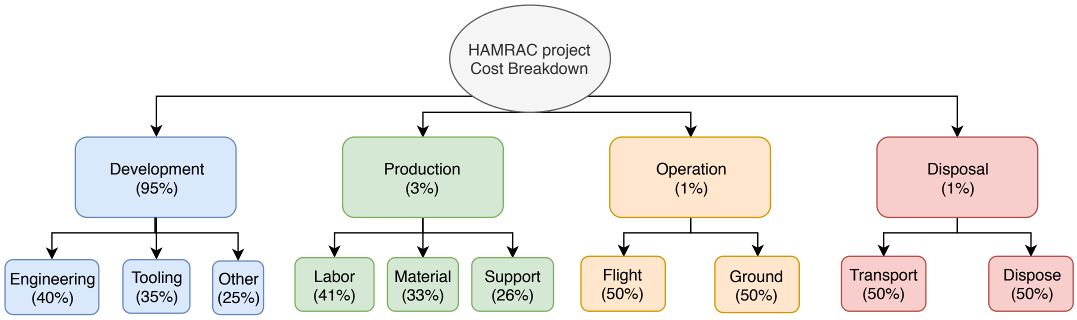

Figure 12.2: *Cost breakdown for the HAMRAC*

tasks grouped together as follows:

- Engineering
  - airframe design/analysis
  - configuration control
  - systems engineering
- Tooling
  - design of tools and fixtures
  - fabrication of tools and fixtures
- Other
  - development support
  - flight testing

The cost breakdown for each of these non-recurring costs during the development phase is shown in Table 12.1 by Markish [50]. This table will be used with the engines of the HAMRAC to estimate the total development cost for the project, which will then be verified by comparing it to the development cost of the Sikorsky X2.

Table 12.1: *Development cost per pound distribution for an aerospace project*

Weight	Engineering 40%	Tooling 35%	Other 25%	Total 100%
Wing	$7093	$6171	$4468	$17,731
Fuselage	$12,837	$12,982	$9273	$37,093
Landing Gear	$999	$874	$625	$2499
Engines	$3476	$3041	$2172	$8691
Systems	$13,722	$12,007	$8576	$34,307
Payloads	$4313	$3774	$2695	$10,783

The engines selected for the HAMRAC each weigh 149.7 kg, and there are two of them. With the non-recurring cost per pound of $8691, the total development cost of the HAMRAC is extrapolated to be 60 million USD, using the given weight to cost ratio as illustrated by Table 12.1 [50]. This is comparable to the production cost of 50 million USD of the Sikorsky X2[2]. Notable differences are the larger rotor for the HAMRAC, a larger maximum take-off weight, and two slightly smaller engines instead of one. Alternatively, changing the engine and rotor for the Sikorsky to match those of the HAMRAC, the Sikorsky would have a development cost estimated at 65 million USD, using the same approach.

However, this is a very imprecise estimate as the data given for the cost estimation is for aerospace instead of rotorcraft, and therefore some of the cost per pound of the HAMRAC is inaccurate. To compensate, the projected cost is deemed too low. This also does not include the need for development for additional, specialised tools for the coaxial rotorcraft, as coaxial rotorcraft are significantly less common than fixed-wing

[2] URL `https://en.wikipedia.org/wiki/Sikorsky_S-97_Raider` [cited 18 January 2019]

aircraft. Therefore, an additional tooling cost will be applied to the existing tooling cost. Additionally, the landing gear mass and wing mass will be reduced by 10% while the fuselage mass and systems mass will be increased by 10% to consider the new development costs for the HAMRAC. This results in a new estimated cost of approximately 95 million USD, or 83.7 million EUR.

The breakdown for the development is also shown in Figure 12.2 given by Markish [50] and based on the weight of the HAMRAC. Using the Table 12.1, the estimated cost for each part of the development in Table 12.2. These costs are increased by 20% with respect to the numbers acquired from the used statistical data, as that data is primarily focused on commercial aircraft. This is because helicopters in general, and the HAMRAC especially due to its coaxial configuration, are rather less conventional compared to competing products. It is assumed that this will lead to significantly increased labour and 'other' costs.

Table 12.2: *Non-recurring costs*

Non-recurring section	Engineering	Tooling	Other	Total
Cost (Million EUR)	21.12	36.96	25.62	52.8

12.2 Production Cost

The recurring costs for an aerospace project are given below:

- Labour
  - fabrication
  - assembly
  - integration
- Material to manufacture
  - raw material
  - purchased outside production
  - purchased equipment
- Production support
  - QA
  - production tooling support
  - engineering support

The cost breakdown for the production is given in Figure 12.2, and the specific costs for production are shown in Table 12.3.

Table 12.3: *Recurring costs*

Recurring leg	Labour	Materials	Other	Total
% of total recurring cost	41%	33%	26%	100%
Cost of HAMRAC production (€)	779,000	628,000	493,000	1,900,000

The learning curve phenomenon is shown in Figure 12.3. The learning curve is an estimate that reduces the cost of successive model outputs by up to 55% of its original production cost as can be seen in Figure 12.3. For the HAMRAC, this indicates that the recurring costs for the HAMRAC could be reduced to as much as €870,000 from its original production cost of 1.9 million EUR. This would increase the return on investment of the HAMRAC and makes successive production of the HAMRAC more affordable for its manufacturers and clients.

12.3 Operational Cost

A requirement regarding the cost states that the operational cost has to be lower than 2500 USD/hr, quoted as: **[SH-08/2-C:OPS] The hourly operational costs of the HAMRAC shall not exceed 2500 €.** In this section, a breakdown is made of all the main contributors to the operational cost and the approximate cost for each

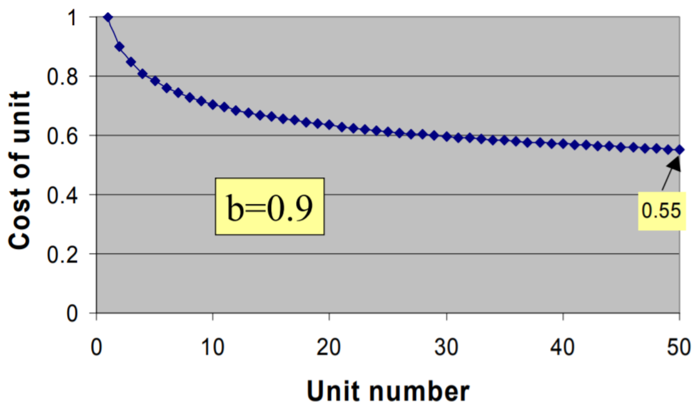

Figure 12.3: *Learning curve*

of them. This can be seen in Table 12.4. The following assumptions have been made regarding the cost predictions:

- 430 annual operational hours.
- The coaxial design introduces more moving and complex parts, therefore an additional factor of 1.4 shall be added to the maintenance costs compared to the standard maintenance costs.
- Duration of a mission is 3 hours.
- Kathmandu Airport is used for airport related fees[3].
- Maintenance, Repair and Overhaul Costs are based on the LH212 Delta I Helicopter with a MTOW of 1135 kg, this has been scaled down to the MTOW of the HAMRAC with additional factor of 1.5 for additional extreme operational conditions[4]/
- Crew salary is based on the average salary of Airbus pilots with an additional factor of 1.4 due to the risk factor of the mission profile[5].
- The cost “others” under fixed costs consists of: unscheduled maintenance and EMS equipment.

It can be noticed that the requirement has been satisfied with an approximate hourly operating cost of $1100. In order to validate this operating cost, this operational cost has to be compared to the hourly operating cost for our reference aircraft (Airbus H135), which is $1144. [6]

12.4 Transport & Disposal Cost

The transport and disposal cost are defined using Figure 12.2, where a disposal cost of 1% is used of the total project cost of the HAMRAC. The 1% of the 3.92 million USD (3.44 million EUR) is $39,200 that is available for both the disposal and the transport cost. The disposal part of the cost is very difficult to estimate due to unavailability of the price from the disposal companies. Furthermore, it is also dependent on the size, weight, internal components and many other factors of the vehicle. However, a rough estimate can be made for the transport cost and therefore an estimated disposal cost can be defined.

In order to execute a disposal operation, a disposal company must be operative in the country where is it stationed or in nearby countries. However, the HAMRAC is stationed at Kathmandu International Airport in Nepal and the availability of disposal companies is not known officially according to Aircraft Fleet Recycling Association (AFRA)[7]. Therefore, companies nearby Nepal should be consulted, which can be found in the

[3]URL `https://dlca.logcluster.org/display/public/DLCA/2.2.1+Nepal+Tribhuvan+International+Airport+Kathmandu` [cited 18 January 2019]
[4]URL `http://www.lcahelicopter.com/wp-content/uploads/2016/06/estimateoperatingcosts-1.pdf` [cited 18 January 2019]
[5]URL `https://www.glassdoor.com/Salary/Airbus-Helicopters-Salaries-E17532.htm` [cited 21 January 2019]
[6]URL `https://www.bjtonline.com/aircraft/airbus-helicopters-h135-p3`[cited 18 January 2019]
[7]URL `https://afraassociation.org/` [cited 18 January 2019]

Table 12.4: *Variable and fixed operational cost breakdown for the HAMRAC mission profile*

Ops. Cost Contributors	**Hourly Costs [1000$/hr]**
Variable costs	
Fuel	0.415
Crew	0.3
Maintenance, Repair & Overhaul	0.3424
Ground Handling	0.012
Control & Communication	0.025
Total	**1.094**

Fixed costs	**Fixed Cost Annually [1000$]**
Mandatory Insurance Crew and Civil Liability	0.85
Insurance Full Helicopter	12.5
Annual Inspection	5
Storage	2.026845
Landing	0.441155
Crew (Outside Mission)	221
Crew Training	10
Others	10
Total	**261.818**
Total Fixed Cost Hourly	**0.03**

People's Republic of China [8]. It is a possibility to transport the HAMRAC both by air and ground transport, however by assuming that there is no transportation time limit, it is much cheaper to transport it over ground due to the sheer size of the HAMRAC (based on transportation of large vehicles such as cars and trucks)[9].

An approximate distance of 6000 km has to be covered in order to transport the vehicle from Kathmandu International airport to the disassembly company. Using transport cost from several USA car transportation companies as reference[10] it can be estimated that the transportation of a SUV of 1500 kg over a range of 4000 km can be done for a price of approximately €1500. Scaling it down for the HAMRAC with an OEW equal to 1400 kg over a distance of 6000 km, it can approximately be determined that the transportation price for the HAMRAC is $2100, however factoring in the sheer size and additional fees, it can end up towards a price of approximately $3000-$4000. Using the transportation cost that has been previously determined, a disposal cost of approximately $35,000 can be expected.

12.5 Return on Investment

The return on investment (ROI) of the project is defined in Equation 12.2[11]. For this calculation, it is assumed that the number of units produced is equal to the number of units sold. The number of units that the HAMRAC is expected to sell during the first 10 years of its operational phase is estimated in section 3.4, and the production cost per unit is given in section 12.2[12]. This would result in a total ROI of the HAMRAC, as can be seen in Equation 12.5, of 26% in 2032 with 95 units sold, when the rotorcraft has been in operation for 10 years. In addition, break-even is predicted to happen after approximately 53 HAMRACs are sold. This is expected to happen at three quarters of the 10 year period, as sales of a new product commonly do not grow linearly.

$$ROI = \frac{\text{Total Revenue}}{\text{Total Investment}} \cdot 100\% - 100\% \tag{12.2}$$

[8] URL `http://cadc-aero.com/Default.aspx` [cited 18 January 2019]

[9] URL `https://www.wcshipping.com/international-car-shipping` [cited 18 January 2019]

[10] URL `https://home.costhelper.com/auto-transport.html` [cited 18 January 2019]

[11] URL `https://study.com/academy/lesson/return-of-investment-definition-formula-example.html` [cited 18 January 2019]

[12] The cost of production for each unit is assumed fixed at 1.9 million EUR, neglecting the learning curve. This is because the learning curve depends on significantly increasing production capacity, and it is assumed this would only happen after the break-even point is met to simplify the estimation

$$\text{Total Revenue} = \text{\# Units Sold} \times \text{Sale price per unit} \tag{12.3}$$

$$\text{Total Investment} = \text{Program cost} + \text{Production Cost per Unit} \times \text{\# Units Produced} \tag{12.4}$$

$$ROI = \frac{95 \cdot 3.5}{83.7 + 1.9 \cdot 95} - 100\% = 26\% \tag{12.5}$$

With an expected ROI of 26%, the HAMRAC could be a successful project, if the forecast of the sales is as expected. There is a risk that for instance one of the markets will not develop as expected, which could have a large impact on the ROI. In order to determine how this will influence the potential ROI, three other scenarios were evaluated. Scenario two assumes that the HAMRAC will not be sold in the primary market as expected, scenario three consists of the HAMRAC will not be sold in one of the smaller potential markets, either OHT or SAR (as described in section 3.4), and the fourth scenario assumes that the HAMRAC will not be sold in the EMS market, the largest potential market, as described in section 3.3. This resulted in the following values for the ROI Table 12.5:

Table 12.5: *Return of investment for variable market success*

Scenario	**1**	**2**	**3**	**4**
Failed Markets	None	HAMR	SAR or OHT	EMS
Units Sold	95	80	80	45
ROI	**26%**	**18%**	**18%**	**-7%**

As can be seen in this table, for scenario 3 or 4, the ROI reduces with 8%, which still results in a promising ROI. If the sales will not be successful in the EMS market a loss of 7% could be a result. However, no sales at all in the EMS-market, consisting of half the global helicopter market, would not be very realistic if HAMRAC would be successful in the other markets. If scenario 4 will be the reality, an additional eight HAMRACs need to be sold in order to break-even. This means that either the other markets need to be more successful than expected, or the EMS market performs marginally with eight HAMRACs sold. To conclude, the overall expectation is that the HAMRAC will generally have good return of investment prospects.

13
System Characteristics

In this chapter, the overall system characteristics of the HAMRAC is thoroughly stated. Firstly, in section 13.1, the RAMS are described which gives an overview of key features that is needed to reliably keep the product effective for the given time. Secondly, the section 13.2 states the production approach and procedures of each segment of the HAMRAC with slight modifications due to the coaxial configuration. Thirdly, in section 13.3, the risks and associated solutions are given regarding the design of the HAMRAC including the mission profile. Lastly, in section 13.4, the sustainability analysis of the HAMRAC design is conducted and gives a brief overview of the sustainability level of the design.

13.1 RAMS

The Reliability, Availability, Maintainability, and Safety (RAMS) characteristics of the system are established in this section.

13.1.1 Reliability

Reliability is of great importance when designing a rescue vehicle. This is because a rescue vehicle is expected to be able to complete its mission, otherwise it can end with catastrophic results. To make sure that the design fulfils the reliability requirements, additional considerations are made. This means that the parts and systems that are used in the design need to be of high quality and therefore highly reliable: they were only chosen on whether they meet the reliability considerations. Standardised components tend to have well documented and accurate reliability characteristics. If these characteristics have been obtained in different operating conditions than the mission of the HAMRAC, additional tests should be performed.

To further increase the reliability of the design some choices were made. The HAMRAC will be built as a category A, this means it shall be able to take off and fly with one engine inoperative from 6705 m. Therefore, if the HAMRAC would get an engine failure on its way back to the hospital it would still be able to get there. However, this means an extra gearbox is needed to facilitate the coupling of the two engines, this means more moving parts and less reliability. The system however is more reliable due to the fact it can keep on flying with an engine failure.

With other coaxial helicopters the swashplate for the top rotor is very complex and prone to failure, for the HAMRAC this is eliminated by the use of servo flaps. This increases the reliability again and makes it overall easier to work with. Finally, the design is equipped with a proven mainly mechanical control system, this means not using a fly-by-wire system. The fly-by-wire systems currently on the market are still to susceptible to failure and therefore not suitable for the design of the HAMRAC.

13.1.2 Availability

Availability is key for the system since the mission should be completed within 6 hours from a distress call, 95 % of the time. Availability is defined as the probability that the system will be ready or available when required for use. Predictive maintenance rather than reactive maintenance shall increase the availability of the

HAMRAC. With a carefully planned maintenance plan this can be achieved. So larger maintenance overhauls shall be planned out of the climbing season where the HAMRAC is stationed. The smaller maintenance operations shall happen on regular bases. However, when bad weather is forecasted for a longer period of time, maintenance can be performed ahead of the planned maintenance. This means weather when there is no possibility of flight due to wind gusts or snow storms. Inherent and operational availability will be discussed next.

Inherent availability, A_i, as defined in the SE lectures [73]:

$$A_i = \frac{MTBF}{MTBF + MTTR} \tag{13.1}$$

In which MTBF is Mean Time Between Failures, and MTTR is Mean Time to Repair.
Inherent availability comes down to the probability that the system, when operated in its environment, with available tools, spares and maintenance, can operate on demand at any point in time. The reason this is inherent is because it excludes preventive or scheduled maintenance actions, logistics and administrative time delays, so it will pertain mainly to the design of the rotorcraft.
Operational Availability, A_o, as defined in the SE lectures [73]:

$$A_o = \frac{MTBM}{MTBM + MTTM} \tag{13.2}$$

In which MTBM is Mean Time Between Maintenance and MTTM is Mean Time To Maintain.
Operational Availability, A_o, refers to the probability that the system can operate on demand at any point in time, given the actual operational environment, including preventive and corrective maintenance times and all delay times. It refers to the availability of the rotorcraft when considering the fact that it needs to interact with other systems such as people and machinery. Factors such as accessibility would then be accounted for here.

Both the inherent and operational availability shall be investigated further in the testing phase of the HAMRAC. Since for some parts of the HAMRAC the overhaul period is not yet known the uncertainty is too high to make an estimation at this point.

13.1.3 Maintainability

Maintainability pertains to the safety, ease, economy and accuracy of maintenance actions. As described above, there will be a predictive maintenance plan for the HAMRAC. Cost and time for maintenance shall be minimized, just as the amount of resources needed to perform the maintenance operations. Where the two engines made the HAMRAC extra reliable during flight, it will also increase the maintenance time. Since the engine is one of the major components of the helicopter, a relatively large amount of time will be spent on maintenance.

In the rotor hub, less parts will be used as described in section 10.3, due to the use of servo flaps on the blades. This will reduce the maintenance time significantly since less parts need to be repaired or replaced. And since there are less parts, it results in parts to be bigger. This will negatively influence the costs of the maintainability, since larger parts will be more expensive. But on the other hand, the time of the maintenance will reduce because less parts need to be examined and replacement is easier for the mechanics.

To be able to place a fairing around the rotor mast, a third mast needs to be there instead of two which results in a more complicated maintainability procedure. Skids are used as landing gear which has less maintenance time with respect to the other two options described in section 8.4. The skids are easy to reach and despite the fact that the part is very large, it is easy and fast to replace. Due to the installed servo flaps at the rotor blades, no hydraulics are present in the HAMRAC. This results in a safer working environment for the mechanics since the hydraulic fluids are dangerous for humans.

13.1.4 Safety

As mentioned at the beginning of this section the HAMRAC is designed to be a category A helicopter, which means it has two engines such that in case of an engine failure it can continue safe flight [39]. Another safety feature of the HAMRAC is the fact that it can perform autorotation in case two engines fail. The safety of the HAMRAC also increases by not having a tail rotor. The main rotors are at such a height that the average person can stand under them easily without being hit. With conventional helicopters, the tail rotor can cause fatal accidents because it is located lower as seen from the ground.

The horizontal stabilizer of the HAMRAC is placed in the wake of the main rotor blades because of safety measures. As already discussed in section 10.5 it could become very dangerous when due to a gust, the rotor wake would suddenly hit the control surface. To prevent this from happening, the control surface is already placed in the rotor wake such that the wake can be taken into account constantly and no sudden changes in air flow will appear at the control surface. For the passengers and crew of the HAMRAC oxygen masks will be present since the fuselage is not pressurized.

13.2 Production Plan

To produce the HAMRAC, components are fabricated from raw materials or purchased from suppliers, this is described in subsection 13.2.1. The produced components are assembled and integrated into the airframe as described in subsection 13.2.2.

13.2.1 Manufacturing

In this section the manufacturing of various components of the HAMRAC is described.

Rotor Blades and Main Rotor Hub Manufacturing The manufacturing of the six rotor blades as well as the flexbeam and torque tube, will be done using composite manufacturing techniques since these parts mainly consist of carbon fibre.

Given the load cases, the fibre orientation for these parts is determined. All these parts have twist and bending loads and so therefore a woven carbon fibre fabric material is most appropriate. Since high tolerances are required for these parts, it makes most sense to use pre-impregnated fibres with high tolerance ply stacking techniques.

Positive moulds should be used to laminate the pre-impregnated fibre. This mould should also be made from carbon fibre. This way, both the mould and the product can achieve high curing temperatures. Additionally, because their coefficient of thermal expansion is similar, no internal stresses will be caused during the cooling part of the curing cycle. The additional benefit of using a carbon fibre mould is that is provides high quality surface finish.

Before laying up the plies, a cleaning agent and release agent should be used to clean the surface from impurities and allow for a smooth release, respectively. After this step, the plies can be stacked on top of each other according to a predefined stacking sequence based on the structural finite element output of the model.

When preparing the product for curing in the oven, peel ply and a vacuum bag should encase the product afterwards. The peel ply should aid in the release of the vacuum bag after curing. And the vacuum back is used to pressurize the product during the curing cycle. This allow for no air to be present within the carbon fibre layers, so that the structural properties are maintained.

To introduce vacuum into the product a hose must be introduced into this vacuum bag, by means of a valve. The pressure difference is achieved using a vacuum pump. Before the product is inserted into the oven, it should be checked for leaks. After a leakage test, the hose valve should be closed and the hose removed.

The oven temperature should match the material specifications of the supplier. A post-cure is a possibility. It can be used to increase the glass transition temperature of the product, so that it holds is strength properties at higher temperatures.

The correct procedure is followed, the product will have the structural properties desired by the HAMRAC's structural department.

Airframe Manufacturing The airframe of the HAMRAC consists of a so-called stressed skin construction. This is a type of rigid construction, intermediate between monocoque and a rigid frame with a non-loaded covering. Relative to a tubular or bonded construction, which are the two other rotorcraft airframe types, this type of construction is easier to manufacture. Furthermore, it has a good precision in terms of fitting tolerance, because of the jigs being used.

The semi-monocoque structure consists of a framework of horizontal and vertical members, covered with a thin metal skin. The heavy longitudinal members, also known as longerons, provide the primary strength of the structure. The relatively lighter longitudinal members, called stringers, give a means of attaching and stiffening the skin. Vertical members called formers or bulkheads provide the shape of the airframe.

Almost all the members within the airframe that have to bear loads, are made of Aluminium 2024-T3 alloys. This alloy first has to be heated up above its melting temperature, after which it can be poured into a mould. If the product does not have the desired shape yet, it can be formed afterwards. This is a popular method used during the manufacturing of stiffeners. Machining processes can be used to make cut outs in sheet material if this is desirable. If the parts have the desired shapes, they can be joined together by bolts, which is preferred over adhesive bonding and welding for maintenance purposes. [1].

13.2.2 Assembly & Integration

Final assembly starts with the receipt of the airframe. Components and pre-assembled subsystems are installed into the airframe. Each installation of a component is called an assembly operations sequence. Each sequence is finished by a quality check by the production facility's quality assurance or quality control department. This does not exclude a total quality management approach but is part of the entire quality management. Assembly will be done according to one of the two following strategies [79]:

A **stations approach** can be taken in which the HAMRAC is assembled in different phases and moved around the production plant from station to station. In this approach the workers, tooling and resources remain stationary, whilst the HAMRAC is moved around. Multiple assembly operations sequences are performed at each station. This method is better suitable for higher production volumes and allows for easier specialization of workers. The disadvantage is that more factory space is required, than with the battleship approach which is described next.

In the **battleship approach** the airframe remains stationary in the same location on the production floor. All assembly operation sequences are performed here. This method is often used for lower production volumes. Battleship assembly approach can be performed on a relatively small production floor but requires more administration and movement of workers, tooling and resources.

Since the HAMRAC design team does not have production facilities available, the assembly strategy depends on partners found for the production. Airbus helicopters as a market leader is known to have large scale production facilities, partnership would allow for a stations approach in the assembly & integration of the HAMRAC.

13.3 Technical Risk Assessment

A risk assessment is performed and presented in this section. The risks are not listed in chronological order, but in association with their phase within the product life cycle. Descriptions have been included for clarification of the risks and describe what it encapsulates. Two risk maps are subsequently presented, showing the likelihood and impact of each risk before and after mitigation, respectively.

Risks associated with manufacturing:

- [$RM1$] Misuse of machinery: Technician may suffer injuries if correct procedures are not followed.
- [$RM2$] Machinery malfunction: Machine needs to be replaced or fixed.
- [$RM3$] Test is destructive, and parts fail during testing.
- [$RM4$] Parts do not pass test.
- [$RM5$] Materials not supplied on time.

[1] URL `https://www.slideshare.net/partyrocka99/1-week-1-helicopter-structure` [cited 20 Janaury 2019]

- [$RM6$] Strike at manufacturing plant.
- [$RM7$] Specified tolerances are not met: Parts cannot be assembled.

Risks associated with vehicle distribution and delivery:
- [$RD1$] Parts lost: During disassembly for transport.
- [$RD2$] Tools for assembly are not available at delivery site.
- [$RD3$] Parts are compromised during transport.
- [$RD4$] Parts cannot be transferred through required road itinerary due to their size.

Risks associated with mission specific performance:
- [$RP1$] Battery management system fails.
- [$RP2$] De-icing system malfunctions.
- [$RP3$] Fuel cap cannot be removed for fuel pump nozzle placement.
- [$RP4$] Fuel redistribution system malfunctions.
- [$RP5$] Oxygen tanks are not available at departure site.
- [$RP6$] Cabin heating malfunctions
- [$RP7$] Communication and/or navigation antennas malfunction
- [$RP8$] Insufficient fuel to complete mission
- [$RP9$] Hoist system malfunctions
- [$RP10$] Gusts higher than 25 kts occur during hover.
- [$RP11$] Fuel tank temperature falls below fuel freeze point.
- [$RP12$] Fuel during refuelling stop is contaminated with water, increasing the fuel freeze point.
- [$RP13$] Facilities at the refuelling stop are inadequate to handle hot refuelling.
- [$RP14$] Door width does not allow for transfer of rescuee to aircraft.

Risks associated with Trade-off:
- [$RTO1$] Grading for each concept is biased: Personal preference has influence on concept chosen.
- [$RTO2$] Weight attributed for each criterion is not appropriate: Reliability, sustainability and cost requirements may not be met by concept because these were given relatively small weights.
- [$RTO3$] Literature research is not thorough: Understanding of the criteria in not reached to appropriate depth for more accurate trade-off.

Risks associated with Requirements:
- [$RR1$] Implication of requirements on design not evident: Misunderstood or overlooked requirements could turn out to be killer.
- [$RR2$] Conflicting requirements: Attempting to meeting one requirement, could result in being unable to meet another.

Miscellaneous:
- [$RMis1$] N2 does not encompass every input/out relation: Chief/System's engineer may lose oversight of system integration.
- [$RMis2$] Costs of development higher than predicted.
- [$RMis3$] Costs of operations are higher than predicted.
- [$RMis4$] Costs of maintenance are higher than predicted.
- [$RMis5$] Insurance companies do not cooperate: Operational cost too high, so they favour competitor's solutions instead.

Risks associate with aerodynamics:
- [$RAero1$] Shock-waves are formed at tips: These could increase likelihood of avalanche.
- [$RAero2$] Blade(s) breaks during flight.
- [$RAero3$] Icing on blade leading edge.
- [$RAero4$] Cross-sections of airframe due to other subsystem requirements is less aerodynamic than preferred.
- [$RAero5$] Down draft of rotor is powerful enough to start an avalanche.
- [$RAero6$] Blade vortex interaction causes rotorcraft to exceed noise limits.

Risks associated with structures:

- [$RS1$] Attachment points fail.
- [$RS2$] Load bearing parts fail due to load.
- [$RS3$] Load bearing parts fail due to fatigue.
- [$RS4$] Different material behaviour: High temperature and humidity variations may decrease performance of materials.
- [$RS5$] Blade deflection exceeds rotor separation.
- [$RS6$] Skin fails due to buckling.

Risks associated with stability and control:

- [$RSC1$] Rotorcraft is not statically stable: May be due to lack of performance during hover, trim condition not reached during cruise or part braking during any flight mode.
- [$RSC2$] Yaw, pitch and/or roll are not controllable: Due to part breaking, poor design, ineffective control augmentation system or harsh environmental condition.
- [$RSC3$] Unstable heave mode at high speeds.
- [$RSC4$] Unstable Dutch roll.
- [$RSC5$] Hoisting becomes dangerous due to the action of strong winds.
- [$RSC6$] Servo flaps freeze.
- [$RSC7$] Fuel tanks are pumped in the wrong order, causing an unstable shift in the centre of gravity.

Risks associated with power:

- [$RPW1$] Not enough power for cruise speed.
- [$RPW2$] Not enough power to hover at 8950 m.
- [$RPW3$] Mechanical power loss is unreasonably high: Power is lost to an unacceptable extent due to poor design.
- [$RPW4$] Engine cuts out in an unsafe autorotation condition.

Risks associated with operations:

- [$RO1$] Clearance from ATC is delayed/not given.
- [$RO2$] Refuelling takes too long: Ground operations are inefficient.
- [$RO3$] Rescuees are not found by crew: Identification of rescuee position for retrieval is not possible.
- [$RO4$] Physical and mental human factors: Misjudgement of landing, (Mental) fatigue.
- [$RO5$] Weather deterioration: Weather changes during operation may extend the mission time.
- [$RO6$] Avalanche takes places when rotorcraft is on ground on mountain.
- [$RO7$] Rotorcraft collides with cables, wires or other rotorcraft whilst performing mission.
- [$RO8$] Craft is struck by lightning.

Scales Definition

Likelihood

- *Almost never*: this event is not expected to occur, but there is the possibility that it will.
- *Rare*: this event may occur, and so the crew of the HAMRAC should be prepared for this event.
- *Moderate*: this event occurs frequently enough to warrant consideration for the design of the HAMRAC.
- *Likely*: this event occurs often enough that the crew and design should anticipate it occurring.
- *Almost certain*: this event is guaranteed to happen in all but the rarest circumstances.

Severity

- *Negligible*: this event will not impact the mission outcome, but it may inconvenience persons.
- *Minimal*: this event does affect the mission outcome, but proper procedures, equipment, and preparation can account for any adverse effects.
- *Moderate*: this event will not jeopardise the mission on its own, but it may compound with other events that may jeopardise the mission's outcome. Additionally, the mission may still succeed, but with adverse consequences, such as a rescued climber getting frostbite, resulting in loss of limb, or damaged equipment requiring immediate maintenance, increasing maintenance time and cost.
- *Severe*: this event jeopardises the mission and prevents the rescue from taking place.
- *Catastrophic*: this event results in a worse situation than if the rescue mission had not taken place, typically due to the crew of the HAMRAC becoming stranded or injured in addition to the rescuees.

13.3.1 Risk Map

After the risks have been discussed and assigned a code, they are organised into a risk map. Colours are used to improve overview, where green shows a very low risk, and red shows a very high risk.

Table 13.1: *Risk map with severity categories on the left, and likelihood on the bottom*

Catastrophic	RD4, RO6, RS5	RP10, RS1, RS2, RS3, RP2,RP9, RO3, RO7, RAero2, RP11, RP12, RSC3, RSC4	RR1, RR2, RSC1, RSC2, RPW4		
Severe	RM6, RD3, RP4, RP8, RO5	RP1,RP5,RP7, RPW1,RPW2, RO8,RSC6	RM1, RMisc1, RAero5, RAero6, RS6	RO4, RAero3	
Moderate	RM4,RD1,RD2, RO1, RO2	RM2,RP3,RTO2,RP14	RS4, RPW3, RAero1, RSC5, RSC7	RM7,RAero4, RP13	
Minimal		RM3,RP6	RTO1	RM5, RMisc2, RMisc3,	
Negligible				RTO3,RMisc4	
	Almost never	Rare	Moderate	Likely	Almost certain

13.3.2 Risk Mitigation

Mitigation can be performed on all risks to reduce either its likelihood or its impact. The mitigation strategies of the most concerning risks are elaborated on here.

- RD4: All possible distribution itineraries should be identified for possible obstructions. Distribution plan should account for all obstructions.
- RP10: Using more reliable models for weather prediction and also better sensing instruments, should decrease the likelihood of the rotor craft encountering high gusts.
- RS1,RS2,RS3: The impact of these risks is reduced by designing a redundant structure and one that has safety factors. Inspection should also decrease the likelihood for these failures.
- RSC1: The static stability performance during hover can be improved with a good aerodynamics and powerful design.
- RSC2: Yaw, pitch and roll capabilities can be modelled. If these models are appropriately verified, the chance the rotorcraft is controllable increase.
- RSC3,RSC4: The autopilot should be very well calibrated such that it can respond quickly when such a mode is induced.
- RO6: The impact for avalanches can be reduced if crew are equipped with avalanche safety gear.
- RO7: Rotorcraft collision probability is reduced by meeting regulatory requirements and enforcing pilot awareness.
- RM1: The likelihood of manufacturing injuries and fatalities is reduced through the appropriate training and supervision of technicians.
- RP2: De-icing malfunction likelihood is mainly reduced by regular inspections of de-icing system. Also, by the appropriate utilization of the rotorcraft during operation. Its impact may potentially be reduced by designing an airfoil that is less prone to icing on leading edges.
- RP9: Hoist system malfunction likelihood is achieved by purchasing one that has a good operational standard. The likelihood of impact one hoist system, can be reduced by mounting two or by having a manual hoist system, i.e. ropes and carabiners.
- R03: The likelihood of the crew finding the stranded rescuees is increased by having an experienced crew. The impact of this risk is reduced by relying on an Electro Optical System instead.
- RR1, RR2: With consistent consideration for requirements, are close collaboration with customer, requires could be adjusted so that customer requirements are met.
- R04: Having a larger pool of crew will allow for a distributed work load, reducing the impact of a single crew member feeling unfit for the mission as well as improving collective judgement.
- RAero2: Good structural design should reduce the likelihood of a blade braking during operations.
- RAero3: With a de-icing system, and shovel equipped rotorcraft, the impact of leading edge ice accumulation is reduced because it can immediately be addressed.
- RAero5: By hovering with sufficient ground clearance the down draft shall not be as powerful at the ground level, reducing avalanche risk.

- RP11, RP12: By heating the fuel with the engine oil waste heat, the temperature will not fall below three degrees Kelvin/Celsius above the freezing temperature of the fuel.
- R08: The airframe shall be designed to act as a Faraday cage in the event of a lightning strike. No hoisting shall take place during thunderstorms.
- RPW4: The HAMRAC shall have two engines in case of such an engine cut out. Furthermore, the airframe and landing gear shall be designed to resist crash landing loads.
- RS6: The airframe shall contain stiffening elements to prevent buckling.
- RSC5: The hoist shall be placed near the centre of gravity to prevent instability of the aircraft during hoisting. No hoisting operation shall be conducted during wind speeds above $13 m/s$.
- RP13: Cold refuelling is used instead of hot refuelling.
- RP14: The door used shall be double hatched at the rear of the aircraft to provide a large opening for rescue operations.
- RSC6: The joints and surfaces of servo flaps are to be heated to prevent freezing.
- RSC7: Automation of the fuel pumping system prevents the wrong order of pump activation.

Table 13.2: *Risk map with severity on the left, and likelihood on the bottom*

Catastrophic	RP10, RS1, RS2, RS3 RSC1, RSC2, RO7, RAero2, RS5, RP11, RP12, RSC3, RSC4				
Severe	RM6, RD3, RP4, RP8, RO5, RP2, RP9, RSC5	RP1, RP5, RP7, RPW1, RPW2, RM1, RAero5	RMisc1, RAero6		
Moderate	RM4, RD1, RD2, RO1, RO2, RO6, RO3, RS6, RP13, RP14, RSC7	RM2, RP3, RTO2, RSC5, RSC6	RS4, RPW3, RAero1	RM7, RAero3, RAero4	
Minimal		RM3, RP6, RO4, RO8	RTO1,RR1, RR2, RPW4	RM5, RMisc2, RMisc3,	
Negligible				RTO3, RMisc4	
	Almost never	Rare	Moderate	Likely	Almost certain

13.4 Sustainability Development Strategy

In this section the sustainability development strategy will be implemented in the design of the HAMRAC. Before this can be done further investigation is needed to expand on the current strategy. The main factors that will be elaborated on are noise, emission and embodied energy. Since noise could possibly be a trigger for avalanches this is investigated first. Next the emission of the HAMRAC will be investigated. Lastly the embodied energy will be elaborated on. In addition, some sustainable design choices of technical departments will be explained.

13.4.1 Noise

Noise is a big part of a helicopter's footprint, it is often experienced as annoying. This is because of the chopping sounds that the rotor blades make. Fortunately for the HAMRAC, flight time above populated areas is limited to only 5% of the time. Since the HAMRAC is a mountain rescue vehicle, it is evident avalanches are an issue during a rescue mission this will be elaborated on later.

For helicopters with an equivalent single rotor with the same gross weight of 6000 lb the noise level would be between 78-90 dB at 150 m distance as given in Figure 13.1. Since the hover out of ground effect will happen at a distance of two rotor diameters from the mountain face. With the current rotor diameter this distance is around 20 m. For the noise level at the mountain face the decibel scale needs to be used. For a doubling of the distance the sound pressure drops by 6 dB. Inversely this is also true. This means that at a distance of 18.75 m, $150/2^3$, the noise level has therefore increased by 18 dB. The new noise level range has increased to 96-108 dB.

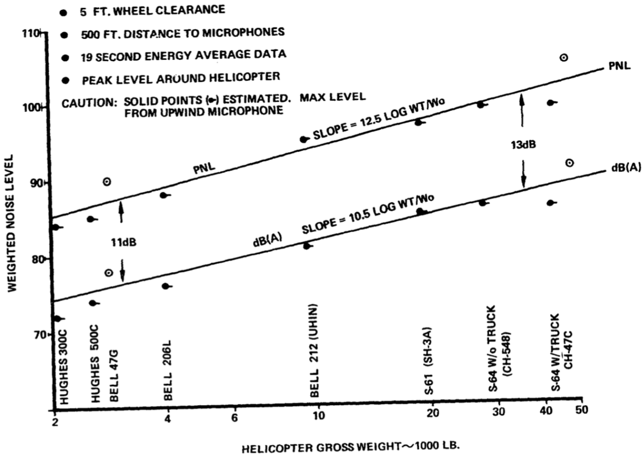

Figure 13.1: *Noise levels single rotor helicopters [45]*

However, the HAMRAC has a coaxial rotor configuration which produces more noise than a conventional helicopter. This increase in noise of a coaxial helicopter would be approximately 10 dB [47]. This increase in noise level is due to the fact that the Blade Vortex Interaction (BVI) noise is higher for the coaxial rotor. The BVI noise increase is a result of the interaction between the top and bottom rotor. The tip vortex of the top rotor collides with the advancing blade of the bottom rotor and therefore creates an impulsive noise [47]. The noise level of the HAMRAC is therefore approximated at 106-118 dB at 18.75 m from the helicopter. This noise level could be experienced as annoying to the people living around the Kathmandu International Airport and in vicinity of the flight path. To mitigate this risk of complains in combination with the needed ground clearance for the expected mountain ranges described in section 6.1, a steeper climb rate has been introduced. This climb rate is higher than the climb rate of the aircraft which are taking off from Kathmandu International Airport.

Avalanches

Most of the avalanches that occur are triggered naturally. Changing weather conditions put enough pressure on the snow to drive it to its breaking point. Human interaction also causes avalanches, in 92% of the cases the avalanche is caused by the victim or victim's party[2]. Noise however does not introduce enough pressure to trigger an avalanche.

To trigger an avalanche from a weak layer of snow where stability is minimal 200-500 Pa is needed [25]. The pressure that is created by an aircraft that is taking off produces 120 dB is around 20 Pa. It is shown that a jet flying supersonic at a 900 m altitude produces 200-500 Pa. In this study it has been shown that only two avalanches were triggered in 20 passes of the supersonic jet [71]. A number of sources and their sound pressure are presented in Table 13.3.

Table 13.3: *Sound pressure from different Sources*

Source	Sound Pressure [Pa]
Loud Scream	2
Jet Plane	20
Supersonic Boom	200-500
Detonation	>1500

With the HAMRAC having a noise level of 118 dB the sound pressure is therefore around 20 Pa. The value is taken of the 120 dB jet plane that is taking off in order to take slight inaccuracy of the measurements into account. Since a minimum sound pressure of 200 Pa is needed to set off an avalanche 10% of the time, a conclusion can be drawn for the HAMRAC. With the sound pressure of the HARMAC being an entire order of magnitude smaller than the minimum requirement to trigger an avalanche, the conclusion can be drawn

[2]URL `https://avalanche.org/avalanche-encyclopedia/trigger/` [cited 22 January 2019]

that the noise produced by the HAMRAC is not enough to trigger an avalanche.

However, the downdraft created by the rotor blades of the HAMRAC has a bigger impact on the snow than the sound. This impact can be calculated using the dynamic pressure equation, since this is the pressure that acts on the snow directly below the helicopter. The HAMRAC will be hovering out of ground effect. This means that it will hover at an altitude of two rotor diameters with respect to the mountain face. With the rotor radius being 5.5 m the altitude with respect to the mountain face will be 22 m.

$$q = \frac{1}{2}\rho v_f^2 \tag{13.3}$$

The speed that is used is the speed of the “far” wake or slipstream velocity. The “far” wake is highest at two rotor diameters down from the rotor blades. Therefore, the pressure that will act on the snow is calculated with this velocity with Equation 13.3. The determination of the ’far’ wake velocity v_f is quite simple since this is twice the induced velocity created by the rotor blades, so $v_f = 2v_i$ [64]. With v_i being 12 m/s an output from the script made for subsection 8.2.2. This leads to a wake velocity of 24 m/s. In combination with the ISA density at 8870 m, altitude of summit of Mount Everest plus two rotor diameters. The dynamic pressure which acts on the snow pack will be 136 Pa. The magnitude of this pressure is still below the trigger threshold of 200 Pa. However, the noise and downdraft both act on the snow at the same time and therefore these pressures should be added together. This results in a total pressure of 156 Pa on the snow. This is worst case scenario since the wake velocity decreases with increasing hover altitude but also decreases with decreasing altitude. Most of the air is curved to the side when decreasing the altitude.

Concluding, with a 22% lower pressure than the lower trigger threshold. It can be assumed that the combined downdraft and noise of the HAMRAC is not enough to set off an avalanche. This however is only theorized and needs to be tested during the first test flights. The procedure that involves this testing is described in chapter 14.

13.4.2 Emission

Since emission has a big impact on environment, extra effort should be put into making sure that the emission of the HAMRAC is as low as possible. During the engine choice the specific fuel consumption is already taken into account. Less fuel use means less emission of carbon dioxide. The engine that has been chosen for the design has one of the lowest specific fuel consumptions in its category. The fuel mass flow needs to be calculated first to determine the emission of the engines. This fuel mass flow has already been calculated to be 0.072 kg/s in subsection 6.1.3. Using methods tailored specifically for twin engine turboshaft engines the emission of Nitrogen Oxide (NO), Unburned Hydro Carbons (HC) and Carbon Monoxide (CO) is calculated. The method used the fuel flow and multiplies it with an emission factor. This emission factor is determined using the installed shaft horsepower per engine. Since the HAMRAC has two engines the outcome needs to be multiplied by two.

$$EINO\left(\frac{g}{kg}\right) \approx 0.2113 * (SHP^{0.5677}) \tag{13.4}$$

$$EIHC\left(\frac{g}{kg}\right) \approx 3819 * (SHP^{-1.0801}) \tag{13.5}$$

$$EICO\left(\frac{g}{kg}\right) \approx 5660 * (SHP^{-1.11}) \tag{13.6}$$

With an installed horsepower of 1038 SHP per engine the emission factors and their respective emissions per engine per hour are given in Table 13.4.

Table 13.4: *Emission numbers for the HAMRAC*

Emitted Molecule	Emission Factor [g/kg]	Emission per engine [g/h]	Emission HAMRAC [g/h]
Nitrogen Oxide	10.89	2818.36	5636.72
Hydro Carbons	2.11	545.70	1091.45
Carbon Monoxide	2.54	657.11	1314.22

Comparing this to other rescue helicopters is very hard since these helicopters are designed for different mission profiles. However, looking back at the initial trade off calculations the coaxial configuration had a lower induced power than the equivalent single rotor by a large margin. Taking into account that the induced power is the main contributor in the power required. Therefore, it can be assumed that if the mission was flown by an equivalent single rotor the power that was needed for the same mission is a lot higher. More power required means bigger engines, bigger engines mean larger fuel flow and a larger fuel flow means a higher emission. Concluding, the HAMRAC is relatively sustainable compared to an equivalent single rotor helicopter which performs the same mission.

13.4.3 Recyclability

As stated in chapter 7 the main materials used for the HAMRAC are $Al2024-T3$, unidirectional carbon fibre reinforced polymer (CFRP), and polycarbonate (plastic). Aluminium, used for the airframe and rotorshaft, is widely used in transportation applications[3]. This is due to its combination of lightness, strength and workability. Beside these favourable features, it is very well recyclable due to its relatively low melting temperature[4]. It is well known that aluminium is near-infinite recyclable and it has flame-retarding properties, which increases the safety of the HAMRAC [69]. It is not only sustainable, but it also reduces the costs of the HAMRAC. Nowadays it is still hard to recycle carbon fibre, however since more and more carbon fibre is used, new ways of recycling are being developed[5]. However, the rotor blades don't necessarily need to be recycled to new rotor blades since this is not possible nowadays. The fibres are not aligned anymore which makes it not possible to re-use the material for the same purpose, but they can also be used for other applications when they are cut into precises[6]. Polycarbonate is used for the windows of the HAMRAC since it is optically transparent and strong. Since it is harmful for the environment, it is important to recycle this plastic[7].

The aluminium airframe and rotorshaft, carbon fibre rotor blades and polycarbonate windows make up the largest part of the HAMRAC. Another large component would be the engines, which is largely made of titanium. It is possible to recycle the engines, however this would take a high amount of energy since the melting temperature of titanium is very high, and thus increase the hereafter discussed embodied energy. To conclude it would be possible to achieve the 90% recyclability requirement since the parts above make up for more than 90% of the materials used for the HAMRAC. The batteries, for example, are non-recyclable and should therefore processed such that it is not harmful for the environment[8].

13.4.4 Embodied Energy

The definition of embodied energy is the amount of energy which is non-renewable per unit of material[9]. The embodied energy can be divided in four parts: The amount of testing for development, materials, maintenance and facilities. Now the HAMRAC is designed, an analysis will be done on these parts, and where needed it will be described how the embodied energy of the HAMRAC can be reduced such that the project will be as sustainable as possible.

Testing for development During the design phase of the HAMRAC, several design choices were made. At every trade-off during this phase the development was taken into account. If possible, and within the budget, a choice was made such that requires marginal testing of a subsystem. Instead of developing new subsystems, one can use existing and tested parts of other aircraft and integrate them in the design of the HAMRAC. It will reduce the total embodied energy significantly, since the production and testing of the subsystems, such as the rotor blades, takes lots of energy.

Materials The main contributor of the embodied energy for a material is the amount of energy that needs to be used to form them in the desired shape. As already discussed in the previous section, aluminium is

[3] `https://www.totalmateria.com/page.aspx?ID=CheckArticle&site=ktn&NM=222` [cited 14 January 2019]
[4] `https://www.azom.com/article.aspx?ArticleID=6652` [cited 14 January 2019]
[5] `https://www.materialstoday.com/carbon-fiber/news/new-way-to-recycle-carbon-fiber-composites/` [cited 14 January 2019]
[6] `https://www.compositesworld.com/articles/recycled-carbon-fiber-update-closing-the-cfrp-lifecycle-loop` [cited 17 January 2019]
[7] `http://polycarbonaterecycling.com/polycarbonate-recycling.html` [cited 15 January 2019]
[8] `https://www.scientificamerican.com/article/lithium-ion-batteries-hybrid-electric-vehicle-recycling/` [cited 21 January 2019]
[9] `http://www.level.org.nz/material-use/embodied-energy/` [cited 15 January 2019]

very well recyclable. The melting temperature is low relative to other metals, which gives aluminium a low embodied energy[10]. Titanium, however, has a very high melting point, which gives it a high embodied energy. Therefore, and due the cost constrains, titanium is only used for the rotor hub. Polycarbonate, a plastic, is a thermoplastic and can therefore be melted at low temperatures.

Maintenance The embodied energy with respect to the maintenance of the HAMRAC can be reduced by making sure the mechanics of helicopters on the current market are also able to perform maintenance on the HAMRAC. This is possible by allowing a maintenance procedure similar to helicopters such as the Airbus H135. In this way the current engineers do not have to follow extensive new training to be able to perform maintenance and replacements on the HAMRAC. Secondly, most of the parts of the HAMRAC should be designed such that most of the individual parts can be replaced instead of replacing a whole subsystem. Finally, lean maintenance should be implemented. This means the maintenance should be active instead of passive. The HAMRAC should be inspected before actual repairs are needed, which will reduce the material and equipment usage[11].

Facilities Since the dimensions of the HAMRAC are comparable with those of conventional helicopters, it should be possible to use the same facilities. Besides that, the same tools can be used on the HAMRAC such as the refuelling system. In this way, no extra energy has to go to changing the facilities to make it possible for the HAMRAC to land and be checked.

13.4.5 Sustainable Design Choices

During the design phase of the HAMRAC choices were made by technical departments which positively increase the sustainability of the project.

Stability & Control Servo-flaps located at the tips of the blades are added. By adding this system, hydraulics can be left out since no moment needs to be created directly to the blade itself as discussed in section 10.3. Skydrol, which is the most common used hydraulic fluid in aviation[12], can be left out of the HAMRAC. This is beneficial from a sustainable point of view since it is a highly toxic substance and adversely affecting the environment as well as the mechanics[13]. The servo-flaps have an already proven technology, and therefore no extra development testing is needed. The rotor hub is designed hingeless and bearing-less, which results in less parts. This will result in less energy needed and less waste produced during production, and since the weight of the rotor hub is less, less fuel needs to be burned during flight.

Configuration and Layout The multifunctional instrument panel that will be used in the HAMRAC as discussed in section 7.1 will not only give a very clear view for the pilot but it will also save a significant amount of weight, which will lead to fuel savings. This is because the multifunctional instrument panel reduces the amount of hardware needed.

Operations & Logistics In the mission profile, an early climb is integrated at the start of the mission. This will result in less flight time over the Gaurishankar Conservation Area, a protected area near the Mount Everest. Because of the high altitude, the sound pressure at the ground of this protected area will be significantly lower. The fuel of the HAMRAC will be heated by pumping the fuel along the hot oil from the engine. As a result, no anti-ice additives are necessary to make sure the jet A-1 will not freeze. This way of heating is very sustainable since the heat, which otherwise wasted is now used in a useful manner. The substance used as anti-ice additive is dangerous to the health and can therefore better be avoided [68].

[10] URL `https://www.lowtechmagazine.com/what-is-the-embodied-energy-of-materials.html` [cited 15 January 2019]
[11] URL `https://www.efficientplantmag.com/2004/10/what-is-lean-maintenance/` [cited 14 January 2019]
[12] URL `https://www.flight-mechanic.com/types-of-hydraulic-fluids/` [cited 15 January 2019]
[13] URL `http://www.aviaoil.com.ua/pdf/skydrol.500b-4.msds.eng.pdf` [cited 15 January 2019]

14 Further Development

In order for the HAMRAC to actually reach the market, it is necessary to investigate and plan (be it on a high level) the different phases that are part of the development, use and disposal of the rotorcraft. This process consists of different phases that together form the product design and development logic in 14.1, and are outlined by Curren and Verhagen [32]. An overview of the process is given in Figure 14.1.

14.1 Project Design & Development Logic

Phase A: VFS After reviewing the feasibility of this project, a letter of intent is written to the VFS to compete in the high-altitude design competition. The project and its stakeholders are redefined and after authorization from the TU Delft, the further development phase is kicked off. The organisational needs and project team are redefined and the design is further refined according to additional information from the VFS. The final submittal of this project is expected to gain the VFS' approval. The preliminary design at this point is finished and reviewed by industry professionals.

Phase B: Detailed Design The next phase in the project would be the detailed design phase. During this phase, components and subsystems are to be designed on a deeper level than during the conceptual design phase. In addition, all the parts are designed that were not investigated so far. More iterations of the design are performed in order to ensure that every subsystem or component is optimised with respect to all the other components. Tests are performed on a component level and the first suppliers are chosen. Wind tunnel tests of scale models are carried out and the design is optimised. The result of this phase is a finalised design for the HAMRAC and all its subsystems and components.

Phase C: Ground and Flight Testing At this point, the rotorcraft is ready for testing on higher levels than the component level. In collaboration with potential and actual suppliers, clients and the government bodies (EASA or FAA) that eventually have to certify the HAMRAC, one or more prototypes are produced and thoroughly tested. These tests shall initially happen on ground, beginning with subsystems and progressing towards full-scale system level tests. After the results of this process are satisfactory, flight tests are performed. These must ensure that the aircraft complies with all safety-related and operational requirements that are established by the relevant airworthiness authorities. Furthermore, it must be absolutely certain that the rotorcraft complies with all user and mission requirements. If the performance of the HAMRAC is unsatisfactory in this phase, the design process shall be re-iterated. For instance, this could result in adjustments being made to the design, alterations with respect to the choice for certain manufacturers of components or alterations regarding the operational procedures.

Phase D: Certification When flight tests are considered to be successful, all adjustments have been made and the design is finalised, the next step is to obtain official certification. If the current design is unable to meet the requirements from the authorities, design iterations and adjustments have to take place. This would lead to additional flight tests as well, and is therefore a very expensive and lengthy process. It is therefore crucial that is the relevant requirements are constantly taken into account during the design and test phases and are checked for compliance.

Phase E: Manufacturing and Distribution After certification is obtained, the rotorcraft manufacturing phase can start. This phase will consist of finalising contracts with suppliers, building production facilities and setting up a supply chain in order to achieve an economically feasible manufacturing process. As well as this, high quality in-line or flight test procedures are to be established. This will result in the HAMRAC living up the quality and safety standards it promises to potential customers. During the manufacturing phase, the sales team is to be expanded to ensure a full orderbook and make the profitability predictions more likely to happen. This is important to secure enough funding, as significant costs accompany this phase while actual sales are most likely limited. After the HAMRAC coaxial helicopters are produced and thoroughly tested, they can be distributed to customers.

Phase F: Operation and Maintenance As soon as the first rotorcraft are delivered to the customers, the project enters its operational phase. This is the longest of all phases, and the manufacturer still has important functions at this point. To begin with, it is responsible for aviation training (procedures and certification) to ensure that qualified pilots know how to fly the rotorcraft and know how it works. In addition, it should provide strict maintenance instructions, procedures and schedules in order to make sure that the rotorcraft keeps performing as designed for. Finally, it is responsible for all certification related activities. The FAA for instance might require the rotorcraft to meet additional requirements to extend the certification. The maintenance strategy should already be developed to a large extent during the design phase, as it is a significant contributor to the operational costs and could lead to different design choices.

Phase G: Disposal At the end of the operational lifetime of the HAMRAC, the product must be disposed of. This is done at a pre-determined disposal location. The HAMRAC must be disassembled and its recyclable components are separated from the non-recyclable components and materials. Recyclable components are then sent off to predetermined partners in order to be recycled, whilst the non-recyclable components are safely disposed of. It is important that it this phase of the rotorcraft life cycle is carefully planned, especially with regard to the sustainability requirements for the rotorcraft.

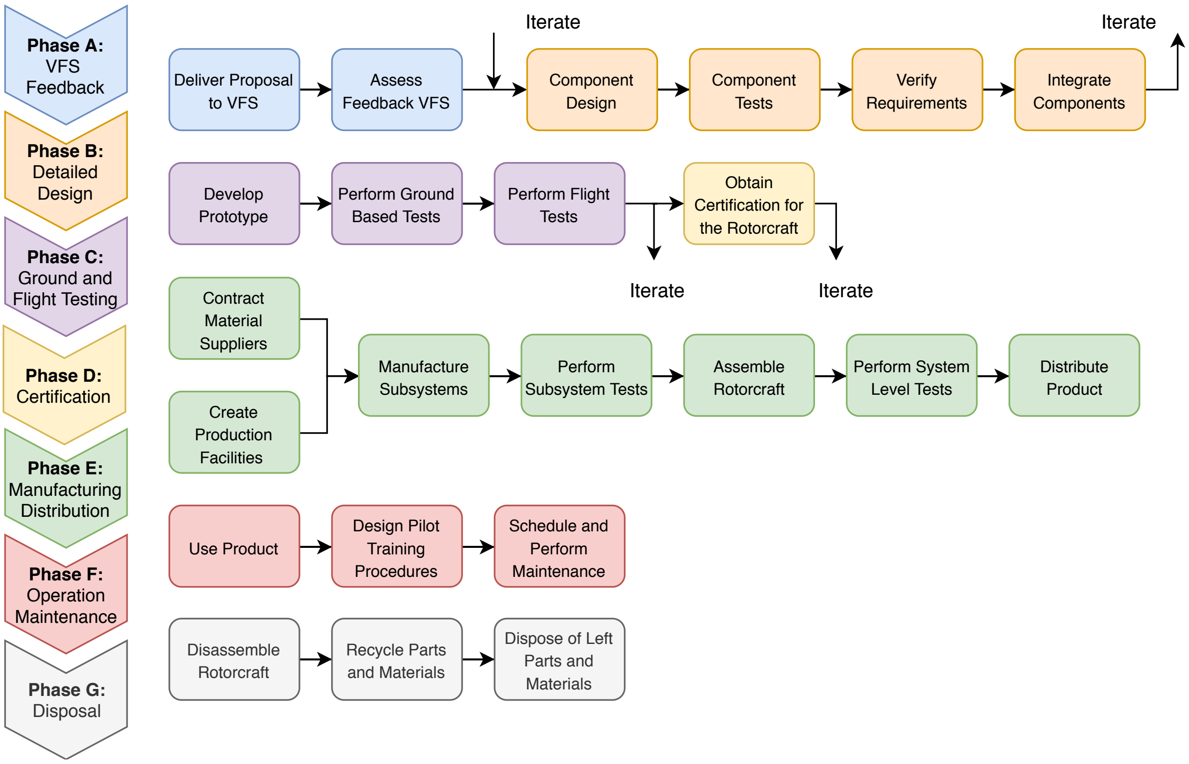

Figure 14.1: *Product design and development logic (post-DSE)*

14.2 Project Gantt Chart

The Project Gantt Chart aims to presents the post-DSE activities and offer a clear overview of the planning of the further project development. All phases described above are represented in the Gantt chart, and the first level task breakdown is visible. Not each individual task is shown, as this would provide little extra information and take up a lot of space. The further in the future, the less precise the proposed timing becomes. The VFS procurement phase and deadlines are well-defined and reasonable timeframes are given, but from there on only estimates of the time required can be made. This is because the team size, available resources and facilities, needed processes etc are all still highly imprecise and will need to be developed further in the detailed design phase. For clarity, only the planning up until the operational phase is broken down. The operational phase is a factor of 10 longer than all other phases and it is not yet clear how much this initial lifetime will be extended by certification.

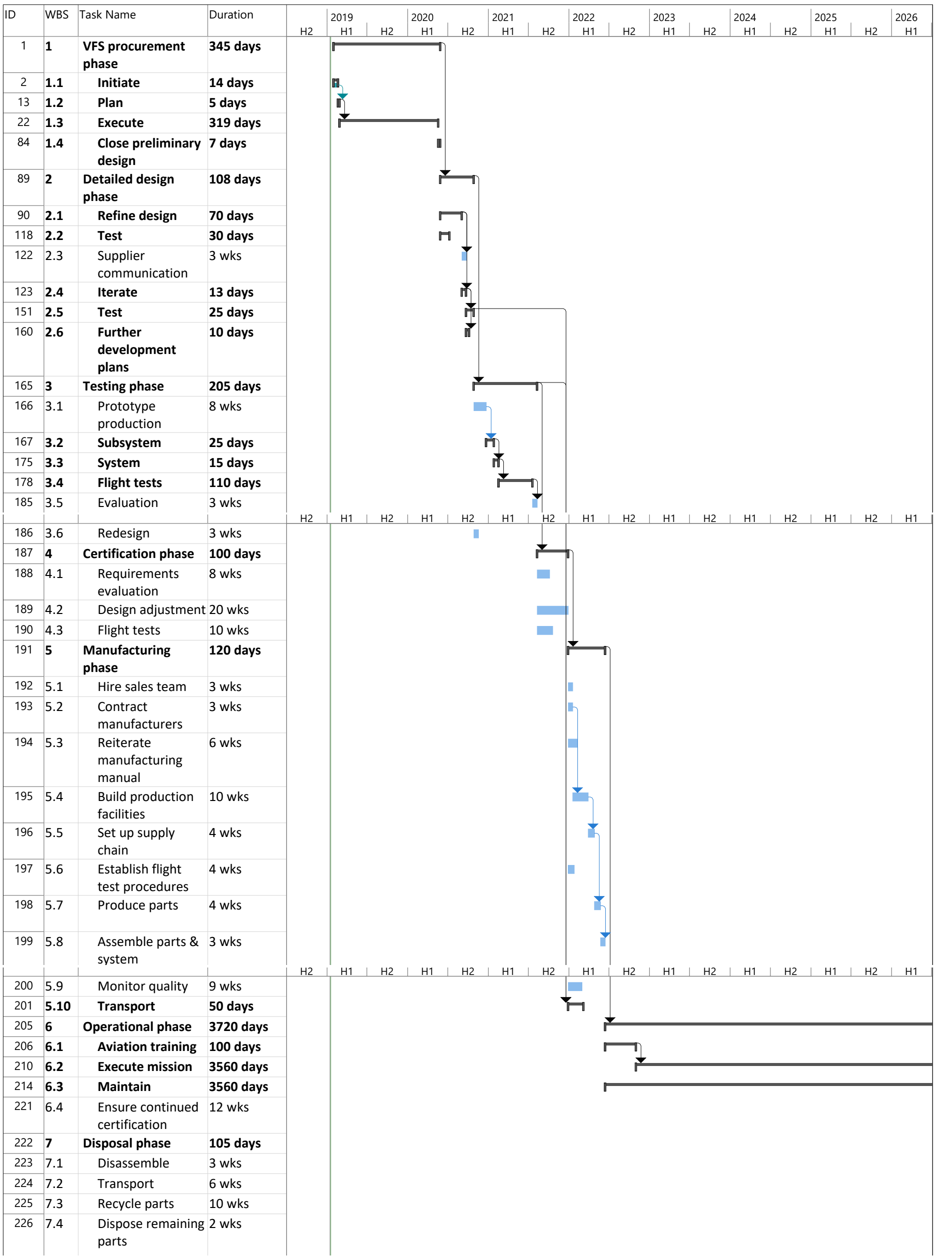

Figure 14.2: *Gantt chart breakdown of the post-DSE project phases*

15

Conclusion & Recommendations

After the conceptual trade-off was performed, a detailed design of a coaxial rotorcraft ensued. The detailed design phase was approached holistically, in the sense that technical, project management and systems engineering aspects were considered.

Market opportunities for extremely high altitude mountain rescues, as proposed to us by our stakeholders, are investigated. The primary market size is estimated to range between 20-29 million EUR per year. The understanding that current rescue helicopters only reach altitudes of 6000 m, makes the HAMRAC team confident that a significant amount of this market share could be immediately captured. It should be noted however, that HAMRAC's multifunctional design, and optional configuration options, permit it to be competitive in other potential markets as well. Namely, the EMS market valued at 26.2 billion EUR with a current annual growth rate of 6%.

Operational mission aspects have been analysed in sufficient detail such that the HAMRAC is capable of carrying out the three hour reference mission. Starting from Kathmandu, the rotorcraft should only have to stop once at an intermediate airport, before finally hovering above Mount Everest's summit. Two people will be saved, despite the harsh operational environment the vehicle is expected to endure. Through optimization, the amount of fuel mass required for the reference mission is a mere 493 kg.

The innovative rear hatch allows for a wide field of view during a rescue. Integrating this feature with an internal hoist system, permits rescuees to be placed on their respective beds with ease, reducing crew workload. The latest avionics system introduced by airbus, Helionix, is chosen for the design, as such a demanding mission profile requires the best navigation and communication hardware available in the market.

Aerodynamic performance took a significant role during the conceptual trade-off. One of the main reasons the coaxial configuration was chosen, was due to the absence of dissymmetry of lift, inherent to a conventional rotorcraft configuration. This allows the HAMRAC to achieve cruise speeds that would have not been possible otherwise. The VR12 and VR14 airfoils have proven to outperform their counterparts when considering the whole range of operations. For this reason, they have been chosen for the rotor blade design of the HAMRAC, where two linear twists and an overall linear taper is used. Further consideration is given to the operational range, whereby two rotational velocities are achieved by means of a dual transmission, increasing the altitude range. In addition to this, the rotor hub fairing, an extremely innovative solution, reduces the rotor hub's parasitic drag, which usually accounts for more than 20% of the total rotorcraft drag. With two LHTEC T800 engines, the HAMRAC is capable of hover at a ceiling of 10,500 m, outperforming its competitors by a significant margin. By introducing two engines to the design, the safety of the vehicle is generally improved and FAR Category A certification requirements can also be met.

The rotor blades will have a sandwich structure, increasing blade inertia, which is crucial for the expected bending loads. The skin itself will be manufactured from lightweight carbon fibre, as performance is paramount to HAMRAC's operations. A control feature coupled with the blade design, is the servo flap. This allows for the design of a single swashplate mechanism, despite two main rotors. The rotor hub chosen is hingeless and bearingless, resulting in a simpler rotor hub with less linkages required for control. The absence of these linkages, which would have been located above the rotor hub fairing, reduces the rotor hub drag further. The hingeless rotor hub has further benefits as it allows for significant control power left to manoeuvre in all flight phases. A 4-axis autopilot will control he HAMRAC, overcoming instability in all controllable axis.

For all analysis models used software verification and model validation is performed where the model outputs and assumptions made in the construction of the analysis model are verified. From this procedure several recommendations have been drawn for further design analysis and these are presented below.
An exhaustive risk analysis is done so that all risks are identified, their probability of occurrence is quantified, impact is clear and appropriate mitigation strategies are accordingly set. Some risks were mitigated by design decision, whilst others still need to be monitored during the manufacturing and assembly phase or operational lifetime. This way the risks encountered in operation of the vehicle are minimised improving the vehicle safety.

When designing in this era, sustainable considerations are crucial to ensure that our planet's ecosystem remains stable for coming generations. Therefore, the impact of the HAMRAC on the environment was carefully considered. The conventional (single rotor) configuration was used as reference, since all current competitor have such design. Unfortunately, a coaxial configuration, does produce 18 dB more sound than a conventional configuration. However, this has little to no effect on setting off avalanches, since the HAMRAC's rotors only produce 106-118 dB, at less than two rotor diameters. By choosing this configuration however, an improvement in fuel consumption is possible. It is believed the latter's benefits, outweigh the former's drawbacks, and therefore, the design team strongly believes the HAMRAC has a net positive effect on the environment when compared to all possible competition.

Using a logarithmic regression, a projected purchase price of 3.44 million EUR is expected. This effectively makes the HAMRAC 60 thousand EUR less expensive than initially budgeted by our stakeholders. Break-even is predicted to happen after approximately 53 HAMRACs are sold. The break-even point is expected to happen after seven and a half years after the HAMRAC enters its manufacturing phase, when 53 HAMRACs are predicted to be sold. It is estimated that a 26% ROI is achievable when all variables are considered.

Further processes are still required before distribution for operational use is possible. The VFS is a body of knowledge regarding vertical take-off aircraft, who will assess the design and its feasibility. Further time must be spent on modelling given that insufficient time was available to create a fully validated structural model. The use of industrial computational tools for FEM and CFD should be acquired to further verify our findings. Flight testing and certification will be required for a green light to manufacture and distribute at scale.

Recommendations A few recommendations are proposed to improve the current design. For a better understanding of the aerodynamic performance of HAMRAC's aerodynamic subsystems, computational fluid dynamic models should be developed and wind tunnel tests should be performed. This will allow for the aerodynamic interference between the servo flaps and the rotor blades to be investigated. Since servo flaps have not been used at such low density flight conditions, their performance in these conditions should be analysed. Design of a multi omega transmission should be done and tested for multiple rotational velocities, so a successful integration with the power train subsystem is possible. A further improved power required model in combination with a further detailed mission profile, accounting for throttle settings, will result in a better understanding of the power required at each phase of the mission. The LHTEC T800 engine should also be tested at high altitudes since it has not been designed for the altitudes the mission profile requires the HAMRAC to reach. The use of more sophisticated software for composite blade design would significantly improve the accuracy of the blade design. The further inclusion of blade torsion in this model would also more accurately represent the true loading conditions.

Appendices

A Task Distribution

Task	Member
List of Abbreviations	Joey
List of Symbols	Joey
Executive Summary	Giel, Ties, Archie
Introduction	Max
Project Definition	
2.1 Mission Objective	Max
2.2 Project Organisation	Ties
2.3 Method and Approach	Max
2.4 Functional Analysis (Flow)	Matt
2.5 Functional Analysis (Breakdown)	José
Market Summary	
3.1 The Helicopter Market	Ties
3.2 Primary Market	Ties
3.3 Potential Markets	Leon
3.4 Forecast Sales 2022-2032	Leon
3.5 SWOT analysis	Ties, Leon
Resource Allocation	
4.1 Mass Budget	José, Archie
4.2 Power Budget	José
Concept Selection	
5.1 Trade-off Approach	Sieglinde
5.2 Trade-off Results	Sieglinde
5.3 Sensitivity Analysis	Sieglinde, Robert
Operations and Logistics	
6.1 Reference Mission	Falco
6.2 Range	Falco
6.3 Operational Conditions	Falco
6.4 Operational Flow	Falco
6.5 Communication Flow	Falco
Configuration and Layout	
7.1 Avionics	José
7.2 Design Configuration	Joey
7.3 Internal Configuration	José, Robert, Joey
7.4.1 Subsystem Layout and Center of Gravity	José, Joey
7.4.2 Critical Center of Gravity Locations	José, Joey
7.4.3 Fuel System	Falco
7.4.4 External 3D CATIA Sketches	Joey
Aerodynamic and Performance Characteristics	
8.1 Initial Sizing Rotorsystem	Leon, Robert
8.2 Rotor Blade Sizing	Matt
8.3 Airfoil Design	Leon, Max
8.4 Fuselage and Aerodynamic Considerations	Robert
8.5 Design of the Propulsive System	Matt, Max

Task	Member
Structural Characteristics	
9.1 Initial Considerations	Archie
9.2 Design of Rotor Blade	Archie, Giel
9.3 Design of Blade Hub Connection	Archie
9.4 Design of Rotorshaft	Archie
9.5 Design of Airframe	Giel
Stability and Control Characteristics	
10.1 Subsystem Description	Ties
10.2 Achieving Balance	Ties
10.3 Helicopter Flight Controls	Ties
10.4 Main Rotor Hub Design	José
10.5 Design of Control Surfaces	Ties, Sieglinde
10.6 Stability Analysis	Sieglinde
10.7 Control Power	Sieglinde
10.8 Flying Qualities	Sieglinde
10.9 Automatic Flight Control System	Ties
Verification and Validation	
11.1 Subsystems	Falco, Archie, Matt, Sieglinde
11.2 Sensitivity Analysis	Max, Ties, Giel
11.3 Compliance Matrix and Feasibility	Falco, Sieglinde
Cost Breakdown	
12.1 Development Cost	Matt
12.2 Production Cost	Matt
12.3 Operational Cost	Joey
12.4 Transport and Disposal Cost	Joey
12.5 Return on Investment	Leon, Matt, Ties
System Characteristics	
13.1 RAMS	Max, Robert
13.2 Production Plan	Falco
13.3 Technical Risk Assessment	Giel, Archie
13.4 Sustainable Development Strategy	Robert, Max
Further Development	
14.1 Design and Development Logic	Ties
14.2 Project Gantt Chart	Sieglinde
Conclusion and Recommendations	José
Others	
Secretarial Tasks	Falco
Report Doctoring	Matt
Communications Coordinator	Sieglinde
Project Management	José
CAD Design	Joey

Bibliography

[1] Bagai A. and Leishman J.G. Free-wake analysis of tandem, tilt-rotor and coaxial rotor configurations. *Journal of the American Helicopter Society*, Vol. 41(No. 3):pp. 196–207, July 1996.

[2] De Sa A. and Al Zubaidy S. Gas turbine performance at varying ambient temperature. *Applied Thermal Engineering*, Vol. 31(No. 14-15):pp. 2735–2739, 2011.

[3] Filippone A. Data and performances of selected aircraft and rotorcraft. *Progress in Aerospace Sciences*, Vol. 36(No. 8):pp. 629–654, 2000.

[4] Krenik A. and Weiand P. *Aspects On Conceptual And Preliminary Helicopter Design.* Deutsche Gesellschaft für Luft-und Raumfahrt-Lilienthal-Oberth eV, Braunschweig, Germany, 2016.

[5] Federal Aviation Administration. *Basic Helicopter Handbook.* U.S. Department of Transportation, Oklahoma City, Oklahoma, 1973.

[6] Federal Aviation Administration. *Instrument Flying Handbook.* U.S. Department of Transportation, Washington D.C., 2012.

[7] Federal Aviation Administration. *Helicopter Flying Handbook.* U.S. Department of Transportation, Washington D.C., 2012.

[8] Federal Aviation Administration. *Flight in Icing Conditions.* U.S. Department of Transportation, Washington D.C., 2015.

[9] Phelps A.E. and Mineck R.E. Aerodynamic characteristics of a counter-rotating, coaxial, hingeless rotor helicopter model with auxiliary propulsion. Technical report, NASA TM 78705, May 1978.

[10] Kaman Aerosystems. *K-MAX, Better by design.* Kaman Corp. of Bloomfield, 2015.

[11] European Aviation Safety Agency. *Certification Specifications and Acceptable Means of Compliance for Small Rotorcraft.* EASA Agency Decisions, Oxford, 2003.

[12] European Aviation Safety Agency. Operational evaluation board report. 2014.

[13] Lefebvre A.H. and Ballal D.R. *Gas Turbine Combustion, Alternarnative Fuels and Emissions.* CRC, Boca Raton, FL, 2010.

[14] Airbus. 36th annual student design competition 2018-19 request for proposal for an extreme altitude mountain rescue vehicle. Vertical Flight Society, 2018.

[15] Ostroff A.J., Downing D.R., and Rood W.J. A technique using a nonlinear helicopter model for determining trims and derivatives. Technical report, NASA TN D-8159, May 1976.

[16] Pasion A.J. Design and evaluation of aircraft heat source systems for use with high-freezing point fuels. Technical Report NASA CR-159568, NASA, May 1979.

[17] Mitchell A.M., Oswald F.B., and Schuller F.T. Testing of yuh-61a helicopter transmission in nasa lewis 2240-kw (3000-hp) facility. 1986.

[18] Bramwell A.R.S., Done G., and Balmford D. *Bramwell's Helicopter Dynamics.* Butterworth-Heinemann, 2nd edition, 2001.

[19] General Aviation Manufacturers Association. *2017 Annual Report.* General Aviation Manufacturers Association, Washington, 2017.

[20] National Fire Protection Association. Standard for aircraft fuel servicing 407, 2017.

[21] Krag B. and Gmelin B. *Flying Qualities - Some History.* Springer International Publishing, 2017.

[22] Marrant B. and Pavel M. *Helicopter Performance, Stability and Control.* Faculty of Aerospace Engineering Delft University of Technology, 2002.

[23] Nuckolls B. *The AeroElectric Connection.* AeroElectric Connection, Medicine Lodge, KS, 2009.

[24] Ren B., Ge S.S., Chen C., Fua C., and Lee T.H. *Modeling, Control and Coordination of Helicopter Systems.* Springer Science+Business Media, 2012.

[25] Reuter B. and Schweizer J. Avalanche triggering by sound: myth and truth. In *Proceedings of the International Snow Science Workshop ISSW*, pages pp. 330–333, 2009.

[26] Andrey S Batrakov, Alexander N Kusyumov, Sergey A Mikhailov, V Pakhov, Artur R Sungatullin, Vladimir V Zherekhov, and George N Barakos. A study in helicopter fuselage drag. *School of Engineers, University of Liverpool*, 2013.

[27] Baskett B.J. *Aeronautical Design Standard - Performance Specification Handling Qualities Requirements for Military Rotorcraft.* United States Army Aviation and Missile Command, Redstone Arsenal, Alabama, March 2000.
[28] Concorde. The rg-25 aircraft battery. Technical report, Concorde Battery Corporation, West Covina, CA, 2017.
[29] Kaman Aircraft Corporation. Helicopter, filed 14-09-1950. US Patent No. 676398.
[30] Coleman C.P. *A survey of theoretical and experimental coaxial rotor aerodynamic research.* NASA Ames Research Center, Moffett Field, CA, 1997.
[31] Filipe Szolnoky Cunha. Helicopter performance.
[32] Verhagen W.J.C. Curran R., Zhao X. Concurrent engineering and integrated aircraft design. 2015.
[33] Carico D. Helicopter controllability. Technical report, Naval Postgraduate School, Monterey, California, September 1989.
[34] Kim D. and Kim S. *The Overview of Kari Bearingless Main Rotor Hub System.* Korea Aerospace Research Institute (KARI), 2013.
[35] Padfield G. D. The making of helicopter flying qualities: a requirements perspective. *The Aeronautical Journal*, December 1998.
[36] Whiteman D. *Mountain Meteorology Fundamentals and Applications.* Oxford University Press, 2000.
[37] Li Liu Daniel Patt and Peretz P. Friedmann. Free-wake analysis of tandem, tilt-rotor and coaxial rotor configurations. *Helicopter Noise Reduction By Actively Controlled Flaps*, page pp. 5, May 2005.
[38] Mu E. and Rojas M.P. Practical decision making. an introduction to the analytical hierarchy process. 2017.
[39] *Annexes to the draft Commission Regulation on 'Air Operations - OPS'*, 2017. EASA.
[40] Cengel Y.A. et al. *Introduction to thermodynamics and heat transfer.* McGraw-Hill New York, 1997.
[41] Smith M. et al. Undermining privacy in the aircraft communications addressing and reporting system (acars). In *Proceedings on Privacy, Enhancing Technologies.* De Gruyter, 2018.
[42] Ruijgrok G. *Elements of Airplane performance.* VSSD, Delft, Netherlands, 2nd edition edition, 2009.
[43] Padfield G.D. *Helicopter Flight Dynamics.* Blackwell Science Ltd, 1996.
[44] Bansemir H. and Emmerling S. Fatigue substantiation and damage tolerance evaluation of fiber composite helicopter components. Technical report, Eurocopter Deutschland GMBH Munchen (Germany), 2000.
[45] True H.C. and Rickley E.J. Noise characteristics of eight helicopters. Technical report, Federal Aviation Administration, Systems Research and Development Centers, Washington DC, 1977.
[46] Airbus Helicopters. H145 technical data. 2018.
[47] Kim H.W., Duraisamy K., and Brown R. Aeroacoustics of a coaxial rotor in level flight. In *64th American Helicopter Society Annual Forum*, 2008.
[48] Chopra I. Design and analysis trends of helicopter rotor systems. *Sadhana*, Vol. 19(No. 3):pp. 427–466, 1994.
[49] Aircraft Industries Association INC. *Aircraft Yearbook 1957-1958.* American Aviation Publications, Washington D.C., 1958.
[50] Markish J. *Valuation techniques for commercial aircraft program design.* PhD thesis, Massachusetts Institute of Technology, 2002.
[51] Roskam J. *Airplane Design VIII: Airplane Cost Estimation: Design, Development, Manufacturing, and Operating.* DARcorporation, 1990.
[52] Shen J. Comprehensice aerolastic analysis of helicopter rotor with trailing-edge flap for primary control and vibration control. 2003.
[53] Watkinson J. *The Art of the Helicopter.* Elsevier Butterworth-Heinemann, 2004.
[54] W. Johnson J. Shen, I. Chopra. Performance of swashplateless ultralight helicopter rotor with trailing-edge flaps for primary flight control. 2003.
[55] Campfens J.A. Preliminary design of a coaxial rotor. 2007.
[56] Crabtree J.A. and Tool H. Weight estimation for helicopter design analysis. In *The Society of Aeronautical Weight Engineers 9inc., Technical Paper No. 177*, pages pp. 7–12. Society of Aeronautical Weight Engineers, May 1958.
[57] Eastman J.N. Characteristics of the naca23012 airfoil from tests in the full-scale and variable-density tunnels. 1936.
[58] Martins J.R.R.A and Lambe A.B. Multidisciplinary design optimization: a survey of architectures. *AIAA journal*, Vol. 51(No. 9):pp. 2049–2075, 2013.

[59] Ferguson K. and Thomson D. A flight dynamics investigation of compound helicopter configurations. Phoenix, AZ, USA, May 2013. AHS 69th Annual Forum and Technology Display.

[60] Ferguson K. and Thomson D. Examining the stability derivatives of a compound helicopter. *Aeronautical Journal*, Vol. 121(No. 1235):pp. 1–20, January 2017.

[61] Ferguson K. and Tu Z. Comparing the flight dynamics characteristics of tandem and conventional helicopters for the purposes of automatic control. September 2015.

[62] Noonan K.W. Aerodynamic characteristics of two rotorcraft airfoils designed for application to the inboard region of a main rotor blade. 1990.

[63] Li L. *Structural design of composite rotor blades with consideration of manufacturability, durability, and manufacturing uncertainties.* PhD thesis, Georgia Institute of Technology, 2008.

[64] J. Gordon Leishman. *Principles of Helicopter Aerodynamics.* Cambridge University Press 2000, 2000. ISBN 0 521 66060 2.

[65] Lonoce M. Helicopter blade twist optimization in forward flight. Master's thesis, Instituto Superior Tecnico, Lisbon, Portugal, November 2016.

[66] B. S. Malyshev. The system of two coaxial main rotors of the aircraft, filed 10-09-2000. RU2155702C1.

[67] Andrew M.J. Co-axial rotor aerodynamics in hover. *University of Southampton*, (No. 27), September 1980.

[68] *Fuel Servicing.* National Air Transport Association, Washington, D.C.

[69] Prasad N.E. and Wanhill R.J.H. *Aerospace materials and material technologies*, volume Vol. 3. Springer, 2017.

[70] Rand O. and Khromov V. Helicopter sizing by statistics. *Journal of the American Helicopter Society*, Vol. 49(No. 3):pp. 300–317, July 2004.

[71] Perroud P. and Lecomte C. Operation "bangvalanches." the sonic boom effect on avalanches. In *Proceedings of the Davos Symposium*, number No. 162, September 1986.

[72] Schindler R. and Pfisterer E. Impacts of rotor hub design criteria on the operational capabilities of rotorcraft systems. Technical report, Industrieanlagen-Betriebsgesellschaft MBH, Ottobrunn, Germany, 1987.

[73] Hamann R.J. and van Tooren M.J.L. Systems engineering and technical management techniques. Delft University of Technology.

[74] Prouty R.W. *Helicopter Performance, Stability, and Control.* Krieger Publishing Company, 1995.

[75] Yoon S., Lee F.C., and Pulliam T.H. Computational study of flow interactions in coaxial rotors. *NASA Ames Research Center*, January 2016.

[76] C Shimansky. Accidents in mountain rescue operation. *Mountain Rescue Association Evergreen, Colorado, USA*, 2008.

[77] J.D. Singleton and Jr. W.T. Yeager. Important scaling parameters for testing model-scale helicopter rotors. *20th AIAA Advanced Measurement and Ground Testing Technology Conference*, 1998.

[78] Gupta S.K. *Aerodynamic Loading on the Blades of a Helicopter Rotor in Steady Translational Flight.* PhD thesis, McMaster University, 1972.

[79] Daigh S.L. Helicopter final assembly critical path analysis. Master's thesis, Massachusetts Institute of Technology, June 2012.

[80] Rindlisbacher T. and Chabbey L. Guidance on determination of helicopter emissions. Swiss Confederation, December 2015.

[81] European Helicopter Safety Team. Techniques for helicopter operations in hilly and mountainous terrain. EASA, 2014.

[82] Megson T.H.G. *Aircraft Structures for Engineering Students.* Elsevier, fifth edition edition, 2012.

[83] Johnson W. *Helicopter Theory.* Princeton University Press, 1980.

[84] Johnson W. Recent developments in the dynamics of advanced rotor systems. 2. *Vertica*, Vol. 10(No. 2): pp. 109–150, 1986.

[85] Johnson W. *Rotorcraft Aeromechanics.* Cambridge University Press, 2013.

[86] Kania W., Stalewski W., and Zwierzchowska B. Design of the modern family of helicopter airfoils. *Prace Instytutu Lotnictwa*, pages pp. 51–82, 2007.

[87] Stalewski W. and Żółtak J. Optimisation of the helicopter fuselage with simulation of main and tail rotor influence. In *Proceedings of the ICAS Congress*, pages pp. 2012–1, 2012.

[88] Stewart W. *Helicopter Behaviour in the Vortex Ring Conditions.* HM Stationery Office, 1959.

[89] Yuan Y., Chen R., and Li P. Trim investigation for coaxial rigid rotor helicopters using an improved aerodynamic interference model. *Aerospace Science and Technology*, Vol. 85:pp. 293–304, 2019.